

**“SYNTHESIS OF WATER SOLUBLE TRIAZATRIANGULENIUM
CATIONS AND STUDIES ON THEIR APPLICATION AS SINGLET
OXYGEN SENSITIZERS IN HOMOGENEOUS AND
HETEROGENEOUS MEDIA”**

*Thesis submitted to the
Cochin University of Science and Technology
In partial fulfilment of the requirements for the degree of*

*Doctor of Philosophy
in
Chemistry*

in the Faculty of Science

By

Seena Sebastian

(Reg. No: 3425)

Under the supervision of

Dr. N. Manoj



**DEPARTMENT OF APPLIED CHEMISTRY
COCHIN UNIVERSITY OF SCIENCE AND TECHNOLOGY
KOCHI - 682 022, KERALA, INDIA**

August 2018

Dedication

To my most beloved parents



DEPARTMENT OF APPLIED CHEMISTRY
COCHIN UNIVERSITY OF SCIENCE AND TECHNOLOGY
KOCHI – 682 022, KERALA, INDIA

Dr. N. Manoj
Associate Professor
E-mail: manoj.n@cusat.ac.in
Ph: 0484-2575804

CERTIFICATE

This is to certify that the thesis entitled **“SYNTHESIS OF WATER SOLUBLE TRIAZATRIANGULENIUM CATIONS AND STUDIES ON THEIR APPLICATION AS SINGLET OXYGEN SENSITIZERS IN HOMOGENEOUS AND HETEROGENEOUS MEDIA”** is a genuine record of research work carried out by **Ms. Seena Sebastian**, under my supervision, in partial fulfilment of the requirements for the degree of Doctor of Philosophy of Cochin University of Science and Technology, and further that no part thereof has been presented before for the award of any other degree. All the relevant corrections and modifications suggested by the audience and recommended by the doctoral committee of the candidate during the pre-synopsis seminar have been incorporated in the thesis.

Kochi-22
August, 2018

Dr. N. Manoj
(Thesis Supervisor)

DECLARATION

I hereby declare that the work presented in the thesis entitled "**SYNTHESIS OF WATER SOLUBLE TRIAZATRIANGULENIUM CATIONS AND STUDIES ON THEIR APPLICATION AS SINGLET OXYGEN SENSITIZERS IN HOMOGENEOUS AND HETEROGENEOUS MEDIA**" is the result of genuine research carried out by me under the supervision of **Dr. N. Manoj**, Associate Professor of Organic Chemistry, Department of Applied Chemistry, Cochin University of Science and Technology, Kochi-22, and the same has not been submitted elsewhere for the award of any other degree.

Kochi-22

August, 2018

Seena Sebastian

Acknowledgements

The work presented here in this could not have been done without the help of many people with whom I am associated. Thanking them with few words is an impossible task but I believe through these acknowledgements I am able to carry my deepest and sincere feelings to them.

*To start with my sincere and deep felt gratitude to my thesis supervisor **Dr. N. Manoj**, Associate Professor, Department of Applied Chemistry, Cochin University of Science and Technology, for giving me an opportunity to be in his research group, for his guidance, constant encouragement, and continuous support throughout my research work.*

I would like to thank Dr. S. Prathapan, Professor, Department of Applied Chemistry, CUSAT for his valuable suggestions and fruitful discussions throughout the research, being my doctoral committee member.

I wish to thank Prof. K. Girish Kumar, Head, Department of Applied Chemistry, CUSAT for the immense support and encouragement extended to me.

I gratefully acknowledge the former Heads of the Department, Dr. K. Sreekumar and Prof. M. R. PrathapachandraKurup for providing me with all the necessary facilities of the department for carrying out my research work. I would like to extend my sincere thanks to all the former and present members of the Faculty of the Department of Applied Chemistry. I thank the administrative staff of the Department and University office, CUSAT.

I express my heartfelt gratitude to Dr. K. R. Gopidas, and Dr. V. Karunakaran NIIST, Trivandrum for providing me the facilities for Laser Flash Photolysis and TCSPC studies. I sincerely thank Ms. Chinju SRF for her support for the laser flash photolysis studies.

My thanks are also due to,

- The Management, Principal, present and former faculties of the department of chemistry, Assumption College Autonomous, Changanacherry, Kottayam for the constant encouragement and supports.*
- Dr. T. K. Manoj Kumar, IITM-K for Theoretical studies*
- Dr. Simon Augustine, St. Thomas College Pala, for XRD Analysis*
- Mrs. Thahira, A. for the LC-MS analysis*
- Ms. Roshini and Ms. Reshma for the IR spectral studies.*

- *Dr. Rishad, Unibiosys Lab for the biological studies*
- *Dr. Manju Thankomoni, Assistant Professor, SreeSankara College, Kalady, for valuable suggestions during thesis correction.*
- *Dr. Aneesh P Sivads for giving wise advices and suggestions.*
- *My seniors, Dr. Gisha George, Dr. Jayakumar, Ms. Dhanya for their advices and valuable suggestions.*
- *My colleagues, Ms. Pravitha, Dr. Jomon, Dr. Sandhya, Dr. Eason, Dr. Sajitha, Dr. Rakesh, Dr. Reshma, Dr. Suma, Dr. Kala and Mr. Senju for the joyful time spent together during the course and for their boundless help and support throughout the work and at the difficult times in my life.*
- *Ms. Vineetha, Mr. Kiran James, Ms. Parvathy, Ms. Aswathy, Ms. Haritha and Mr. Midhun for their support and cooperation.*
- *My friends, Ms. Manjula, Ms. Minu, Ms. Cisy, Ms. Remya L., Ms. Soumya, Ms. Nithya, Ms. Ligi, Mr. Shandev, Mr. Tomson, Ms. Nishad, Mr. Jith, Ms. Amrutha, Ms. Remya, Ms. Aswathy, Ms. Rani, Ms. Jesna for their timely help*
- *Late Mr. Vishnu P., Alpha Chemicals and Diagnostics for supplying chemicals in time.*
- *Friends of other groups in the Department of Applied Chemistry for their endless care and support.*
- *All my respected teachers and well-wishers.*
- *SAIF, CUSAT for the analytical and spectral data.*
- *University Grants Commission (UGC) for the research fellowship.*

My family have been unbelievably supportive throughout my life, without which it would have been impossible to finish the work in due time. I have no words to extend my deep sense of gratitude to my parents, husband, daughter, my chechy, chettai, their son Cyriac and all other family members who contributed their patience, moral support, encouragement, co-operation and blessings throughout this work.

*It is to **God Almighty** that I owe all my achievements. His blessings showered on me gave me strength to complete the course successfully.*

Seena Sebastian

PREFACE

Oxygen the most important element required to sustain life on earth. It accounts for nearly half of the mass of the earth crust and two thirds of the mass of the human body. Oxygen molecule is paramagnetic due to its electronic configuration where there are two unpaired electron in its valence orbital. In terms of spin multiplicity its ground state has a triplet multiplicity. Though there are two unpaired electrons in its valence orbital it is less reactive to many organic molecules and this low reactivity is key to sustaining life on earth. However, in its lowest energy excited states it has singlet multiplicity and are termed as “delta” oxygen and “sigma” oxygen where the latter one has a higher energy (Figure 1). The transition from $^1\Delta_g$ to $^3\Sigma_g$ is a spin forbidden transition where as the transition from $^1\Sigma_g$ to $^1\Delta_g$ is a spin allowed transition and this is evident from their respective lifetime data. In the gaseous phase $^1\Delta_g$ has a lifetime of 45 min where as $^1\Sigma_g$ exists only 7-12 seconds.

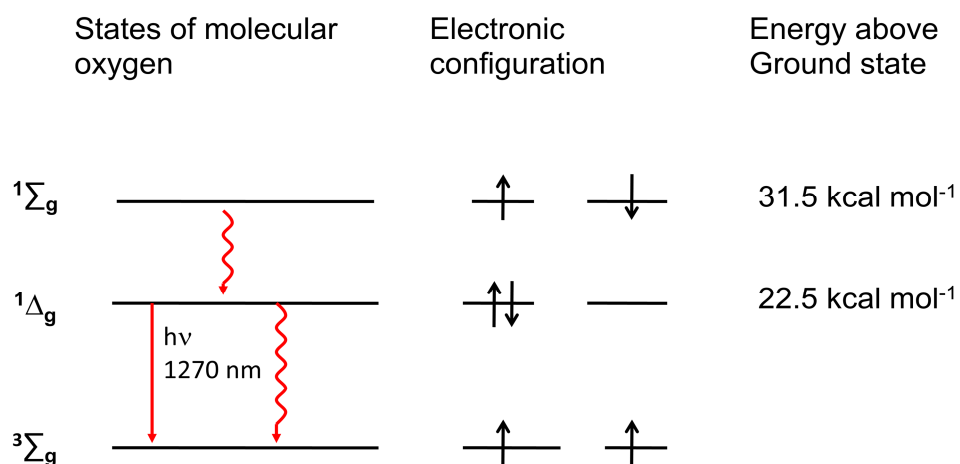


Figure 1 The energy levels of molecular oxygen

This electronically excited molecular oxygen is commonly called as singlet oxygen which is highly electrophilic and reactive with unsaturated compounds, heterocyclic compounds etc. This high and selective reactivity has its advantages and is considered as a good technique of oxygenation of organic molecules. Alkenes and arene reacts with singlet oxygen to form an endoperoxide via a cycloaddition reaction and further rearrangement or disproportionation give oxidation products. In addition to this singlet oxygen also give 'ene' reaction where addition of singlet oxygen to an alkene followed by a sigmatropic shift of hydrogen produce a hydroperoxide. This specificity of its reaction finds it as an important reagent for oxygenation in synthetic organic chemistry. Singlet oxygen has also an important role in the natural oxidative damages happen to living cells. For example some of the naturally occurring molecules do aid in the intracellular generation of singlet oxygen chemically or photochemically when exposed to light. Singlet oxygen thus produced do react with cellular components such as unsaturated lipids, amino acids such as tryptophan, cysteine, histidine etc., nucleic acid bases such as purines and pyrimidines leading to formation of oxygenated products. Newly formed products either modify cell functions or even cause cell death. This mechanism of oxygenation reaction under exposure of sunlight is termed as photodynamic action of singlet oxygen. Though it induce considerable damages to living cells there are applications which take advantage of this mechanism. One is in the Photodynamic therapy of cancer and another photodynamic remediation of contaminated water with pathogens such as bacteria and viruses. The present thesis is an attempt in this direction where a triaryl cation derivative is used as a potential agent for the generation of singlet oxygen.

Photosensitized generation of singlet oxygen is the method of choice in application domains such as photodynamic therapy or photoremediation of

water. It requires oxygen, light of suitable wavelength, and a photosensitizer capable of absorbing light and transfer that energy to oxygen molecule in the ground state to form the singlet excited molecular oxygen.

For a molecule to act as a singlet oxygen sensitizer it should have, (1) high absorption coefficient in the spectral region of the light used for the excitation, (2) the excited state energy should be greater than $22.5 \text{ kcal mol}^{-1}$ so that the effective energy transfer occurs between the triplet state of the sensitizer and molecular oxygen in the ground state, (3) it should be thermally and photochemically stable, (4) it should not react with the singlet oxygen and (5) it should have high triplet quantum yield and have long triplet lifetime. Rose bengal, phenalenone, dicyanoanthracene etc., are some of the commonly used singlet oxygen sensitizers.

Photochemical water disinfection based on the photodynamic action of oxygen has gained much attention compared to the conventional methods of water disinfection such as chlorination, ozonization and UV irradiation. These methods faces the limitations such as harmful side products, high cost, long time duration, limited water volume etc. The photodynamic water disinfection involves only three components the photosensitizer, light of suitable wavelength and molecular oxygen. The major advantage is the possibility to use visible light absorbing molecules as the sensitizer so that sunlight can be used as the light source. The singlet oxygen generated reacts with the cell components of the pathogen such as lipids of the membranes, amino acids, proteins, and nucleic acids leading to the cell death. Since the lifetime of singlet oxygen in water is low compared to other solvents, for the effective inactivation of microorganisms in aqueous medium require the pathogen's affinity to sensitizer. This is usually through an electrostatic association between the bacteria and the sensitizer. Because of the presence of lipopolysaccharide in the outer membrane most of the bacteria have a

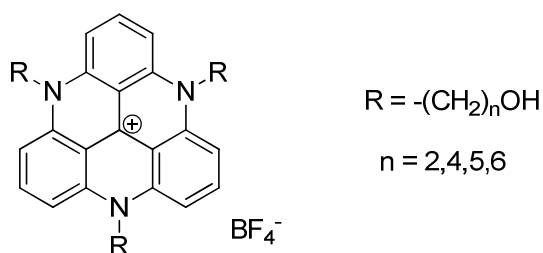
negative charge in the outer shell at physiological pH values. Therefore, cationic dyes are effective in the photodynamic action compared to neutral and anionic dyes. Solubility and stability of these sensitizers in water is an important criteria for effective use in disinfection.

The present thesis reports a study of a class of cationic triarylmethane dyes hitherto have not been known as singlet oxygen sensitizers. These are a group of bridged highly planar triarylcarbocations known as trianguleniums having remarkable thermal stability. Triangulene is the trivial name given to a group of molecules having, six membered rings arranged in a triangular fashion. In 1963 Martin and Smith reported the best known Triangulonium salt, trioxatriangulonium (TOTA^+) tetrafluoroborate. Triangulonium cations are very stable in aqueous medium and generally the stability of a carbocation is expressed in terms of its pK_{R^+} value. The TOTA^+ has a pK_{R^+} value of 9.05. The structurally similar N bridged cation known as triazatriangulonium is another group of triangulonium ions that show remarkable stability in a wide range of pH's. The triazatriangulonium cations with various alkyl chain lengths are reported in the literature, but are insoluble in aqueous medium. For potential biological applications solubility in particular water solubility is an important criteria. In the present thesis we report the synthesis of a few water soluble triazatriangulonium cations and results of the studies on their photophysical properties and singlet oxygen generation properties in aqueous and non-aqueous medium. The main objectives of the thesis are

- ❖ To synthesize water soluble triazatriangulonium salts by incorporating polar functional groups
- ❖ Study their photophysical properties
- ❖ Study the efficiency of Triplet state formation and singlet oxygen sensitization

- ❖ Synthesis and study of lipophilic triazatriangulenium cations in microheterogeneous medium
- ❖ Tether covalently or intercalate triazatriangulenium salts to solid supports or layered materials
- ❖ Study the singlet oxygen production by these heterogeneous sensitizer systems
- ❖ Study the photodynamic action of singlet oxygen generated by these heterogeneous sensitizers and explores their ability in disinfection of contaminated water.

The thesis is divided in to five chapters. **Chapter 1** of the present thesis is a review on the generation and applications of singlet oxygen as well as the chemistry and applications of triazatriangulenium cations. In **Chapter 2** we report the synthesis, photophysical and singlet oxygen generation studies of a few water soluble triazatriangulenium (TATA) cations (Chart 1).



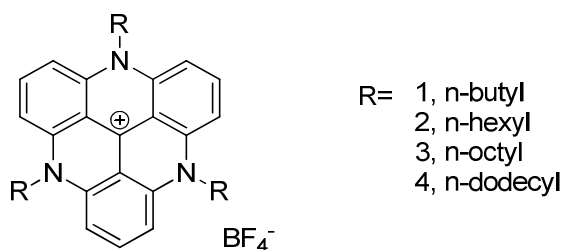
H-TATA 1-4

Chart 1

The photophysical studies such as steady – state and time - resolved absorption and emission spectroscopy were carried out in water as well as in acetonitrile. The respective absorption maxima, singlet and triplet state

energy levels, their lifetimes and quantum yields were determined. The triplet state properties were determined using nanosecond laser flash photolysis studies. The photophysical properties of TATA⁺ in the triplet state shows that it can be effectively used as a singlet oxygen sensitizer. The quantum efficiency of singlet oxygen generation was estimated by chemical actinometry using disodium-9, 10-anthracenedipropionic acid and 1, 3-diphenylisobenzofuran as the chemical actinometers and rose bengal as the reference. The apparent quantum yield for singlet oxygen generation by these cations was found to be 0.36 in water and 0.21 in acetonitrile.

Chapter 3 is the studies of triazatriangulenium cations in microheterogeneous medium. The lipophilic derivatives show significant distortion in planarity in their ground and excited state. This is indicated as a progressive shift in their emission maximum as a function chain length of the N-alkyl substituent. The theoretical calculations are also done for confirming the observed change in the geometry. The structures of the compounds are shown in Chart 2.



TATA 1-4

Chart 2

In **chapter 4**, a series of triazatriangulenium cations covalently anchored to silica surfaces were prepared and their singlet oxygen generation efficiencies were compared. The synthesis of heterosensitizers gain attention in recent times and found application in many fields including

photosensitized disinfection of waste water as they have many advantages over the homogeneous photosensitizers. Among the heterosensitizers silica gel supported organic compounds received great attention. Silica is cheap, inexpensive, thermally stable and biocompatible. The main objective of this work is to synthesize a heterogeneous photosensitizer in which triazatriangulenium covalently anchored on silica. The silica is functionalized with amino groups using the aminopropyltrimethoxysilane and with a mixture of aminopropyltrimethoxysilane and methyltrimethoxysilanes. The starting material for the synthesis of triazatriangulenium cation is tris-(2,6-dimethoxyphenyl) carbenium tetrafluoroborate. The tris-(2, 6-dimethoxyphenyl) carbenium tetrafluoroborate is cyclised with amino functionalized silica resulting in the loading of triazatriangulenium on the silica surface. The singlet oxygen production capacity of the triazatriangulenium-silica composites can be monitored using the molecular probe disodium-9,10-anthracenedipropionic acid. The disinfection studies are also conducted in order to determine the effectiveness of the synthesized triazatriangulenium-silica composites for the waste water treatment. All the four types of synthesized triazatriangulenium-silica composites produced the singlet oxygen as it is evident from the photobleaching of molecular probe disodium-9, 10-anthracenedipropionic acid. By the use of four types of synthesized triazatriangulenium-silica composites there is large decrease in the survival of bacterial pathogens as it is evident from the disinfection studies. The structure of the triazatriangulenium loaded on silica is represented in the following Chart.

List of Abbreviations

ADPA	:	Anthracene-9, 10-dipropionic acid
APTMS	:	(3-aminopropyl)trimethoxysilane
C	:	centigrade
CMC	:	critical micelle concentration
CTAB	:	Cetyltrimethylammonium Bromide
d	:	doublet
DCA	:	9, 10-dicyanoanthracene
DFT	:	Density Functional Theory
DMA	:	9, 10-dimethylantracene
DMF	:	Dimethylformamide
DNA	:	Deoxyribonucleic acid
DPA	:	2, 2'-dipyridylamine
DPBF	:	1, 3-diphenylisobenzofuran
E. coli	:	Escherichia coli
Φ_F	:	fluorescence quantum yield
FT IR	:	fourier transform infrared
g	:	gram
hrs	:	hours
HOMO	:	highest occupied molecular orbital
LED	:	Light emitting diode
LIOAC	:	Laser-induced optoacoustic calorimetry
LPS	:	Lipopolysaccharide
LUMO	:	lowest unoccupied molecular orbital
m	:	multiplet
MB	:	Methylene blue
MeCN	:	acetonitrile
mg	:	milligram

min	:	minute
mL	:	millilitre
mp	:	melting point
MTS	:	methyltrimethoxysilanes
NaCl	:	Sodium Chloride
nm	:	nanometer
ns	:	nanosecond
NMR	:	nuclear magnetic resonance
PDT	:	Photodynamic Therapy
ppm	:	parts per million
RB	:	Rose bengal
ROS	:	Reactive oxygen species
RT	:	Room temperature
s	:	singlet
SDS	:	Sodium dodecyl sulfate
SEM	:	Scanning Electron Microscopy
SODIS	:	Solar disinfection method
t	:	triplet
TADF	:	Thermally Assisted Delayed Fluorescence
TATA ⁺	:	Triazatriangulenium cation
TCSPC	:	Time Correlated Single Photon Counting
TD-DFT	:	Time Dependent Density Functional Theory
TEM	:	Transmission electron microscopy
TGA	:	Thermogravimetric Analysis
TMS	:	tetramethylsilane
TOTA ⁺	:	Trioxatriangulenium cation
TPP	:	Tetraphenylporphyrins
TRANES	:	Time - Resolved Area Normalized Emission Spectra

TRES	:	Time resolved emission spectra
TRTL	:	Time-resolved thermal lensing
UV	:	ultraviolet
XRD	:	X-Ray Diffraction
Φ_{Δ}	:	Singlet oxygen quantum yield

CONTENTS

TITLE	PAGE NO
Chapter 1	
A Review on the Generation and Applications of Singlet Oxygen...	1-62
1.1. Introduction.....	1
1.2. Methods for the generation of singlet oxygen	4
1.2.1. Chemical methods for singlet oxygen generation	4
1.2.2. Direct optical excitation.....	5
1.2.3. Photosensitization	5
1.3. Types of Singlet oxygen Sensitizers.....	6
1.3.1. Organic dyes and aromatic hydrocarbons.....	7
1.3.2. Porphyrins, phthalocyanines, and related tetrapyrroles	8
1.3.3. Transition metal complexes	9
1.4. Detection and Quantification of singlet oxygen	10
1.4.1. Direct Methods	10
1.4.1.1. Emission spectroscopy	10
1.4.1.2. Time-resolved thermal lensing (TRTL)	11
1.4.1.3. Laser-induced optoacoustic calorimetry (LIOAC)	11
1.4.2. Indirect Methods	12
1.4.3. Chemical Actinometry	13
1.5. Reactions of singlet oxygen	16
1.5.1. Reactions with biomolecules	18
1.6. Applications of singlet oxygen	19
1.6.1. Organic Synthesis	19

1.6.2. Photodynamic therapy (PDT)	23
1.6.3. Water purification and disinfection	28
1.7. Immobilized singlet oxygen sensitizers	35
1.7.1. Polymer supported singlet oxygen sensitizers	36
1.7.2. Silica supported singlet oxygen sensitizers	36
1.7.3. Zeolite supported singlet oxygen sensitizers	37
1.7.4. Clay supported singlet oxygen sensitizers	37
1.7.5. Graphene oxide supported singlet oxygen sensitizers	38
1.8. Cationic singlet oxygen sensitizers in PDT and Photochemical disinfection	39
1.9. Triazatriangulenium salts	40
1.9.1. Applications of triazatriangulenium salts	47
1.10 The Objectives	48
1.11 References	50

Chapter 2

Synthesis, Photophysical and Singlet Oxygen Generation Studies of a Few Water Soluble Triazatriangulenium Salts..... 63-115

2.1. Abstract	63
2.2. Introduction	63
2.3. Results and Discussion	68
2.3.1. Synthesis of hydroxyl group bearing triazatrinagulenium cations (H-TATA 1-4)	68
2.3.2. Photophysical studies	69
2.3.2.1. Absorption spectra of triazatriangulenium salts	69
2.3.2.2. Fluorescence spectra of triazatriangulenium salts	71

2.3.2.3. Phosphorescence spectra of triazatriangulenium salts	74
2.3.2.4. Thermally Assisted Delayed Fluorescence (TADF) in triazatriangulenium cations	76
2.3.2.5. Laser flash photolysis	79
2.3.2 .6. Laser flash photolysis studies: Triplet quenching by oxygen	84
2.3.3. Singlet oxygen generation studies	87
2.3.3.1. Determination of singlet oxygen quantum yield of H-TATA 1-4 in acetonitrile.....	95
2.3.3.2. Determination of singlet oxygen quantum yield of H-TATA 1-4 in aqueous medium	100
2.4. Conclusions.....	106
2.5. Experimental Section.....	107
2.6. References.....	113

Chapter 3

Studies of Lipophilic Triazatriangulenium Cations in Microheterogeneous Medium	117-157
3.1. Abstract.....	117
3.2. Introduction.....	117
3.3. Results and discussion	126
3.3.1. Synthesis of lipophilic triazatriangulenium cations (TATA 1-4).....	126
3.3.2. Photophysical Studies.....	126
3.3.2.1. UV-Visible absorption properties of triazatriangulenium salts in micellar medium.....	126
3.3.2.2. Emission properties of triazatriangulenium salts in micellar medium.....	130

3.3.2.3. Fluorescence quantum yield of lipophilic triazatriangulenium cations (TATA 1-4) in SDS micelles.....	133
3.3.2.4. Fluorescence lifetime measurements of lipophilic triazatriangulenium cations (TATA 1-4) in SDS micelles.....	134
3.3.2.5. Time – resolved emission spectra of lipophilic triazatriangulenium cations (TATA) in SDS micelles	135
3.3.2.6. Time – resolved decay associated spectra and Time - Resolved Area Normalized Emission Spectra (TRANES) of lipophilic triazatriangulenium cations in SDS micelles.....	139
3.3.2.7. The binding topology and “disc to bowl” shape transformation of lipophilic triazatriangulenium cations (TATA) in SDS micelles	144
3.3.2.8. Effect of temperature on the fluorescence emission spectra of lipophilic triazatriangulenium cations (TATA) in SDS micelles.....	148
3.3.3. Theoretical Calculations	150
3.4. Conclusions.....	154
3.5. Experimental.....	155
3.6. References.....	156

Chapter 4

Synthesis, Characterization and Study of Surface-Tethered Triazatriangulenium Cations	159-200
4.1. Abstract.....	159
4.2. Introduction.....	160

4.3. Results and Discussion	165
4.3.1. Functionalization of silica surface	165
4.3.2. Synthesis of Tris-(2, 6-dimethoxyphenyl) carbenium tetrafluoroborate	166
4.3.3. Synthesis of triazatriangulenium silica composites	166
4.3.4. Characterization of triazatriangulenium silica composites	170
4.3.4.1. CHN Analysis	170
4.3.4.2. IR spectral studies	172
4.3.4.3. Scanning Electron Microscopy (SEM) studies	177
4.3.4.4. Transmission Electron Microscopy (TEM)	178
4.3.4.5. TGA Analysis	180
4.3.5. Photophysical properties	181
4.3.5.1. Absorption spectral properties	181
4.3.5.2. Emission spectral properties	182
4.3.5.3. Lifetime Measurements	183
4.3.6. Singlet oxygen generation studies	185
4.3.6.1. Comparison of singlet oxygen production of triazatriangulenium silica composites in the presence of ultrabright green LED light	188
4.3.7. Photosensitized inactivation of bacteria	189
4.4. Conclusion	194
4.5. Experimental	194
4.6. References	199

Chapter 5

Synthesis, Characterization and Study of Intercalated Triazatriangulenium Cations in Layered Materials201-238

5.1. Abstract.....	201
5.2. Introduction.....	201
5.3. Results and discussion	209
5.3.1. Characterization of the H-TATA 1 and H-TATA 4 intercalated clay samples.	209
5.3.1.1. X-ray diffraction studies	209
5.3.1.2. CHN Analysis	214
5.3.1.3. Thermogravimetric analysis	214
5.3.1.4. Scanning Electron Microscopy (SEM) studies	217
5.3.1.5. Transmission Electron Microscopy (TEM)	219
5.3.2. Photophysical properties.....	221
5.3.2.1. Absorption spectral properties	221
5.3.2.2. Emission spectral properties	222
5.3.2.3. Lifetime Measurements	224
5.3.3. Singlet oxygen generation studies	225
5.3.4. Photosensitized inactivation of bacteria	228
5.4. Conclusions.....	232
5.5. Experimental.....	233
5.6. References.....	236
Summary and Conclusions	239
List of Publications	243

CHAPTER 1

A Review on the Generation and Applications of Singlet Oxygen

1.1. Introduction

Oxygen, the most important element required for sustaining life on earth accounts for nearly half the mass of the earth crust, two-third, the mass of the human body and nine tenth, the mass of water. Oxygen identified by Carl Wilhelm Scheele and by Joseph Priestly in the late 18th century, is a colourless, odourless and tasteless gas with the molecular formula O₂ and referred to as dioxygen at standard temperature and pressure. The linear combinations of the atomic orbitals from two individual oxygen atoms result in the formation of molecular orbitals with a bond order two. The bonding in oxygen occurs in such a way that the two unpaired electrons are distributed in the highest occupied degenerate state. This uncoupled pair of electrons classified oxygen as a triplet in its ground state. The molecular orbital diagram of oxygen is given in figure 1.1. This triplet multiplicity is the reason why most of the reactions of oxygen with organic molecules do not proceed at room temperature even though they are exergonic and the key to sustaining life in an oxygen-containing atmosphere.

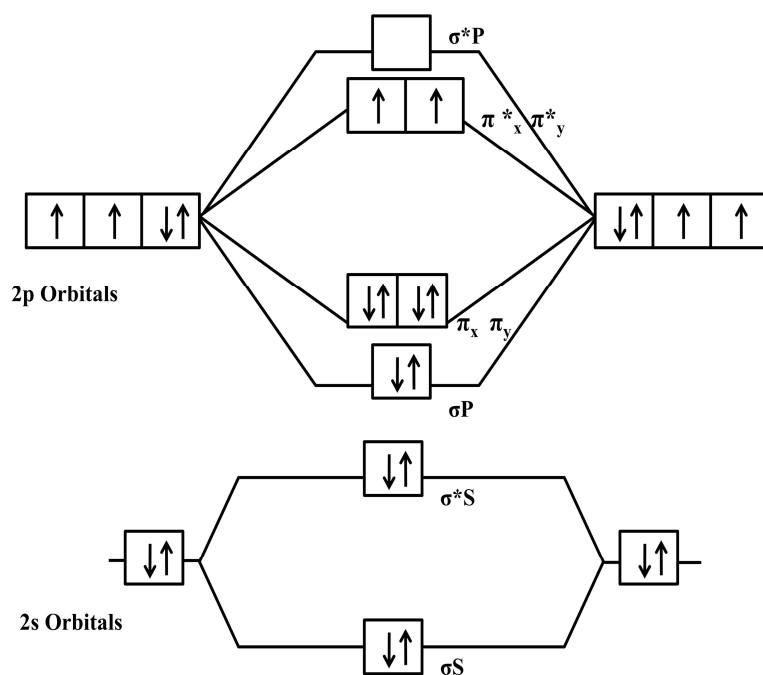


Figure 1.1 The molecular orbital diagram of oxygen in the ground state

According to Hund's rule, when two electrons are distributed in a degenerate level, the triplet state has the lower energy with molecular term symbol ${}^3\Sigma_g^-$. There are two higher energy excited states possible for the molecular oxygen and they are denoted by term symbol ${}^1\Delta_g$ and ${}^1\Sigma_g^+$, with both these excited states having singlet multiplicity. The latter is known as the sigma oxygen and the former is called singlet oxygen. The transition from the ${}^1\Delta_g$ state to the ${}^3\Sigma_g^-$ state is spin forbidden and the transition from ${}^1\Sigma_g^+$ to the ${}^1\Delta_g$ is a spin allowed transition. This reflects in their lifetime data; 45 min and 7-12 seconds being the radiative lifetimes in the gaseous phase respectively.¹ The molecular orbital diagram of the molecular oxygen in the excited state is shown in figure 1.2.

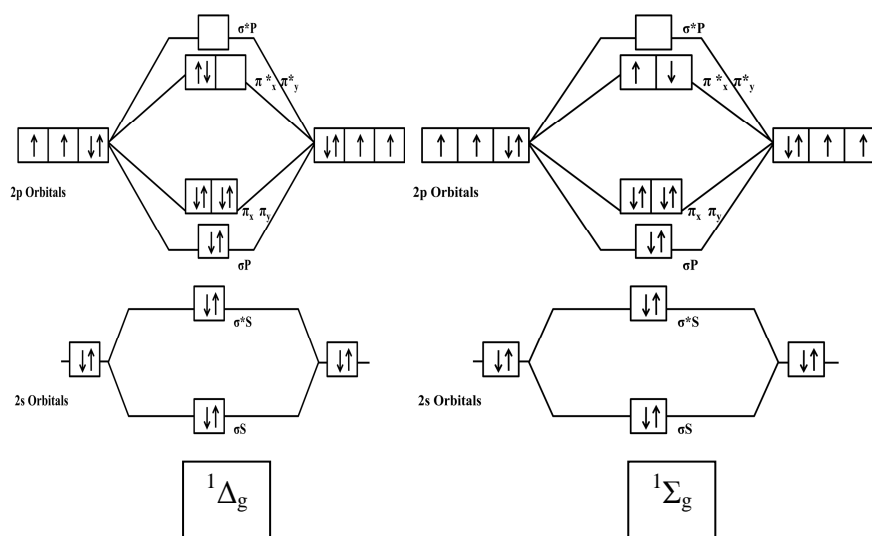


Figure 1.2 The molecular orbital diagram of oxygen in the excited state

The three electronic states, the triplet ground state and two singlet excited states of molecular oxygen differ only in the spin multiplicity and the occupancy in two degenerate antibonding π_g -orbitals. The three electronic states of molecular oxygen are represented in figure 1.3.

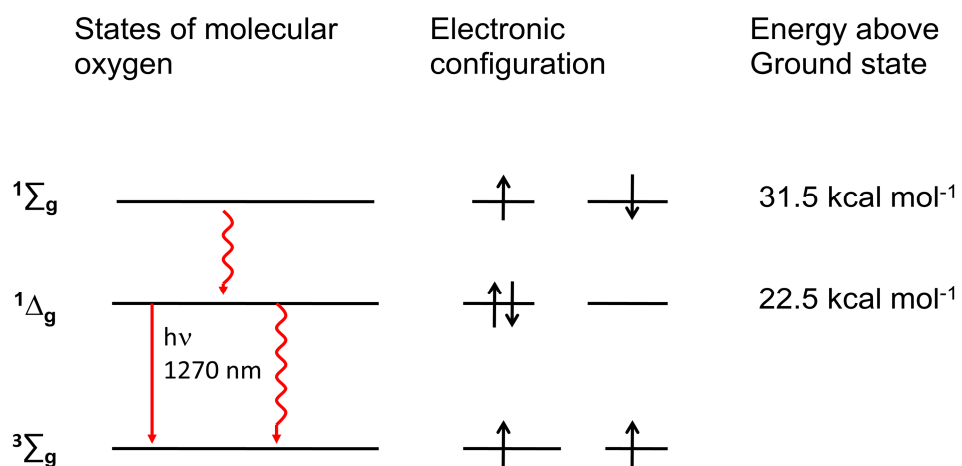


Figure 1.3 The three energy states of molecular oxygen

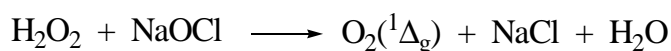
Singlet oxygen was first detected and reported by Fritzsche in 1867 in his study of transformations of naphthacene in the presence of light and

oxygen. He found out that one of the product formed, upon heating regenerated the naphthacene.² In those era, the chemical structures of both naphthacene and the product of the photochemical reaction were unknown. In 1924, Lewis predicted the unpaired electronic structure and the possibility of a spin paired electronic state for the molecular oxygen.³ Katusky in 1930 reported the presence of a metastable intermediate species in some of the photooxygenation reactions he has studied.⁴ All these experimental evidences along with Mulliken's prediction using molecular orbital theory about two low-lying oxygen excited states ($^1\Delta_g$ and $^1\Sigma_g^+$) initiated research on the chemistry of singlet oxygen.⁵ The development of novel luminescent singlet oxygen probes,⁶⁻⁹ the time-resolved detection of $O_2(^1\Delta_g)$ in a transmission microscope,¹⁰ the first time-resolved measurements of singlet oxygen luminescence *in vivo*,¹¹ are some of the recent advancements in this field of research.

1.2. Methods for the generation of singlet oxygen

1.2.1. Chemical methods for singlet oxygen generation

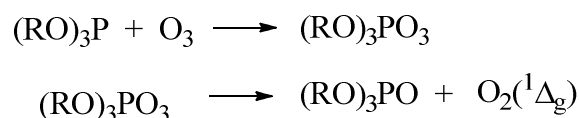
Several chemical methods of generation of singlet oxygen are known. The most common method is the aqueous phase reaction of hydrogen peroxide with sodium hypochlorite.¹²



The thermal decomposition of triethylsilyl hydrotrioxide generated *in situ* by the reaction of triethylsilane with ozone can act as a source of singlet oxygen.¹³



Similarly phosphite ozonides are also a source of singlet oxygen.¹⁴



Nardello et al., reported a Lanthanum (III) catalysed disproportionation reaction that involves the decomposition of hydrogen peroxide into singlet molecular oxygen.¹⁵ The method has the advantage that this source can generate the singlet oxygen in basic, neutral and even slightly acidic condition.

1.2.2. Direct optical excitation

The transitions between the ground state and two singlet excited states ($^1\Delta_g$ and $^1\Sigma_g$) of molecular oxygen are spin forbidden. However, in the condensed phase interactions of oxygen molecule with other atoms or molecules in its vicinity can cause changes in molecular symmetry and can lead to the breakdown of the selection rules. In such a scenario, the direct optical excitation can lead to formation of excited molecular oxygen in very low yields.¹⁶ The most adequate light sources for direct optical excitation of $^3\text{O}_2$ are lasers. Some are: Nd: YAG and Nd-based,¹⁷⁻¹⁹ Yb-based,²⁰ He-Ne,²¹⁻²³, semiconductor (diode),²⁴⁻²⁶ Raman-shifted,^{27,28} and dye-based,^{29,30} lasers.

1.2.3. Photosensitization

Photosensitized generation is simple and controllable method for the production of $^1\text{O}_2$; requiring only oxygen, light of an appropriate wavelength, and a photosensitizer capable of absorbing and using that energy to excite molecular oxygen to its excited state. The photosensitization of singlet oxygen is illustrated in the following Jablonski diagram (figure 1.4).

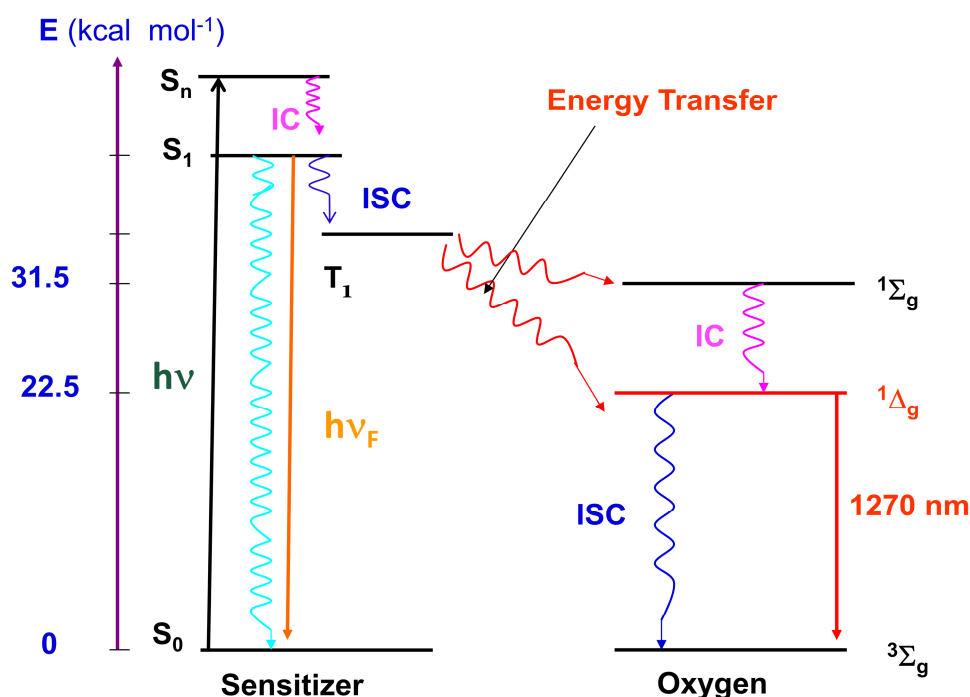


Figure 1.4 The photosensitized production of singlet oxygen (solid line indicate radiative transitions and courly lines non-radiative transitions, IC: internal conversion, ISC: intersystem crossing)

1.3. Types of Singlet oxygen Sensitizers

A number of molecules have been identified as good singlet oxygen sensitizers. A good singlet oxygen sensitizer should have the following qualities. (1) High molar absorption coefficient in the spectral region of the light used for the excitation, (2) the excited state energy should be greater than $22.5 \text{ kcal mol}^{-1}$ so that energy transfer should be exergonic, (3) it should have high triplet quantum yield and have long triplet lifetime, (4) it should be thermally and photochemically stable, (5) it should not react with the singlet oxygen as well as the other components in the medium where it is used.³¹ Based on the molecular structure, the sensitizers are grouped as dyes, aromatic molecules, porphyrins and transition metal complexes.

1.3.1. Organic dyes and aromatic hydrocarbons

Among dye based sensitizer systems, most commonly used are methylene blue, rose bengal, eosin blue, fluorescein, erythrocin B etc. Rose bengal is a common sensitizer that can be used in water. It is a xanthene dye with intense absorption at 549 nm in water. The peculiar properties of rose bengal are large molar absorption coefficient (ϵ), high solubility and high quantum yield of singlet oxygen generation (0.76). It is soluble in water up to a concentration of 10^{-3} M but at higher concentration H-type aggregates are formed with lower molar absorptivity.³²⁻³⁵ In non-polar solvents rose bengal is photochemically not stable compared to that in polar protic solvents.

Methylene blue is another water soluble dye, belonging to the phenothiazinium class that has been used for singlet oxygen and related photooxygenation studies. It also forms aggregates at higher concentrations which limits its applications.³⁶ Methylene blue exhibits a moderate triplet quantum yield of 0.52 in water but not an exclusive singlet oxygen generator as it also produces superoxide radical ions.^{36,37} Another example is the family of Rhodamine dyes. But, high fluorescence quantum yield and low triplet quantum yield limits its utility.³⁸

The singlet oxygen production capacity of various aromatic hydrocarbons has also been reported. Naphthalenes, anthracenes, and biphenyls are studied in this regard. In these cases there occur a competition between charge transfer interaction with the energy transfer pathway.³¹ Many aromatic hydrocarbons reacts with singlet oxygen and thus not considered as good for photosensitization. Dicyanoanthracene is a special case, where, both the singlet and triplet state of the molecule produces the singlet oxygen. The singlet oxygen production occurs by the energy transfer from the singlet state of the molecule to the triplet oxygen with or without the production of triplet

state of the molecule. An alternative path is the normal intersystem crossing from singlet state to the triplet followed by the energy transfer to the triplet oxygen. The singlet oxygen quantum yield of the molecule is 2.0 in acetonitrile and 1.56 in benzene.³⁹

The aromatic ketone, phenalenone is used as a universal singlet oxygen reference sensitizer. It is soluble in a large number of solvents and has high singlet oxygen quantum yield which is close to unity.⁴⁰ In protic solvents, the triplet state of the molecule competes with the hydrogen atom abstraction from the solvents. Because of this, under continuous irradiation in polar protic solvents it is not a sensitizer of choice.

1.3.2. Porphyrins, phthalocyanines, and related tetrapyrroles

Porphyrins, phthalocyanines, and related tetrapyrroles are groups of singlet oxygen sensitizers which are well studied with respect to their role in oxidative damages to living cells as many molecules of this class are naturally occurring. They are known to produce singlet oxygen and have been used as a singlet oxygen sensitizer in a variety of medium and application domains. The strong absorption in the visible region, low dark toxicity, high triplet quantum yield are the main advantages of the porphyrin based systems. Though their long wavelength absorption bands have smaller values of ϵ , they are sensitizers of choice under physiological conditions. These long wavelength absorption (> 600 nm) is well above the light absorption limit or filter effect by living tissues.³¹ Haematoporphyrin, tetraphenylporphyrin, phthalocyanine are the most commonly studied sensitizers of this class.⁴¹

In phthalocyanines, the presence of peripheral benzene gives extended absorption than porphyrins. Metallophthalocyanines containing diamagnetic metal ions such as Zn^{2+} or Al^{3+} have relatively good lifetime and

triplet quantum yield. Zn (II) phthalocyanine tetrasulfonate, has a long triplet lifetime, 245 μ s, and a moderate triplet quantum yield of 0.56.⁴² Naphthalocyanines are another group of macrocycles having longer wavelength absorption compared to phthalocyanines.⁴²

1.3.3. Transition metal complexes

Transition metal complexes of Ruthenium (II), are the most studied group because of the straight forward synthesis, stability of the complexes with polypyridyl type ligand and excellent light absorption properties.⁴³ They have relatively strong absorption in the uv-vis regions of the spectrum. Many Ru(II) diimine complexes can photosensitize formation of singlet oxygen. Tris(bipyridine)ruthenium(II) chloride, is the well known sensitizer among this class of molecules with a singlet oxygen quantum yield of 0.86.⁴⁴ Pefkianakis et al., in 2013 synthesized and studied a series of Ru(II) based photosensitizers as singlet oxygen sensitizers.⁴³ The ligand used to coordinate ruthenium was a pyridine–quinoline hybrid bearing an anthracene moiety and it was combined with 2,2'-bipyridine (bpy) for the preparation of heteroleptic complexes. The singlet oxygen production in these complexes was studied by monitoring the photobleaching of 1,3-diphenylisobenzofuran at 410 nm. The complexes shows the singlet oxygen quantum yield higher than those in the parent $[\text{Ru}(\text{bpy})_3]^{2+}$ complex.

The singlet oxygen production from the mixed ligand complexes of Pt(II) and Pd(II) with halides and pseudohalides were also reported. Anbalagan et al., synthesized eight new complexes of the formula $[\text{M}(\text{X-X})(\text{DPA})]$ where M is Pd(II) or Pt(II), DPA is 2,2'-dipyridylamine and X-X are various dianions of catechol and its derivatives.⁴⁵ The synthesized new complexes sensitize the oxidation of 2,2,6,6-tetramethyl-4-piperidinol in DMF to the corresponding nitroxide radical.

1.4. Detection and Quantification of singlet oxygen

To understand the role of singlet oxygen in various systems, analytical tools are required to detect the presence and quantify the amount of singlet oxygen produced. Since it is a highly reactive species the identification and quantification is a difficult task. There are various methods used in the literature for the detection and measurements. It involves the direct methods and indirect methods. Direct method involves the detection of the weak phosphorescence emission from the singlet excited state to the triplet ground state appearing at 1270 nm. Indirect methods make use of spectrophotometric, fluorescent or chemiluminescent probes for the measurement of singlet oxygen. Chemical actinometry is the commonly used method for the singlet oxygen quantification.

1.4.1. Direct Methods

1.4.1.1. Emission spectroscopy

The characteristic phosphorescence emission of singlet oxygen observed at 1270 nm was frequently used for its detection and characterization.⁴⁶ It is a forbidden transition and is weak. Another way is to monitor its dimol emission (the simultaneous emission from two singlet oxygen molecules upon collision) which is observed as a red glow at 603 nm and 730 nm. This is possible only when there is a high concentration of singlet oxygen present in the medium. To understand the kinetics of singlet oxygen production, time-resolved experiments are used. Molnar et al., studied the singlet oxygen generation of haematoporphyrin derivatives and protoporphyrin derivatives in liposomes using this technique.⁴⁷ Since the emission at 1270 nm is a weak emission, a cryogenically cooled germanium-diode detector is used. This is necessary to minimise the background signal due to thermal effects. The sensitivity of this detector is poor and this limits

the application of this detector.⁴⁶ The low signal to noise ratio observed in the detection at NIR region is another limitation of the process. The methods have the advantages such as the signal obtained is distinct and not mistaken even with solvent change. The luminescence from other species usually occurs at wavelength lower than 1000 nm. Recently NIR sensitive photomultiplier tubes were used with very good time resolution so as to be used in a time-resolved emission spectroscopy mode in addition to the steady – state emission measurements. Such sensitive detectors have also been used in imaging techniques where singlet oxygen is used as a luminescent probe.⁴⁸

1.4.1.2. Time-resolved thermal lensing (TRTL)

In this method the heat released through the nonradiative processes of the excited state molecule is detected and analysed.⁴⁹ It involves the calorimetric determination of the minute temperature gradient induced by the relaxation of the excited species.⁵⁰ The enthalpy changes associated with a photophysical or photochemical reaction can be measured using this technique. This method has the advantage that the absolute yield of the transient species can be understood from the experiment without the help of a standard reference compound. The photophysical parameters can also be extracted directly. The relaxation dynamics of singlet oxygen in water can be studied using this technique. Cheng et al., studied the lifetime, absolute quantum yield and the singlet oxygen generation efficiency of 1H-phenalen-1-one in various solvents.⁵¹

1.4.1.3. Laser-induced optoacoustic calorimetry (LIOAC)

The absolute quantum yield of singlet oxygen can be determined with the laser-induced optoacoustic calorimetry (LIOAC) method.⁵² In this method the pressure wave formed by the expansion of solvent due to release

of heat during a non-radiative process is measured by a piezo-electric transducer. In its measurement a comparison of the optoacoustic wave signals generated by the sample and a photocalorimetric reference is made. If they are of identical shape, absolute value of quantum yield of singlet oxygen generation can be obtained from the optoacoustic wave maximum. Oliveros et al., determined the absolute quantum yield of singlet oxygen production by phenalenone using this technique.⁵³ In 1, 4-dioxane and in N,N'-dimethylacetamide they have reported singlet oxygen quantum yields as 0.99 and 0.87 respectively. The experiment confirms the applicability of phenalenone as an efficient singlet oxygen sensitizer.

1.4.2. Indirect Methods

Indirect method for detection and analysis of singlet oxygen involves a specific chemical reaction of singlet oxygen to form a product. The progress of the reaction is monitored by a spectroscopic or chromatographic technique to extract kinetic information. In methods that use spectrophotometry or fluorescence spectroscopy the product of the oxygenation reaction and other component/s should not have any overlapping absorption or emission. If the reaction system used meet this condition, then a sensitive and convenient method for the detection of singlet oxygen is possible. The common trap molecules are dienes capable of efficient [4+2] cycloaddition with singlet oxygen to produce an endoperoxide. For a molecule to act as a probe there are certain requirements. (1)It should react with singlet oxygen in a 1:1 stoichiometry without any side reactions, (2) the product formed should not have overlapping absorption /emission with other components of the reaction which produce singlet oxygen, (3)The product formed should neither react with the probe nor with the singlet oxygen.⁵⁴ The commonly used chemical probes are, 9,10-dimethylanthracene, 2,5-dimethylfuran, anthracene-9,10-diyl-diethyl disulfate, bis-9,10-anthracene-(4-

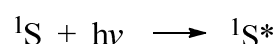
trimethyl-phenylammonium)dichloride (BPAA), anthracene-9,10-divinylsulfonate (AVS), anthracene-9,10-bisethanesulfonic acid (AES), anthracene-9,10-dipropionic acid (ADPA), and 1,3-diphenylisobenzofuran (DPBF). In organic solvents DPBF is the commonly used probe. It has the largest rate constant for the reaction with singlet oxygen.⁵⁵ 2, 5-dimethylfuran is only soluble in lipid matrices and ADPA is widely used in aqueous medium.

1.4.3. Chemical Actinometry

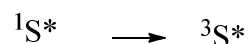
Quantum yield determination is very important in photosensitized singlet oxygen production. For the quantum yield determination the incident photon rate should be known. Actinometry is the method for the determination of the incident photon rate for a system of specific geometry and in a well-defined spectral domain. Chemical actinometry is based on the behaviour of a reference substance (chemical actinometer) for which the quantum yield is known. Theoretically any substance which by irradiation undergoes a photochemical transformation and whose quantum yield Φ is known can be used as a chemical actinometer. The requirements of a chemical actinometer are well defined. A chemical actinometer should satisfy the following requirements. (1) The photoreaction considered should be reproducible, controllable and the quantum yield should be accurately known for a large number of wavelengths of irradiation. (2) The chemical components should be thermally stable, (3) The analytical methods adopted should be simple and the direct spectrophotometric analysis is preferred, (4) The system should display large sensitivity towards light, (5) The actinometric molecules should be easily available and should have the highest possible purity.⁵⁶

Chemical actinometry can be used for the quantification of singlet oxygen. An ideal actinometer for singlet oxygen quantification should have the following qualities: (1) The absorption spectra of actinometer and sensitizer must not overlap, (2) No ground state or excited state interactions between actinometer and substrate should exist, (3) The reaction between the actinometer and $O_2(^1\Delta_g)$ must be the only reaction path and role of physical quenching must be negligible, (4) The presence of actinometer does not change the quantum yield of singlet oxygen generation.⁵⁷ The different kinetic phenomena that occur in the case of a photosensitizer in the presence of oxygen and the actinometer are given below.

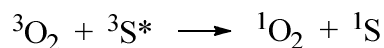
(1) Light absorption by the sensitizer:



(2) Intersystem crossing:



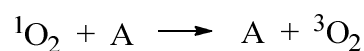
(3) Energy transfer:



(4) Singlet oxygen deactivation by the solvent (rate constant k_d):



(5) Physical quenching of 1O_2 by actinometer (rate constant k_p):



(6) Actinometer oxidation by 1O_2 (rate constant k_R):



Upon continuous stationary irradiation with light of intensity I_{abs} , $[^1O_2]$ is constant and the differential equations describing the changes in concentrations of actinometer and singlet oxygen kinetics are:

$$\begin{aligned}
\frac{d[{}^1\text{O}_2]}{dt} &= \Phi^{\text{S}}I_{\text{abs}} - k_{\text{R}}[A][{}^1\text{O}_2] - K_{\text{P}}[A][{}^1\text{O}_2] - k_{\text{d}}[{}^1\text{O}_2] \\
&= \Phi^{\text{S}}I_{\text{abs}} - (k_{\text{R}} + k_{\text{p}})[A][{}^1\text{O}_2] - k_{\text{d}}[{}^1\text{O}_2] = 0 \\
\implies [{}^1\text{O}_2] &= \frac{\Phi^{\text{S}}I_{\text{abs}}}{(k_{\text{R}}+k_{\text{p}})[A]+k_{\text{d}}} \\
\frac{d[A]}{dt} &= -k_{\text{R}}[A][{}^1\text{O}_2] \\
&= -k_{\text{R}}[A] \frac{\Phi^{\text{S}}I_{\text{abs}}}{(k_{\text{R}}+k_{\text{p}})[A]+k_{\text{d}}}
\end{aligned}$$

Under conditions when $(k_{\text{R}} + k_{\text{p}})[A] \ll k_{\text{d}}$, the change in actinometer concentration is simply expressed as

$$\begin{aligned}
\frac{d[A]}{dt} &= -k_{\text{R}}[A] \frac{\Phi^{\text{S}}I_{\text{abs}}}{k_{\text{d}}} = -k_{\text{s}}[A], \text{ where } k_{\text{s}} = k_{\text{R}}[A] \frac{\Phi^{\text{S}}I_{\text{abs}}}{k_{\text{d}}} \\
\implies \ln[A] &= \ln[A]_0 - k_{\text{s}}t
\end{aligned}$$

ie., the kinetics of the actinometer bleaching can become first order and this can be employed in the estimation of apparent quantum yield of singlet oxygen generation (Φ_{sen}). The singlet oxygen quantum yield of a particular sensitizer is determined by relative actinometry in the presence of a chemical actinometer and compared with a reference sensitizer of known singlet oxygen quantum yield under identical conditions of irradiation. Kinetic profiles for the actinometer consumption are obtained for the sample and reference. Slopes of the kinetic profiles for the sensitizer and the reference were determined by linear regression and singlet oxygen quantum yield of the sensitizer is determined by comparing the slopes for the sensitizer and the reference. Using the absolute value of Φ_{Δ} reported for the reference compound the quantum yield of singlet oxygen generation of the sensitizer can be calculated by the equation **1.1**. This method of estimation of

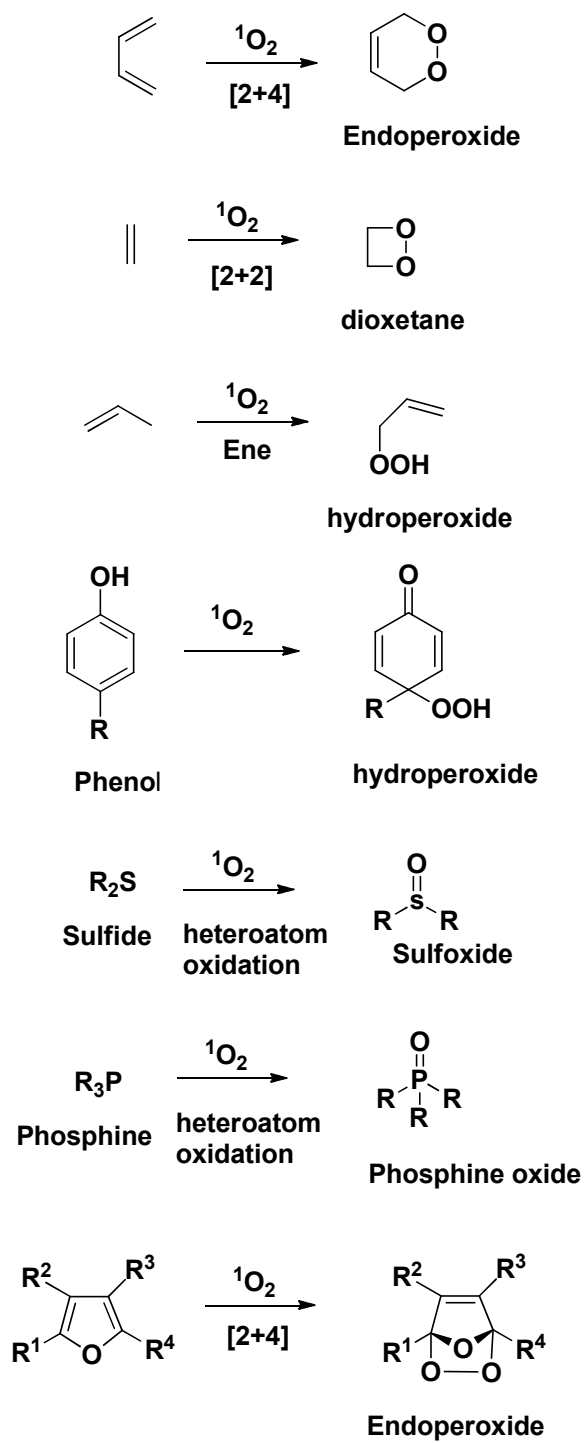
Φ_{sen} is valid only when the solvent induced deactivation is much faster than the scavenging or deactivation of singlet oxygen by the actinometer. If Φ_{R} , the quantum yield of the reference is known, Φ_{sen} is determined using the equation **1.1**.

$$\Phi_{\text{sen}} = \Phi_{\text{R}} \frac{I_{\text{R}} k_{\text{sen}}}{I_{\text{sen}} k_{\text{R}}} \quad (1.1)$$

Where k_{sen} and k_{R} are the first order rate constants of the actinometer disappearance induced by sensitizer and the reference compound respectively. I_{sen} and I_{R} are the total intensities absorbed by the sensitizer and the reference respectively.

1.5. Reactions of singlet oxygen

Even though singlet oxygen is a highly reactive species it is a reagent for oxidation/oxygenation in synthetic organic chemistry. The major chemical reactions of singlet oxygen are: [2+2] and [4+2] cycloaddition, ene reaction, and heteroatom oxidations (Scheme **1.1**)



Scheme 1.1

The [4+2] cycloaddition leads to formation of endoperoxides. These endoperoxides are versatile intermediates that can be transformed via a variety of synthetic procedures to specifically oxygenated products.^{58,59} The [2+2] cycloaddition is observed with electron rich alkenes especially those which do not have or geometrically inaccessible, allylic hydrogens. The dioxetane products are often sensitive molecules that thermally decompose in a fascinating chemiluminescent process to carbonyl compounds.⁶⁰ The ene reaction generates allylic hydroperoxides which can be converted to synthetically valuable allylic alcohols.⁶¹

1.5.1. Reactions with biomolecules

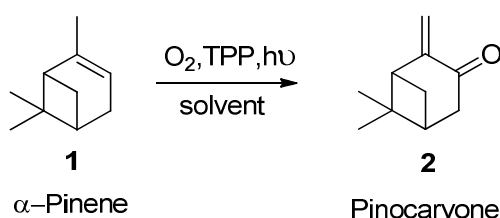
Because of this versatile reactivity of singlet oxygen with alkenes, aromatics and heterocycles, it do react with the biomolecules such as lipids, proteins, nucleic acids, etc. If singlet oxygen is generated within the cell, it can interact with the biomolecules and cause damage. Lipids are susceptible to oxidative damage due to reaction of lipids with reactive oxygen species (ROS) (lipid peroxidation). These lipid peroxidation with singlet oxygen is implicated in haemolysis of erythrocytes, damage to cardiomyocytes and degeneration of cellular membranes. Since lipid peroxides are polar they disrupt structure and functions of cell membranes. There are evidences for the involvement of singlet oxygen *in vivo* in the etiology of certain diseases.⁶² Also other toxic products of lipid peroxidation attack DNA.⁶³ Oxidation of amino acids having sulfur or heterocyclic groups by singlet oxygen produce sulphoxides and endoperoxides which lead to formation of other ROS's, which are toxic to cells. Among amino acids, histidin, tryptophan, methionine, and tyrosine are more reactive towards singlet oxygen. Oxidation of crystallins, the proteins of the eye, by singlet oxygen produces high molecular weight cross links leading to cataract.⁶⁴ DNA reacts with singlet oxygen causes strand breakes and formation of altered bases.

Bases like guanosins, which is the most susceptible base undergoes cycloaddition mechanism has high reactivity with single stranded DNA. This change of guanosine has serious biological effects. For example, termination of DNA replication occurring at the position of modified guanine results in misleading by DNA polymerase which results in mutagenesis and carcinogenesis.⁶³

1.6. Applications of singlet oxygen

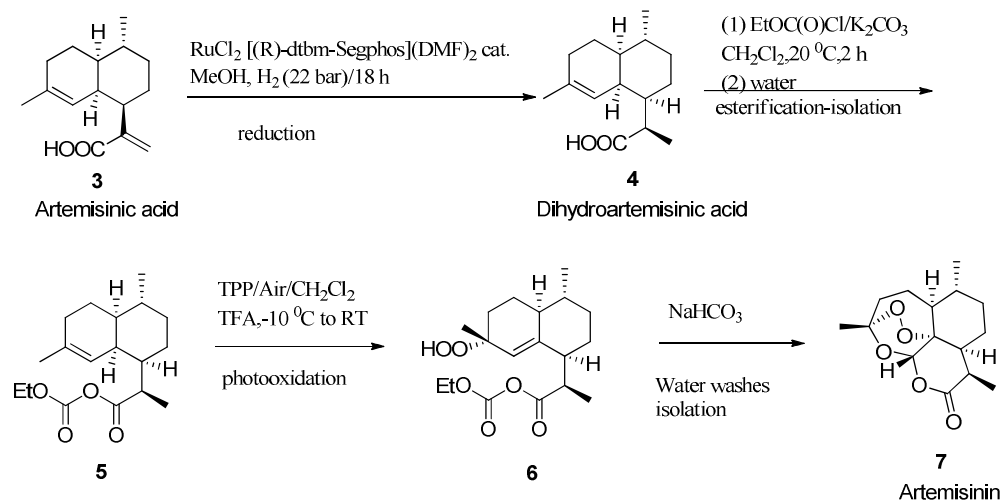
1.6.1. Organic Synthesis

The versatility and the high degree of stereo selectivity make singlet oxygen as powerful reagent in synthetic organic chemistry. Pinocarvone (2) is an important compound as it can be used as a building block for antimalarial peroxides and chiral ligands for catalysis. It can be synthesized by the singlet oxygen mediated photooxygenation of α -pinene (1).⁶⁵ (Scheme 1.2)



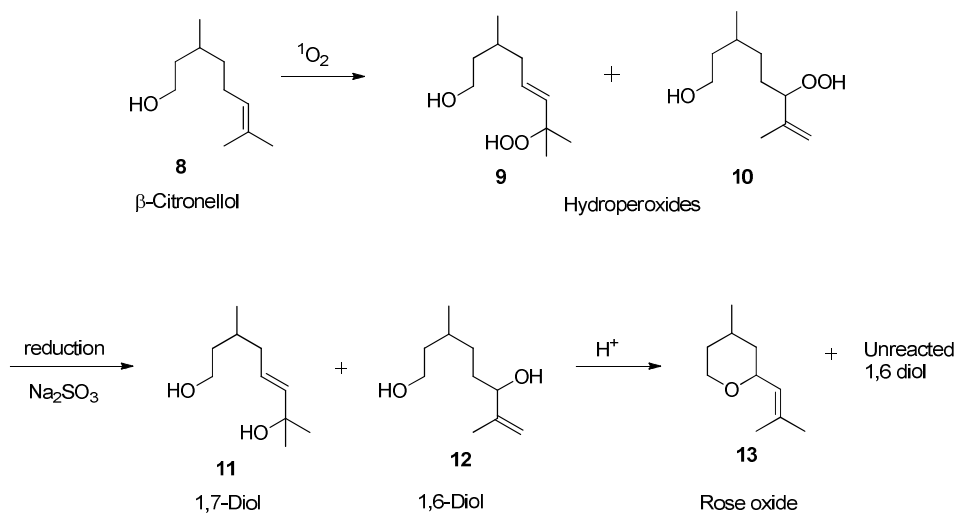
Scheme 1.2

Artemisinin (7) and its semi-synthetic derivatives are the drugs used against *Plasmodium falciparum* malaria.⁶⁶ Its synthesis involves a continuous flow conversion of dihydroartemisinic acid (4) into artemisinin (7) by a three-step reaction sequence. It consists of singlet oxygen mediated photooxidation, acid-catalyzed Hock cleavage and oxidation with 3O_2 . (Scheme 1.3).



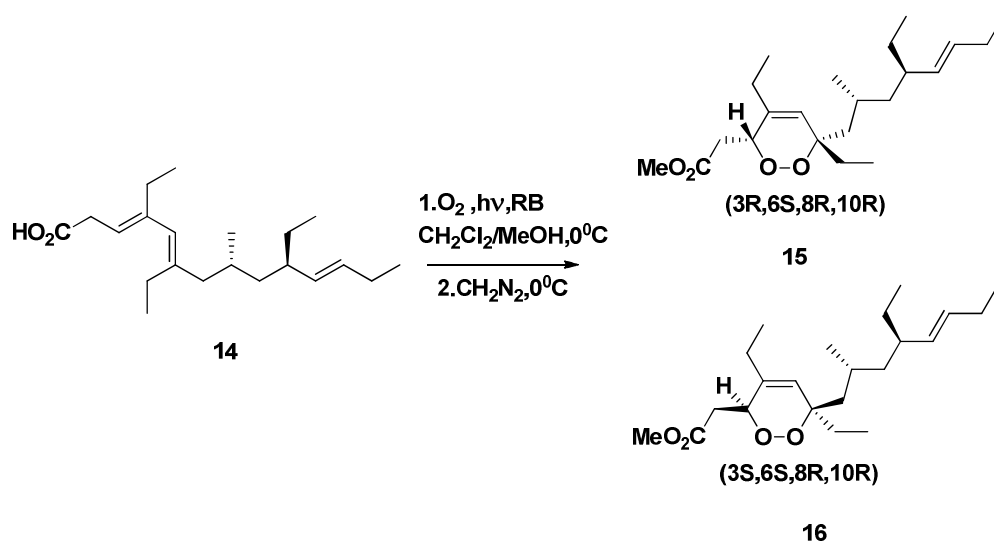
Scheme 1.3

The synthesis of rose oxide (13), an important fragrance chemical involves the photooxidation of β -citronellol (8) in methanol.⁶⁷ The mixture of secondary and tertiary hydroperoxides thus obtained on reduction with bisulfite, yields the corresponding alcohols. Acid-catalyzed ring closure of the main tertiary product (1, 7-diol) leads to a mixture of the stereoisomeric rose oxide (13). (Scheme 1.4).



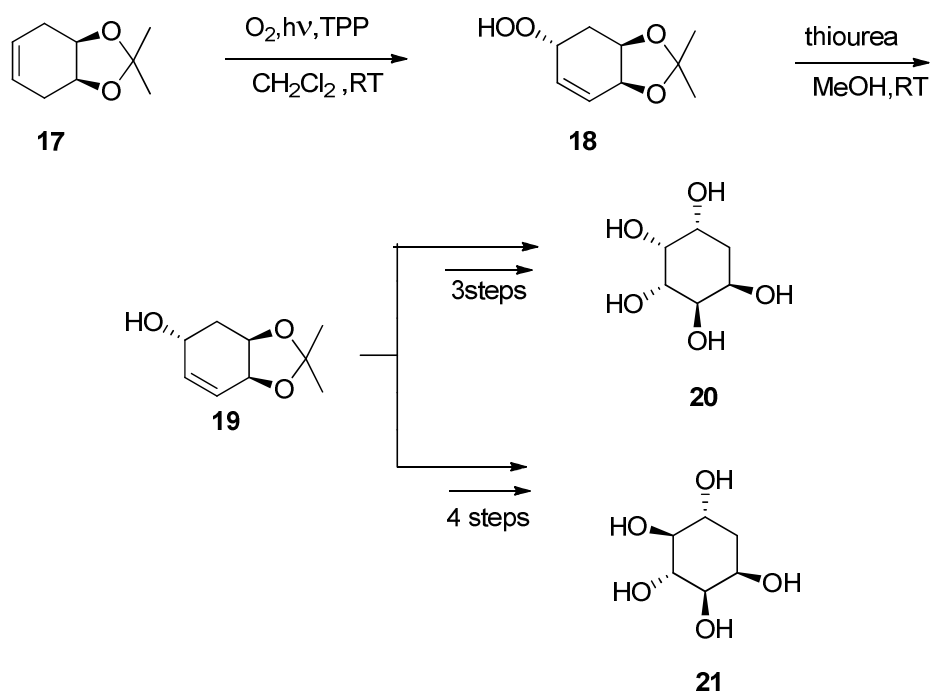
Scheme 1.4

Yao et al., in 2002 used the [4+2] cycloaddition of singlet oxygen to a triene to construct the 3, 6-dihydro-1,2-dioxin ring in his 18 step synthesis of the bioactive natural products **15** and **16** (Scheme 1.5).⁶⁸ The product was a mixture of diastereomeric endoperoxides formed by the photooxidation followed by the reaction with diazomethane. The carboxylic acid derivatives of the endoperoxide have cytotoxic and antifungal activity.



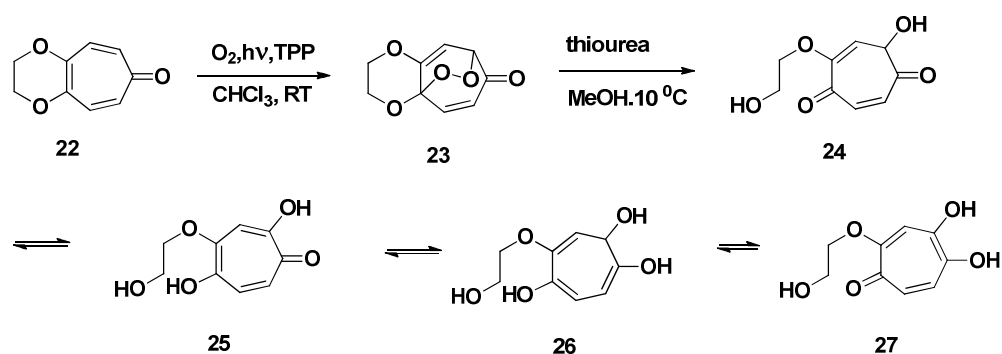
Scheme 1.5

Maras et al., reported the use of ene reaction of singlet oxygen for the synthesis of DL-*vibo*-quercitol (**20**) and DL-*talo*-quercitol (**21**).⁶⁹ In the TPP sensitized photooxidation of dioxolane (**17**) to DL-*vibo*-quercitol (**20**) and DL-*talo*-quercitol (**21**), the hydroperoxide product of the ene reaction (**18**) on reduction with thiourea to form an alcohol (**19**) with the desired stereochemistry (Scheme 1.6).



Scheme 1.6

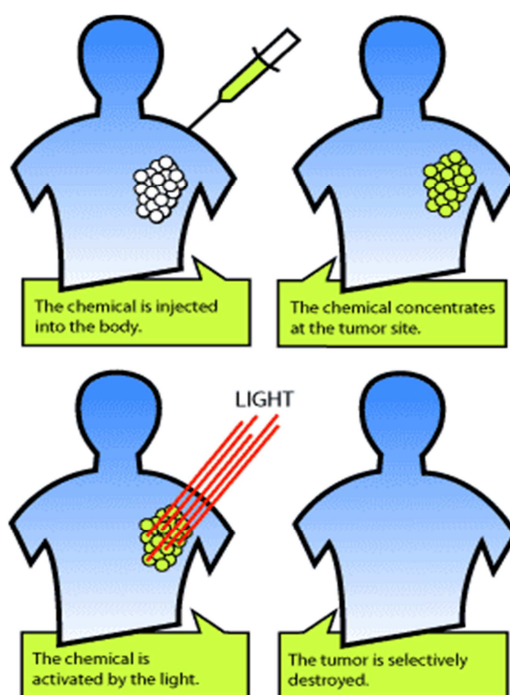
Tropones and tropolones are examples for highly oxygenated natural products widely seen in nature. The TPP sensitized synthesis of tropolone compound was (27) reported by Dastan et al.⁷⁰ Here the tricyclic endoperoxide was formed (23) in about 94% yield was reduced to the enol (24) by thiourea (Scheme 1.7).



Scheme 1.7

1.6.2. Photodynamic therapy (PDT)

Cancer is a group of diseases that account for 16.6 % of the death among world population. It involves abnormal cell growth often detected by the formation of a tumour, and invade or spread to other parts of the body. The preliminary step in the cancer treatment is the killing of malignant cells in order to prevent the spread of cancer. The important cancer treatment modes are surgery, radiation therapy and chemotherapy. Photodynamic therapy is used to treat some cancers and precancerous conditions such as skin, head, neck, mouth, lung and gullet cancers. This treatment modality involves the combination of light, a light sensitive drug (photosensitizer) and oxygen leading to the production of singlet oxygen capable of inactivating the malignant cells. The mechanism of photodynamic therapy is represented in the following Scheme 1.8.



Scheme 1.8 The mechanism of Photodynamic therapy

The advantageous feature of photodynamic therapy lies in the localization of the sensitizer drug in the tumour and the ability to control the activation of the photosensitizer drug by illumination only in the tumour region. This selected area activation keeps a normal tissue unaffected during the treatment, which is a major goal in the cancer treatment. There are three major steps involved in the photodynamic therapy. Initially the drug i.e., the photosensitizer is administered orally, topically or intravenously. Then the drug equilibrates for a limited period of time in order to get maximum tumour/normal tissue differentiation. Using a light of suitable wavelength the tumour is then irradiated. Finally the lethal agents generated from the excited photosensitizer destructs the tumour without affecting the normal tissue.

A compound used as a sensitizer for photodynamic therapy should satisfy certain conditions. The compound should have minimal dark toxicity. The compound should selectively accumulate in the tumour. Amphiphilic compounds are preferable photosensitizers in photodynamic therapy. A water-soluble compound containing a hydrophobic matrix is a suitable candidate for photodynamic therapy because this feature facilitates in crossing the cell membranes. For easy and fast removal after the treatment the compound used as photosensitizer should have minimum in vivo stability. The absorption in the visible region with high molar extinction coefficient is a favourable criterion to act an efficient sensitizer.³¹ The absorption band of the sensitizer should not overlap the absorption bands of other chromophores present in the tissues. The compounds should be stable and stable in body's tissue fluids.

Haematoporphyrin derivatives are the first generation photosensitizers used for PDT. They exist as mixtures consisting of monomers, dimers and oligomers. In the case of photofrin the intensity of light absorption at maximum wavelength is low as a result the tissue penetration length is only

2-3 nm. The long term phototoxicity is another drawback of this drug. It is an approved drug for head, neck, skin, breast and cervical cancer. Porphyrins are the second generation photosensitizers, *meta*-tetra(hydroxyphenyl) porphyrin was 25 to 30 times as potent as haematoporphyrin derivatives in tumour photonecrosis when irradiated at 648 nm.³¹ 1,5-aminolevulinic acid is an approved drug for non-oncological PDT treatment of actinic keratosis. Chlorins are another class of molecules belongs to the second generation photosensitizers. Chlorins differ from the porphyrins by the presence of two extra hydrogen atoms in one pyrrole ring. As a result, a bathochromic shift in the absorption from 640 nm to 700 nm was observed.⁷¹ Benzoporphyrin derivative monoacid ring A(BPD-MA), *meta*-tetra(hydroxyphenyl) chlorine (*m*-THPC) are examples for molecules belongs to this class. BPD-MA has the advantage that it requires a lower time interval of skin phototoxicity than Photofrin.⁷² Pthalocyanine metal complexes are used to treat stomach, lip, skin and breast cancer.⁷³ Long term skin phototoxicity is the limitation of this class of molecules. Non porphyrin photosensitizers are also involved in the PDT. Hypericin is a naturally occurring anthraquinone derivative, known to produce the reactive oxygen species. It is used to treat squamous cell carcinoma and basal cell but the results are unsatisfactory and needs more optimization studies.⁷⁴ Methylene blue which belong to the phenothiazinium family shows positive PDT action against melanoma cell cultures.⁷⁵ Rose bengal, the water soluble xanthene dye is an experimental agent for PDT treatment of breast carcinoma and metastatic melanoma.⁷⁶ Merocyanine 540, a cyanine based dye targets leukemia and lymphoma cells.⁷⁷ Third generation photosensitizers uses tumour targeting moieties which have the advantage of direct delivery of the PDT agent to the tumour tissue. This is achieved through the conjugation of the photosensitizer to the biomolecules such as monoclonal antibodies (mAB).The tumour cells have cell surface antigen

that is different from normal cells. The mAB attached to the photosensitizer specifically bind to the tumour tissue and cause destruction of tumour tissue specifically. Avidin-biotin system can be used for the delivery of the photosensitizer specifically to the tumour tissue.⁷⁸

Dos.Santos et al., in 2017 reported that methylene blue (MB) photodynamic therapy induces selective and massive cell death in human breast cancer cells.⁷⁹ Even in the middle of the technological advances, breast cancer is a serious health problem for women. The poor efficiency in killing the cancer cells in the primary treatment is the reason for the failure of complete eradication of the disease. In this study they selected the breast epithelial cell lines MCF-7, an ER, PR and HER-2-positive, luminal A cell line; MDAMB-231, a TNBC cell line; and MCF-10A, a normal-like cell line. The cell lines are irradiated with 20 μ M MB for 24 hrs. The treatment shows considerable effect on malignant cells. The highest cell death was reported (98 %) in the TNBC cell line followed by MCF-7 cell line (93 %). Even the low concentration of MB cause massive cell death, but at the same time the normal cells were less sensitive to MB-PDT. The preferential lysosomal localization of MB was reported instead of mitochondrion or the nucleus. The authors argue that apoptosis may not be the predominant process that mediates cell death induced by PDT. They propose regulated necrosis pathways (i.e. necroptosis) as more relevant mechanisms involved in MB-PDT induced cell death. The authors conclude that MB-PDT could be an effective alternative to surgery for the breast cancer.

Hill et al., reported a series of selenorhodamines useful in a combination therapy to treat Colo-26 cells in vitro.⁸⁰ The chart 1.1 shows the structure of the synthesized rhodamines. Since rhodamines are delocalized lipophilic cations, they are concentrated in the mitochondria of the cancer cells. The preferential uptake of the rhodamines may be taking place because

of the electrostatic interaction of the positively charged rhodamine dye and the mitochondria of the cancer cells. The cancer cells have an altered mechanism of increased mitochondrial membrane potential.⁸¹ The selenorhodamine obtained by the incorporation of selenium atom in the xanthylium core of the rhodamines shows $\lambda_{\text{max}} > 600 \text{ nm}$ and the singlet oxygen quantum yield of the dyes was reported as 0.44. These are favourable for a photosensitizer used in PDT. Among the synthesized molecules thioamide derivatives are effective photosensitizers and have the potential to be used in PDT.

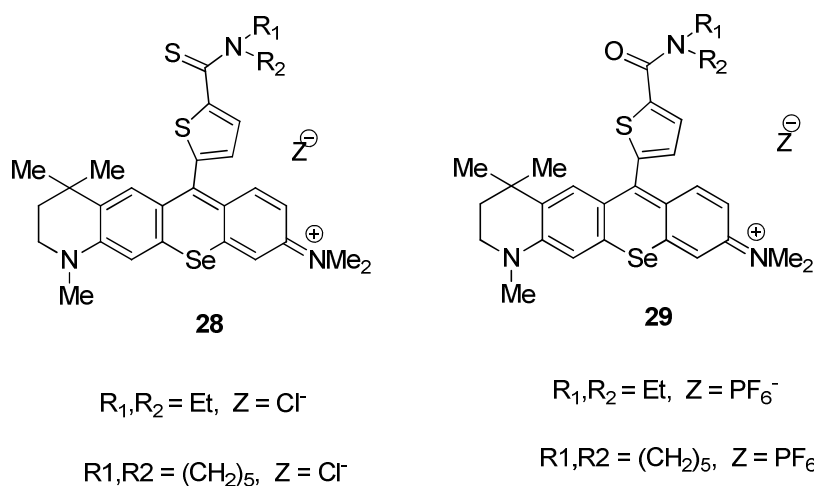


Chart 1.1

Rose bengal, is an anionic xanthyne dye having very good singlet oxygen quantum yield. It is a Type II photosensitizer.⁸² The photodynamic action of oxygen proceeds through a Type I process or through a Type II process. Type I pathway involves electron or hydrogen atom transfer, producing radical forms of the photosensitizer or the substrate. These intermediates may react with oxygen to form peroxides, superoxide ions, and hydroxyl radicals, which initiate free radical chain reactions. Type II mechanism is mediated by an energy transfer process with ground state

oxygen.³¹ Because of the anionic nature, in the absence of a carrier, RB shows decreased efficiency in crossing the cell membranes. It has been observed that PDT can cause cell death by apoptosis, autophagy and necrosis. The rose bengalacetate (RBAC) which is hydrophobic can easily cross the cell membrane and can produce ROS inside the cell when treated with green light. RBAC-PDT produces apoptosis through intrinsic, extrinsic, endoplasmic reticulum stress and caspase independent pathways in HeLa cells.⁸³

Ramaiah et al., reported that squaraines dyes could be useful for PDT.⁸⁴ The halogenated squaraines like bromo and iodo produces cytotoxicity and genotoxicity of Chinese hamster ovary cells. The mouse lymphoma cells proliferation was inhibited by photoexcited bromo and iodo derivatives of squaraine dyes. In the absence of light only a few mutations was observed. The bromo derivative produce micronuclei that cause photogenotoxicity in the absence of light in comparison to the iodo derivative and the iodo derivative is recommended for PDT applications.

1.6.3. Water purification and disinfection

Clean water to drink and clean air to breath are essential for sustaining a healthy life. The water sources are getting polluted day by day. In December 2016, the UN General Assembly adopted the resolution “International Decade (2018–2028) for Action – Water for Sustainable Development” to help put a greater focus on water during ten years.⁸⁵ A very large section of the world population still lack safely managed water for drinking purpose. This UN intervention points out the urgent need for developing new practical methods for the water disinfection. The first solar water disinfection studies were reported in 1904, where some fluorescent dyes have the potential to inactivate the microorganisms when exposed to

sunlight.⁸⁶ It was based on the studies of acridine dye on paramecia. The term photodynamic action was coined after this report and then the role of ROS in photodynamic action was well-studied. Chlorination, ozonization, and UV irradiation are the conventional method for the water disinfection. But these methods face limitations like production of harmful by-products, involving high cost, limited water volume, and long time duration. The simplest procedures for reducing the microbiological contamination of very small volumes of water are either boiling water or make use of solar disinfection process. Solar disinfection method (SODIS) involves the combined action of solar UV radiation and the temperature inside a bottle filled with water. As a result of this, the inactivation of many water borne pathogenic organisms occur by the ROS generated within the microorganism. The method has the advantages like zero cost, use sunlight as the energy source, absence of the adverse effect of the taste of the treated water but at the same time faces the limitations like limited effectiveness against certain viruses and protozoa, relatively long treatment time, the limited water volume and the climatic dependence. Even with these limitations, SODIS method is currently used by more than 4.5 million people in 55 countries.⁸⁷

Solar disinfection method can be used along with the singlet oxygen sensitizers.⁸⁸⁻⁹² Many water-soluble singlet oxygen sensitizers are used in PDT and antimicrobial photodynamic treatments of localized infection.⁹³⁻⁹⁵ Since the removal of the sensitizer are essential after the treatment, supported sensitizers are favourable for the water disinfection. Most of the previous work, make use of rose bengal, methylene blue and some porphyrin derivatives. In order to perform as a good photosensitizer for water treatment the compound should have high absorption coefficient, long lived triplet excited state, good photostability, broad spectrum of action, low toxicity in the dark. A factor which influences the phototreatment of water is the

concentration of the photosensitizer. The inactivation rate of bacteria increases with increase in the photosensitizer concentration.^{96,97} Another factor that affect the phototreatment of water is the pH. With methylene blue as the photosensitizer, Acher et.al observed that the increase in pH from 7.1-7.6 to 8.6 to 8.9 improves the inactivation efficiency but Cooper et al., observe that the change in pH from 7 to 10 had no significant effect on disinfection with same photosensitizer.^{98,99} The wavelength and the intensity of incident light also affect the photodisinfection process. Visible light absorbing sensitizers scores better and a clean and less turbid water ensures better transmission of solar radiation facilitating disinfection process.

Singlet oxygen mediated water disinfection has certain advantages compared to other methods. Organic dyes are commonly used singlet oxygen sensitizers as it shows absorption in the visible region with high absorption coefficients and in this case lower amount of photosensitizing materials are required. The 3-4 μ s lifetime available for singlet oxygen in the aqueous medium is enough to interact with the microorganisms. The targets within 0.1 μ m from the point of generation of singlet oxygen are exposed to attack, and at the same time non toxic towards other microorganisms. As an oxidizing species singlet oxygen is more selective.⁸⁷

Bartusik et al., developed a microphotoreactor having device to generate bubbles.¹⁰⁰ The bubble carries the singlet oxygen generated has a concentration at a level toxic to bacteria and fungus.

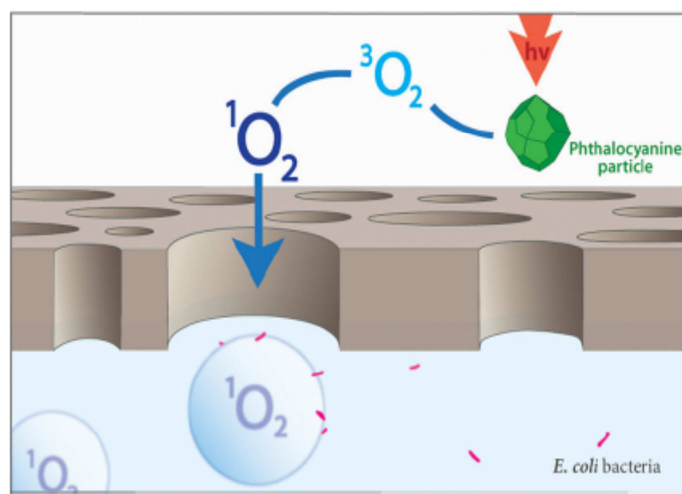


Figure 1.5 The schematic representation of a bubble generating microphotoreactor (Adapted from reference 100)

The advantage of the singlet oxygen bubble technology is that there is no waste or by products generated as a result of the reaction. The device was loaded with phthalocyanine sensitizer particles and was coupled to a diode laser via an optical fiber and to an O_2 gas tank via a feed tube. Oxygen gas flows over the sensitizer particles while the particles, kept dry by a polyethethylene membrane, are illuminated with 669 nm laser light. From a comparative study of the inactivation of the *Escherichia coli* and *Aspergillus fumigates* in deaerated, air saturated, and oxygenated solutions it was concluded that the singlet oxygen bubble toxicity was inversely proportional to the amount of dissolved oxygen in solution. For the photoinactivation of bacteria two mechanisms were proposed. The first mechanism propose that the inactivation occurs by an oxygen gradient formed inside and outside of the bubble, the singlet oxygen formed is solvated and diffuses through the aqueous solution until it reacts with the target organism. The second mechanism involves the interaction of the singlet oxygen directly with the *E.coli* that accumulates the gas –liquid interface. This mechanism operates at

a slower rate compared to the first mechanism. The actual mechanism is determined by the addition of detergent molecules and Ca^{2+} ions. The results reveal that the second mechanism is operated during the inactivation of bacteria through singlet oxygen bubble technology.

Villén et al., reported the use of a solar photocatalytic reactor to generate $^1\text{O}_2$.¹⁰¹ The reactor was fabricated with an aim to provide daily domestic water disinfection for people in the less favoured regions of the planet. A ruthenium (II)tris–chelate complex supported on porous silicone acts as the singlet oxygen sensitizer. Pilot experiments have been carried out using the solar reactor containing a compound parabolic collector (CPC).



Figure 1.6 Solar photoreactor for water disinfection test with the photosensitizing material into the glass tubes of the CPC. (Adapted from reference 101)

The efficiency is tested with two CPC prototypes with different configuration of the photosensitizing material, namely, a coaxial- and a fin-type one. The water containing the pathogenic microorganisms *Escherichia coli* or *Enterococcus faecalis* with a flow rate of 2 L/min was subjected to the photocatalytic treatment for 5 hrs. The average rate for the disinfection was similar for both the photoreactor designs. A reduction of 1 % and 0.1 %

highly stable and sustain their magnetic behaviour and photoinactivation efficiencies for several cycles.

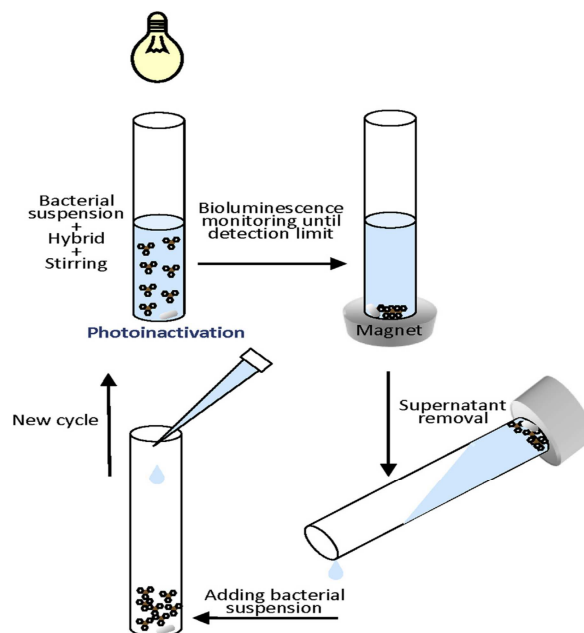


Figure 1.8 Schematic illustration of the nanomagnet-porphyrin hybrids recycling (Adapted from reference 102)

Fouling of membranes by bacteria, fungus and algae is a problem in the reverse osmosis based water purification systems. A combined water disinfection and anti-fouling method has been proposed. Here, a singlet oxygen sensitizer present on the membrane prevents accumulation of pathogens on the membrane when used in conjunction with light.¹⁰³⁻¹⁰⁸

The waste water discharge from industries such as paper, dye manufacturing and from refineries contains toxic compounds such as phenol and its derivatives. The photosensitized oxidation of phenol was studied using the photosensitizers such as eosin, rose bengal, methylene blue, riboflavin, and Zn(II) tetraphenylporphyrin. Nowakowska et al., reported the oxidation of phenol using immobilized rose bengal.¹⁰⁹ Gerdes et al., studied

the same using immobilized phthalocyanines.¹¹⁰ Gerdes et al., used Al(III), Zn(II), and Ga(III) complexes of 2,9,16,23-tetrasulfophthalocyanine, as well as 5,10,5,20-tetrakis(4-carboxyphenyl)porphyrin, rose bengal, methylene blue, and di(N,N,-trimethylammonium-propylene)-3,4,9,10-perylenebiscarboxyimide for investigating degradation of phenols and monochlorophenols in aqueous solution.¹¹¹ Sulfide salts are the by-product of industrial processes such as petroleum refining, tanning, coking, natural gas purification, and food processing so the oxidation of sulfide salts to sulfates are also important in waste water treatment. Photosensitized singlet oxygen mediated conversion of sulfide to sulfate was shown by almost all phthalocyanines, exception of the Co (II) complexes.^{112,113}

1.7. Immobilized singlet oxygen sensitizers

Most of the above mentioned application scenarios, in particular water treatment using singlet oxygen require immobilization of singlet oxygen sensitizers on solid and inert supports. The main advantages for the supported sensitizers are we can control the aggregation and self quenching of the sensitizer, increasing the photostability, carrying out the reactions in various medium including water, easy separation of the products, conducting solvent free reactions and deploying in water purification systems. Various supports are reported in the literature for the singlet oxygen sensitizers. The basic requirement for a photosensitizer carrier is that it should not quench singlet oxygen. When the photosensitizer is attached to the support aggregation of the sensitizer is prevented and the monomeric forms prevail. The photosensitizers adsorbed on porous medium shows reduced singlet oxygen quantum yield because of the reduced oxygen diffusion. Commonly used solid supports are polymers, silica, clays, graphene, chitosan, silicone, cellulose membranes etc. The immobilization process includes adsorption, dissolution, casting, covalent bonding and electrostatic attraction.

1.7.1. Polymer supported singlet oxygen sensitizers

Several polymer supports have been used for the purpose, for example, polystyrene derivatives, silicone,^{114,115} polyurethane,^{116,117} and polyethylene¹¹⁸ etc. Common methods of attaching sensitizers to the polymer support are via polymerisation of a sensitizer monomer, covalent grafting of the sensitizer in a post functionalization process and dopping while casting of the devices. The applications of polystyrene based supports are limited because of its hydrophobic nature. A way to overcome this is to use copolymers with monomers having polar side chains or groups. Rose bengal attached to a copolymer of chloromethylstyrene and methacrylate ester of ethyl glycol was found to be efficient for photooxygenation in aqueous medium. In biomedical applications, plastics used to fabricate instruments used in hospitals mainly contain methylene blue and toluidine blue to aid photochemical disinfection process.¹¹⁴⁻¹¹⁸ Electrospinning technique is used to dop polymeric surfaces with pthalocyanines to make photoantimicrobial surfaces.¹¹⁹⁻¹²¹ Many attempts have been reported in the literature where such supported sensitizers have been successfully applied for the photo-disinfection of both gram positive and gram negative bacteria.^{122,123}

1.7.2. Silica supported singlet oxygen sensitizers

Silica materials offer the advantages of large surface area, modulated porosity and mostly inert to many application scenarios. Roy et al., reported a novel system in which photosensitizer molecules are covalently attached to organically modified silica nano particles.¹²⁴ The photosensitizer molecule retains its photophysical properties after the incorporation and effectively produces the singlet oxygen. The tumour cells take up the synthesized particles and effective phototoxic action was reported. The main advantage in this system is that drug is not released during the systemic circulation.

Ronzani et al., synthesized and characterized three silica immobilized organic photocatalysts based on rose bengal, anthraquinone-2-carboxylic acid, and a cyanoanthracene derivative.¹²⁵ Amino-alkylated silica supported halogenated porphyrin was synthesized by Pineiro et al.¹²⁶ Guo et al., synthesized a heterogeneous singlet oxygen sensitizer-silica nanoparticles decorated with rose bengal to inactivate gram-positive bacteria, including Methicillin-resistant *Staphylococcus aureus* (MRSA), with high efficiency through photodynamic action.¹²⁷ A series of silica immobilized singlet oxygen photosensitizers are prepared by immobilizing phthalocyanines on aminopropyl groups on silica lengthened by grafting additional propyleneimine units. Singlet oxygen generation efficiency did not change with the length of the spacer but the photobactericidal function markedly increased with length of the spacer.¹²⁸

1.7.3. Zeolite supported singlet oxygen sensitizers

Zeolites are aluminosilicates characterized by a network of silicon and aluminium. Li et al., in 1996 reported the selective oxidation of olefins within the dye cation exchanged Zeolites.¹²⁹ The singlet oxygen is generated within the Zeolite by irradiating the thiazine dye entrapped within the zeolite. Smolinská et al., reported a methylene blue–zeolite hybrid system to generate singlet oxygen and show photoinactivation of pathogenic microorganisms.¹³⁰ In another immobilization strategy a trisphenanthroline iridium (III) complex was prepared by a Ship-in-a-bottle synthesis routine and singlet oxygen generation property was studied with the degradation of 9,10-dimethylanthracene.¹³¹

1.7.4. Clay supported singlet oxygen sensitizers

Clays are layered materials of natural origin and are abundant. They are suitable and cost effective supports if a sensitizer can be intercalated in

the interlayer space. Cationic photosensitizers are mainly used and intercalated via an ion exchange process. Cenens et al., in 1988 reported the photooxidation of tryptophan by the methylene blue adsorbed on clay.¹³² 5, 10, 15, 20-tetrakis(4-carboxyphenyl)porphyrin was shown to intercalate in Cloisite 30B, a monotallow bis(hydroxyethyl)ammonium-modified montmorillonite clay. The material was used for the photooxidation of phenol in aqueous solution.¹³³ Madhavan et al., reported the oxidation of a series of dialkyl, alkyl and aryl sulfides to the corresponding sulfoxide using clay bound methylene blue.¹³⁴ The triphenylmethane dyes encapsulated in clay are used in the preparation of a carbonless copying paper. Here singlet oxygen generated in a photosensitized process is used for developing the images.¹³⁵ Methylene blue adsorbed clay particles are found to be very effective in antimicrobial treatment. However, aggregation of the dye molecules on the clay surface reduced the singlet oxygen production but showed anti-microbial activity.¹³⁶

1.7.5. Graphene oxide supported singlet oxygen sensitizers

Graphene oxide has been extensively studied for *in vitro* and *in vivo* drug delivery due to its low cost, scalable production, simple functionalization, high stability in biological environments.^{137,138} Graphene oxide contains functional groups such as epoxides, carbonyl groups, carboxylic acids and isolated double bonds. They can be used in covalent anchoring of sensitizers. The methylene blue-graphene oxide nano composite prepared found to have the potential photodynamic activity against human breast cancer.¹³⁹ In another report Wojtoniszak et al., showed methylene blue-graphene oxide composite can be obtained by the noncovalent functionalization. He has demonstrated an enhanced singlet oxygen generation capacity for the composite compared to the pristine methylene blue.¹⁴⁰ Zhou and co-workers reported a novel GO-hypocrellin-A hybrid prepared by the noncovalent adsorption. The stability of the hybrid was

superior compared to free hypocrellin-A. Better tumour targeting and significant cell death was demonstrated and suggest the composite as a promising drug for clinical photodynamic therapy.¹⁴¹

1.8. Cationic Singlet Oxygen Sensitizers in PDT and Photochemical Disinfection

Photodynamic antimicrobial treatment involves the combined use of photosensitizers, visible light and oxygen to kill the pathogens. Among bacteria, there are Gram-positive bacteria and Gram negative bacteria. A common pathogen encountered in the potable water is *E. coli* which is a gram negative bacteria. Gram-positive bacteria have generally been sensitive to photoinactivation but gram-negative bacteria have been reported to be relatively insensitive unless the photosensitizers are administered in the presence of additional substances, for example, CaCl_2 , Tris-EDTA, or polymyxin B nonapeptide (PMBN), that alter the permeability of the outer membrane.¹⁴²⁻¹⁴⁵ The difference in the reactivity is mainly because of the structural difference between the two types of bacteria (figure 1.9)

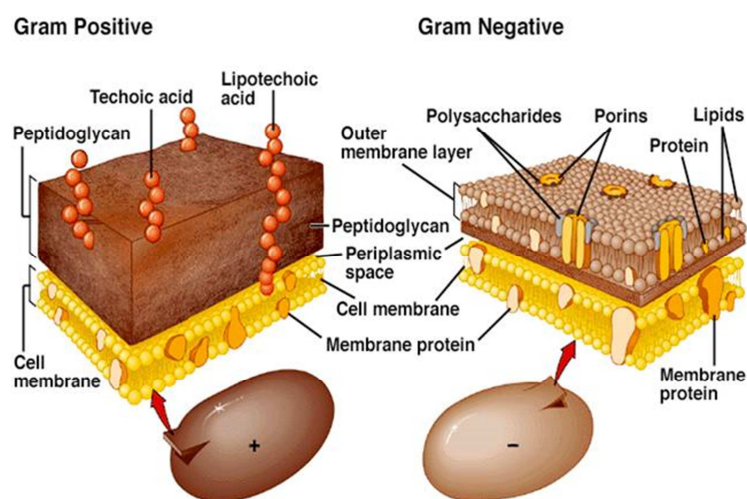


Figure 1.9 Schematic representations of the cell wall and cytoplasmic membrane structure in gram positive and negative bacteria. (Image taken from www.water.me.vccs.edu)

The insensitivity of gram-negative bacteria to photoinactivation was attributed to the presence of an outer membrane rich in lipopolysaccharide (LPS) which is highly negatively charged. This membrane generally limit the permeability of external drug molecules compared to that of usual biological membranes, containing a thick and permeable peptidoglycan layer.¹⁴⁶ Within this LPS there are many negatively charged groups which endow the surface of gram-negative bacteria with a strong negative charge.^{147- 149} Inorder to improve the efficiency of the photosensitizer in the disinfection of the gram negative bacteria two features are to be important: (1) the presence of positive charge on the photosensitizer that promote a tight interaction with the negatively charged bacterial cell wall (2) a degree of lipophilicity.

Costa et al., tested the effect of six cationic porphyrin derivatives with two to four charges on the photoinactivation of a sewage bacteriophage.¹⁵⁰ The rate of bacteriophage photoinactivation and the efficiency of the photosensitizer appeared to vary with the charge and with the substituents in the *meso*-positions of the porphyrin macrocycle. Tetra- and tricationic porphyrins were, therefore, recommended as a new method for inactivating sewage bacteriophages. A similar work in this direction by Orlandi, et al., used two dicationic 5,15-di(N-alkyl-4-pyridyl) porphyrins in the antibacterial photodynamic treatment. The results of the study showed the importance of lipophilicity along with positive charge in the disinfection of gram negative bacteria.¹⁵¹

1.9. Triazatriangulenium Salts

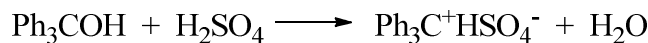
A carbocation is a molecule in which a carbon atom bears three bonds and a positive charge. In carbocations carbon atom typically adopts sp^2 hybridization at the cationic carbon center, with a trigonal planar molecular geometry. They are often very reactive in order to complete the

octet of valence electrons and to be neutral. The stability of a carbocation is expressed in terms of its pK_{R^+} value. It is a thermodynamic parameter that expresses the affinity of a carbocation towards hydroxide ions. It is the equilibrium constant for the acid-base reaction that converts a carbenium ion into the corresponding carbinol. The higher the pK_{R^+} the more stable the carbocation towards nucleophilic attack. In other words, it means that a carbocation of which the pK_{R^+} value is 9.0 would be 50 % converted into its carbinol at pH 9.0.

$$pK_{R^+} = \text{pH} + \log \left(\frac{[R_3C^+]}{[R_3COH]} \right)$$



In 1902 J.F. Norris, F. Kehrmann and F. Wentzel discovered independently that colourless triphenylmethanol gave deep yellow solutions in concentrated sulfuric acid.^{152,153}



Similar coloured triaryl cations like triarylmethylum, acridinium and xanthenium cations were subsequently discovered and they find applications as dyes in chemical, medical and biological fields. Some of the specific application includes use as colorants in photographic, food, textiles and cosmetics industry. They are also used as laser dyes and fluorescent probes for clinical and biological purposes.¹⁵⁴⁻¹⁵⁶

Triangulene is the trivial name for the class of compounds characterized by a ring system of six, six-membered rings fused in a triangular fashion (Chart 1.2). In 1963 Martin and Smith synthesized the triangulenium system which is a planarised triphenyl cation having O-bridges connecting phenyl rings called a trioxatriangulenium (TOTA⁺) cation or a

sesquixanthylum.¹⁵⁷ According to systematic naming it is a dibenzopyrene (**31**) and named as 4, 8, 12-trioxa-4,8,12,12c-tetrahydrodibenzo[*cd,mn*]pyrenium. TOTA⁺ was noted by the research community for its properties as a highly stable carbocation with a pK_{R^+} value of 9.05.

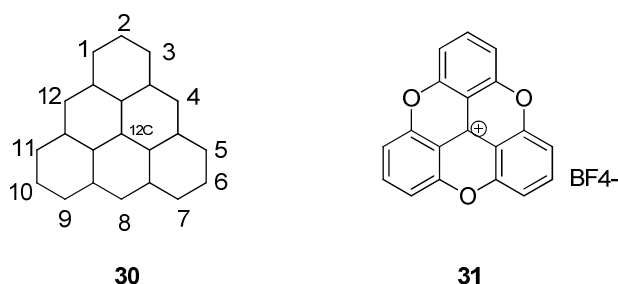


Chart 1.2 Triangulene system with numbering used in the naming of derivatives(**30**), trioxatriangulenium tetrafluoroborate (TOTA⁺) (**31**).

Changing the bridge atom in heterocyclic carbenium ions from oxygen to nitrogen significantly increases the cation stability. Hence, on going from the 9-phenyl-xanthenium ion (**32**) (pK_{R^+} 1.0) to the 10-methyl-9-phenyl-acridinium ion (**33**) (pK_{R^+} 11.0) the stability increases by ten pK_{R^+} units.^{158,159}

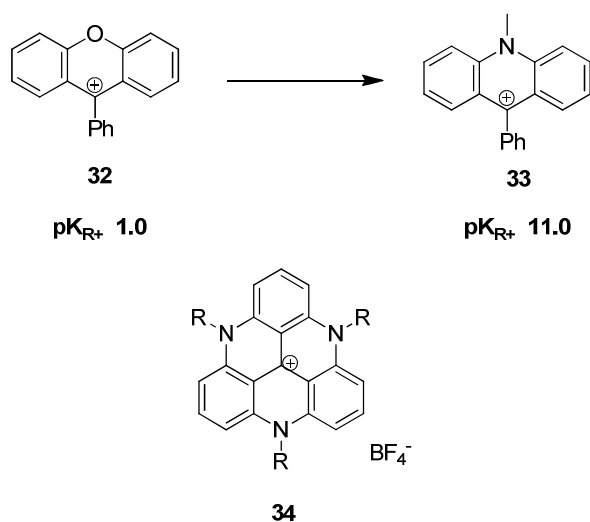
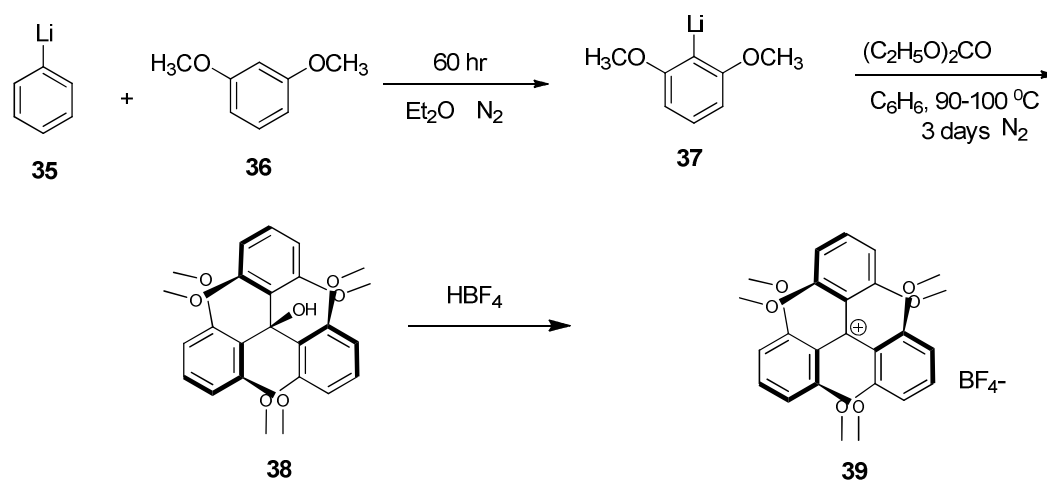


Chart 1.3 Structures of 9-Phenyl-xanthenium (**32**), 10-methyl-9-phenyl-acridinium (**33**) and triazatriangulenium tetrafluoroborate (**34**).

In a similar way changing the bridge atom in the TOTA⁺ with nitrogen resulting in a very highly stable heterocyclic compound known as triazatriangulenium salts (Chart 1.3).¹⁶⁰ The present thesis reports the design, synthesis and studies of a series of water soluble triazatriangulenium salts. Among the triphenylmethane dyes triazatriangulenium compounds gain attention due to its high stability with pK_{R^+} value 23.7.

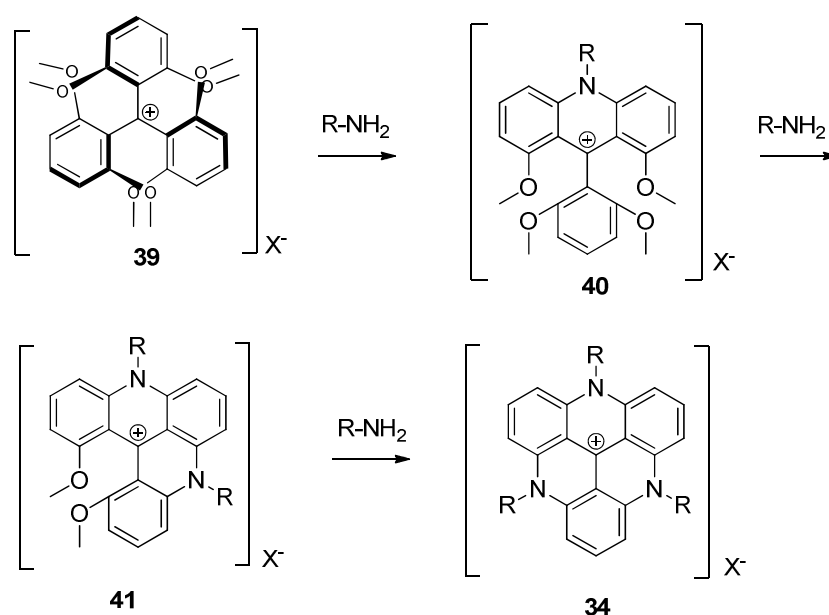
Laursen et al.,^{160,161} reported the synthesis and Dileesh et al.,¹⁶² reported the photophysical and electron transfer properties of a series of N-alkyl substituted triazatriangulenium salts. The precursor for the synthesis of this class of triangulenium cations is the cation tris-(2,6-dimethoxyphenyl) carbenium ion and the general synthetic procedure is shown in scheme 1.9.¹⁵⁷



Scheme 1.9

The transformation of tris-(2,6-dimethoxyphenyl) carbenium ion to the triazatriangulenium ion is effected through a series of consecutive S_NAr reactions where the six orthomethoxy groups present in the tris-(2,6-dimethoxyphenyl) carbenium tetrafluoroborate serve as leaving groups when

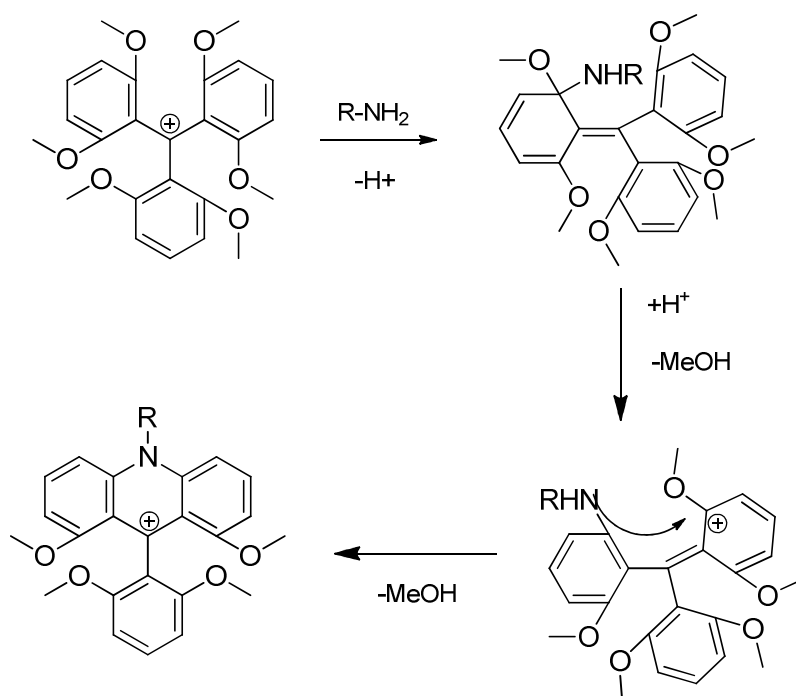
nucleophiles like primary amines are used (Scheme 1.10). In these reactions the steric bulk of the methoxy groups protects the central carbon atom in the tris-(2,6-dimethoxyphenyl) carbenium tetrafluoroborate from nucleophilic addition.



Scheme 1.10

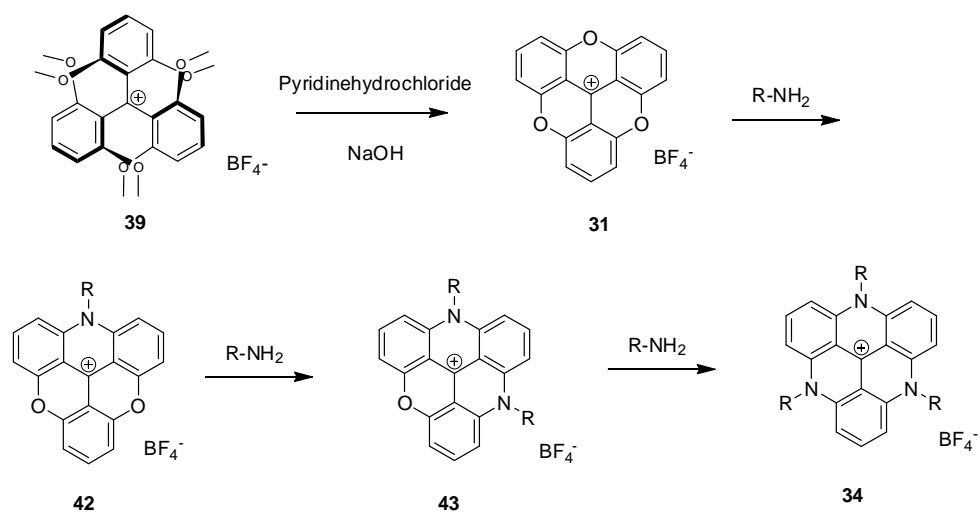
By controlling the reaction temperature, it is possible to obtain products having one, two, or three nitrogen bridges, respectively. Room temperature stirring of tris-(2,6-dimethoxyphenyl) carbenium tetrafluoroborate with primary amine give the monoazabridged cation **40**. A temperature rise upto 100 °C and heating for 45 minutes yield diaza-bridged cation **41**. The triazatriangulenium cation **34** is obtained when heating the reaction above 160 °C with excess primary amine for longer durations. The decreased reactivity associated with the introduction of second and third nitrogen atoms is because of the delocalization of the positive charge on the central carbon to the new bridging N atom leading to a reduced electrophilicity of aromatic

rings. As a result the S_NAr reactions are irreversible. The proposed mechanism for this S_NAr reaction is given in Scheme 1.11.¹⁶¹



Scheme 1.11

An alternative pathway for the production of triazatriangulenium salt is through trioxatriangulenium salt¹⁶¹ again in a stepwise process resulting into azadioxa(42), diazaoxa(43) and triazatriangulenium cations(34) (Scheme 1.12).



Scheme 1.12

The crystal structure and the packing modes of triazatriangulenium salts were also reported in relation to the electrostatic and spacefilling requirements of the ions. In the case of *n*-propyl-TATA and *n*-octyl-TATA the cation forms staggered dimers.¹⁶¹ The staggering forces the alkyl groups away from the plane of the ring system and as a result the dimers become isolated. The dimers formed in the case of *n*-propyl-TATA and *n*-octyl-TATA are shown in the figure 1.10.

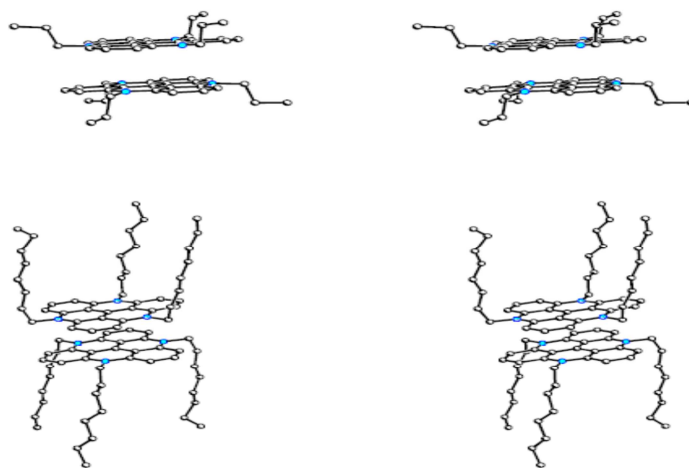


Figure 1.10 Stereo view showing the dimmers of *n*-propyl-TATA and *n*-Octyl-TATA (Adapted from reference 161).

1.9.1. Applications of triazatriangulenium salts

The remarkable stability along with visible light absorption properties of these cations prompted researchers to explore various application scenarios. Laurson et al., and Dileesh et al., have studied the photophysical and electron transfer properties of these cations in detail.^{161,162} The trioxa triangulenium cation was found to intercalate with DNA and under light it led to strand cleavages.¹⁶³ Cyril Nicolas et al., reported the use of N-alkyl substituted triazatriangulenium salts with varying chain length in phase transfer catalysis.¹⁶⁴

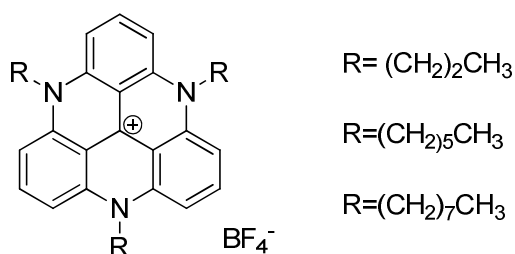


Chart 1.3

The efficiency of phase transfer catalysis was found to depend on the cations partition ability between aqueous and organic medium. The applicability of these compounds as a successful catalyst for several classical organic reactions under basic and nucleophilic conditions has been demonstrated. The biological applications of triazatriangulenium salts were also reported. Sørensen et al., reported the application of azadioxatriangulenium salt in anisotropic assay for the detection of binding events of large sized biomolecules.¹⁶⁵ The major limitation of biofluorescence anisotropy is that the label used should be comparable to the tumbling time of the biomolecule which is labelled. In this study a new fluorescent label for high molecular weight biomolecule based on azadioxatriangulenium motif was used. The esterified form of triangulenium was conjugated to *anti*-rabbit Immunoglobulin G which has the long fluorescence lifetime matches with the

high molecular weight antibody and it complexes with rabbit Immunoglobulin G. Shivalingam et al., reported that triangulenium compounds can be used as a unique fluorescent probe for studying the existence and *invivo* functions of nonduplex topologies adopted by the nucleic acids.¹⁶⁶ Since this probe can be used *in vivo* it points towards the possibility of live-cell imaging studies. A continuous glucose monitoring device was reported by conjugating triangulenium dye to ovalbumin. The assay shows varying intensity with the glucose level ranging from 0-500 mg/dL.¹⁶⁷ The limitations of glucose sensing technology of ConA-beased glucose sensors is overcome by conjugation with the red emitting long lifetime azadioxatriangulenium dye to ovalbumin.

Though these triazatriangulenium cations show extreme stability in both acidic and alkaline conditions but their solubility in many solvents are poor. This has prevented using these cations for diverse applications in material science or in medicine. Solubility in aqueous medium is an important criteria required in the biological applications. Polar substituents or substituents having polar end groups at suitable positions can enhance the solubility of triazatriangulenium salts. Moreover, the present known studies have not explored the properties of these cations as potential singlet oxygen sensitizers as they possess high triplet yield, energy and lifetime suitable for being a good singlet oxygen sensitizer.

1.10. The Objectives

The main objectives of the thesis are

- ❖ To synthesize water soluble triazatriangulenium salts by incorporating polar functional groups
- ❖ Study their photophysical properties in the aqueous medium
- ❖ Study their efficiency of singlet oxygen generation by photosensitization

- ❖ Synthesis and study of lipophilic triazatriangulenium cations in microheterogeneous medium
- ❖ Tether covalently or intercalate triazatriangulenium ions to solid supports or layered materials
- ❖ Study the singlet oxygen photosensitization properties of these heterogeneous sensitizer systems
- ❖ Study the applicability of these heterogeneous sensitizers in the photodynamic disinfection of water containing pathogens.

1.11. References

1. Arnold, S.J.; Kubo, M.; Ogryzlo, E.A. *Adv. Chem. Ser.* **1968**, *77*, 133.
2. Fritzsche, M. *Compt. Rend.* **1867**, *64*, 1035.
3. Lewis, G. N. *Chem. Rev.* **1924**, *1*, 231.
4. Kautsky, H.; de Bruijn, H. *Naturwissenschaften* **1931**, *19*, 1043
5. Clennan, EL.; Pace, A. *Tetrahedron* **2005**, *61*, 6665.
6. Zou, J.; Jiang, J.; Han, Z.; Lin, L.; Li, Y.; Huang, Z. *J. Biomed. Opt.* **2018**, *10820*, 108203C.
7. Ronzani, F.; Trivella, A.; Bordat, P.; Blanc, S.; Lacombe, S. *Photochem.Photobiol.* **2014**, *284*, 8.
8. Boso, G.; Ke, D.; Korzh, B.; Bouilloux, J.; Lange, N.; Zbinden, H. *Biomed opt. express.* **2016**, *7*, 211.
9. Gemmell, R.; McCarthy, A.; Kim, M.; Veilleux, I.; Zhu, C.; Buller, S.; Wilson, C.; Hadfield, H. *J. Biophotonics.* **2017**, *10*, 320.
10. Qiu, J.; Ha, G.; Jing, C.; Baryshev, V.; Reed, W.; Lau, W.; Zhu, Y. *Ultramicroscopy.* **2016**, *161*,130.
11. Risco, C.; Sanmartín, E.; Tzeng, P.; Frey, K.; Seybold, V.; Groot, J. *Structure.* **2012**, *20*, 759.
12. Khan, A.U.; Kasha, M. *J. Chem. Phys.* **1963**, *39*, 2105.
13. Corey, E.J.; Mehrotra, M.M.; Khan, A.U. *J. Am. Chem. Soc.* **1986**, *108*, 2472.
14. Murray, R. W.; Kaplan, M. L. *J. Am. Chem. Soc.* **1969**, *91*, 5358.
15. Nardello, V.; Barbillat, J.; Marko, J.; Witte, P.T.; Alsters, P.L.; Aubry, J.M. *Chem. Eur. J.* **2003**, *9*, 2435.
16. Blázquez-Castro, A. *Redox biology.* **2017**, *13*, 39.

17. Houreld, N.N.; Abrahamse, H. *Laser Chem.* **2007**, *80*, 536.
18. Landry, M.P.; McCall, P.M.; Qi, Z.; Chemla, Y.R. *Biophys. J.* **2009**, *97*, 2128.
19. Matheson, I.B.C.; Lee, J. *Chem. Phys. Lett.* **1970**, *7*, 475.
20. Aabo, T.; Perch-Nielsen, I.R.; Dam, J.S.; Palima, D.Z.; Siegumfeldt, H.; Glückstad, J.; Arneborg, N. *J. Biomed. Opt.* **2010**, *15*, 041505.
21. Dube, A.; Bock, C.; Bauer, E.; Kohli, R.; Gupta, P.K.; Greulich, K.O. *Radiat. Environ. Biophys.* **2001**, *40*, 77.
22. Zakharov, S.D.; Ivanov, A.V. *Quant. Electron.* **1999**, *29*, 1031.
23. Evans, D.F.; Tucker, J.N. *J. Chem. Soc. Faraday Trans.* **1976**, *2*, 1661.
24. Neuman, K.C.; Chadd, E.H.; Liou, G.F.; Bergman, K.; Block, S.M. *Biophys. J.* **1999**, *77*, 2856.
25. Spitler, R.; Berns, M.W. *J. Biomed. Opt.* **2014**, *19*, 038001.
26. Almeida-Lopes, L.; Rigau, J.; Zângaro, R.A.; Guidugli-Neto, J.J.; Martins Marques Jaeger, M. *Surg. Med.* **2001**, *29*, 179.
27. Saenko, Y.V.; Glushchenko, E.S.; Zolotovskii, I.O.; Sholokhov, E.; Kurkov, A. *Lasers Med. Sci.* **2016**, *31*, 405.
28. Anquez, F.; Courtade, E.; Sivéry, A.; Suret, P.; Randoux, S. *Opt. Express.* **2010**, *22*, 22928.
29. Koroll, G.W.; Singh, A. *Photochem. Photobiol.* **1978**, *28*, 611.
30. Armichev, A.V.; Ivanov, A.V.; Panasenko, N.A.; Perov, S.N.; Zakharov, S.D. *J. Rus. Laser Res.* **1995**, *16*, 186.
31. DeRosa, M.C.; Crutchley, R.J. *Coord. Chem. Rev.* **2002**, *233*, 351.
32. Neckers, D.C. *J. Photochem. Photobiol. A.* **1989**, *47*, 1.

33. Xu, D.; Neckers, D.C. *J. Photochem. Photobiol. A*. **1987**, *40*, 361.
34. Srinivasan, V.S.; Podolski, D.; Westrick, N.J.; Neckers, D.C. *J. Am. Chem. Soc.* **1978**, *100*, 6513.
35. Redmond, R.W.; Gamlin, J.N. *Photochem. Photobiol.* **1999**, *70*, 391.
36. Tardivo, J.P.; Del Giglio, A.; de Oliveira, C.S.; Gabrielli, D.S.; Junqueira, H.C.; Tada, D.B.; Severino, D.; de Fátima Turchiello, R.; Baptista, M.S. *Photodiagn. photodyn.* **2005**, *2*, 175.
37. Severino, D.; Junqueira, H.C.; Gugliotti, M.; Gabrielli, D.S.; Baptista, M.S. *J. Photochem. Photobiol. A*. **2003**, *77*, 459.
38. Stracke, F.; Heupel, M.; Thiel, E. *J. Photochem. Photobiol. A*. **1999**, *126*, 51.
39. Kanner, R.C.; Foote, C.S. *J. Am. Chem. Soc.* **1992**, *114*, 678.
40. Oliveros, E.; Bossmann, S.H.; Nonell, S.; Martí, C.; Heit, G.; Tröscher, G.; Neuner, A.; Martínez, C. *New J. Chem.* **1999**, *23*, 85.
41. Darwent, J.R.; Douglas, P.; Harriman, A.; Porter, G.; Richoux, M.C. *Coord. Chem. Rev.* **1982**, *44*, 83.
42. Soncin, M. *J. Photochem. Photobiol. B*. **1998**, *42*, 202.
43. Pefkianakis, E.K.; Christodouleas, D.; Giokas, D.L.; Papadopoulos, K.; Vougioukalakis, G.C. *Euro. J. Inorg. Chem.* **2013**, *26*, 4628.
44. Demas, J.N.; Harris, E.W.; McBride, R.P. *J. Am. Chem. Soc.* **1977**, *99*, 3547.
45. Anbalagan, V.; Srivastava, T.S. *J. Photochem. Photobiol. A*. **1994**, *77*, 141.
46. Wu, H.; Song, Q.; Ran, G.; Lu, X.; Xu, B. *Trends Anal. Chem.* **2011**, *30*, 133.

47. Molnár, A.; Džedić, R.; Svoboda, A.; Hála, J. *J. Lumin.* **2008**, *128*, 783.
48. Snyder, J.W.; Zebger, I.; Gao, Z.; Poulsen, L.; Frederiksen, P.K.; Skovsen, E.; McIlroy, S.P.; Klinger, M.; Andersen, L.K.; Ogilby, P.R. *Acc. Chem. Res.* **2004**, *37*, 894.
49. Whinnery, J. R. *Acc. Chem. Res.* **1974**, *7*, 225.
50. Fuke, K.; Ueda, M.; Itoh, M. *J. Am. Chem. Soc.* **1983**, *105*, 1091.
51. Cheng, C.C.; Wu, G.R.; Chiou, C.S.; Yu, J.K.; Chou, P.T. *J. Chin. Chem. Soc.* **2003**, *50*, 31.
52. Braslavsky, S. E.; Heibel, G. E. *Chem. Rev.* **1992**, *92*, 1381.
53. Oliveros, E.; Bossmann, S.H.; Nonell, S.; Martí, C.; Heit, G.; Tröscher, G.; Neuner, A.; Martínez, C. *New J. Chem.* **1999**, *23*, 85.
54. Spiller, W.; Kliesch, H.; Wöhrle, D.; Hackbarth, S.; Röder, B.; Schnurpfeil, G. *J. Porphyr. Phthalocyanines.* **1998**, *2*, 145.
55. Mayeda, E.A.; Bard, A.J. *J. Am. Chem. Soc.* **1973**, *95*, 19.
56. Kuhn, H.J.; Braslavsky, S.E.; Schmidt, R. *Chemical Actinometry (IUPAC technical report). Pure and Applied Chemistry.* **2004**, *7612*, 2105.
57. Günther, S.; Lemp, M.; Zanocco, A.L. *Boletín de la Sociedad Chilena de Química.* **2000**, *45*, 637.
58. Bloodworth, A. J.; Eggelte, H. J. Endoperoxides. In Singlet oxygen. Reaction Modes and Products, Part 1, Frimer, A. A., Ed. CRC Press: Boca Raton, FL, 1985; *Vol. II*, pp 93–203.
59. Clennan, E. L.; Foote, C. S. Endoperoxides. In Organic Peroxides, Ando, W., Ed. John Wiley & Sons Ltd.: New York, 1992; pp 255–318.

60. Baumstark, A. L. The 1,2-Dioxetane Ring System: Preparation, Thermolysis, and Insertion Reactions. In Singlet O₂. Reaction Modes and Products, Frimer, A. A., Ed. CRC Press:Boca Raton, FL, 1985; *Vol. II*, pp 1–35.
61. Frimer, A. A.; Stephenson, L. M. The Singlet Oxygen Ene Reaction. In Singlet O₂. Reaction Modes and Products, Frimer, A. A., Ed. CRC Press: Boca Raton, FL, 1985; *Vol. II*, pp 67–9.
62. Yamazaki, S.; Ozawa, N.; Hiratsuka, A.; Watabe, T. *Free Radical Biol.Med.* **1999**, *27*, 301.
63. Devasagayam, T.; Kamat, J.P. *Indian J. Exp. Biol.* **2002**, *40*, 680.
64. Moreau, K.L.; King, J.A. *Trends Mol. Med.* **2012**, *18*, 273.
65. Shannon, S.; Stahl.; Paul L.A. Liquid phase aerobic oxidation catalysis,Wiley-VCH Verlag GmbH & Co.KGaA, Boschstr. 12, 69469 Weinheim, Germany, 2016; p 384.
66. Shannon, S.; Stahl.; Paul L.A. Liquid phase aerobic oxidation catalysis,Wiley-VCH Verlag GmbH & Co.KGaA, Boschstr. 12, 69469 Weinheim, Germany, 2016; p 390.8
67. Shannon, S.; Stahl.; Paul L.A. Liquid phase aerobic oxidation catalysis,Wiley-VCH Verlag GmbH & Co.KGaA, Boschstr. 12, 69469 Weinheim, Germany, 2016; p 391.
68. Yao, G.; Steliou, K. *Org. Lett.* **2002**, *4*, 485.
69. Maraş, A.; Seçen, H.; Sütbeyaz, Y.; Balcı, M. *J.Org. Chem.* **1998**, *63*, 2039.
70. Dastan, A.; Balci, M. *Tetrahedron.* **2006**, *62*, 4003.
71. Ormond, A.B.; Freeman, H.S. *Materials.* **2013**, *6*, 817.

72. Fingar, V.H.; Kik, P.K.; Haydon, P.S.; Cerrito, P.B.; Tseng, M.; Abang, E.; Wieman, T.J. *Br. J. Cancer*. **1999**, *79*, 1702.
73. Zimcik, P.; Miletin, M. Photodynamic Therapy. In *Dyes and Pigments: New Research*; Lang, A.R., Ed.; Nova Science Publishers: New York, NY, USA, 2008.
74. Sanovic, R.; Krammer, B.; Grumboeck, S.; Verwanger, T. *Int. J. Oncol.* **2009**, *35*, 921.
75. Chen, Y.; Zheng, W.; Li, Y.; Zhong, J.; Ji, J.; Shen, P. *Cancer Sci.* **2008**, *99*, 2019.
76. Mousavi, S.H.; Tavakkol-Afshari, J.; Brook, A.; Jafari-Anarkooli, I. *Food Chem. Toxicol.* **2009**, *47*, 855.
77. Tsujino, I.; Miyagi, K.; Sampson, R.W.; Sieber, F. *Photochem. Photobiol.* **2006**, *82*, 458.
78. Wöhrle, D.; Hirth, A.; Bogdahn-Rai.; T, Schnurpfeil, G.; Shopova, M. *Russ. Chem. Bull.* **1998**, *47*, 807.
79. Dos Santos, A.F.; Terra, L.F.; Wailemann, R.A.; Oliveira, T.C.; de Moraes Gomes, V.; Mineiro, M.F.; Meotti, F.C.; Bruni-CardosoA, BaptistaM.S.; Labriola, L. *BMC Cancer*. **2017**, *17*, 194.
80. Hill, J.E.; Linder, M.K.; Davies, K.S.; Sawada, G.A.; Morgan, J.; Ohulchansky, T.Y.; Detty, M.R. *J. Med. Chem.* **2014**, *57*, 8622.
81. Johnson, L. V.; Walsh, M. L.; Bockus, B. J.; Chen, L. B. *J. Cell Biol.* **1981**, *88*, 526.
82. Bottiroli, G.; Croce, A.C.; Balzarini, P.; Locatelli, D.; Baglioni, P.; Lo Nostro, P.; Monici, M.; Pratesi, R. *Photochem. Photobiol.* **1997**, *66*, 374.

83. Panzarini, E.; Inguscio, V.; Dini, L. *Int J. Photoenergy*. **2011**, 2011, 1.
84. Ramaiah, D; Eckert, I; Arun, K.T; Weidenfeller, L; Epe, B. *J. Photochem. Photobiol.* **2002**, 76, 672.
85. <http://www.unwater.org/new-decade-water/>. Accessed, January 30, 2018.
86. Von Tappeiner, H.; Jodlbauer, A. *Dtsch. Arch. Klin. Med.* **1904**, 80, 427.
87. Garcí'a-Fresnadillo, D. *Chem.Photo. Chem.* **2018**, 2, 1.
88. Jori, G.; Magaraggia, M.; Fabris, C. et al., *J. Environ. Pathol. Toxicol. Oncol.* **2011**, 30, 261.
89. Chong, M. N.; Jin, B.; Chow, C. W. K.; Saint, C. *Water Res.* **2010**, 44, 2997.
90. Alves, E.; Faustino, M. A. F. ; Neves, M. G.P.M.S. ; Cunha, A.; Nadais, H.; Almeida, A. *J. Photochem. Photobiol. C. Photochemistry Reviews.* **2015**, 22, 34.
91. Ergaieg, K.; Chevanne, M.; Cillard, J.; Seux, R. *Sol. Energy.* **2008**, 82, 1107.
92. Costa, L.; Faustino, M. A. F.; Tom'e, J. P. C. et al., *J. Photochem. Photobiol. B.* **2013**, 120, 10.
93. Ethirajan, Y.; Chen, P.; Joshi, R.; Pandey, K. *Chem. Soc. Rev.* **2011**, 40, 340.
94. Awuaha, S. G.; You, Y. *RSC Adv.* **2012**, 2, 11169.
95. Yin, R.; Agrawal, T.; Khan, U.; Gupta, G. K.; Rai, V.; Huang, Y. Y.; Hamblin, M. R. *Nanomedicine.* **2015**, 10, 2379.
96. Rinc'on, A. G.; Pulgarin, C. *Appl. Catal. B- Environ.* **2003**, 44, 263.

97. Schwegmann, H.; Ruppert, J.; Frimmel, F. H. *Water Res.* **2013**, *47*, 1503.
98. Acher, A.; Fischer, E.; Zellingher, R.; Manor, Y. *Water Res.* **1990**, *24*, 837.
99. Cooper, A. T.; Goswami, D. Y. *J. Sol. Energy. Eng.* **2002**, *124*, 305.
100. Bartusik, D.; Aebisher, D.; Lyons, A.M.; Greer, A. *Environ. Sci. Technol.* **2012**, *46*, 12098.
101. Villén, L.; Manjón, F.; García-Fresnadillo, D.; Orellana, G. *Appl. Catal. B.* **2006**, *69*, 1.
102. Alves, E.; Rodrigues, J.M.; Faustino, M.A.; Neves, M.G.; Cavaleiro, J.A.; Lin, Z.; Cunha, Â.; Nadais, M.H.; Tomé, J.P.; Almeida, A. *Dyes Pigm.* **2014**, *110*, 80.
103. Daels, N.; De Vrieze, S.; Sampers, I.; Decostere, B.; Westbroek, P.; Dumoulin, A.; Dejans, P.; De Clerck, K.; Van Hulle, S. W. H. *Desalination.* **2011**, *275*, 285.
104. Yoon, K.; Kim, K.; Wang, X.; Fang, D.; Hsiao, B. S.; Chu, B. *Polymer.* **2006**, *47*, 2434.
105. Basri, H.; Ismail, A. F.; Aziz, M.; Nagai, K.; Matsuura, T.; Abdullah, M. S.; Ng, B. C. *Desalination.* **2010**, *261*, 264.
106. Barakat, N. A. M.; Abadir, M. F.; Sheikh, F. A.; Kanjwal, M.A.; Park, S. J.; Kim, H. Y. *Chem. Eng. J.* **2010**, *156*, 487.
107. Sheikh, F. A.; Kanjwal, M. A.; Saran, S.; Chung, W.-J.; Kim, H. *Appl. Surf. Sci.* **2011**, *257*, 3020.

108. Goethal, S.A.; Mugadza, T.; Arslanoglu, Y.; Zügler, R.; Antunes, E.; Van Hulle, S.W.; Nyokong, T.; De Clerck, K. *J. Appl. Polym. Sci.* **2014**, *131*, 40486.
109. Nowakowska, M.; Kepczynski, M. *J. Photochem. Photobiol. A.* **1998**, *116*, 251.
110. Gerdes, R.; Bartels, O.; Schneider, G.; Woehrl, D.; Schulz-Ekloff, G. *Polym. Adv. Technol.* **2001**, *12*, 152.
111. Gerdes, R.; Woehrl, D.; Spiller, W.; Schneider, G.; Schruppfeil, G.; Schulz-Ekloff, G. *J. Photochem. Photobiol. A.* **1997**, *111*, 65.
112. Iliev, V.; Prahov, L.; Bilyarska, L.; Fischer, H.; Schulz-Ekloff, G.; Woehrl, D.; Petrov, L. *J. Mol. Catal. A: Chem.* **2000**, *151*, 161.
113. Spiller, W.; Woehrl, D.; Schulz-Ekloff, G.; Ford, W.T.; Schneider, G.; Stark, J. *J. Photochem. Photobiol. A.* **1996**, *95*, 161.
114. Piccirillo, C.; Perni, S.; Gil-Thomas, J.; Prokopovich, P.; Wilson, M.; Pratten, J.; Parkin, I.P. *J. Mater. Chem.* **2009**, *19*, 6167.
115. Ismail, S.; Perni, S.; Pratten, J.; Parkin, I.; Wilson, M. *Infect. Control Hosp. Epidemiol.* **2011**, *32*, 1130.
116. Naik, A.J.T.; Ismail, S.; Kay, C.; Wilson, M.; Parkin, I.P. *Mater. Chem. Phys.* **2011**, *129*, 446.
117. Perni, S.; Prokopovich, P.; Piccirillo, C.; Pratten, J.R.; Parkin, I.P.; Wilson, M. *J. Mater. Chem.* **2009**, *19*, 2715.
118. Cahan, R.; Schwartz, R.; Langzam, Y.; Nitzan, Y. *Photochem. Photobiol.* **2011**, *87*, 1379.
119. Osifeko, O.L.; Nyokong, T. *Dyes Pigm.* **2014**, *111*, 8.

120. Masilela, P.; Kleyi, Z.; Tshentu, G.; Priniotakis, P.; Westbroek, T.; Nyokong. *Dyes Pigm.* **2013**, *96*, 500.
121. Tombe, S.; Antunes, E.; Nyokong, T. *J. Mol. Catal. A. Chem.* **2013**, *371*, 125.
122. Bonnett, R.; Buckley, D.G. ; Burrow, T.; Galia, A.B.B. ; Savilleb, B.; Songca, S.P. *J. Mater. Chem.* **1993**, *3*, 323.
123. Frochot, P.; Krausz. *Biomacromolecules.* **2011**, *12*, 1716.
124. Roy, I.; Ohulchanskyy, T.Y.; Pudavar, H.E.; Bergey, E.J.; Oseroff, A.R.; Morgan, J.; Dougherty, T.J.; Prasad, P.N. *J. Am. Chem. Soc.* **2003**, *125*, 7860.
125. Ronzani, F.; Costarramone, N.; Blanc, S.; Benabbou, A.K.; Le Behec, M.; Pigot, T.; Oelgemöller, M.; Lacombe, S. *J. Catal.* **2013**, *303*, 164.
126. Pineiro, M.; Ribeiro, S.M.; Serra, A.C. *ARKIVOC***2010**, *5*, 51.
127. Guo, Y.; Rogelj, S.; Zhang, P. *Nanotechnology.* **2010**, *21*, 1.
128. Kuznetsova, N.A.; Yuzhakova, O.A.; Strakhovskaya, M.G.; Slivka, L.K.; Kaliya, O.L.; Lukyanetsa, E.A. *Macroheterocycles.* **2013**, *6*, 363.
129. Li, X.; Ramamurthy, V. *J. Am. Chem. Soc.* **1996**, *118*, 10666.
130. Smolinska, M.; Cik, G.; Sersen, F.; Caploviciva, M.; Takacova, A.; Copani, M. *Int. J. Environ. Sci. Technol.* **2015**, *12*, 61.
131. Trinidad, L.J.; Usman, K.A.; Payawan, Jr L.M. *Appl. Mech. Mater.* **2017**, *863*, 89.
132. Cenens, J.; Schoonheydt, R.A. *Clay Miner.* **1988**, *23*, 205.

133. Drozd, D.; Szczubiałka, K.; Skiba, M.; Kepczynski, M.; Nowakowska, M. *J. Phys. Chem. C* **2014**, *118*, 9196.
134. Madhavan, D.; Pitchumani, K. *Tetrahedron*. **2001**, *57*, 8391.
135. Caine, M.A.; McCabe, R.W.; Wang, L.; Brown, R.G.; Hepworth, J.D. *Dyes Pigm.* **2001**, *493*, 135.
136. Bujdak, J.; Jurecekova, J.; Bujadakova, H.; Lang, K.; Sersen, F. *Environ. Sci. Technol.* **2009**, *43*, 6202.
137. Chen, Y.; Qi, Y.; Liu, B. *J. Nanomater.* **2013**, *2013*, 1.
138. Liu, J.-H.; Wang, T.; Wang, H.; Gu, Y.; Xu, Y.; Tang, H.; Jia, G.; Liu, Y. *Toxicol. Res.* **2015**, *4*, 83.
139. Hosseinzadeh, R.; Khorsandi, K.; Hosseinzadeh, G. *J. Biomol. Struct. Dyn.* **2017**, *6*, 1.
140. Wojtoniszak, M.; Rogin´ ska, D.; Machalin´ ski, B.; Drozdziak, M.; Mijowska, E. *Mater. Res. Bull.* **2013**, *48*, 2636.
141. Zhou, L.; Wang, W.; Tang, J.; Zhou, J.H.; Jiang, H.J.; Shen, J. *Chem. Eur. J.* **2011**, *17*, 12084.
142. Bachmann, B. *J. Microbiol. Rev.* **1990**, *54*, 130.
143. Bertoloni, G.; R. Sacchetto.; G. Jori.; Vernon, D. I.; Brown, S. B. *Lasers Life Sci.* **1993**, *5*, 267.
144. Bertoloni, G.; B. Salvato.; Dall' Acqua, M.; Vazzoler, M.; Jori. G. *Photochem. Photobiol.* **1984**, *39*, 811.
145. Malik, Z.; H. Ladan; Nitzan, Y. *J. Photochem. Photobiol. B.* **1992**, *14*, 262.
146. Nikaido, H. *J. Bacteriol.* **1996**, *178*, 5853.

147. Nikaido, H.; Vaara, M. *Microbiol. Rev.* **1985**, *49*, 1.
148. Plesiat, P.; Nikaido, H. *Mol. Microbiol.* **1992**, *6*, 1323.
149. Vaara, M. *Microbiol. Rev.* **1992**, *56*, 395.
150. Costa, L.; Alves, E.; Carvalho, C.M.; Tomé, J.P.; Faustino, M.A.; Neves, M.G.; Tomé, A.C.; Cavaleiro, J.A.; Cunha, Â.; Almeida, A. *Photochem. Photobiol. Sci.* **2008**, *7*, 415.
151. Orlandi, V.T.; Caruso, E.; Tettamanti, G.; Banfi, S.; Barbieri, P. *J. Photochem. Photobiol. B.* **2013**, *127*, 123.
152. Kehrmann, F.; Wentzel, F. *Ber. Dtsch. Chem. Ges.* **1901**, *34*, 3815.
153. Norris, J. F.; Franklin, A. I. *J. Am. Chem. Soc.* **1899**, *21*, 499.
154. Duxbury, D. F. *Chem. Rev.* **1993**, *93*, 381.
155. Waring, D. R.; Hallas, G. *The Chemistry and Application of Dyes*; Plenum Press: New York, N.Y, 1990.
156. Mason, W. T. *Fluorescent and Luminescent Probes for Biological Activity, Second Edition: A Practical Guide to Technology for Quantitative Real-Time Analysis*; Academic: London, U.K, 1999.
157. Martin, J. C.; Smith, R. G. *J. Am. Chem. Soc.* **1964**, *86*, 2252.
158. Arnett, E.M.; Flowers, R.A., II in "Coordination and Electron Transfer to Carbocations - Direct Access to Heterolysis and Homolysis Energies in Solution; Stable Carbocation Chemistry, G.K. Surya Prakash; P. von R. Schleyer, Eds.; John Wiley & Sons: N.Y, 1997; pp 265-296.
159. Bunting, J. W.; Meathrel, W. G. *Can. J. Chem.* **1973**, *51*, 1965.
160. Laursen, B. W.; Krebs, F. C. *Angew. Chem. Int. Ed. Engl.* **2000**, *39*, 3432.

161. Laursen, B. W.; Krebs, F. C. *Chem. Eur. J.* **2001**, 7, 1773.
162. Dileesh, S.; Gopidas, K.R.J. *Photochem. Photobiol. A* **2004**, 162, 115.
163. Reynisson, J.; Schuster, G.B.; Howerton, S.B.; Williams, L.D.; Barnett, R.N.; Cleveland, C.L.; Landman, U.; Harrit, N.; Chaires, J.B. *J. Am. Chem. Soc.* **2003**, 125, 2072.
164. Nicolas, C.; Lacour. *J. Org. Lett.* **2006**, 8, 4343.
165. Sørensen, T.J.; Thyraug, E.; Szabelski, M.; Luchowski, R.; Gryczynski, I.; Gryczynski, Z.; Laursen, B.W. *Methods Appl. Fluoresc.* **2013**, 1, 025001.
166. Shivalingam, A.; Vyšniauskas, A.; Albrecht, T.; White, A.J.; Kuimova, M.K.; Vilar, R. *Chem. Eur. J.* **2016**, 22, 4129.
167. Cummins, B.; Simpson, J.; Gryczynski, Z.; Sørensen, T.J.; Laursen, B.W.; Graham, D.; Birch, D.; Coté, G. *In Optical Diagnostics and Sensing XIV: Toward Point-of-Care Diagnostics.* **2014**, 8951, 89510A.

CHAPTER 2

Synthesis, Photophysical and Singlet Oxygen Generation Studies of a Few Water Soluble Triazatriangulenium Salts

2.1. Abstract

In this chapter we report the synthesis, studies on photophysical properties and singlet oxygen generation of a few water soluble triazatriangulenium (TATA) cations. The photophysical studies such as steady – state and time - resolved absorption and emission spectroscopy were carried out in acetonitrile as well as in water. The respective absorption maxima, singlet and triplet state energy levels, their lifetimes and quantum yields were determined. The triplet state properties were determined using nanosecond laser flash photolysis studies. The quantum efficiency of singlet oxygen generation was estimated by chemical actinometry using disodium-9,10-anthracenedipropionic acid (ADPA) and 1,3-diphenylisobenzofuran (DPBF) as the chemical actinometers and rose bengal as the reference. The apparent quantum yield for singlet oxygen generation by these cations was found to be 0.36 in water and 0.21 in acetonitrile.

2.2. Introduction

For a dye to be used as a sensitizer in aqueous medium it must satisfy the following requirements:

1. Should have excellent thermal stability
2. Should have excellent photochemical stability

3. Should be stable for wide range pH
4. Good solubility in aqueous medium
5. Long wavelength absorption maximum and suitable excited state properties to act as a singlet oxygen sensitizer.
6. No reactivity to singlet oxygen and other reactive oxygen species such as peroxides, hydroperoxides or dioxetanes generated from singlet oxygen induced reactions of substrates other than the sensitizer.

The commonly used singlet oxygen sensitizers are represented in Chart 2.1

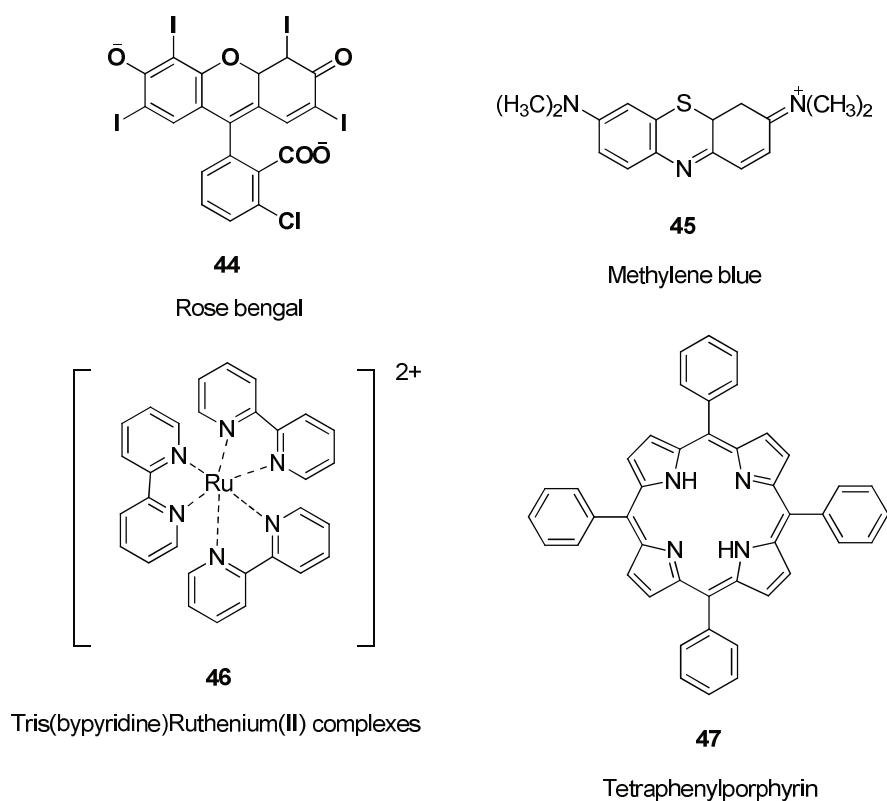


Chart 2.1

Rose Bengal (RB) is an anionic water soluble xanthene singlet oxygen sensitizer widely used as a reference sensitizer, as light active agent

in photooxidation, photodynamic therapy or in disinfection reactions. It is soluble in water with λ_{max} 549 nm. The peculiar properties of rose bengal are large molar extinction coefficient, high solubility and high quantum yield of singlet oxygen generation (0.76). It is soluble in water up to a concentration of 10^{-3} M but at higher concentration H-type aggregates are formed with lower molar absorptivity.¹⁻⁴ In non-polar solvents rose bengal is photochemically unstable compared to the situation in polar protic solvents. The uptake and intracellular localization of a photosensitizer in cells is crucial to the photodynamic process.⁵ The low lipid solubility and anionic nature of rose bengal limit its capacity to cross biological barriers such as cell membranes. Consequently, its clinical application remains limited, but with the help of drug carriers such as liposomes or use of the acylated rose bengal derivative this sensitizer have been used with some success in some of the photobiological applications.^{6,7} Photobleaching was also observed in the case of rose bengal during irradiation especially in aqueous solutions.⁸

Methylene blue (MB) is another water-soluble cationic dye used in the clinical applications of photodynamic therapy. The high molar extinction coefficient, good singlet oxygen quantum yield, minimal dark toxicity are its advantages.^{9, 10} The dye is prone to aggregation at higher concentrations and also it is not a specific type II photosensitizer. Type I photooxidation pathways are also reported for this sensitizer. Because of the poor cell/tissue accumulation and low biological activity in the free molecular form its use in *in vivo* PDT of cancer is limited.¹¹⁻¹³

Porphyrin derivatives are well known singlet oxygen sensitizers because of their unique photochemical and photophysical properties.¹⁴ The delocalized 18π electrons present in the porphyrin system is responsible for the large absorption and strong emission characteristics in the visible region.¹⁵ Among the porphyrins tetraphenylporphyrins (TPP) are the widely

used molecules. It possess some disadvantages such as poor solubility, low singlet oxygen efficiency and photodegradation.¹⁶ Aggregation is another limitation possessed by the porphyrin derivatives.¹⁷

The unique properties of the transition metal complexes make them as a suitable platform for making new singlet oxygen sensitizers.¹⁸ These compounds undergo rapid intersystem crossing because of heavy atom effect.¹⁹ Transition metal complexes of Ruthenium (II) with polypyridyl ligands are the most studied group because of the straight forward synthesis and excellent visible light absorption properties.²⁰ The photoinitiated decomposition arising from the population of the low-lying dd states limits the use of ruthenium polypyridyl complexes in photochemical applications.²¹ Poor water solubility is another problem observed in many ruthenium complexes. The $\text{Ru}(\text{bpy})_3^{2+}$ undergoes photooxidation in aqueous acidic solution containing the dissolved oxygen.²²

Aggregation of the sensitizers, pH or ionic strength effects, competitive formation of superoxide ions are the main problems associated with the singlet oxygen sensitizers in aqueous condition. The main applications of singlet oxygen sensitizers are in water disinfection, photodynamic therapy and in organic synthesis. The focus of the thesis is the development of photochemically and thermally stable photosensitizer systems with a wide range of pH stability when used in aqueous media. Also sensitizers with specific type II photooxidation pathway are also important for the apoptotic cell death than the necrotic pathway where the reactive enzymes in the cells spread easily to other locations in the tissue. Another desirable factor is the control of solubility and lipophilicity by suitable chemical modifications. Also chemical modifications to achieve tumour or carcinoma targeting with minimal dark toxicity is a criterion while choosing sensitizer systems for photobiological applications. For example presence of

positive charges, conjugation to nanoparticles, graphene and other 2D layered materials, monoclonal antibodies etc. were found to have added advantages in tumour targeting. In the present chapter we propose the use of a well known triazatriangulenium cation as a potential singlet oxygen sensitizer. The known derivatives are insoluble in water and have very poor solubility in non-aqueous media. A series of triazatriangulenium cations are designed such that it has high solubility in water with groups to control lipophilicity. Being cationic we expect triazatriangulenium cations can have better tumour targeting as well as activity towards gram negative pathogens.

To improve solubility of the proposed dye we plan to introduce polar groups such as hydroxyl, amino, carboxylic acid, sulfonic acid or phosphoric acid group either on the aromatic rings or as part of the N-alkyl side chains. Substitution of the aromatic rings with polar groups is synthetically demanding as the synthesis of the parent triaryl cation requires protection deprotection strategies. Such substitution may also alter the electronic properties of the triaryl cation and may not undergo efficient aryl-aryl bridging reaction to produce the triangulenium cation. Substitution of the side chain is a viable synthesis strategy to achieve very good solubility in polar medium. This strategy is not synthetically demanding and one can use a modified synthesis strategy that uses the method reported by Krebs and coworkers.^{23,24} In the present thesis we propose to use aminoalcohols as the reagents for the aromatic nucleophilic substitution based bridging reaction of the three phenyl rings in the triphenyl cation derivative (**39**). The structures of the proposed cations are given in chart 2.2.

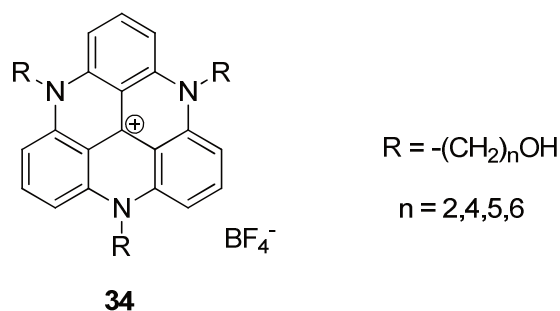
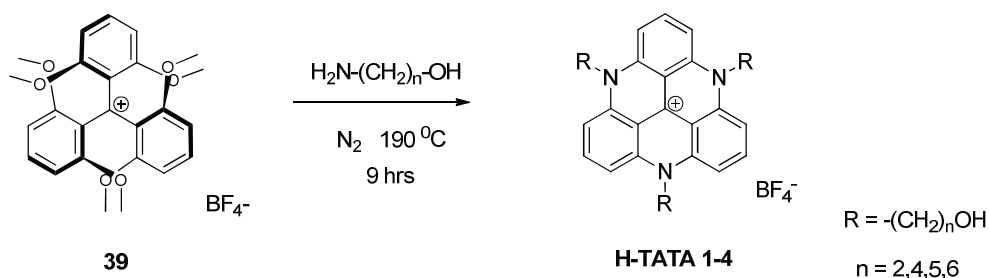


Chart 2.2

2.3. Results and Discussion

2.3.1. Synthesis of hydroxyl group bearing triazatriangulenium cations (H-TATA 1-4)

Tris-(2,6-dimethoxyphenyl) carbenium tetrafluoroborate (**39**) is synthesized according to a reported procedure.²⁵ The N-alkyl substituted triazatriangulenium cations (**H-TATA1-4**) were prepared from **39** using literature procedure reported by Krebs, F. C. and coworkers (Scheme 2.1).^{23,24}



Scheme 2.1

These cations were initially formed as their tetrafluoroborates and were soluble in aqueous medium. However, tetrafluoroborates are not very stable in aqueous medium as these anions are known to hydrolyse under acidic and alkaline pH and ambient temperatures.²⁶ One of the product of this hydrolysis reaction is HF where solvent molecule does a nucleophilic

displacement of fluorine on the tetrafluoroborate anion.²⁷ This is not desirable for potential applications of this molecule as a sensitizer because, the product HF is corrosive and may interfere with the chemistry under study. An alternative is to do an ion exchange by using KPF_6 where a saturated solution of KPF_6 in water was added to an aqueous solution of the tetrafluoroborate salt. The hexafluorophosphate salt was insoluble in water and precipitated and was purified by repeated washing with water. The hexafluorophosphate was found to dissolve in aqueous saline medium (0.1 M NaCl) with 1-1.5 mg/mL solubility with the cation having six carbon side chain showing maximum solubility. **H-TATA PF₆** (**H-TATA1- 4**) thus prepared were characterized using ^1H NMR, ^{13}C NMR, FT-IR and mass spectrometry (ESI-MS).

2.3.2. Photophysical studies

2.3.2.1. Absorption spectra of triazatriangulenium salts

Absorption spectra of the tri-N-alkyltriazatriangulenium salts in acetonitrile were reported earlier by Laursen and Krebs.²³ **H-TATA 1-4** were also showing a similar spectral profile. The compounds show absorption bands in the 250-570 nm region. The absorption band around 270 nm is very intense and sharp. There are two relatively weak bands, one at 350 nm and the other centered around 530 nm. The absorption spectrum of **H-TATA1-4** in water (0.1 M NaCl) and acetonitrile is shown in figure 2.1. The spectral profile observed in acetonitrile was similar to the one reported for the N-butyl bridged triazatriangulenium cations. In water (0.1 M NaCl) the spectrum is red shifted by 5 nm compared to that in acetonitrile with the shoulder band at 505 nm. A concentration dependence on spectral profile was studied by recording the absorption spectrum at various concentrations and no change in the spectral profile was observed.

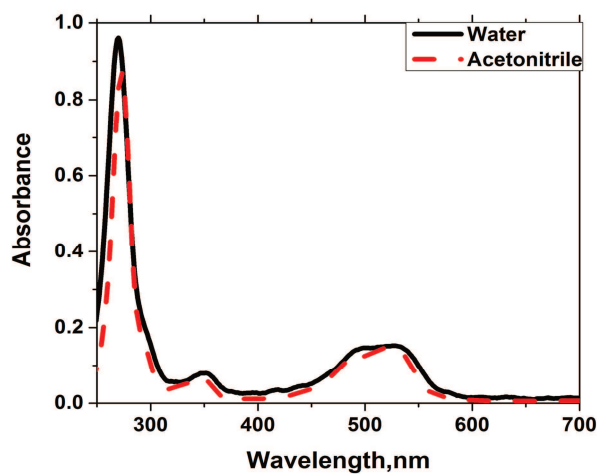


Figure 2.1 Comparison of normalized absorption spectrum of H-TATA1 in acetonitrile and water

Since at higher concentration the spectrum is devoid of any profile changes one can rule out the aggregation of dye under the concentration range used for our studies. Figure 2.2 and 2.3 show the spectra obtained for **H-TATA 1** at two different concentrations in acetonitrile and water (0.1 M NaCl).

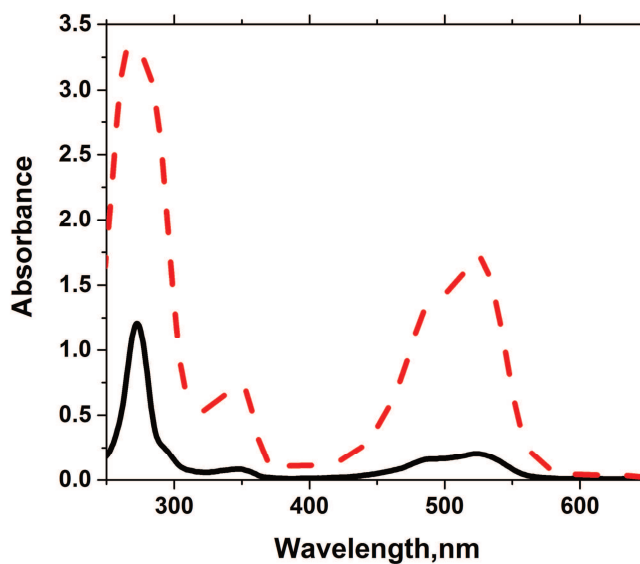


Figure 2.2 Absorption spectra of H-TATA 1 in acetonitrile at 1.7×10^{-5} M (---) and 1.7×10^{-6} M (—)

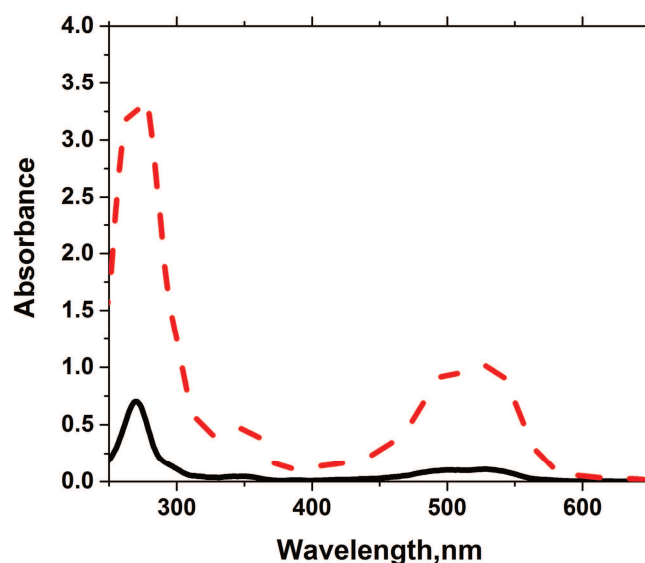


Figure 2.3 Absorption spectra of H-TATA 1 in water at 1.7×10^{-5} M (---) and 1.7×10^{-6} M (—)

2.3.2.2. Fluorescence spectra of triazatriangulenium salts

The fluorescence emission spectra of the H-TATA cations were recorded in both acetonitrile and water (0.1 M NaCl) by exciting at 480 nm. All compounds exhibited the fluorescence in the 500-700 nm region with no significant changes in the emission spectral profile. Figure 2.4 is a typical fluorescence spectrum recorded for **H-TATA 1** in water (0.1 M NaCl) and acetonitrile. The compound shows a red shifted emission at 571 nm in water (0.1 M NaCl) compared to the emission maximum at 558 nm in acetonitrile. In solutions saturated with nitrogen the emission intensity was marginally increased by about 15% of the corresponding solution under air saturation. All the fluorescence experiments were carried out in air equilibrated solutions.

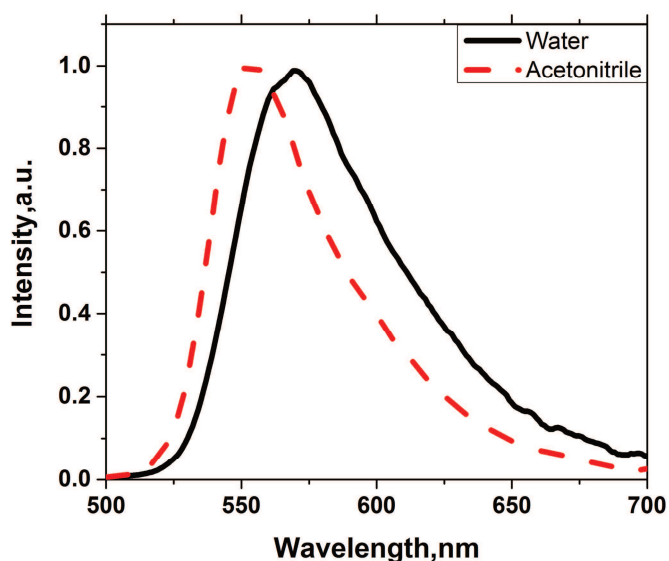


Figure 2.4 Normalized emission spectra of the compound H-TATA 1 in acetonitrile (---) and water (—), $\lambda_{\text{ex}}=480$ nm

The fluorescence quantum yield (Φ_F) of the compounds was determined in water (0.1 M NaCl) and acetonitrile by using the method of relative actinometry. Optically matched solution of Rhodamine-6G in ethanol was used as the standard and the following equation was used for calculation.

$$\Phi_F = \frac{A_S F_U N_S^2}{A_U F_S N_U^2} \times \Phi_S \quad (2.1)$$

Where the subscripts 'S' and 'U' represent the standard and unknown respectively. A_S and A_U , are the optical densities at the excitation wavelength. F_S , and F_U , are the peak areas of the fluorescence spectrum. N_S , and N_U are the refractive indices of the solvents used and Φ_S , is the fluorescence quantum yield of the standard. We have used a value of $\Phi_S=0.90$ for the standard in ethanol.²⁸

The fluorescence decay profiles of the compounds were obtained by the method of Time Correlated Single Photon counting (TCSPC) in water (0.1 M NaCl) and acetonitrile. The decay was found to be monoexponential for all compounds in both solvents and no significant changes in fluorescence lifetime was observed in the absence of air. The figure 2.5 shows a typical fluorescence decay profile obtained for **H-TATA 1** in water (0.1 M NaCl) and acetonitrile.

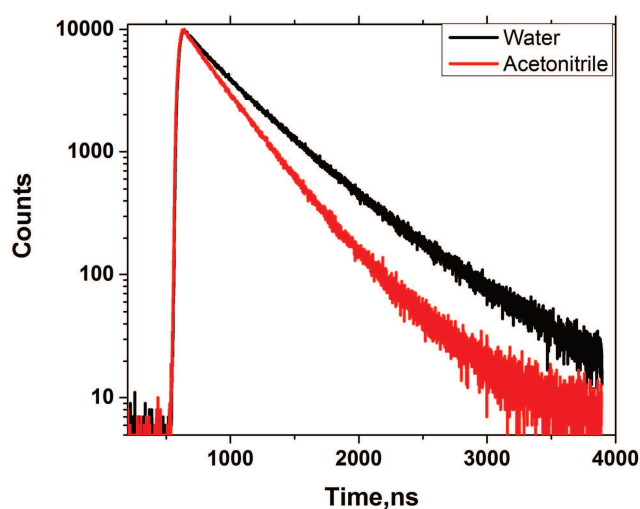


Figure 2.5 The fluorescence decay profile ($\lambda_{\text{ex}} = 510 \text{ nm}$ & $\lambda_{\text{em}} = 560 \text{ nm}$) for H-TATA 1 in acetonitrile and water (0.1 M NaCl).

The radiative and non radiative rate constants of all the samples were determined using the equations 2.2 and 2.3.

$$k_r = \frac{\Phi}{\tau} \quad (2.2)$$

$$k_{\text{nr}} = \frac{(1-\Phi)}{\tau} \quad (2.3)$$

Where Φ and τ are the fluorescence quantum yield and fluorescence lifetime respectively.

The photophysical properties of the compounds **H-TATA 1-4** in acetonitrile and water (0.1 M NaCl) are summarized in table 2.1. The singlet state energy for the compounds **H-TATA 1-4** was estimated from the point of intersection of the absorption and fluorescence spectra and the value obtained was 53 kcal M⁻¹

Table 2.1 Absorption maximum ($\lambda_{\max}(\text{abs})$), extinction coefficient (ϵ_{\max}), emission maximum ($\lambda_{\max}(\text{em})$), singlet lifetime (τ_F) and singlet quantum yield Φ_F of triazatriangulenium salts in acetonitrile and water (0.1 M NaCl). Values given in parentheses are those obtained in acetonitrile.

Compounds	$\lambda_{\max}(\text{abs})$ nm	$\epsilon_{\max}^{\text{M}^{-1}\text{cm}^{-1}}$ $^1(\log \epsilon)$	$\lambda_{\max}(\text{em})$ nm	Φ_F	τ_F ns	$k_r(\text{s}^{-1})$ $\times 10^{-2}$	$k_{nr}(\text{s}^{-1})$ $\times 10^{-2}$
H-TATA 1	530 (525)	4.6(5)	571 (558)	0.15 (0.20)	11 (8.1)	1.36 (2.46)	7.72 (9.8)
H-TATA 2	530 (525)	4.6(5)	571 (558)	0.15 (0.20)	10.9 (8.1)	1.37 (2.46)	7.79 (9.8)
H-TATA 3	530 (525)	4.6(5)	571 (558)	0.15 (0.20)	10.5 (8.2)	1.42 (2.43)	8.09 (9.7)
H-TATA 4	530 (525)	4.6(5)	571 (558)	0.15 (0.20)	10.5 (8.1)	1.42 (2.46)	8.09 (9.8)

2.3.2.3. Phosphorescence spectra of triazatriangulenium cations

The low fluorescence quantum yield of the prepared cations suggests alternative modes of deactivation of their singlet excited states. This has prompted us to look for phosphorescence emission of the cations. It was

observed that the compounds exhibited the phosphorescence at 77 K in ethanol glass with an emission maximum at 563 nm. The phosphorescence spectrum obtained for **H-TATA 1** at 50 μ s delay after the excitation flash in ethanol glass at 77 K is given in figure 2.6.

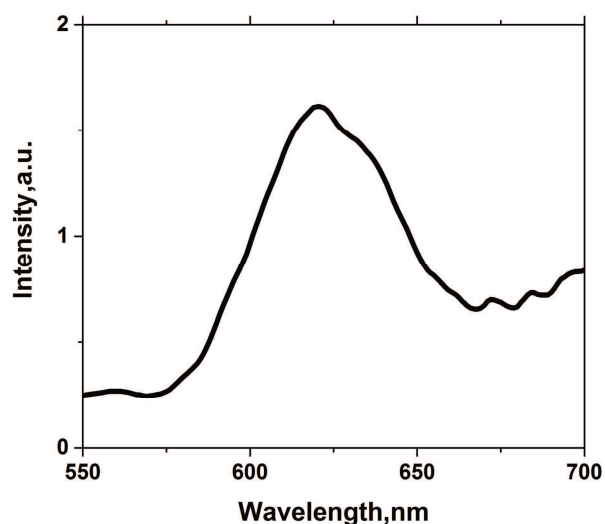


Figure 2.6 Phosphorescence spectrum of triazatriangulenium salt (H-TATA 1) in ethanol glass at 77 K

The triplet energy of 49.72 kcal M^{-1} was estimated from the point of intersection between the normalized excitation and phosphorescence spectra, i.e., the wavelength corresponding to the 0-0 band position in the phosphorescence spectrum. The photophysical studies thus enabled us to determine the energy levels of first singlet and triplet excited states of these compounds. A schematic diagram showing the singlet and triplet energy level is given in figure 2.7. The S-T energy gap for the compounds is estimated as 3.28 kcal M^{-1} .

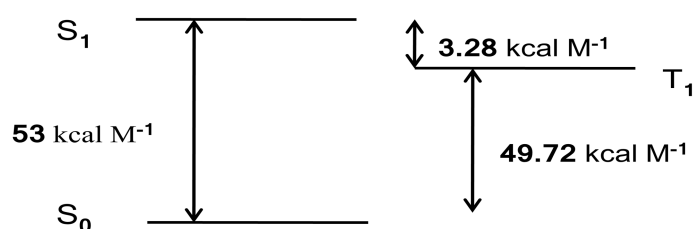


Figure 2.7 Schematic representation of various energy levels of triazatriangulenium salts.

2.3.2.4. Thermally Assisted Delayed Fluorescence (TADF) in triazatriangulenium cations

The effect of oxygen on the fluorescence intensity and the small singlet - triplet energy gap in these molecules prompted us to investigate on the occurrence of a delayed emission. Such small singlet – triplet energy gap can cause thermally assisted reverse intersystem crossing between triplet and singlet states leading to the observation of a delayed emission as shown in figure 2.8. This reverse intersystem crossing is thermally activated and its efficiency increases with decrease in the singlet – triplet energy gap.

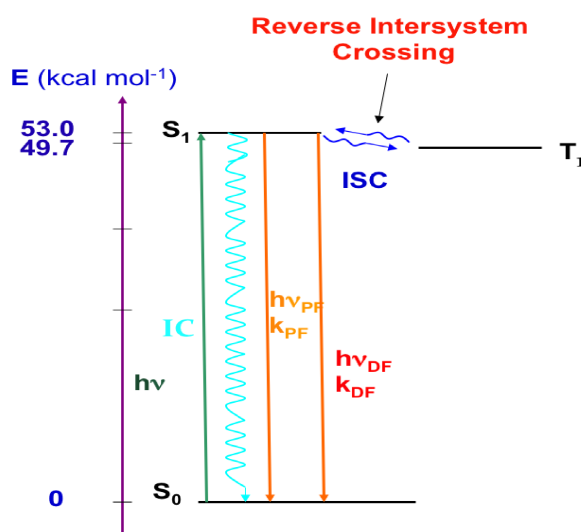


Figure 2.8 Energy level diagram showing TADF emission in the triazatriangulenium cations

Delayed emissions were recorded on a Phosphorescence spectrometer with a pulsed xenone lamp and the spectra were recorded at a delay of 10 - 50 μs after the excitation pulse. All compounds were showing delayed emission both in acetonitrile and water. The lifetime of the delayed fluorescence was also recorded in these solvents in both air saturated and nitrogen saturated solutions. To confirm the existence of reverse intersystem crossing and the observation of the delayed emission we have recorded the emission spectrum of an air saturated solution and nitrogen saturated solution with the pulsed xenon lamp as the excitation source. Here we have observed an approximately four fold enhancement in the emission intensity for nitrogen saturated solutions. This result indicates the quenching of a fraction of the triplet states by oxygen in air leading to a reduction in the population of triplet states in comparison to the solution under nitrogen saturation. This oxygen quenching leads to a decrease in the number of molecules adopting the pathway leading to thermally activated reverse intersystem crossing and results in a reduced intensity for the delayed emission (figure 2.9 and 2.10). This confirms the role of triplet states in the delayed emission and the observed emission is an E-type delayed emission. The emission decay profile was also recorded after an initial delay of 25 μs for nitrogen saturated and air saturated solutions of **H-TATA 1**. The decay profiles were analysed and fitted to exponential decay function. Figure 2.11 show the decay profiles and the fitted curves. Both decays gave good fit to a single exponential function and obtained emission lifetimes as 15 μs and 4 μs respectively for the nitrogen saturated and air saturated solutions. The value obtained in the absence of air is very close to the value of triplet lifetime obtained for the same compound in water in the absence of oxygen.

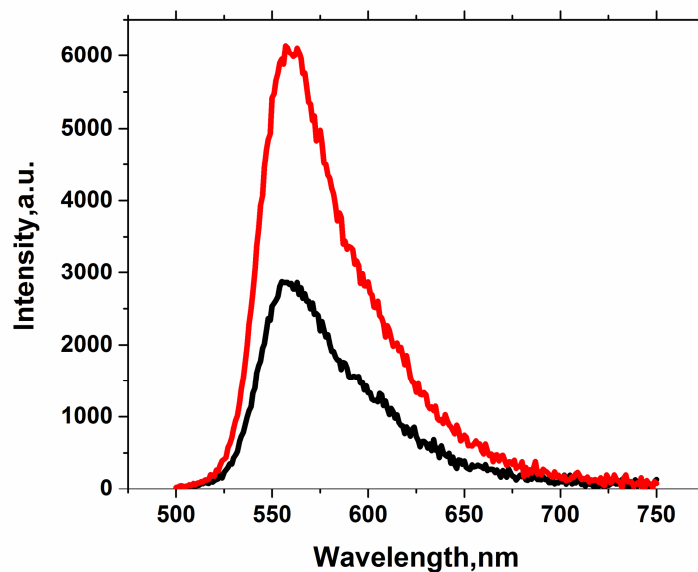


Figure 2.9 Delayed emission observed for H-TATA 1 in air saturated (—) and nitrogen saturated solution in acetonitrile (—)

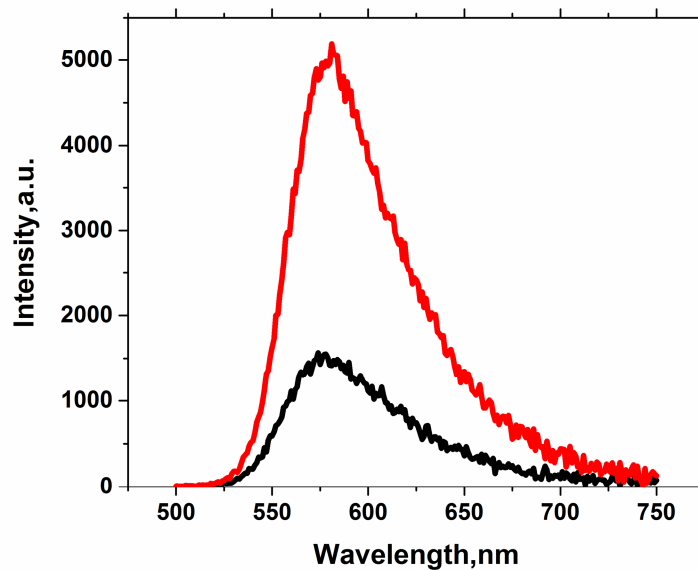


Figure 2.10 Delayed emission observed for H-TATA 1 in air saturated (—) and nitrogen saturated solution in water (0.1 M NaCl) (—)

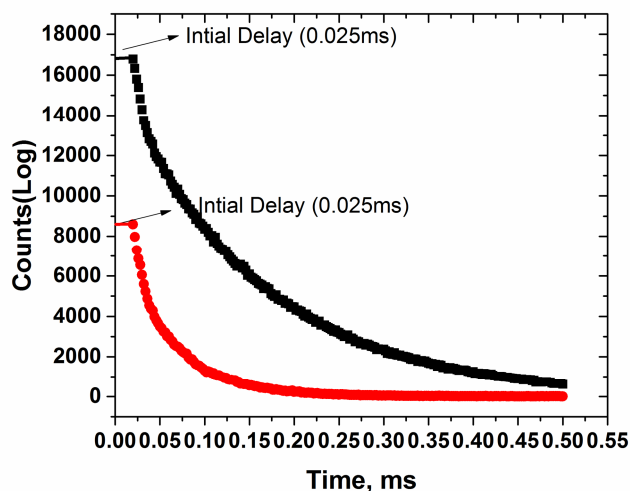


Figure 2.11 TADF decay profiles of H-TATA 1 recorded in water (●) and acetonitrile (●)

2.3.2.5. Laser flash photolysis

Laser flash photolysis experiments are carried out to characterize the triplet excited state properties of the triazatriangulenium compounds. These data are essential to assess the feasibility of triplet oxygen sensitization by these dyes. From the calculated triplet state energy it is clear that these compounds have suitably placed triplet excited state to facilitate energy transfer to molecular oxygen. The flash photolysis experiments were carried out in argon saturated acetonitrile and water (0.1 M NaCl) as solvents. Excitation of the compounds was made by using the 532 nm second harmonic output from a Nd:YAG laser and the transient changes in the concentration of the ground and excited state species were probed by using a kinetic spectrometer. The pulse width of the laser was 7 ns and used focussing optics for an orthogonal excitation of the samples. The kinetic spectrometer used a 150 W pulsed xenon lamp and absorbance changes were monitored at 10 nm intervals using a monochromator, PMT and a digital storage oscilloscope. The spectra obtained for **H-TATA 1** in acetonitrile and

water (0.1 M NaCl) at various time intervals after the laser pulse are given in figures 2.12 and 2.13 respectively. All compounds showed similar transient absorption spectrum and did not show any significant change according to the length of the side chain.

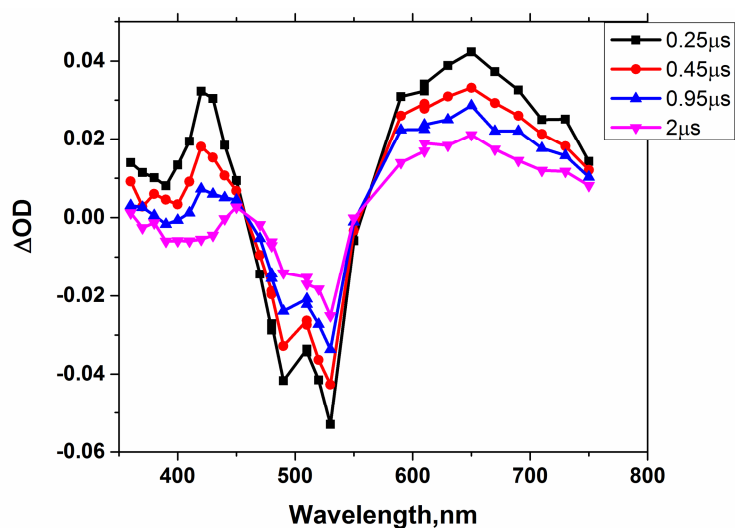


Figure 2.12 The transient absorption spectrum of H-TATA 1 in acetonitrile recorded with different time delays after laser excitation. ($\lambda_{\text{ex}}=532$ nm)

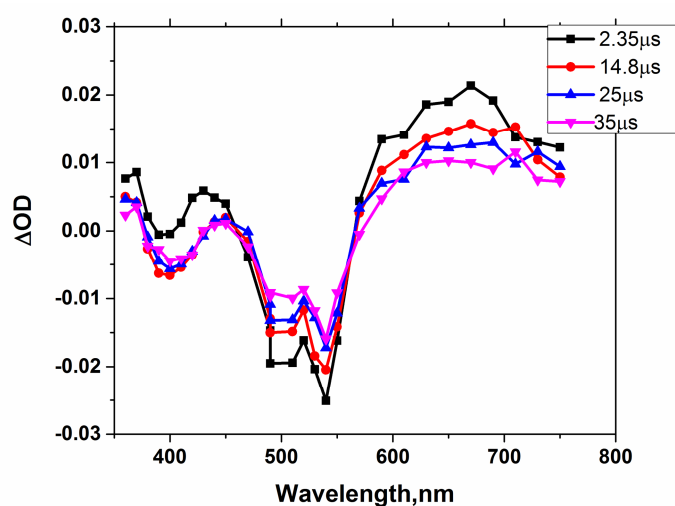


Figure 2.13 The transient absorption spectrum of H-TATA 1 in water (0.1 M NaCl) recorded with different time delays after laser excitation. ($\lambda_{\text{ex}}=532$ nm).

The transient absorption spectrum thus obtained in acetonitrile showed absorption maxima at 370 nm, 420 nm and 650 nm with a bleaching in the 450-600 nm region. The bleaching in the 450-600 nm region correspond well with the ground state absorption of the compounds. A similar spectrum was also obtained for the compounds in water (0.1 M NaCl). Figures 2.14 and 2.15 show the transient decay profiles obtained at 650 nm and at 530 nm for H-TATA 1 in acetonitrile and water (0.1 M NaCl) respectively. The decay profiles obeyed first order decay kinetics and the estimated triplet excited state lifetime was 1.85 μs and 21.6 μs in acetonitrile and water (0.1 M NaCl) respectively.

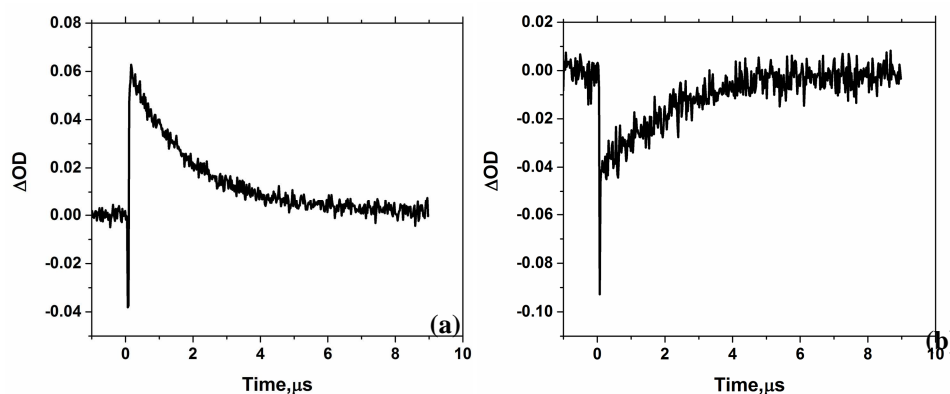


Figure 2.14 Kinetic profiles of H-TATA 1 in acetonitrile recorded at (a) 650 nm and (b) 530 nm.

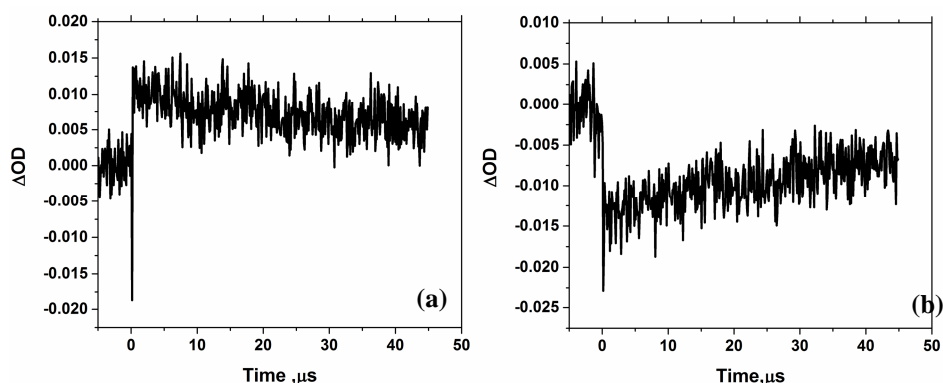


Figure 2.15 Kinetic profiles of H-TATA 1 in water (0.1 M NaCl) recorded at (a) 650 nm and (b) 530 nm.

Triplet excited states interact with oxygen which also has a triplet multiplicity leading to quenching of the triplet states. This interaction can be both a physical deactivation to the ground state or an energy transfer to the oxygen singlet state. This energy transfer process is possible because the calculated triplet energy of these cations lie well above the singlet energy of oxygen molecule. All compounds show efficient triplet quenching indicated by a faster decay in both air saturated and oxygen saturated solutions. Hence, the observed bands in the transient absorption spectrum can be assigned to the triplet state of these compounds. The observation of a bleach or negative difference absorption corresponding to the absorption maximum of the studied compounds lead us to determine the molar extinction coefficient of triplet – triplet absorption (T-T absorption) by the method of singlet depletion.²⁹ In this method it is assumed that the optically pumped molecules completely return either to the S_0 state or populate the lowest triplet state within the time scale of observation. Under these conditions, the change in optical density can be expressed by equation 2.4.

$$\Delta OD = (\epsilon_T - \epsilon_S) [^3M] l \quad (2.4)$$

In equation 2.4, [3M] is the concentration of the triplet states present at the time of observation, l is the optical path length of the solution, ϵ_S is the extinction coefficient of the S_0 - S_n absorption at the monitoring wavelength and ϵ_T is the extinction coefficient of the T-T absorption at this wavelength. If the bleaching minimum (λ_1 , largest negative absorption) coincides with the absorption maximum of the compound, then it is generally assumed that the triplet does not absorb at this wavelength (i.e., $\epsilon_T = 0$). Under this condition equation 2.4 reduces to equation 2.5.

$$\Delta OD (\lambda_1) = - \epsilon_S [^3M] l \quad (2.5)$$

In equation 2.5 ΔOD is the change in the optical density due to singlet depletion at λ_1 . Since ϵ_S at λ_1 is known, the concentration of the triplet species ($[^3M]$) can be calculated using equation 2.5. If $[^3M]$ is known, ϵ_T at all wavelengths can be calculated using equation 2.4. Using this method, we obtained a value around $5400 \text{ M}^{-1}\text{cm}^{-1}$ for ϵ_T at 650 nm for the compounds in water and around $8100 \text{ M}^{-1}\text{cm}^{-1}$ for ϵ_T at 650 nm in acetonitrile. Once the extinction coefficient of the T-T absorption is known, the triplet quantum yield (Φ_T) can be estimated using the method of relative actinometry.³⁰ Decay profiles at respective T-T absorption maxima of optically matched solutions at excitation wavelength (532 nm), for the reference compound and the compounds studied were obtained. Triplet quantum yield (Φ_T) was estimated by using the equation 2.6.

$$\Phi_T = \frac{\Phi_R \Delta OD_T \epsilon_R}{\Delta OD_R \epsilon_T} \quad (2.6)$$

In Equation 2.6, T refers to the triplet of the compounds and R refers to a reference compound. Φ 's are the quantum yields, ϵ 's are the extinction coefficients and ΔOD 's are the end-of pulse optical densities of the transients. In our study we have used an aqueous solution of the Tris-(2,2'-bipyridine)Ruthenium(II)chloride($[\text{Ru}(\text{bpy})_3]^{2+}$) as the reference. For the reference, we have used $\Phi_R=0.95$ and $\epsilon_R= 27300 \text{ M}^{-1}\text{cm}^{-1}$ at 370 nm in acetonitrile and water to estimate the Φ_T values of triazatriangulenium cations.²⁹ Using these values, we obtained the quantum yield of intersystem crossing or the quantum yield of triplet excited state as $\Phi_T= 0.64$ in acetonitrile and $\Phi_T= 0.68$ in water for the compounds. The triplet state properties of the compounds **H-TATA 1-4** are summarized in **table 2.2**.

Table 2.2 Triplet-triplet absorption maxima ($\lambda_{\text{max}}^{\text{T}}(\text{abs})$), extinction coefficients ($\epsilon_{\text{max}}^{\text{T}}$), Triplet quantum yield (Φ_{T}), triplet lifetime (τ_{T}), Triplet energy (E_{T}), oxygen quenching rate constant ($k_{\text{q}}(\text{O}_2)$) for **H-TATA 1-4** in water. Values given in parenthesis are those recorded in acetonitrile.

	$\lambda_{\text{max}}^{\text{T}}(\text{abs})$ nm	$\epsilon_{\text{max}}^{\text{T}}(\text{abs})$ $\text{M}^{-1} \text{cm}^{-1}$	Φ_{T}	$\tau_{\text{T}} \mu\text{s}$	E_{T} eV	$k_{\text{q}}(\text{O}_2)$ $\text{M}^{-1} \text{s}^{-1}$
H-TATA 1	650 (650)	5.43×10^3 (8.0×10^3)	0.68 (0.64)	21.6 (1.85)	2.11 (2.11)	1.41×10^7 (1.9×10^6)
H-TATA 2	650 (650)	5.45×10^3 (8.1×10^3)	0.68 (0.64)	27.2 (1.52)	2.11 (2.11)	1.43×10^7 (1.9×10^6)
H-TATA 3	650 (650)	5.43×10^3 (8.1×10^3)	0.68 (0.64)	21.6 (1.67)	2.11 (2.11)	1.41×10^7 (1.9×10^6)
H-TATA 4	650 (650)	5.42×10^3 (8.1×10^3)	0.68 (0.64)	27.3 (1.95)	2.11 (2.11)	1.42×10^7 (1.9×10^6)

2.3.2.6. Laser flash photolysis studies: Triplet quenching by oxygen

In order to study the kinetics of interaction of the triplets of triazatriangulenium cations by oxygen we have carried out the flash photolysis experiments in the presence of air, oxygen and argon. The solutions used for the study was saturated with respective gases. We have observed that the triplet absorption due to **H-TATA 1** at 650 nm is quenched very efficiently by oxygen indicated by faster decay dynamics in air or oxygen saturated solutions. The decay rate constants were estimated by using the triplet decay profiles as well as the ground state bleach recovery profiles. The decay rate constants obtained under these three oxygen concentrations were analysed by Stern - Volmer method and calculated the rate constant for oxygen quenching. The bimolecular quenching rate constants were obtained by plotting the data according to equation 2.7.

$$k_{\text{obs}} = k_0 + k_q^T [\text{Q}] \quad (2.7)$$

In equation 2.7 $k_0 = (1/\tau_0)$ is the decay rate in the absence of any quencher and k_q^T represents the triplet quenching constant. The decay profiles observed in argon, air and oxygen saturated solutions of these compounds in acetonitrile and water (0.1 M NaCl) are presented in figure 2.16 and 2.17 respectively. The solubility of oxygen is higher in acetonitrile than in water. The k_q^T values obtained for the prepared triazatriangulenium cations were of the order of $10^7 \text{ M}^{-1} \text{ s}^{-1}$ and indicating a very efficient quenching interaction with oxygen. The values obtained are given in table 2.2.

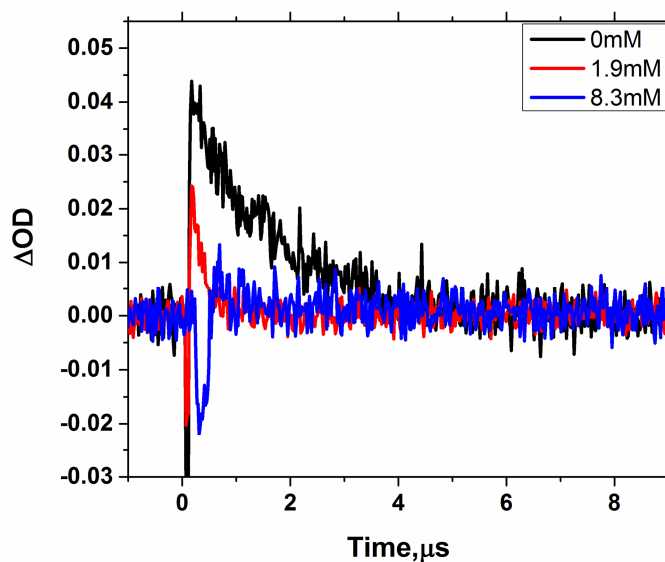


Figure 2.16 Decay profile at 650 nm for H-TATA 1 in acetonitrile. (a) Argon saturated $[\text{O}_2] = 0 \text{ mM}$, (b) Air saturated $[\text{O}_2] = 1.9 \text{ mM}$ and (c) Oxygen saturated $[\text{O}_2] = 8.3 \text{ mM}$.

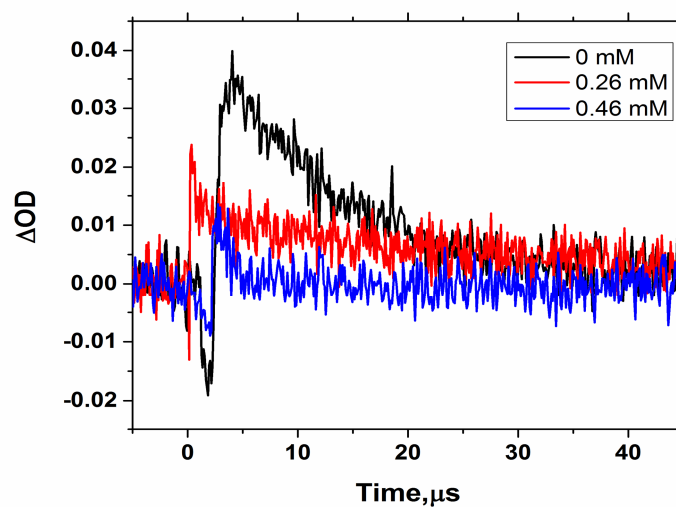


Figure 2.17 Decay profile at 650 nm in the flash photolysis of H-TATA 1 in water (0.1 M NaCl). (a) Argon saturated, $[O_2] = 0$ mM (b) Air saturated, $[O_2] = 0.26$ mM and (c) Oxygen saturated $[O_2] = 0.46$ mM.

Representative examples for the Stern - Volmer plots for oxygen quenching are given in figure 2.18 and 2.19.

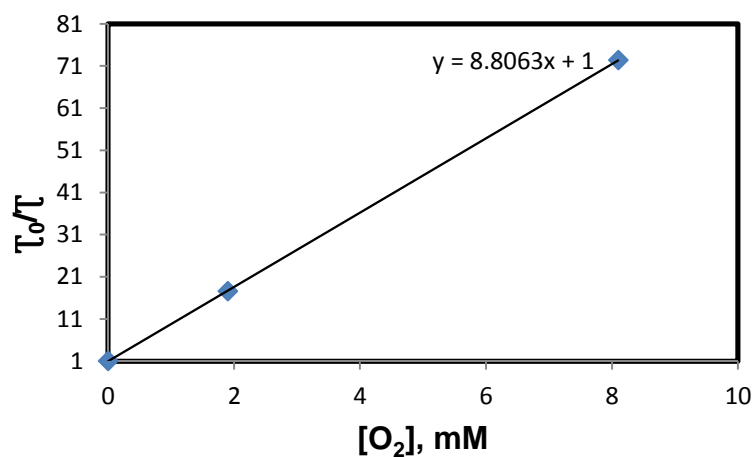


Figure 2.18 Stern -Volmer plot for oxygen quenching of H-TATA 1 triplet excited states in acetonitrile

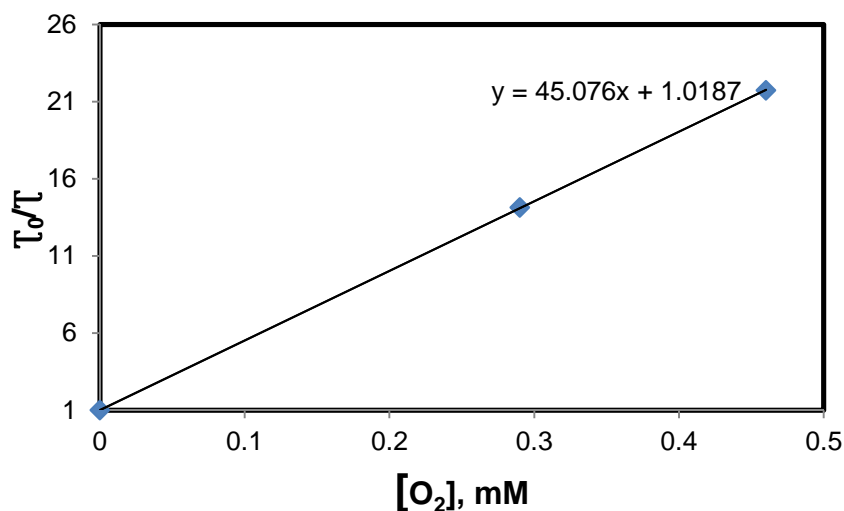


Figure 2.19 Stern - Volmer plot for oxygen quenching of H-TATA 1 triplet excited states in water.

Oxygen quenching rate constant is found to be $1.9 \times 10^6 \text{ M}^{-1} \text{ s}^{-1}$ and $1.4 \times 10^7 \text{ M}^{-1} \text{ s}^{-1}$ in acetonitrile and water respectively as shown in table 2.2.

2.3.3. Singlet oxygen generation studies

Photosensitization is the most popular method for the production of singlet oxygen. The singlet oxygen generation is generally occurs via an energy transfer to molecular oxygen. Triazatriangulenium cations possess the required triplet state energy for an effective energy transfer to molecular oxygen to produce singlet oxygen. By laser flash photolysis experiments, it was showed that triplet states of these cations are efficiently quenched by molecular oxygen. In addition, the delayed emission observed for these cations was also affected by the presence of molecular oxygen indicating an oxygen quenching process for the triplet excited states. The energy profile diagram for the photosensitized production of singlet oxygen by H-TATA is represented in figure 2.20.

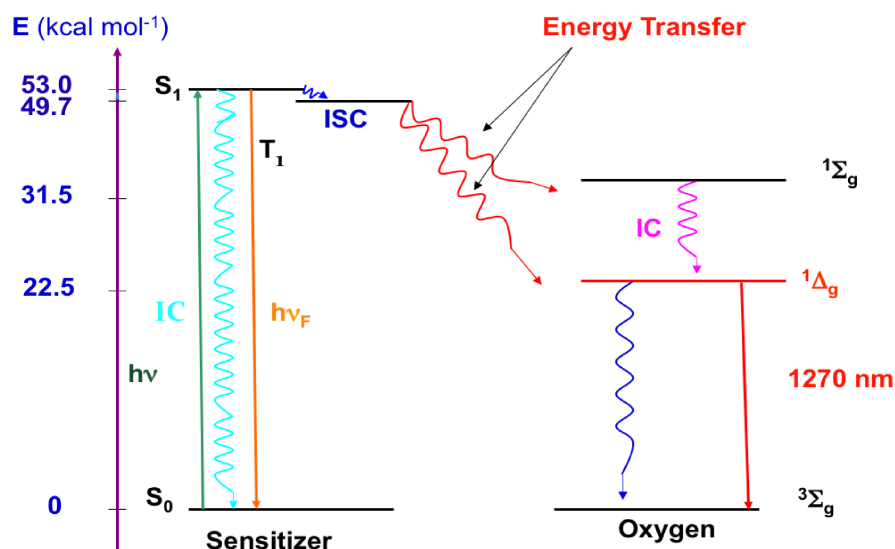
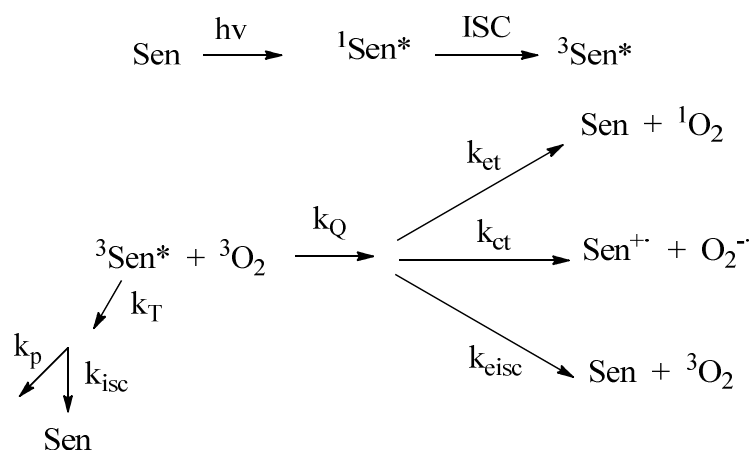


Figure 2.20 The energy profile diagram for the photosensitized production of singlet oxygen by **H-TATA**

The quantum yield of singlet oxygen is a parameter that describe the potential of a sensitizer in generating singlet oxygen. Triazatriangulenium cations are having high triplet yield ($\Phi_{isc}=0.68$ in water) and is expected to be a good singlet oxygen sensitizer. Scheme 2.2 describes possible pathways of interaction available for an excited sensitizer with molecular oxygen.



Scheme 2.2 The interaction of photo excited sensitizer with molecular oxygen

The quantum yield of intersystem crossing (Φ_{isc}) provide information on the quantum efficiency of triplet state formation. This parameter however will not imply the quantum efficiency of singlet oxygen formation as there are various other pathways for the deactivation of the triplet other than the energy transfer to molecular oxygen. The triplet state deactivate (k_T) radiatively by emission of phosphorescence characterised by the rate constant 'k_p' and non-radiatively via an intersystem crossing to the ground state (k_{isc}). The interaction of triplet states with molecular oxygen (k_Q) can lead to energy transfer (k_{et}) generating singlet oxygen, an electron transfer generating superoxide anion (k_{ct}) or an enhanced intersystem crossing to sensitizer ground singlet state (k_{eisc}). Therefore, for a sensitizer with a quantum yield of intersystem crossing ' Φ_{isc} ' the quantum efficiency of energy transfer to oxygen and the quantum yield of singlet oxygen generation are given by the equations:

$$\phi_{et} = \frac{k_{et} [^3O_2]}{k_T + k_Q [^3O_2]} = \frac{k_Q [^3O_2]}{k_T + k_Q [^3O_2]} \frac{k_{et}}{k_Q} = F_{O_2}^T f_{\Delta}^T$$

$$\Phi_{\Delta} = \Phi_{ISC} \phi_{et} = \Phi_{ISC} F_{O_2}^T f_{\Delta}^T$$

where, $F_{O_2}^T$ is the fraction of triplet states quenched by oxygen and f_{Δ}^T is the fraction of the triplets quenched by oxygen yielding singlet oxygen. Because of these possibilities it is imperative that one should determine the actual quantum yield of singlet oxygen by an appropriate method. Moreover, an ideal singlet oxygen sensitizer should not have a reaction with oxygen that lead to superoxide radical anion either from the singlet state or from the triplet excited state. The laser flash photolysis of **H-TATA** in air saturated solutions did not reveal any new transient other than the band due to the triplet state. An estimation of the free energy of electron transfer between

singlet and triplet excited states of **H-TATA**'s with molecular oxygen was also made using the Rehm – Weller equation (Equation 2.8)³¹⁻³³

$$\Delta G_{\text{el}} = \left[23.06 \left(E_{D^+/D}^0 - E_{A/A^-}^0 \right) - \frac{e^2}{\epsilon a} \right] - E_{0,0} \quad (2.8)$$

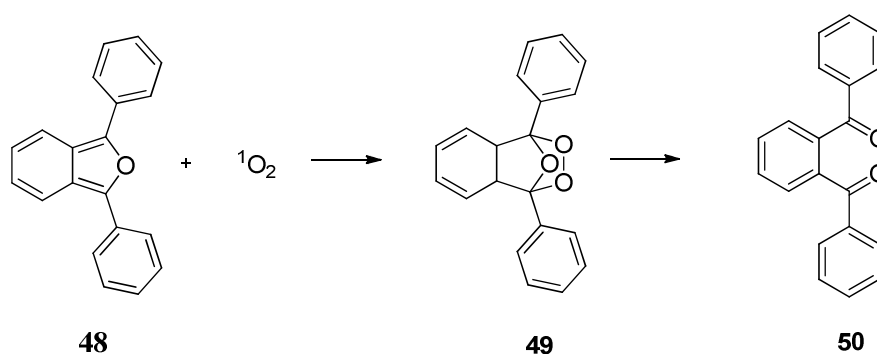
Where $E_{D^+/D}^0$ is the oxidation potential of the donor, E_{A/A^-}^0 is the reduction potential of the acceptor, e is the electronic charge ϵ is the dielectric constant of the solvent, 'a' is the molecular diameter and $E_{0,0}$ is the energy of the singlet/triplet state from which the electron transfer takes place. The oxidation potential of structurally similar trialkylsubstituted triazatriangulenium cation ($E_{\text{ox}} = 1.20$ vs SCE in acetonitrile)³⁴ and the reduction potential of oxygen ($E^0(\text{O}_2/\text{O}_2^-) = -0.82$ V vs. SCE in acetonitrile),³⁵ was used for the calculation. A value of 10 \AA^0 was assumed for the molecular diameter 'a' for the triazatriangulenium cation. A singlet energy of 53 kcal/mol and a triplet energy of 49.72 kcal/mol for acetonitrile medium was used for the electron transfer from singlet and triplet states of the triazatriangulenium cation. The estimated values were -6.41 kcal/mol from the singlet and -3.1 kcal/mol from the triplet. These values show that the electron transfer to singlet oxygen is exergonic and the formation of superoxide anion cannot be ruled out. Darmany et al., earlier studied singlet oxygen sensitization by molecules with moderately to highly feasible electron transfer between the sensitizer triplet states and molecular oxygen.³⁶ The study revealed the role of exciplexes in the oxygen quenching process along with energy transfer and electron transfer. As illustrated in scheme 2.2 the exciplex further proceed towards enhanced intersystem crossing to sensitizer (singlet) ground state. According to the report, the rate constant for energy transfer (k_{et}) and rate constant for electron transfer (k_{ct}) are in the order of diffusion rate constants ($\sim 10^{10} \text{ M}^{-1}\text{s}^{-1}$). The rate constant for the enhanced intersystem crossing (k_{eisc}) when such exciplexes are involved is

estimated as $3 \times 10^7 \text{ s}^{-1}$. Therefore, in such molecules the singlet oxygen generation could compete with electron transfer as well as the oxygen enhanced intersystem crossing and the quantum yield of singlet oxygen generation could be lower than the value of Φ_{isc} would imply.

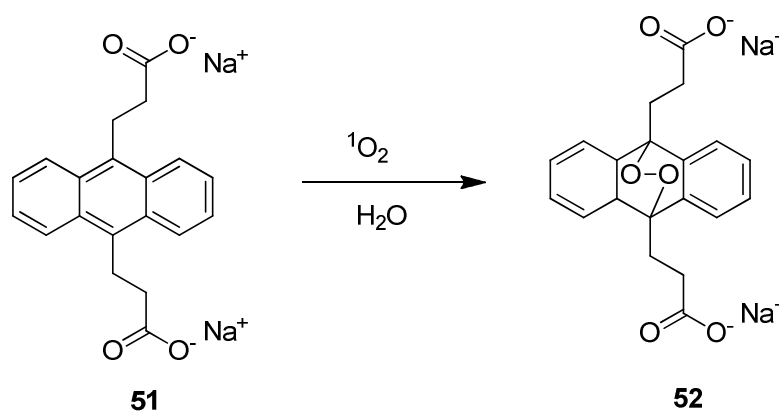
For a molecule to be an ideal sensitizer it should not have any interaction or reaction with the singlet oxygen being generated. To verify this we have attempted to record the singlet oxygen luminescence in aqueous as well as acetonitrile medium using the NIR sensitive InGaAs detector cooled to 77 K. However, due to the very short singlet oxygen lifetimes in these solvents and also due to an overlapping of a tailing delayed emission we could not successfully observe the singlet oxygen luminescence and its lifetime.

The singlet oxygen quantum yield is defined as the number of molecules of singlet oxygen generated per number of photons absorbed by the sensitizer. As discussed earlier the singlet oxygen quantum yield depend on the quantum efficiency of energy transfer and the fraction of the triplet state quenched by oxygen yielding singlet oxygen. Therefore the quantum yield of singlet oxygen generation is either close to the Φ_{isc} or less. In rare cases it is higher than the Φ_{isc} value, for example it is ~ 2 for dicyanoanthracene (DCA).³⁷ In this case both singlet and triplet states generate singlet oxygen. There are direct and indirect methods available for the determination of singlet oxygen quantum yield. The direct method includes time-resolved near-infrared (NIR) luminescence, time-resolved thermal lensing (TRTL), and laser-induced optoacoustic calorimetry (LIOAC).³⁸⁻⁴¹ Chemical trapping and oxygen consumption methods are the indirect methods available for singlet oxygen quantum yield determination and termed as chemical actinometry. Based on the trapping species selected the chemical traps were monitored by changes in fluorescence, EPR, absorption and others.⁴²⁻⁴³ We have adopted the chemical

actinometry method using 1,3-diphenylisobenzofuran (DPBF) as the actinometer in acetonitrile and disodium salt of anthracene-9,10-dipropionic acid (ADPA) in aqueous medium. Both actinometers produce oxygenated products that do not have overlapping absorption with the actinometers (Scheme 2.3 and 2.4). This enabled us to monitor the disappearance of the actinometers as a function of irradiation time.



Scheme 2.3



Scheme 2.4

The method chemical actinometry and the determination of the singlet oxygen quantum yield have been described earlier in chapter 1, 1.4. Since the solubility of the triazatriangulenium salts and the rose bengal was sufficiently high we were able to prepare solution with absorbance > 2 at 530

nm. This enabled us to use total absorption conditions for the actinometry experiments. Besides this another advantage was that there was no overlap between the absorption band of the actinometers and the sensitizers enabling us to monitor the disappearance of the actinometers with maximum sensitivity.

We have used ultrabright green LED light as the light source for the excitation of the sensitizer cations and rose bengal, the reference compound. The LED has the advantages that it gives narrow band monochromatic emission, low power consumption and stable intensity of light emission. By using the ultrabright green LED with an emission maximum at 530 nm selective excitation of the sensitizer was possible. The emission spectrum of the used LED light used in the actinometry experiments is shown in figure 2.21.

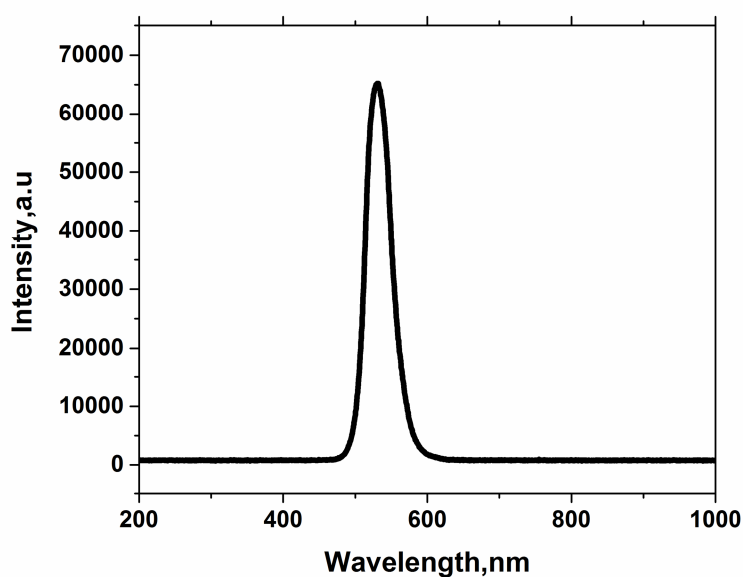
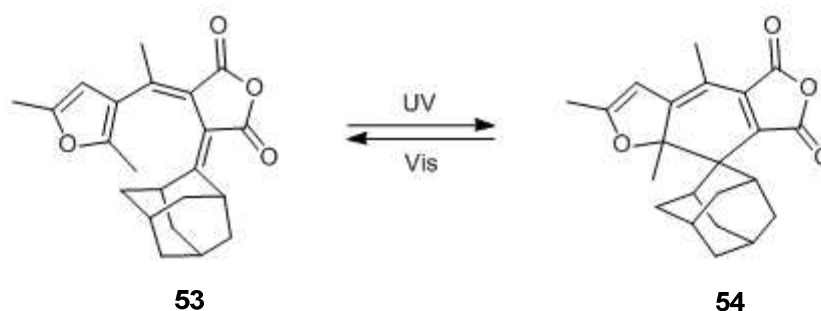


Figure 2.21 The emission spectrum of the ultrabright green LED light used for the excitation of the sensitizer

Chemical actinometry was used to determine the incident photon rate reaching the solution used for photooxidations. The incident photon rate was

monitored periodically using aberchrome 670 as the chemical actinometer. Aberchrome 670 is a photochromic actinometer applicable in the uv and visible region. The compound is the (*E*)-3-(Adamantan-2-ylidene)-4-[1-(2,5-dimethyl-3-furyl)ethylidene]dihydro-2,5-furandione(**53**), which under irradiation in the spectral range 316-366 nm, yield the highly dark red cyclised form (DHBF)(**54**) (Scheme 2.5).⁴⁴



Scheme 2.4

The incident photon rate was calculated using the equation 2.9.

$$P_{0,\lambda} = \frac{\Delta n_{Ac}}{\Phi_{Ac,\lambda} t} \quad (2.9)$$

Where $P_{0,\lambda}$ is the incident photon rate at the excitation wavelength, Δn_{Ac} is the number of actinometric molecules which are reacted during a given irradiation period 't'. $\Phi_{Ac,\lambda}$ is the quantum yield of the actinometer at the excitation wavelength λ . Δn_{Ac} was calculated using the equation 2.10.

$$\Delta n_{Ac} = \frac{NV\Delta OD_{519}}{10^3 \epsilon_{519} l} \quad (2.10)$$

N is the Avogadro number, V is the total volume of the solution irradiated, ΔOD_{519} is the variation in the absorbance at 519 nm (analyzing wavelength) during the irradiation of cyclised form (5×10^{-4} M) with ultrabright green LED in a 2 mm cuvette, ϵ_{519} is the extinction coefficient at

519 nm, l is the optical pathlength of the cuvette in which ΔOD_{519} is measured. Using equations 2.9 and 2.10, the incident photon rate under our irradiation conditions is calculated as $9.5 (+/- 0.5) \times 10^{16}$ photons s^{-1} .

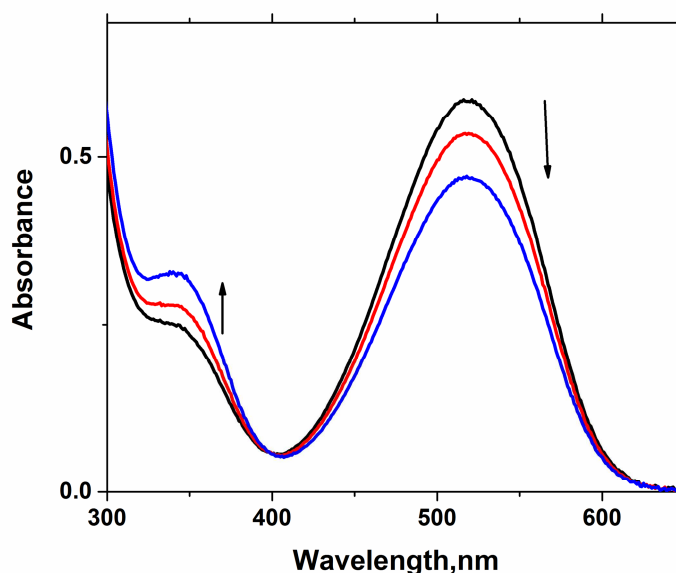


Figure 2.22 Change in the absorbance of (DHBF) (5×10^{-4} M) during the irradiation with ultrabright green LED

2.3.3.1. Determination of singlet oxygen quantum yield of H-TATA 1-4 in acetonitrile

For determining the singlet oxygen quantum yield of the compounds **H-TATA 1-4** chemical actinometry was used with rose bengal as a standard and DPBF as the chemical actinometer. DPBF satisfies all the requirements of the chemical actinometer⁴⁵⁻⁴⁷ except that it showed a fluorescence quenching interaction with the triazatriangulenium cations. Since the concentration of the DPBF used were very small we expected a minor role for this quenching interaction in the overall singlet oxygen sensitization process. A blank irradiation in the absence of the sensitizer was also carried out which did not show any change in the concentration of the actinometer

used. An air saturated solution of **H-TATA 1** (1.5×10^{-4} M) in acetonitrile containing DPBF (5.3×10^{-5} M) was irradiated using 530 nm light. The photooxidation of DPBF was monitored spectrophotometrically. During the irradiation, no change in the absorbance of the dye solutions was observed indicating that no photobleaching occurred under our experimental condition. Under identical condition the reference rose bengal, (8.3×10^{-5} M) also irradiated in the presence of DPBF (figure 2.23). For total absorption of the incident light the absorbance at the irradiation wavelength was ensured to be above 2 absorbance units. Figure 2.24 to 2.27 show the evaluation of absorbance of **H-TATA 1-4** during the irradiation at 530 nm of a solution of DPBF and **H-TATA**.

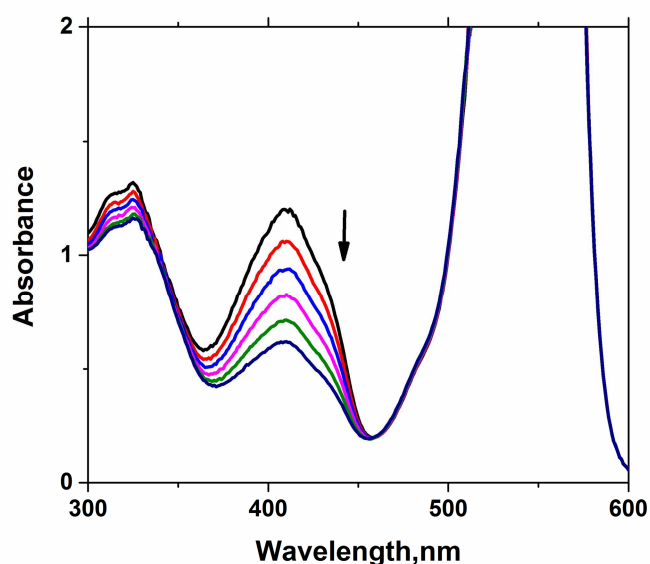


Figure 2.23 Change in absorbance during the irradiation at 530 nm of a solution of DPBF (5.3×10^{-5} M) and rose bengal (8.3×10^{-5} M) in acetonitrile

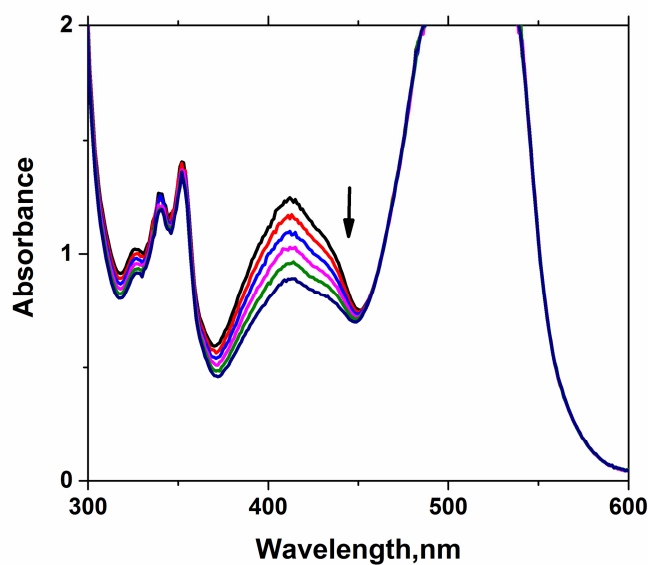


Figure 2.24 Change in absorbance during the irradiation at 530 nm of a solution of DPBF (5.3×10^{-5} M) and H-TATA 1 (1.5×10^{-4} M) in acetonitrile

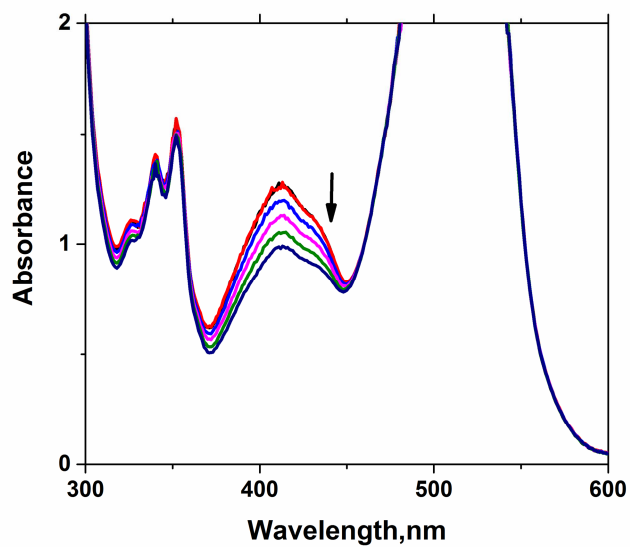


Figure 2.25 Change in absorbance during the irradiation at 530 nm of a solution of DPBF (5.3×10^{-5} M) and H-TATA 2 (1.5×10^{-4} M) in acetonitrile

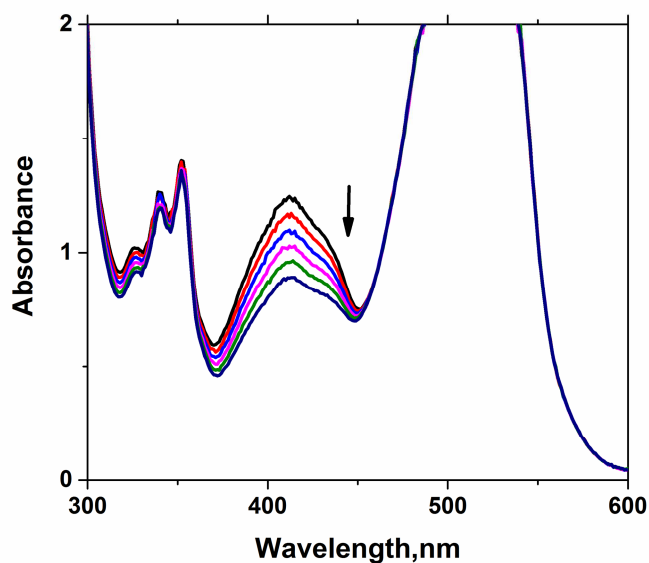


Figure 2.26 Change in absorbance during the irradiation at 530 nm of a solution of DPBF (5.3×10^{-5} M) and H-TATA 3 (1.5×10^{-4} M) in acetonitrile

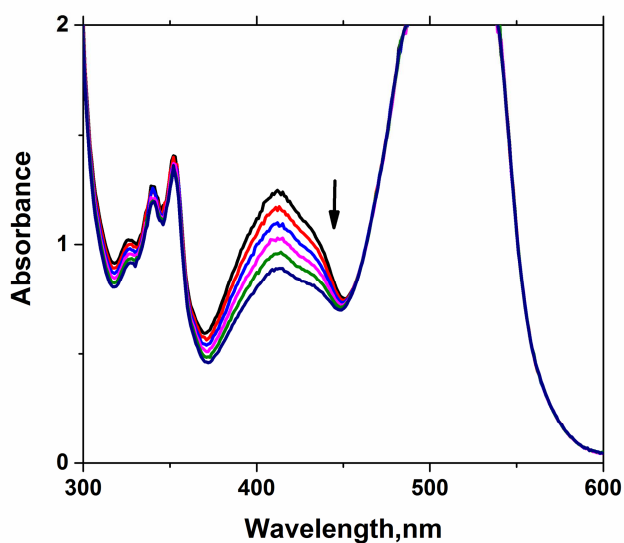


Figure 2.27 Change in absorbance during the irradiation at 530 nm of a solution of DPBF (5.3×10^{-5} M) and H-TATA 4 (1.5×10^{-4} M) in acetonitrile

The rate constant for the consumption of singlet oxygen by DPBF can be calculated in the presence of the triazatriangulenium dye as well as the reference sensitizer rose bengal. The ratio of rate constants for the dye and the reference sensitizer is proportional to their ratios of singlet oxygen generation efficiency. Rose bengal has a singlet oxygen quantum yield of 0.42 in acetonitrile.⁴⁸ From these data the apparent quantum yield of singlet oxygen generation can be estimated using the equation 2.11. Figure 2.28 shows comparison of a plot of absorbance at 410 nm as a function of irradiation time.

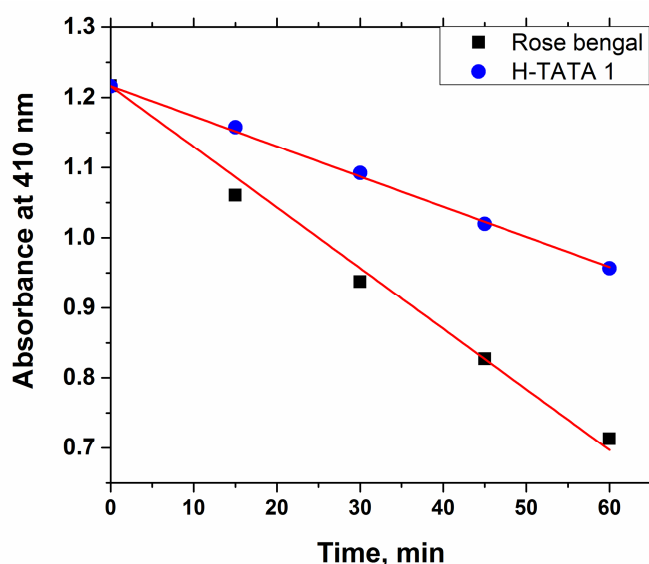


Figure 2.28 Comparison of the decrease in the absorbance at 410 nm of DPBF in the presence of rose bengal and H-TATA 1 in acetonitrile

The apparent singlet oxygen quantum yield of **H-TATA 1-4** in acetonitrile was determined using the equation 2.11.

$$\Phi_{\Delta} = \frac{\Phi_R k_R^{\text{TATA}}}{k_R^{\text{RB}}} \quad (2.11)$$

Where Φ_{Δ} is the singlet oxygen quantum yield, Φ_R is the singlet oxygen quantum yield of the reference, k_R^{TATA} is the rate constant for the disappearance of the actinometer in the presence of TATA, k_R^{RB} is the rate constant for the disappearance of the actinometer in the presence of rose bengal. The apparent quantum yield of singlet oxygen generation by the triazatriangulenium cation in acetonitrile was estimated as 0.21. Table 2.3 shows the values of Φ_{Δ} for all the synthesized triazatriangulenium cations in acetonitrile.

Table 2.3 The values of singlet oxygen quantum yield (Φ_{Δ}) obtained for the compounds H-TATA 1-4 in acetonitrile.

Compound	Φ_{Δ}
H-TATA 1	0.21
H-TATA 2	0.21
H-TATA 3	0.21
H-TATA 4	0.21

2.3.3.2. Determination of singlet oxygen quantum yield of H-TATA 1-4 in aqueous medium

The singlet oxygen quantum yield in water is determined using disodium salt of 9, 10-anthracenedipropionic acid as the chemical actinometer. In order to understand whether ADPA interfere with the excited state of triazatriangulenium salts, the emission spectra of H-TATA 1 (1.0×10^{-6} M) were recorded at various ADPA concentrations ranging from (1.4×10^{-4} M - 2.6×10^{-4} M). It is shown in figure 2.29.

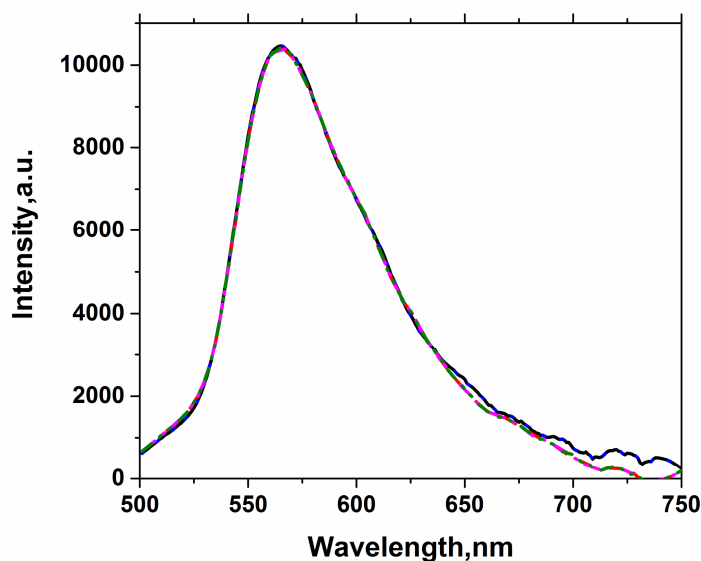


Figure 2.29 Emission spectrum of H-TATA 1 (1.0×10^{-6} M) in water in the presence of increasing concentrations of ADPA (1.4×10^{-4} M - 2.6×10^{-4} M). $\lambda_{ex} = 480$ nm

ADPA satisfies all the requirements of the chemical actinometer⁴⁹⁻⁵² and it is not interfering with the excited state processes of the sensitizer. A blank irradiation in the absence of the sensitizer was carried out which did not show any change in the concentration of the actinometer used. An air saturated solution of **H-TATA 1** (1.6×10^{-4} M) in water (0.1 M NaCl) containing ADPA (1.8×10^{-4} M) was irradiated with ultrabright green LED light. The photooxidation of ADPA was monitored spectrophotometrically and indicated by a decrease in the absorbance in the range of 350 – 400 nm. During the irradiation, no change in the absorbance of the dye solutions indicates that photobleaching of the dye has not taken place under such experimental condition. Under identical condition rose bengal (4.0×10^{-5} M) the reference sensitizer, was also irradiated in the presence of ADPA (figure 2.30). For total absorption of the incident light the absorbance at the irradiation wavelength was ensured to be above 2 absorbance units. Figure

2.31 to 2.34 shows change in absorbance of **H-TATA1-4** during the irradiation at 530 nm of an aqueous solution of ADPA and H-TATA.

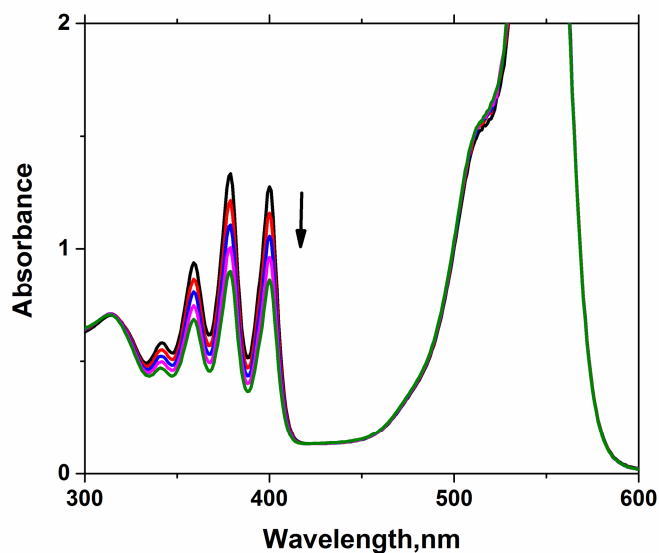


Figure 2.30 Change in absorbance during the irradiation at 530 nm of a solution of ADPA (1.8×10^{-4} M) and rose bengal (4.0×10^{-5} M) in water

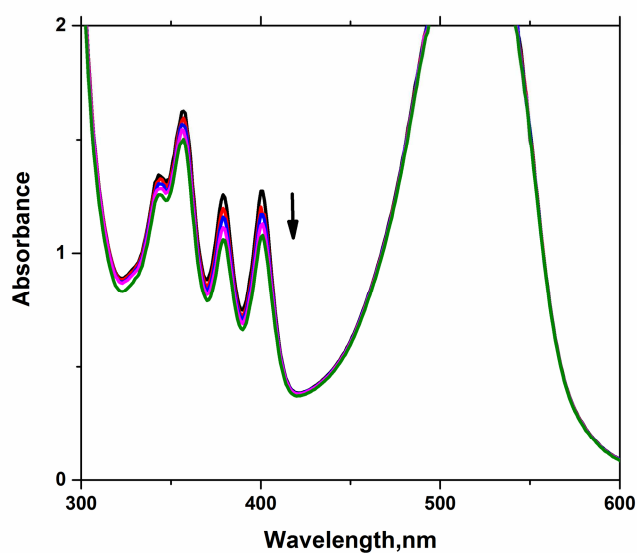


Figure 2.31 Change in absorbance during the irradiation at 530 nm of a solution of ADPA (1.8×10^{-4} M) and H-TATA 1 (1.6×10^{-4} M) in water

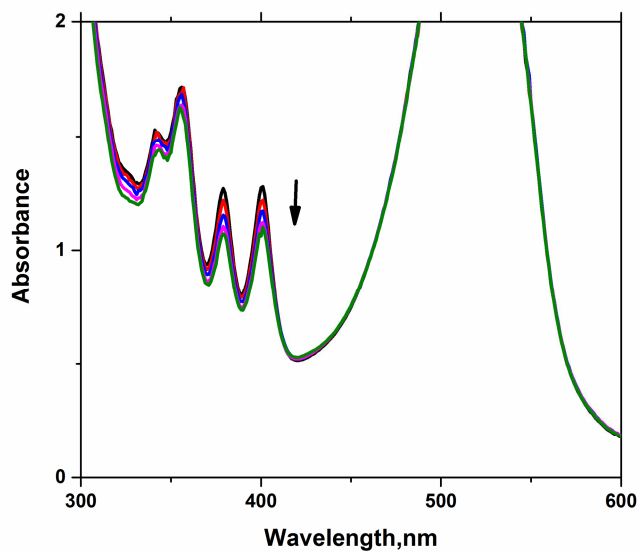


Figure 2.32 Change in absorbance during the irradiation at 530 nm of a solution of ADPA (1.8×10^{-4} M) and H-TATA 2 (1.6×10^{-4} M) in water

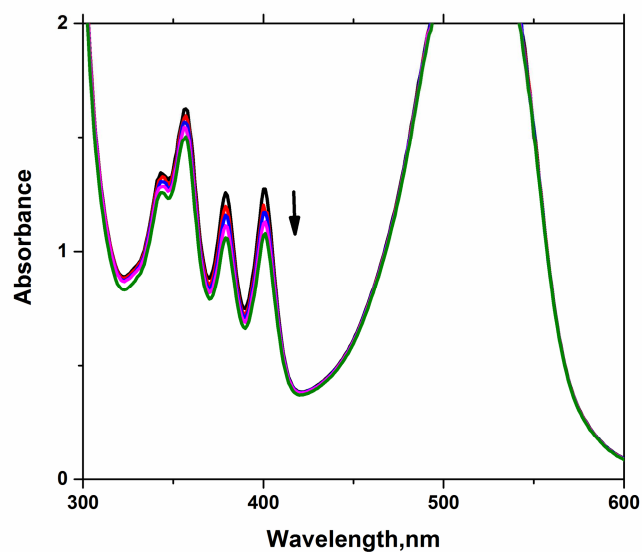


Figure 2.33 Change in absorbance during the irradiation at 530 nm of a solution of ADPA (1.8×10^{-4} M) and H-TATA 3 (1.6×10^{-4} M) in water

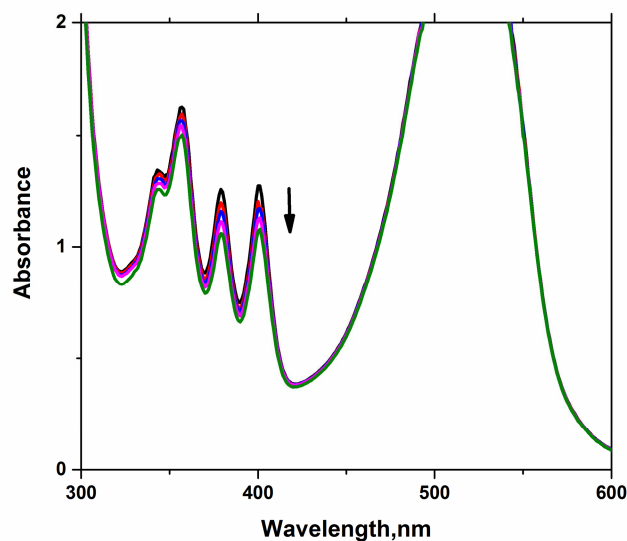


Figure 2.34 Change in absorbance during the irradiation at 530 nm of a solution of ADPA (1.8×10^{-4} M) and H-TATA 4 (1.6×10^{-4} M) in water.

The rate constant for the consumption of singlet oxygen by ADPA can be calculated in the presence of the triazatriangulenium dye as well as the reference sensitizer rose bengal. The ratio of rate constants for the dye and the reference sensitizer is proportional to their ratios of singlet oxygen generation efficiency. Rose bengal has a singlet oxygen quantum yield of 0.76 in water.⁴⁸ From these data the apparent quantum yield of singlet oxygen generation can be estimated using the equation 2.11. Figure 2.35 shows comparison of a plot of absorbance at 400 nm as a function of irradiation time.

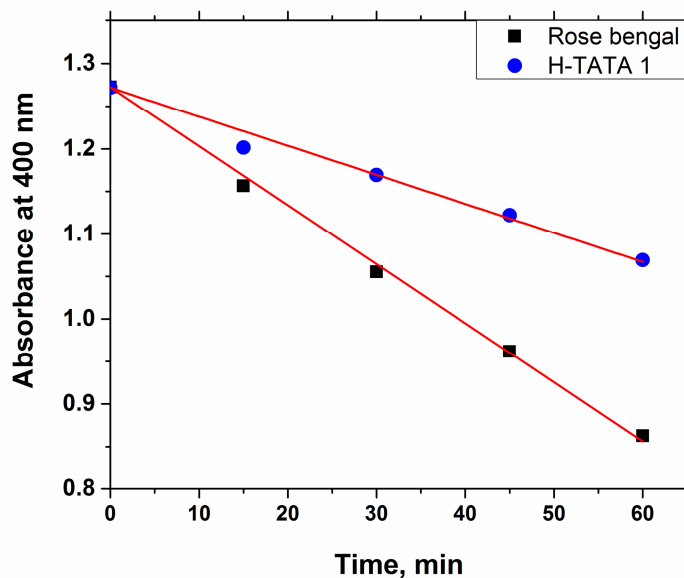


Figure 2.35 Comparison of the decrease in the absorbance at 400 nm of ADPA in the presence of rose bengal and **H-TATA 1**

From the ratio of rate constants the apparent quantum yield of singlet oxygen generation by the triangulenium ions were estimated as 0.36 in water. Table 2.4 shows the Φ_{Δ} values of all the synthesized triazatriangulenium cations in water.

Table 2.4 The values of singlet oxygen quantum yield (Φ_{Δ}) obtained for the compounds **H-TATA 1-4** in water.

Compound	Φ_{Δ}
H-TATA 1	0.36
H-TATA 2	0.36
H-TATA 3	0.36
H-TATA 4	0.36

2.3.3.1.1. Determination of the role of singlet oxygen in dye sensitized photooxidation

The competition kinetics between ADPA and a singlet oxygen quencher N_3^- (NaN_3) was carried out to establish the role of $^1\text{O}_2$ in dye sensitized photooxidation. The presence of azide ion quenches the $^1\text{O}_2$, such an experiment reveal whether the dye sensitized photooxidation proceeds through $^1\text{O}_2$ mechanism or through a free radical intermediate. Figure 2.36 shows the results of the competition between ADPA and N_3^- in the presence of TATA as the sensitizer. The rate of singlet oxygen consumption has steadily decreased as a function of the azide anion concentration establishing the role of singlet oxygen in the photooxygenation of ADPA.

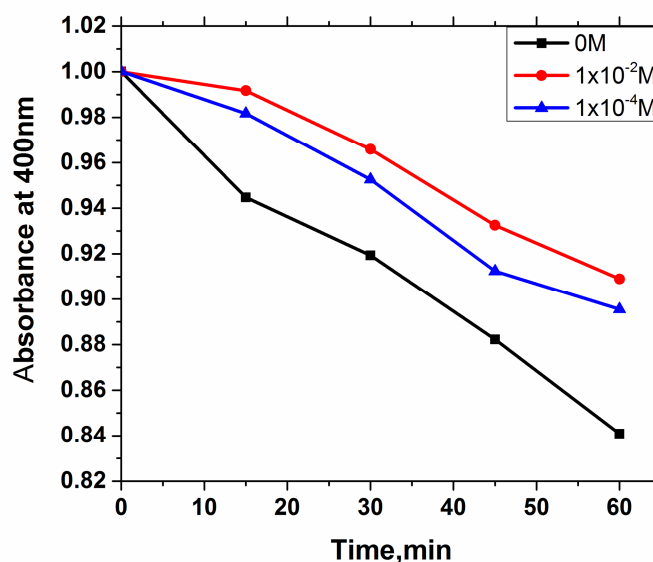


Figure 2.36 Competition for singlet oxygen between ADPA and N_3^- in the presence of TATA with various quencher concentrations

2.4. Conclusions

In this chapter we have described the synthesis, photophysical properties and singlet oxygen generation efficiencies of a series of water

soluble triazatriangulenium salts. The properties of these compounds in water and acetonitrile are compared. Both singlet and triplet lifetime of the compounds are higher in aqueous medium. Using absorption, fluorescence and phosphorescence spectra, the energy levels of the singlet and triplet excited states of the triazatriangulenium salts are determined. The singlet oxygen generation capacities of the synthesized compounds are determined using ADPA and DPBF as the chemical actinometers and rose bengal as the reference. The singlet oxygen quantum yield is found to be higher in aqueous medium.

2.5. Experimental Section

2.5.1 General Techniques

All reactions were carried out using oven dried glass wares. The solvents used were distilled and dried prior to use. All reagents were purchased from either Sigma –Aldrich or Spectrochem Pvt. Ltd and were used as received. ADPA is synthesized based on the reported procedure.⁵³ Aberchrome 670 was purchased from TCI Chemicals Pvt. Ltd. Absorption spectra were recorded using Evolution 201 UV-visible spectrophotometer. Fluorescence, Phosphorescence and Fluorescence lifetime studies were carried out using Jobin-YvonFluorolog3-211UV-Vis-NIR fluorescence spectrometer with a TCSPC attachment. IR spectra were recorded on JASCO 4100 model, FTIR spectrometer. The ¹H NMR spectra were recorded on 400 MHz on Bruker FT-NMR spectrometer with tetramethylsilane(TMS) as internal standard. Chemical shifts were reported in parts per million (ppm) downfield to TMS. Molecular mass was determined by Waters 3100 mass detector with an Electro-Spray-Ionization unit. Laser flash photolysis experiments were carried out by employing an Applied Photophysics model LKS-60 laser kinetic spectrometer equipped with a GCR-12 Series Quanta

Ray Nd:YAG laser. The analysing and laser beams were fixed at right angles to each other. The laser energy was 90 mJ at 532 nm. Singlet oxygen quantum yield was determined by chemical actinometry by using 1,3-diphenylisobenzofuran in acetonitrile and disodium salt of 9,10-anthracenedipropionic acid in water as the chemical actinometers respectively and rose bengal as standard.

2.5.2. Synthesis of Tris-(2,6-dimethoxyphenyl)carbenium tetrafluoroborate (39).

Tris-(2,6-dimethoxyphenyl) carbenium tetrafluoroborate (39) was synthesized according to a reported procedure.²⁵ Yield: 52%. MS (ESI, m/z): 423. Mp 164 °C. FT-IR (cm^{-1}) 3450, 1596, 1487, 1262, 1085, 810, 643.¹H NMR (400 MHz, CDCl_3 ,) δ (ppm): 7.620-7.557 (t, 1H), 6.546-6.525 (d, 2H), 3.596 (s, 6H). ¹³C NMR (400 MHz, CDCl_3 ,) δ (ppm): 162.69, 142.47, 125.37, 104.96.

2.5.3. Synthesis of 4,8,12-Tri-hydroxyethyl-4,8,12-triazatriangulenium tetrafluoroborate (H-TATA 1)⁵⁴

In a round bottom flask tris-(2,6-dimethoxyphenyl) carbenium tetrafluoroborate (1.0 g., 2.0 mmol) is mixed with ethanolamine (3.0 g., 49 mmol). The reaction flask was fitted with a reflux condenser and heated to 190 °C under nitrogen atmosphere for 9 hr. The resulting solid was then triturated several times with dichloromethane and hexane. Selective crystallization occurred from methanol to give 0.40 g of compound H-TATA 1. Yield: 40%. MS (ESI, m/z): 414. mp: >300 °C. FT-IR (cm^{-1}) 3318, 2919, 2858, 1625, 1532, 1330, 1057, 857, 820, 760. ¹H NMR (400 MHz, DMSO,) δ (ppm): 8.046-8.004 (t, 1H), 7.479-7.458 (d, 2H), 5.131-5.105 (t, 1H), 4.556 (s, 2H), 3.926-3.914 (t, 2H). ¹³C NMR (100 MHz, D_2O) δ (ppm): 169.69, 139.98, 137.68, 126.75, 105.38, 71.83, 56.94.

2.5.4. Synthesis of 4, 8, 12-Tri-hydroxybutyl-4, 8, 12-triazatriangulenium (H-TATA 2)

In a round bottom flask tris-(2,6-dimethoxyphenyl) carbenium tetrafluoroborate (0.2 g, 0.38 mmol) is mixed with 4-amino-1-butanol (1 g, 11 mmol). The reaction flask was fitted with a reflux condenser and heated to 190 °C under nitrogen atmosphere for 9 hr. The resulting solid was then triturated several times with dichloromethane and hexane. Selective crystallization occurred from methanol to give compound **H-TATA 2**. Yield: 35%. MS (ESI, m/z): 498. mp: >300 °C. FT-IR (cm^{-1}) 3418, 2924, 2860, 1620, 1330, 1030, 835, 760. ^1H NMR (400MHz, DMSO) δ (ppm): 8.032-7.990 (t, 1H), 7.317-7.295 (d, 2H), 4.649 (s, 1H), 4.292 (s, 2H), 3.553 (s, 2H), 1.808 (s, 2H), 1.718-1.687 (t, 2H). ^{13}C NMR (100MHz, CDCl_3) δ (ppm): 144.84, 114.81, 110.19, 65.51, 34.05, 26.58.

2.5.5. Synthesis of 4, 8, 12-Tri-hydroxypentyl-4, 8, 12-triazatriangulenium (H-TATA 3)

In a round bottom flask tris-(2,6-dimethoxyphenyl)carbenium tetrafluoroborate(0.2 g, 0.38 mmol) is mixed with 5-amino-1-pentanol (1.17g, 11 mmol). The reaction flask was fitted with a reflux condenser and heated to 190 °C under nitrogen atmosphere for 9 hr. The resulting solid was then triturated several times with dichloromethane and hexane. Selective crystallization occurred from methanol to give compound **H-TATA 3**. Yield 42%. MS (ESI, m/z): 540. mp: >300 °C. FT-IR (cm^{-1}) 3396, 2934, 2867, 1616, 1530, 1337, 1073, 837, 762. ^1H NMR (400 MHz, DMSO) δ (ppm): 8.034-7.992 (t, 1H), 7.291-7.269 (d, 2H), 4.468-4.445 (t, 1H), 4.248(s, 2H), 3.462-3.443 (t, 2H), 1.752 (s, 2H), 1.559-1.553 (d, 4H). ^{13}C NMR (100MHz, DMSO,) δ (ppm): 139.51, 137.58, 109.47, 104.92, 79.40, 60.56, 46.99, 32.08, 24.34, 22.64.

2.5.6. Synthesis of 4,8,12-Tri-hydroxyhexyl-4,8,12-triazatriangulenium tetrafluoroborate(H-TATA 4)

In a round bottom flask tris-(2,6-dimethoxyphenyl)carbenium tetrafluoroborate (0.2 g, 38 mmol) is mixed with 6-amino-1-hexanol (1.28 g., 11 mmol). The reaction flask was fitted with a reflux condenser and heated to 190 °C under nitrogen atmosphere for 9 hr. The resulting solid was then triturated several times with dichloromethane and hexane. Selective crystallization occurred from methanol to give compound **H-TATA 4**. Yield 40%. MS (ESI, m/z): 582. mp: >300 °C. FT-IR(cm^{-1}) 3408, 2928, 2857, 1615, 1333, 1080, 840, 762. ^1H NMR (400MHz, DMSO) δ (ppm):8.001-7.959(t, 1H), 7.254-7.234 (d, 2H), 4.415-4.391 (t, 1H), 4.196 (s, 2H), 3.445-3.405 (t, 3H), 1.717 (s, 2H), 1.545-1.417 (m, 6H). ^{13}C NMR (100 MHz, DMSO) δ (ppm): 139.63, 137.64, 109.63, 104.96, 60.56 ,32.43, 24.77.

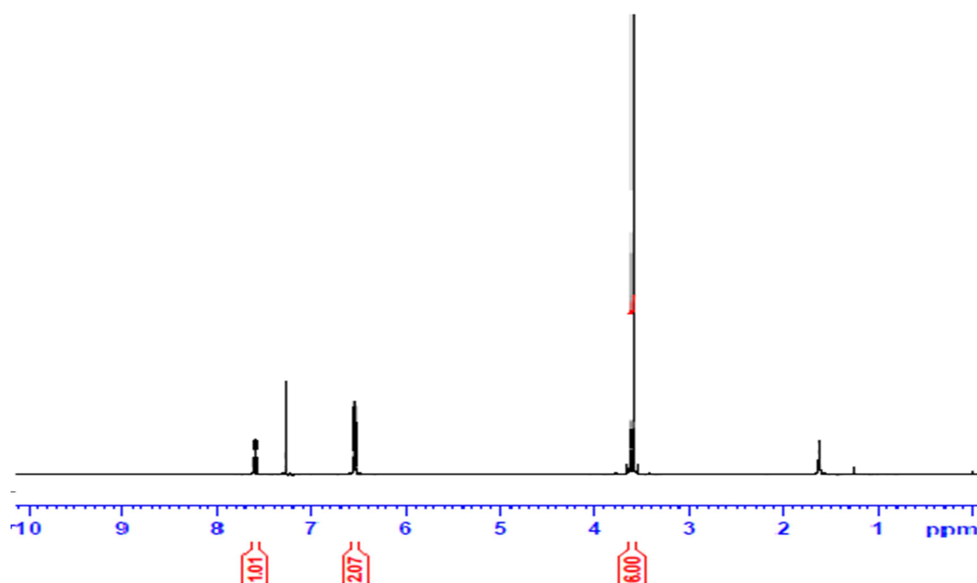


Figure 2.37 ^1H NMR spectrum of tris-(2,6-dimethoxyphenyl)carbenium tetrafluoroborate (39)

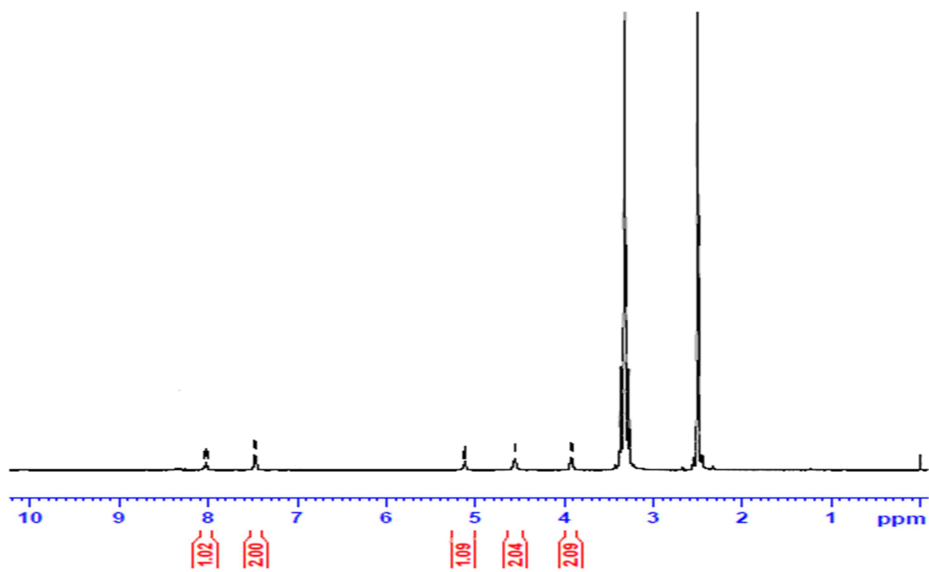


Figure 2.38 ^1H NMR spectrum of H-TATA 1

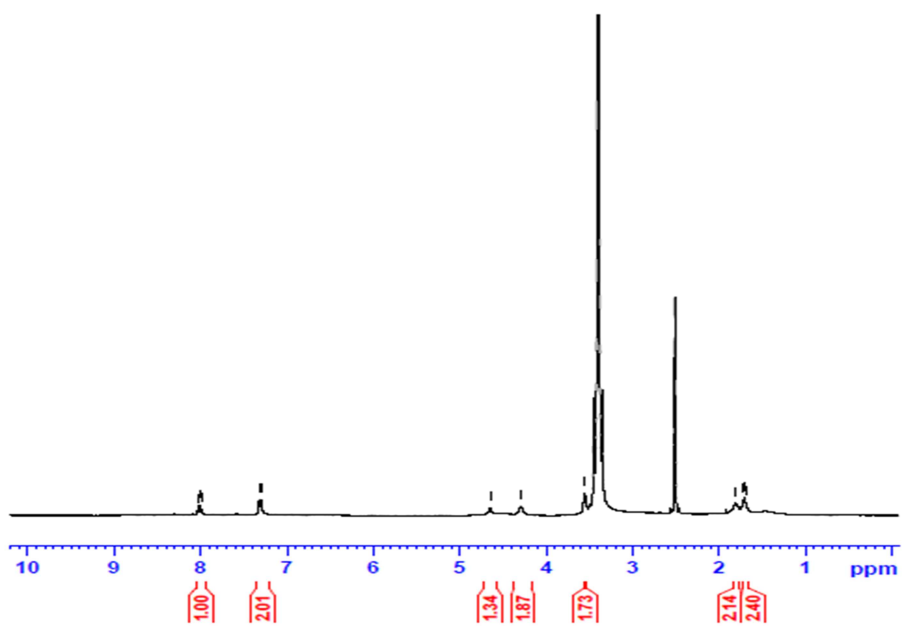


Figure 2.39 ^1H NMR spectrum of H-TATA 2

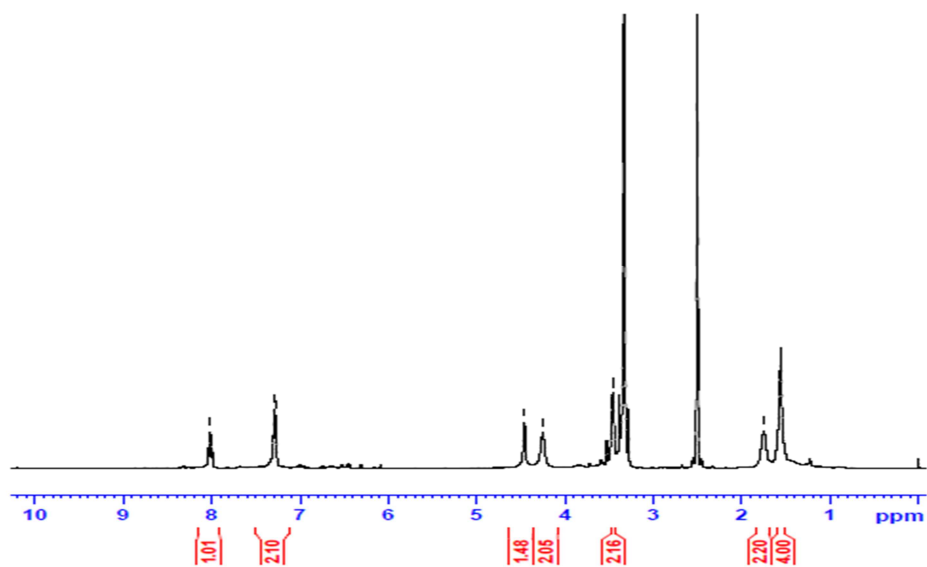


Figure 2.40 ^1H NMR spectrum of H-TATA 3

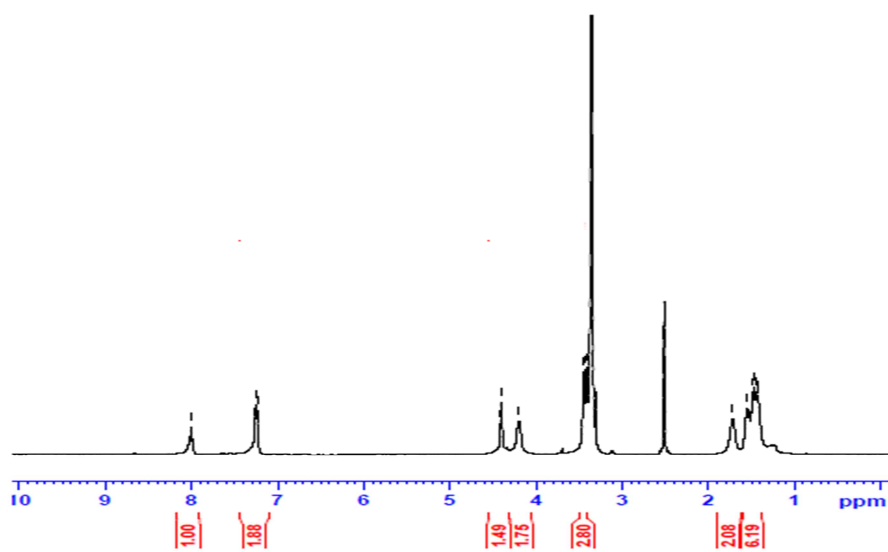


Figure 2.41 ^1H NMR spectrum of H-TATA 4

2.6. References

1. Neckers, D.C.; *J. Photochem. Photobiol. A*. **1989**, *47*, 1.
2. Tedesco, A.C.; Primo, F.L.; deJesus, P.D. *In Multifunctional Systems for Combined Delivery, Biosensing and Diagnostics*. **2017**, *1*, 9.
3. Wang, P.; Qin, F.; Zhang, Z.; Cao, W. *Opt. express*. **2015**, *23*, 22991.
4. Redmond, R.W.; Gamlin, J.N. *Photochem. Photobiol.* **1999**, *70*, 391.
5. Fadel, M.; Kassab, K. *Trop. J. Pharm. Res.* **2011**, *10*, 289.
6. Kumar, A.; Thirumalesh, M.B. *J.Clin.Ophthalmol.* **2013**, *1*, 55.
7. Chang, C.C.; Yang, Y.T.; Yang, J.C.; Wu, H.D.; Tsai, T. *Dyes Pigm.* **2008**, *79*, 170.
8. Gutierrez, M.I.; Garcia, N.A. *Dyes Pigm.* **1998**, *38*, 195.
9. Redmond, R.W.; Gamlin, J.N. *Photochem. Photobiol.* **1999**, *70*, 391.
10. DeRosa, M.C.; Crutchley, R.J. *Coord. Chem. Rev.* **2002**, *233*, 351.
11. Dos Santos, A.F.; Terra, L.F.; Wailemann, R.A.; Oliveira, T.C.; de Moraes Gomes, V.; Mineiro, M.F.; Meotti, F.C.; Bruni-CardosoA, BaptistaM.S.; Labriola, L. *BMC Cancer* **2017**, *17*, 194.
12. Wainwright, M. *Chem. Soc. Rev.* **1996**, *25*, 351.
13. Tang, W.; Xu, H.; Kopelman, R.; Philbert, M.A. *Photochem. Photobiol.* **2005**, *81*, 242.
14. Ribeiro, A.O.; Tome, J.P.C.; Neves, M.G.P.M.S.; Tome, A.C.; Cavaleiro, J.A.S.; Iamamoto, Y.; Torres. T. *Tetrahedron Lett.* **2006**, *47*, 9177.
15. Jeong, H.G.; Choi, M.S. *Isr. J. Chem.* **2016**, *56*, 110.
16. Bonnett, R.; Djelal, B. D.; Nguyen,A. *J. Porphyr. Phthalocyanines.* **2001**, *5*, 652.
17. Hunter, C.A.; Sanders, J.K.M.; Stone, A. *J. Chem. Phys.* **1989**, *133*, 395.

18. García-Fresnadill, D.; Georgiadou, Y.; Orellana, G.; Braun, A.M.; Oliveros, E. *Helvetica chimicaacta*. **1996**, *79*, 1222.
19. Jiang, X.; Zhu, N.; Zhao, D.; Ma, Y. *Sci China Chem*. **2016**, *59*, 40.
20. Pefkianakis, E.K.; Christodouleas, D.; Giokas, D.L.; Papadopoulos, K.; Vougioukalakis, G.C. *Eur. J. Inorg. Chem*. **2013**, *2013*, 4628.
21. Vaidyalingam, A.; Dutta, P.K. *Anal. Chem*. **2000**, *72*, 5219.
22. Das, A.; Joshi, V.; Kotkar, D.; Pathak, V.S.; Swayambunathan, V.; Kamat, P.V.; Ghosh, P.K. *J. Phys. Chem. A*. **2001**, *105*, 6945.
23. Laursen, B. W.; Krebs, F. C. *Angew. Chem. Int. Ed. Engl*. **2000**, *39*, 3432.
24. Laursen, B. W.; Krebs, F. C. *Chem. Eur. J*. **2001**, *7*, 1773.
25. Martin, J. C.; Smith, R. G. *J. Am. Chem. Soc*. **1964**, *86*, 2252.
26. Freire, M.G.; Neves, C.M.; Marrucho, I.M.; Coutinho, J.A.; Fernandes, A.M. *J. Phys. Chem. A*. **2009**, *114*, 3744.
27. Cho, C.W.; Pham, T.P.; Jeon, Y.C.; Yun, Y.S. *Green Chem*. **2008**, *10*, 67.
28. Würth, C.; González, M.G.; Niessner, R.; Panne, U.; Haisch, C.; Genger, U.R. *Talanta*. **2012**, *90*, 30.
29. Carmichael, I.; Hug, G. L. *J. Phys. Chem. Ref. Data*. **1986**, *15*, 1.
30. Lutz, W.; Brehert, E.; Lindquist, L. *J Phys. Chem*. **1973**, *77*, 1758.
31. Rehm, D.; Weller, A. *Isr. J. Chem*. **1970**, *8*, 259.
32. Kavarnos, G. J.; Turro, N. *J. Chem. Rev*. **1986**, *86*, 401.
33. Kavarnos, G. J. *Fundamentals of Photoinduced Electron Transfer*, VCH Publishers, Inc., New York, 1993.
34. Dileesh, S.; Gopidas, K.R. *J. Photochem. Photobiol. A*. **2004**, *162*, 115.
35. Peover, M. E.; White, B. S. *Electrochim. Acta*. **1966**, *11*, 1061.
36. Darmany, A.P.; Lee, W.; Jenks, W.S. *J. Phys. Chem. A*. **1999**, *103*, 2705.
37. Kanner, R.C.; Foote, C.S. *J. Am. Chem. Soc*. **1992**, *114*, 678.

38. Krasnovsky, A. A. *Membr. Cell Biol.* **1998**, *12*, 665.
39. Niedre, M.; Patterson, M. S.; Wilson, B. C. *Photochem. Photobiol.* **2002**, *75*, 382.
40. Redmond, R.W.; Braslavsky, S.E. *Chem. Phys. Lett.* **1988**, *148*, 523.
41. Martı́neza, C. G.; Neunera, A.; Martı́b. C.; Nonellb, S.; Brauna, A.M.; Oliveros, E. *Helv.Chim.Acta.* **2003**, *86*, 384.
42. Alegria, A. E.; Ferrer, A.; Santiago, G.; Sepulveda, E.; Flores, W. *J.Photochem. Photobiol. A.* **1999**, *127*, 57.
43. Tanielian, C.; Heinrich, G. *Photochem. Photobiol.* **1995**, *61*, 131.
44. Bossi, M.; Fölling, J.; Dyba, M.; Westphal, V.; Hell, S.W. *New J. Phys.* **2006**, *16*, 275.
45. Spiller, W.; Kliesch, H.; Wohrle, D.; Hackbarth, S.; Roder, B.; Schnurpfeil, G. *J. Porphyr. Phthalocyanines.* **1998**, *2*, 145.
46. Amat-Guerri, F.; Lempe, E.; Lissi, E. A.; Rodriguez, F. J.; Trull, F. *J. Photochem. Photobiol. A.* **1996**, *93*, 49.
47. Mayeda, E.A.; Bard, A. *J. Am. Chem. Soc.* **1973**, *95*, 6223.
48. Neckers, D.S. *J. Photochem. Photobiol. A.* **1989**, *47*, 1.
49. Lindig, B.; Rodgers, M. *Photochem. Photobiol.* **1981**, *33*, 627.
50. Barbara, A.; Lindig, Michael, A. J.; Rodgers, A.; Paul, Schaap. *J. Am. Chem. Soc.* **1980**, *102*, 5590.
51. Kim, S.; Fujitsuka, M.; Majima, T. *J. Phys. Chem. B.* **2013**, *117*, 13985.
52. Moreno, M.; Monson, E.; Reddy, R.; Rehemtulla, A.; Ross, B.; Philbert, M. *Sens. Actuators B. Chem.* **2003**, *90*, 82.
53. Icli, S.; Demic, S.; Dindar, B.; Doroshenko, A.O.; Timur, C. *J. Photochem. Photobiol. A.* **2000**, *136*, 15.

CHAPTER 3

Studies of Lipophilic Triazatriangulenium Cations in Microheterogeneous Medium

3.1. Abstract

The chapter presents the studies of a series of lipophilic triazatriangulenium cations in microheterogeneous medium. To vary lipophilicity symmetrically substituted triazatriangulenium cations having N-alkyl groups with varying length of alkyl chains ($n = 4, 6, 8$ and 12) were prepared. The photophysical properties of the triazatriangulenium cations were studied in anionic, cationic and neutral micelles. Triazatriangulenium cations showed changes in the photophysical properties that can be correlated with the length of the alkyl side chain. Solubilization of the cations having long alkyl chain substituents ($n=8$ and 12) led to a progressive shift in their respective absorption and emission maximum. This change in absorption and emission property is attributed to a distortion in the planarity of the structure upon binding with the micellar assemblies. This conclusion was supported by temperature dependence of emission properties, time resolved emission studies, and theoretical study on their geometry and electronic properties by DFT calculations at 6-31g (d, p) level.

3.2. Introduction

Microheterogeneous media such as micelles, microemulsions and liposomes serve as mimics of biological membranes. This is because of the

resemblance between the interfacial properties of these microheterogeneous media with those of biological membranes and serve as a model for biological studies of certain drug molecules. In chapter 2 we have demonstrated that triazatriangulenium cations can be good singlet oxygen sensitizers and are potential drug candidates for the photodynamic therapy. The photodynamic action of the molecules depends not only on the singlet oxygen production but also on other factors such as bio-distribution of the dye molecules in the cytoplasmic and mitochondrial membranes, the retention and the nature of binding inside the cell.¹ The properties of the dye molecules inside the cell are complex and this may affect their photophysical properties. Hence, using micelles or liposomes as mimics of the cell one must develop an understanding on the photophysical properties of these cations. This insight on the nature of interaction and the localization of these cations inside the cell will be valuable to predict their suitability as a potential dye for photodynamic applications. Among micelles, liposomes and microemulsions, micelles are the best primary model due to ease of handling and preparation compared to liposomes and micro emulsions.

Micelle is a self assembly of amphiphilic surfactant molecules with distinct hydrophilic and hydrophobic regions. In aqueous solution the surfactant molecule self assemble in such a way that the hydrophobic groups align and exclude water molecules to create this distinct hydrophilic and hydrophobic regions. Typically in a normal micelle, the polar head groups align towards the surrounding water molecules and the hydrophobic regions form the inner core. Similarly, in reverse micelles the hydrophilic head groups are oriented inwards and the hydrophobic groups are oriented towards the non-aqueous solvent bulk. Since micelles have diameters of 10-80 nm range, it do not sediment under gravity and provide a medium with long term stability. In solution the self assembly leads to the formation of colloidal

clusters in which 40–100 surfactant molecules assemble to the micellar assemblies and are characterized by a critical micellar concentration (CMC) and aggregation number.

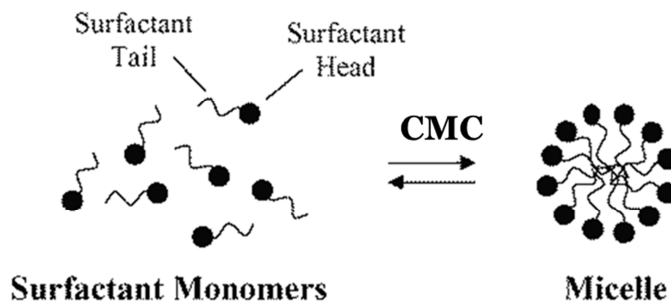


Figure 3.1

The number of surfactant molecules in a micelle is known as the aggregation number. The concentration at which the micelle formation begins is known as critical micelle concentration (CMC). Micelles are normally spherical in shape however, other shapes such as cylindrical assemblies or lamellae are also possible. The shape and the size of the micelles depend on the factors such as surfactant concentration, temperature, pH and ionic strength. The various types micelles are shown in figure 3.2.

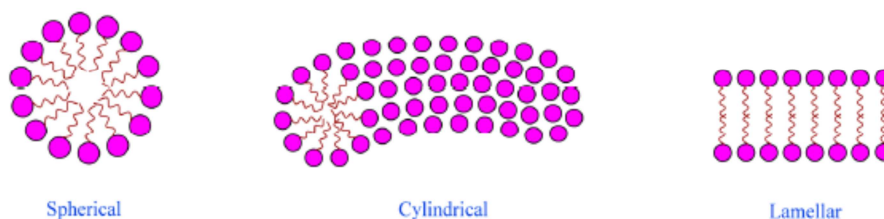


Figure 3.2 Various types of micelles

The surfactants are classified based on different factors such as their origin, structural features, behavior in solutions etc. A typical classification is based on the type of head group they possess. Based on this the surfactants

are classified into four types: anionic, cationic, nonionic and zwitterionic. In an anionic surfactant the head group is negatively charged and is electrically neutralized by an alkali metal cation. The well known examples for anionic micelle are soaps ($\text{R-COO}^-\text{Na}^+$) and alkyl benzene sulfonates ($\text{R-C}_6\text{H}_4\text{SO}_3^-\text{Na}^+$). The cationic surfactants have a positively charged head group. Long chain amines (RNH_3^+X^-) and quaternary ammonium salts [$\text{RN}(\text{CH}_3)^3\text{X}^-$] belongs to the group of cationic surfactants. Non-ionic surfactants do not possess any significant electric charge on their polar head group. The examples for nonionic surfactants are alkyl phenol ethoxylate, alcohol ethoxylate, polyoxypropylene glycols. Zwitterionic surfactants possess both positive and negative charge on their polar head group. lauryldimethylamine N-oxide, amidosulfobetaine-16, hexadecylphosphocholine etc. are examples for this group of surfactants.

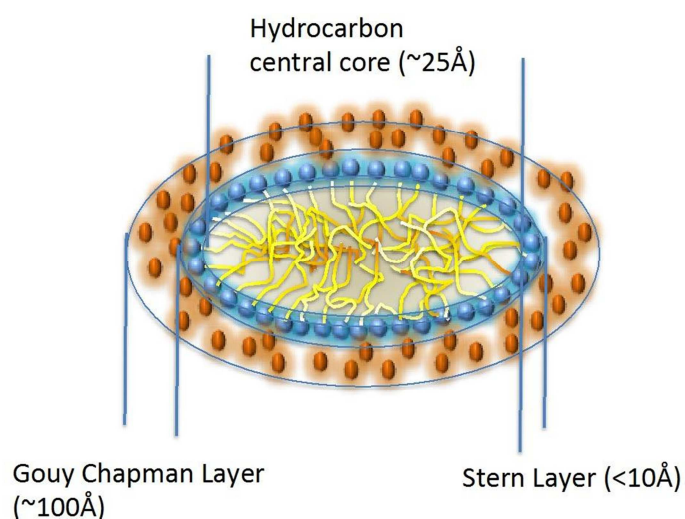


Figure 3.3A cross section of an ionic micelle

The cross section of a typical ionic surfactant micellar assembly is given in figure 3.3. The micelle formed by the self-assembly of 'n' number of surfactant molecules has liquid like core consisting of the hydrophobic alkyl chains with the ionic head groups projecting out to the aqueous bulk.

The charged region with the ionic groups formed the inner part of the electrical double layer surrounding the hydrophobic core is termed as the Stern layer. Along with the ionic head groups this layer also contains the respective counter ions. The outer and more diffused hydrodynamic shear surface containing some of the counter ions and the water molecules is called the Gouy – Chapman layer. The hydrophobic core and the Stern layer forms the kinetic micelle. Here the surfactant molecule is in equilibrium with the micellar assembly. The association constant for the anionic micelle formed from SDS is 7800 M^{-1} with the rate constant for association of the surfactant molecule is $\sim 1 \times 10^9 \text{ M}^{-1} \text{ s}^{-1}$ and the dissociation rate constant of $1 \times 10^7 \text{ s}^{-1}$. These thermodynamically stable self-assemblies of surfactant molecules solubilize molecules especially those ones having a poor solubility in the bulk medium in which the surfactants are assembled. The micropolarity gradient in these assemblies also assist the partitioning of the solutes. For example, polarity of aqueous bulk decreases gradually from the bulk to the surface and then to the hydrocarbon core. The location of the solute in these dynamic assemblies is difficult to predict and only a time average loci can be assumed based on the changes in spectroscopic properties of the solute. In anionic micelle the possible locations for the solutes are:

- a. adsorption at the micellar surface or in the Stern layer
- b. association within the Gouy – Chapman layer
- c. intercalated between the polar head groups
- d. further deep but closer to the polar head groups
- e. in the inner hydrophobic core

Typically solubilization in the micelle is indicated in the UV-Vis, Fluorescence or NMR spectral properties etc. For example, molecules having

polarity dependent absorption and emission spectra, the solubilization of the solute is indicated by changes in the absorption or emission maxima, quantum yield or lifetime of fluorescence emission. These changes are often used in the determination of binding constants of the solutes with the micellar assemblies.

Most of the dyes proposed for photodynamic applications were studied in these micro heterogeneous media to derive an understanding on how these dyes are distributed in a true biological matrix and how their properties change due to interfacial phenomena. The spectroscopic and photophysical properties of some rhodamine derivatives (Chart 3.1) in cationic, anionic and neutral micelles was reported by Pal et al.^{2,3}

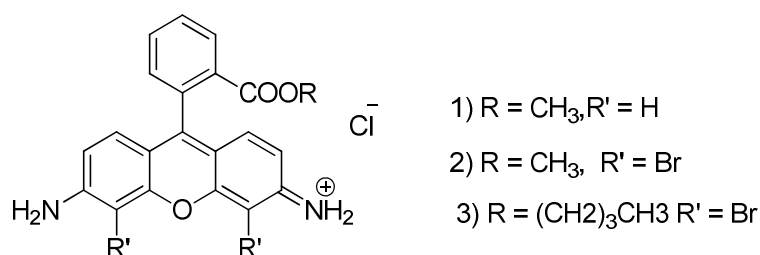
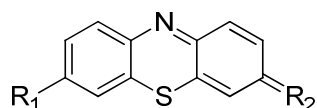


Chart 3.1

The studies are conducted in anionic sodium dodecyl sulfate (SDS), the cationic cetyltrimethylammoniumbromide (CTAB) and neutral triton X-100 (TX) micelles. The results showed a substituent dependent interaction between these dyes and the surfactants. The interaction was predominantly electrostatic when anionic SDS micelles are used with Dye 1. The dye-SDS aggregate formation was found at lower SDS concentration but monomeric form of the dye was observed above critical micellar concentration. Dye 2 and 3 showed interaction with the cationic micelles formed from CTAB. Here, the hydrophobic interactions dominated over the coulombic interaction whereas, in Dye 1 the coulombic interaction is the dominating factor.

Thiazine dyes or azure dyes (Chart 3.2) are promising photosensitizers for PDT.⁴ These dyes are more soluble in aqueous media and in contrast to MB⁺ they do not undergo demethylation.⁵ Havelcová et al.,⁶ studied the photophysical properties of these dyes in aqueous solution and in micelles



1) R1 = N(CH₃)₂ R2 = N(CH₃)₂

2) R1 = N(CH₃)₂ R2 = NH₂

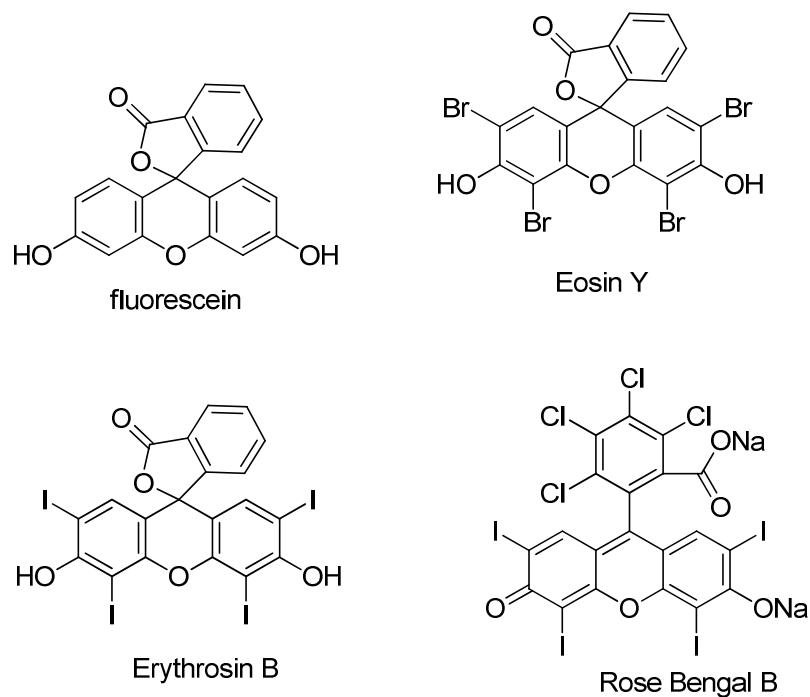
3) R1 = N(CH₃)₂ R2 = NH(CH₃)

4) R1 = NH(CH₃) R2 = NH₂

Chart 3.2

Depending on the pH of the solution these dyes show excited state protonation, deprotonation behavior. The transient spectra of these cations are characterized by the unprotonated and protonated triplet states and radical cations with absorption maxima at 370 nm, 420 nm and 520 nm respectively. This absorption profile obtained in the micellar medium was similar to that observed in water. The triplet states are effectively quenched by oxygen and singlet oxygen production was observed. In anionic surfactant (SDS) the lifetime of the triplet state is increased. The singlet oxygen quantum yield of these dyes is found to be increased in micellar medium compared to those in water. Similar results were reported in the case of methylene blue.⁷

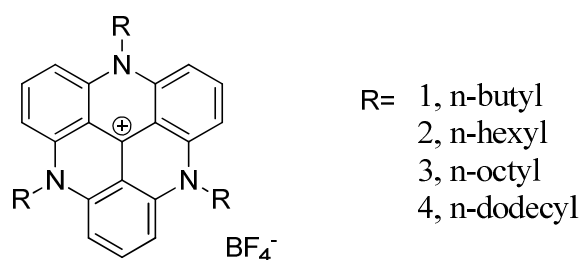
The photophysical properties of a series of xanthene dyes (Chart 3.3) in SDS, CTAB and pluronic P-123 micellar medium was reported by Pellosi et al.⁸

**Chart 3.3**

The partition coefficient values were determined for all the dyes and concluded that eosin, erythrosine and rose bengal has an amphiphilic nature. For all the xanthenes dyes investigated there occurs a red shift as the medium change from water to micelle. The emission maximum was red shifted by 8-10 nm in P-123 micelles and 12-15 nm in CTAB but no change reported in the case of SDS micelles. At physiological pH values the ability of the dyes to be positioned inside the micelle and the nature of interaction with the micelle depends not only on the hydrophobicity of the dye but also on the micellar surface charge. The Stern–Volmer analysis of quenching interaction with a quencher molecule confirms the existence of the erythrocin and rose bangal inside the micelle. Since these dyes are anionic in nature the dye – micelle interaction was maximum in neutral P-123 and cationic CTAB micelles. Solubilisation of the dye in micellar assemblies is indicated by a

high fluorescence quantum yield. Erythrosin and rose bengal are found to show enhanced singlet oxygen generation upon solubilization in the micelles.

In the present work we have used micellar medium as a model to study the properties of a series of lipophilic triazatriangulenium cations (**TATA 1-4**, Chart 3.4) so that an understanding on the behavior of these cations in a true biological system can be obtained. The studies are conducted in anionic sodium dodecyl sulfate (SDS), the cationic cetyltrimethylammoniumbromide (CTAB) and neutral triton X-100(TX) micelles. As given in the chart 3.4, the cations chosen for the present study are planar with D_{3h} symmetry and contain linear N-alkyl side chains having 4, 6, 8 and 12 carbon atoms. The cationic-triangular -tripodal nature of the molecule is expected to prevent the binding interaction with the micelle but, the presence of long alkyl chains are expected to favour the binding interaction. Lengths of the alkyl chains are varied to tune the hydrophobicity and solubility in non-aqueous medium. The cationic-triangular-tripodal molecule with side chains of sufficient length is expected to associate with the micelles with a “spider-on-the-apple” like binding topology.



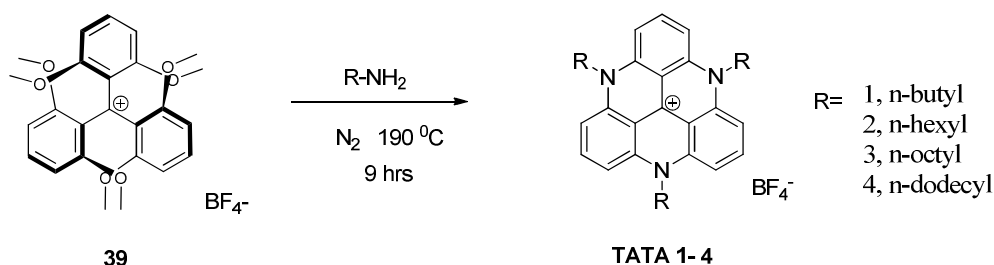
TATA 1-4

Chart 3.4

3.3. Results and discussion

3.3.1. Synthesis of lipophilic triazatriangulenium cations (TATA 1-4)

Tris-(2,6-dimethoxyphenyl) carbenium tetrafluoroborate (**39**) was synthesized according to a reported procedure.⁹ The N-alkyl substituted triazatriangulenium cations (**TATA 1-3**) were prepared from **39** using literature procedure reported by Krebs, F. C. and coworkers (Scheme 3.1).^{10,11} A similar procedure was adopted for the synthesis of **TATA 4** using *n*-dodecylamine as the primary amine for the aza-bridging reaction.



Scheme 3.1

These cations were formed as their tetrafluoroborates and showed moderate solubility in acetonitrile (~1 mg/mL for **TATA 1-3** and ~0.5 mg/mL for **TATA 4**) and were insoluble in aqueous medium.

3.3.2. Photophysical Studies

3.3.2.1. UV-Visible absorption properties of triazatriangulenium salts in micellar medium

The solutions for the photophysical characterization in micellar media were prepared by mixing 1-10 μL of a concentrated stock solution in acetonitrile with an appropriate volume of the micelle solution (100 mM) in water. Distribution of the solute in the micelle medium was ensured by stirring or ultrasound sonication prior to spectroscopic experiments. Among the three micellar medium, in anionic micelle the solutions were stable and

did not become turbid. The solutions prepared in cationic and neutral micellar medium were less stable and showed increasing turbidity on standing. In terms of solubility, solutions with dye concentration up to 1×10^{-3} M in anionic micelle medium could be prepared. The better stability of the solutions in the anionic micellar medium can be ascribed to the electrostatic association of the triazatriangulenium cations with the anionic surfactant molecules. Due to the poor solubility behavior in cationic and neutral micelles we have chosen the anionic micellar medium for the detailed photophysical studies.

Absorption spectra of the tri-N-alkyltriazatriangulenium salts in acetonitrile were reported earlier by Laursen and Krebs.¹⁰ Similar spectral profiles and maxima were observed for **TATA 1-4** in the same solvent with absorption maxima at 270 nm, 350 nm and at 525 nm (figure 3.4). All compounds showed similar spectra and did not show any variation in the absorption maxima or spectral profile as the length of the alkyl chain is varied. **H-TATA 2**, the newly prepared cation reported in chapter 2 of the present thesis are soluble in aqueous medium its spectrum in water is also presented for comparison. In aqueous medium triazatriangulenium chromophores shows a red shift of 5 nm for the long wavelength absorption maximum and other bands are relatively unaffected by the change in the polarity on moving from acetonitrile to water. The absorption spectra of **TATA 1-4** were also recorded in 100 mM solutions of the anionic SDS micelle, cationic CTAB micelles and neutral Triton X-100 micelles and are presented in figures 3.5, 3.6 and 3.7.

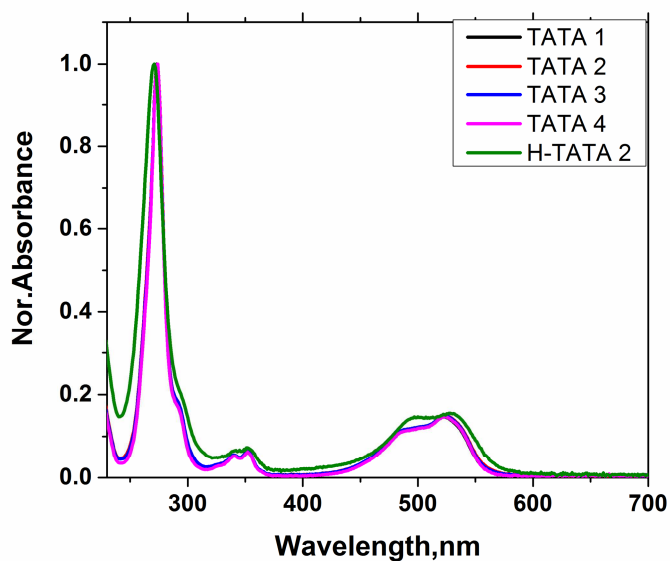


Figure 3.4 Normalized absorption spectrum of **TATA 1-4** in acetonitrile and **H-TATA 2** in water

In the anionic micelle, **TATA 1-4** showed a chain length dependent absorption spectrum. It showed a progressive red shift in the absorption maximum of the long wavelength transition with increase in the alkyl chain length. In cationic and neutral micelles this shift is less prominent and is limited to **TATA 4**, the cation having the dodecyl chains as the pods. The absorption maxima and the molar absorption coefficients of these cations in the micellar media are summarized in table **3.1**.

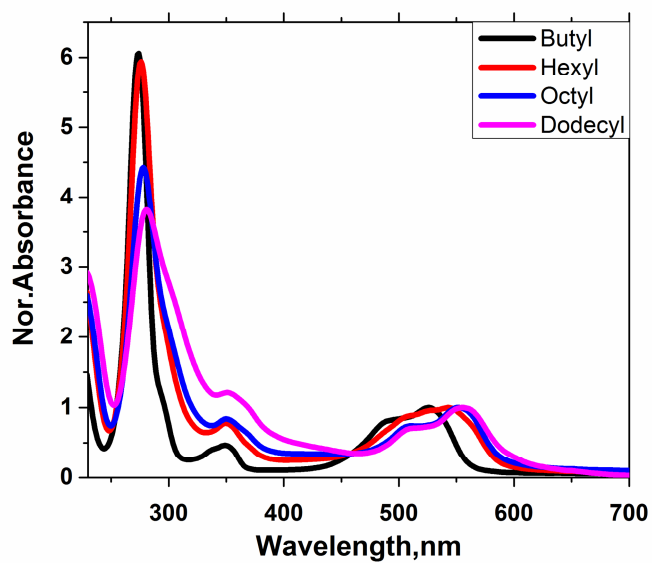


Figure 3.5 Absorption spectra of TATA 1-4 in anionic micelle (SDS)

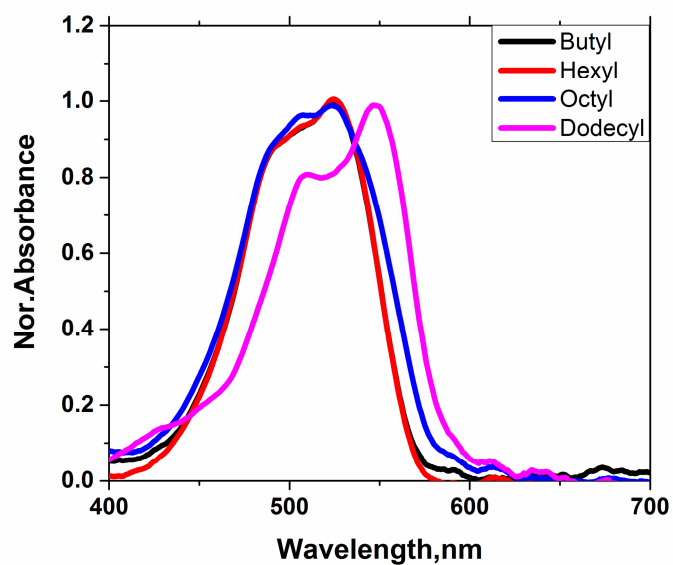


Figure 3.6 Absorption spectra of TATA 1-4 in cationic micelle (CTAB)

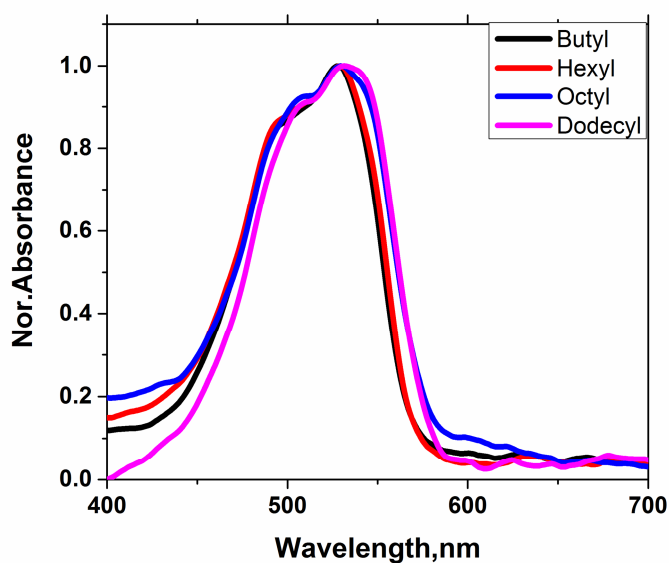


Figure 3.7 Absorption spectra of **TATA 1-4** in neutral micelle (Triton X-100)

3.3.2.2. Emission properties of triazatriangulenium salts in micellar medium

Emission spectra of the tri-N-alkyltriazatriangulenium salts (**TATA 1-4**) recorded in acetonitrile were similar to the data reported by Gopidas and coworkers.¹² The compounds exhibited the fluorescence in the 500-700 nm region (figure 3.8) with a maximum at 558 nm in acetonitrile. The emission spectrum of the water soluble derivative **H-TATA 2** is also given in figure 3.8 for comparison. This molecule too has similar spectral features but with a 13 nm (571 nm) red shifted emission maximum in water.

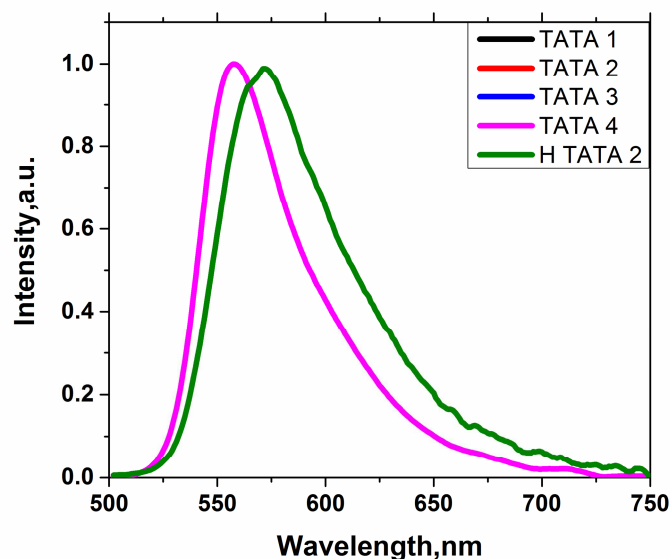


Figure 3.8 Normalized emission spectra of **TATA 1-4** in acetonitrile and **H-TATA 2** in water. $\lambda_{\text{ex}} = 480$ nm

The emission spectral properties of the lipophilic triazatriangulenium salts were also recorded in the anionic micelle (SDS), cationic micelle (CTAB) and in neutral micelle (triton X-100) solutions. The spectra obtained are given in figures 3.9, 3.10 and 3.11. As observed in the absorption spectrum of these cations the solubilization in the micellar medium is evident from their respective shifts in the emission spectrum. In the anionic micelle solution the data showed a clear dependence on the chain length of the alkyl substituents. In this case the cations having octyl and dodecyl chains showed a clear red shift in the emission maximum with appearance of the new band at 629 nm. In cationic micelle and neutral Triton X-100 solutions too the emission spectra of the cations with *n*-octyl and *n*-dodecyl derivatives indicated red shift in the emission maximum indicating solubilization of these cations in these micelles.

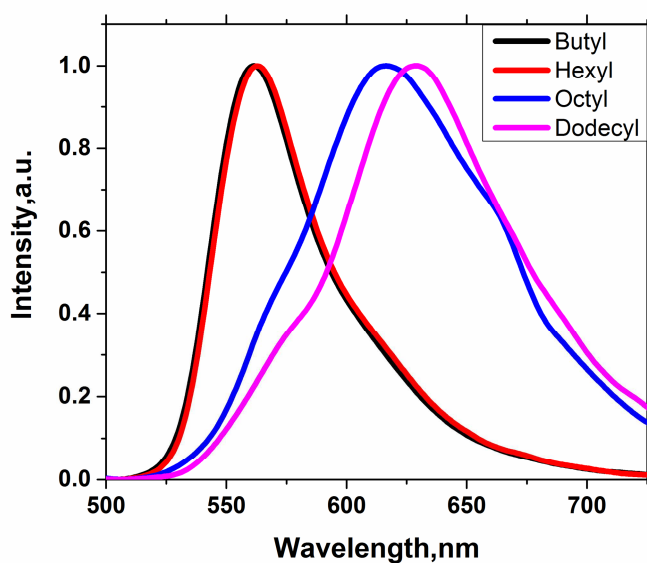


Figure 3.9 Normalized emission spectra of the compound **TATA 1-4** in anionic micelle (SDS) $\lambda_{\text{ex}}=480$ nm

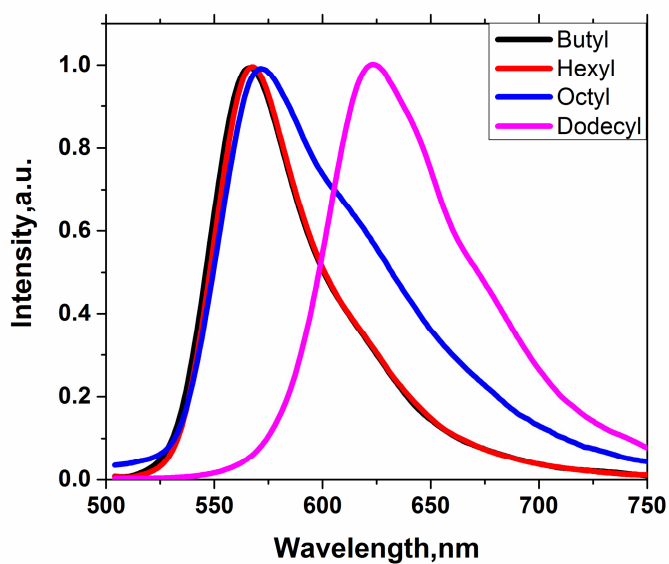


Figure 3.10 Normalized emission spectra of the compound **TATA 1-4** in cationic micelle (CTAB) $\lambda_{\text{ex}}=480$ nm

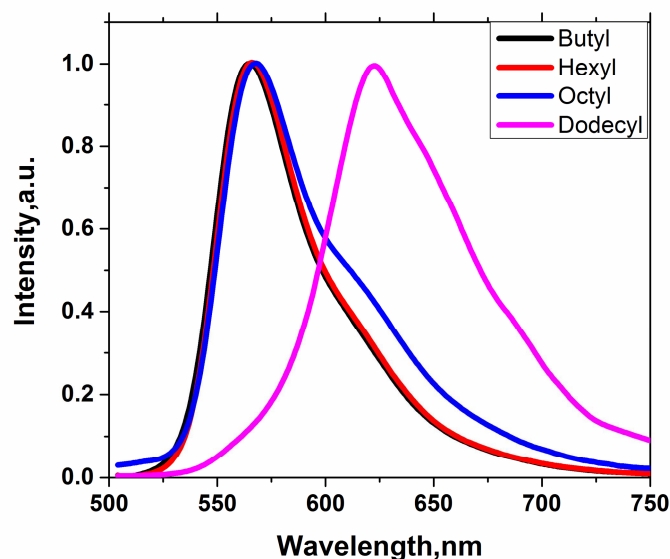


Figure 3.11 Normalized emission spectra of the compound **TATA 1-4** in neutral micelle (triton X-100) $\lambda_{\text{ex}}=480$ nm

3.3.2.3. Fluorescence quantum yield of lipophilic triazatriangulenium cations (TATA 1-4) in SDS micelles

Typically solubilization in micelles modulates fluorescence quantum yield (Φ_F) as the dye molecules due to a more rigid environment, screening from potential quenchers such as water molecules or due to polarity effects. In order to find out how the fluorescence quantum yield of these lipophilic cations gets affected due to this micellar medium we have determined the absolute fluorescence quantum yield by using an integrating sphere accessory. The data obtained are presented in table **3.1**. The results show a decreasing trend in the fluorescence quantum yield with increasing lipophilicity. This is contrary to the commonly observed phenomena for majority of molecules in such medium. This result points to the fact that there exist other channels for the deactivation of the excited chromophores when they get associated with anionic micelles.

3.3.2.4. Fluorescence lifetime measurements of lipophilic triazatriangulenium cations (TATA 1-4) in SDS micelles

The fluorescence decay of all the compounds were recorded in acetonitrile and in the anionic micellar medium by the method of Time Correlated Single Photon Counting (TCSPC). The decays observed in acetonitrile were monoexponential and did not show any dependence on the length of the alkyl chains. However, in anionic micellar medium the decays obtained were found to be emission wavelength dependent and fitted well with a biexponential model.

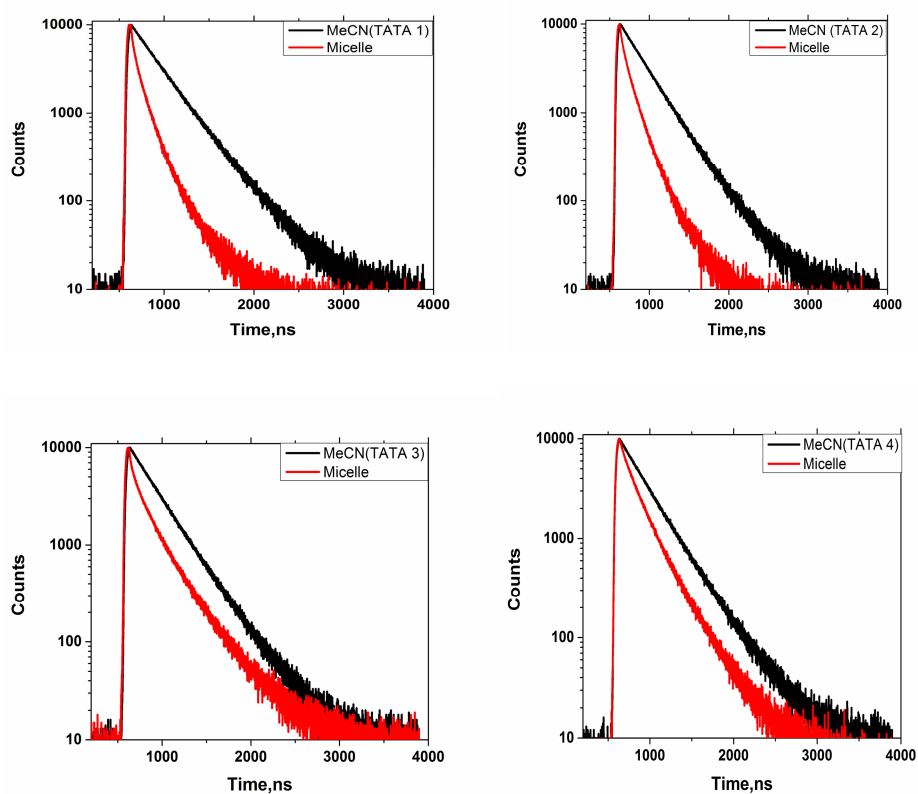


Figure 3.12 The fluorescence decay profile in acetonitrile and in anionic micellar medium (SDS). The excitation and monitoring wavelength were 480 nm and 560 nm, 563 nm, 616 nm, 629 nm for TATA 1-4) respectively

The figure 3.12 shows the fluorescence decay profiles of TATA 1-4 recorded in acetonitrile and in anionic micellar medium at their respective emission maximum. The average lifetime observed in the micellar medium showed an increasing trend from 1.69 ns for the cation having *n*-butyl side chains (TATA 1) to 4.72 ns for the cation with *n*-dodecyl side chains (TATA 4).

Table3.1. Absorption maxima ($\lambda_{\max}(\text{abs})$), extinction coefficient (ϵ_{\max}), fluorescence emission maximum ($\lambda_{\max}(\text{em})$), fluorescence quantum yield (Φ_{F}), average fluorescence lifetime ($\tau_{\text{F(av)}}$), radiative rate constant (k_{r}) and non-radiative rate constant (k_{nr}) of triazatriangulenium salts in anionic micellar medium (SDS). Values given in parentheses are those in acetonitrile.

Compound	$\lambda_{\max}(\text{abs})$ nm	ϵ_{\max} $\text{M}^{-1} \text{cm}^{-1}$ ($\times 10^2$)	$\lambda_{\max}(\text{em})$ nm	Φ_{F}	$\tau_{\text{F(av)}}$, ns	k_{r} (s^{-1}) $\times 10^{-2}$	k_{nr} (s^{-1}) $\times 10^{-1}$
TATA 1	525 (525)	7.0	560 (558)	0.21	1.69 (9.4)	12.4	4.6
TATA 2	544 (525)	7.6	563 (558)	0.15	2.14 (9.4)	7.0	3.9
TATA 3	552 (525)	9.0	616 (558)	0.10	2.6 (9.4)	3.8	3.4
TATA 4	556 (525)	10.1	629 (558)	0.04	4.72 (9.4)	0.8	2.0

3.3.2.5. Time-resolved emission spectra of lipophilic triazatriangulenium cations (TATA 1-4) in SDS micelles

Analysis of the emission spectral properties of these cations reveals that it has a complex emission behavior. This is evident from the following facts:

1. An alkyl chain length dependent red shift in the emission maximum.
2. The observed emission spectrum appears as an envelope of two emission bands

3. The fluorescence decay profiles are emission wavelength dependent and this is more prominent with **TATA 3** and **TATA 4** having n-octyl and n-dodecyl side chains.
4. The fluorescence decay profiles fits well to a biexponential model with two distinct lifetimes of emission

Such complex emission behavior is commonly observed in microheterogeneous medium. These properties when carefully analysed can throw light on to the topology of binding and also on the dynamics of excited state deactivation. The emission wavelength dependent biexponential fluorescence decay profiles and the alkyl chain length dependent red shifted emission band indicate the following:

1. Existence of two types of fluorophores in the micellar medium each having distinct photophysical behaviors.
2. An additional non-radiative process from the excited state leading to the formation of a more stabilized excited state.

A clear understanding on the photophysical properties in such complex systems can be obtained from the analysis of time resolved emission spectra (TRES) of the surfactant solutions. TRES is a convenient method that gives fruitful information regarding excited state dynamics and reactions of fluorophores. In this method, a set of TRES is obtained for the fluorophore, which is analysed with respect to different kinetic models that represent the system under study. There are two methods of acquiring TRES, one in which the decay profiles were accumulated for a fixed time and for fixed wavelength steps and in the second method which is a decay associated TRES reconstruction from the steady – state spectrum using lifetime information at each wavelength. In the first method, the array of decay profiles in 3D with both intensity and wavelength axes are sliced to get the

intensity – wavelength spectra for various time delays after excitation. Typical TRES spectra obtained for **TATA 3** and **TATA 4** in SDS micelles when excited at 510 nm are presented in figures 3.13 and 3.14. For **TATA 3** the TRES is characterized by a maximum at 575 nm at 0.45 ns after the excitation pulse. The same solution shows a maximum at ~ 620 nm at a time delay of 5.95 ns after the excitation. TRES of **TATA 4**, on the other hand showed the maximum of emission at 620 nm, which remain the same even after longer time delays.

The results of this study point to two possible scenarios. One in which there is solvent relaxation in the excited state. Such solvent relaxation is typical for chromophores where there is a significant change in the molecular dipole upon excitation.¹³ Another possibility is the existence of a second emissive species and the observed steady-state emission spectrum could be an envelope of emissions from these two species. In the case of **TATA 3**, the results show that there is a short wavelength emitting component which decays fast and a long wavelength emitting component that prevail at longer time delays after excitation. TRES obtained by this simple method of slicing the decays for different emission wavelengths is less informative and limited by time resolution and the number of emissive states involved.

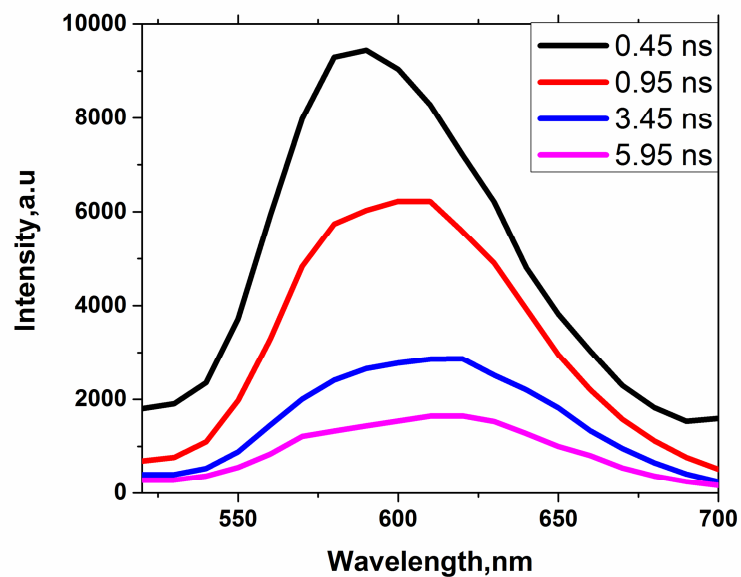


Figure 3.13 The time resolved emission spectra of **TATA 3** in SDS. The excitation wavelength is 510 nm

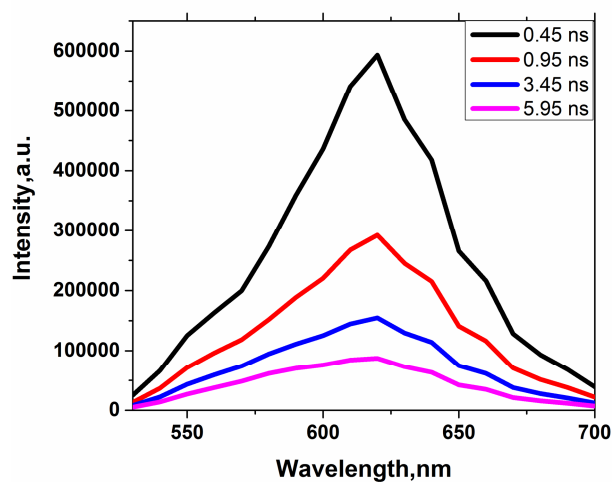


Figure 3.14 The time resolved emission spectra of **TATA 4** in SDS. The excitation wavelength is 510 nm

3.3.2.6. Time-resolved decay associated spectra and Time - Resolved Area Normalized Emission Spectra (TRANES) of lipophilic triazatriangulenium cations (TATA 1-4) in SDS micelles

Time - resolved decay associated spectra are more informative and can be obtained by a complex deconvolution analysis of the array of decay profiles acquired for a specific number of counts at fixed intervals of emission wavelengths. Here, global analysis of the array of decay profile yields the various lifetime components and their respective contributions to the overall fluorescence decay. This analysis resolves the emission spectra into different components which are associated to specific lifetimes. Sum of such spectra can give the steady – state spectra of the system under study. Further, results of the TRES analysis can be used to derive time – resolved area normalized emission spectra (TRANES) by the method described by Periasamy, N. and co-workers.¹⁴ The TRANES is a model free method to get conclusive evidence on the existence of multiple emissive states (only up to two) and are applicable to states that are kinetically coupled either reversibly, irreversibly or not coupled at all. The observation of an isoemissive point in the TRANES spectra is the important feature that helps one to conclude that there are two states present that contribute to the observed steady – state emission spectrum of a complex system.

A similar study of the present complex system of triazatriangulenium cations **TATA 3** and **TATA 4** in SDS micelle was carried out. The reconstruction of the decay associated TRES and TRANES involves different steps. In the first step, the fluorescence decays of the triazatriangulenium cations **TATA 3** and **TATA 4** were obtained over the entire fluorescence spectrum at 20 nm intervals by exciting at 455 nm using a pulsed LED with a pulse width of 1.5 ns. The decays were accumulated for upto 5000 counts along with the instrument response function. The decay

profiles thus obtained were deconvoluted using the instrument response function and fitted to a multiexponential decay function ($I(t)$, Equation 3.1) by global analysis using up to two exponential functions.

$$I(t) = \sum \alpha_i e^{-t/\tau_i}, i = 1 - 4 \quad (3.1)$$

Where α_i is the pre-exponential factor that represents the fraction of fluorophores with lifetime τ_i .

The lifetime values found for **TATA 3** were 5.5 ns for the short-lived species and 12.64 ns for the longer lived species. For **TATA 4** they were 4.55 ns and 12.87 ns respectively. Figure 3.15 and 3.16 represent the plot of fitted decay functions $I(t)$ for representative wavelengths obtained for **TATA 3** and **TATA 4**.

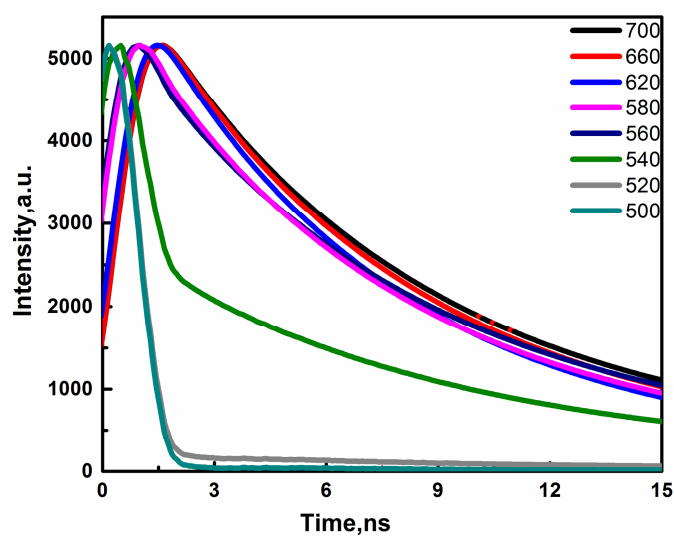


Figure 3.15 Fitted intensity decay functions at different emission wavelengths obtained after deconvolution of the experimental decays of **TATA 3** in SDS. $\lambda_{\text{ex}} = 455$ nm.

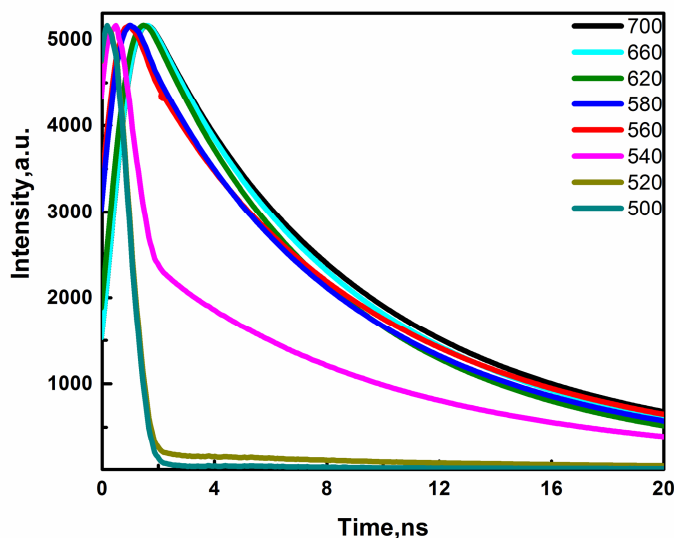


Figure 3.16 Fitted intensity decay functions at different emission wavelengths obtained after deconvolution of the experimental decays of **TATA 4** in SDS. $\lambda_{\text{ex}} = 455 \text{ nm}$.

Decay assisted TRES were constructed using the fitted parameters $\alpha_i(\nu)$ & $\tau_i(\nu)$ and the steady – state emission spectrum recorded with 455 nm as the excitation wavelength for the respective cation in SDS. The intensity at wavenumber ν (cm^{-1}) for delay time t was calculated using the following equation (Equation 3.2).

$$I(\nu, t) = I_{ss}(\nu) \frac{\sum_j \alpha_j(\nu) e^{-t/\tau_j(\nu)}}{\sum_j \alpha_j(\nu) \tau_j(\nu)} \quad (3.2)$$

Where $I_{ss}(\nu)$ is the intensity of the steady-state emission at ν (cm^{-1}) and $\alpha_j(\nu)$ & $\tau_j(\nu)$ are the fit parameters. Figure 3.17 and 3.18 are the TRES calculated for **TATA 3** and **TATA 4** for various time delays. It is clear from the TRES data obtained for **TATA 3** that its steady state spectrum is an envelope of two bands, one with a maximum at 588 nm (17006 cm^{-1}) and another long wavelength band at 653 nm (15307 cm^{-1}). In the case of **TATA**

4 the TRES data did show the short wavelength emission as a slight onset with the long wavelength emission band at 631 nm (15844 cm^{-1}) as the principal component in the TRES data.

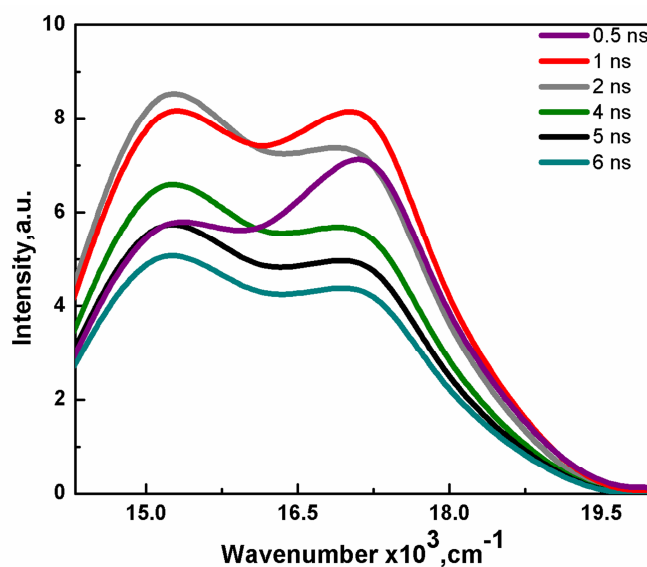


Figure 3.17 Time – resolved emission spectra (TRES) calculated for **TATA 3** in SDS at delays 0.5 ns, 1 ns, 2 ns, 4 ns, 5 ns and 6 ns. $\lambda_{\text{ex}}=455\text{ nm}$

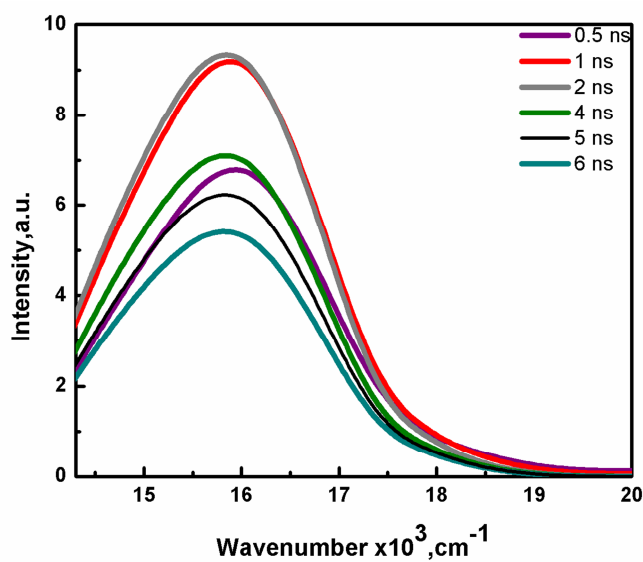


Figure 3.18 Time – resolved emission spectra (TRES) constructed for **TATA 4** in SDS at delays 0.5 ns, 1 ns, 2 ns, 4 ns, 5 ns and 6 ns. $\lambda_{\text{ex}}=455\text{ nm}$

Time-resolved area normalized spectra (TRANES) were constructed for **TATA 3** and **TATA 4** in SDS by normalizing the area under each spectrum in the TRES data with the spectrum obtained at 0.5 ns. Figure 3.19 and 3.20 are the TRANES spectra calculated for **TATA 3** and **TATA 4** for various time delays.

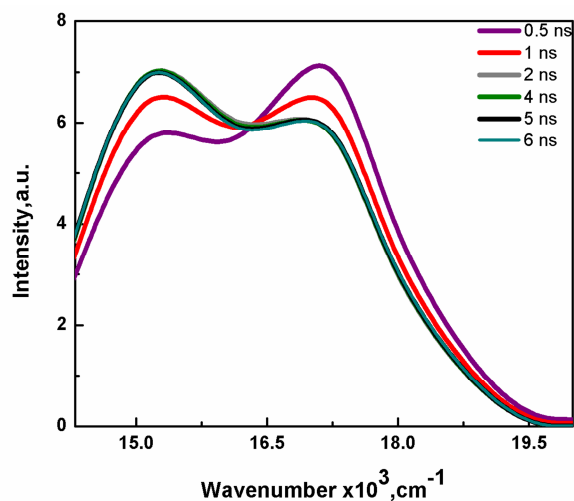


Figure 3.19 Time – resolved area normalized emission spectra (TRANES) constructed for **TATA 3** in SDS at delays 0.5 ns, 1 ns, 2 ns, 4 ns, 5 ns and 6 ns. $\lambda_{\text{ex}}=455$ nm

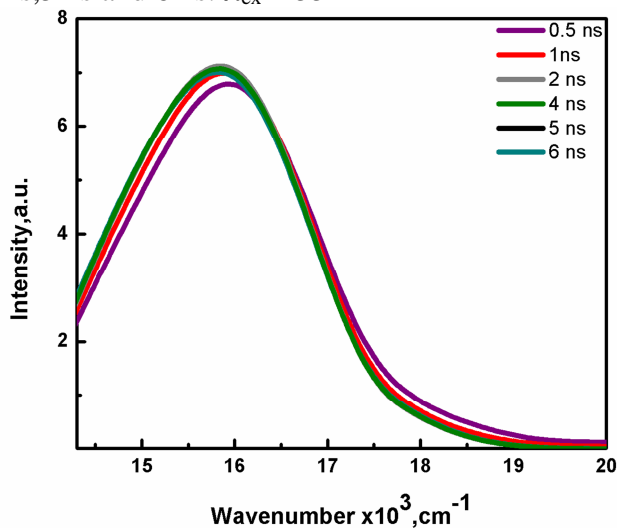


Figure 3.20 Time – resolved area normalized emission spectra (TRANES) constructed for **TATA 4** in SDS at delays 0.5 ns, 1 ns, 2 ns, 4 ns, 5 ns and 6 ns. $\lambda_{\text{ex}}=455$ nm

TRANES spectra of both **TATA 3** and **TATA 4** in SDS solutions showed isoemissive points at $16.31 \times 10^3 \text{ cm}^{-1}$ (613 nm). The observation of the same isoemissive point in the TRANES spectra of **TATA 3** and **TATA 4** show that there exists two emissive states when triazatriangulenium cations with lipophilic groups are bound to anionic micelles. This fact also rules out the solvent relaxation as the cause of redshift in the emission spectrum in the micellar medium. Moreover, in **TATA** the low energy electronic transition involves a charge transfer from the filled π orbitals of the phenyl rings and the n orbital of the N atoms to the vacant p orbital on the central carbon atom. Being symmetrical this electronic transition do not create large dipole moment change that is responsible for a solvent relaxation phenomena.

3.3.2.7. Binding topology and “disc to bowl” shape transformation of lipophilic triazatriangulenium cations (TATA) in SDS micelles

Binding interaction of the triazatriangulenium cations with the anionic SDS micelle and the corresponding photophysical properties are summarized below.

1. a red shift in the absorption spectrum for **TATA 2 - 4**
2. a red shifted emission maximum observed for **TATA 3** and **TATA 4**
3. a strong alkyl chain length dependence on absorption and emission data
4. a complex biexponential decay kinetics for **TATA 3** and **TATA 4**
5. two clear emission maxima in the decay assisted TRES data of **TATA 3**
6. TRANES data revealed the presence of two possible emissive states when associated with the micellar medium

7. presence of a growth kinetics feature for the long wavelength emission band in **TATA 3** and **TATA 4**.

Based on these results one can make an assessment on the possible location and mode of binding of the triazatriangulenium cations in anionic micelles. Based on simple polarity arguments we cannot predict the location and mode of binding in this complex system. The two species observed in the TRANES data can be viewed as a bound cation and an unbound cation. But the absorption maximum does not indicate the presence of an unbound cation, which is freely solvated by the aqueous bulk. If this is the case, then, the absorption maximum should have been similar to **H TATA**, the water-soluble triazatriangulenium cation. The observed absorption maximum however, is red shifted by a larger extent than the value of 530 nm in aqueous medium.

Being cationic the most probable location of **TATA** is the surface of the micelle i.e, the Stern layer. This association can be by two modes. One, in which the plane of the molecule is tangential to the surface of the micelle and another, as an intercalated cation between the anionic sulfonate head groups in the micelle. The absorption maximum also shows chain length dependence. These changes in absorption and emission properties are indicative of a destabilization of the ground state possibly a geometrical perturbation as a result of association with the micelle.

Facts 2-6 are more related to the excited state of these cations when dissolved in SDS micelles. Here the red shifted emission maximum, complex decay kinetics and alkyl chain length dependence and the resolution of two emission bands for **TATA 3** with the presence of an isoemissive point suggest two emissive states that are present when these cations are in the micellar medium. For **TATA 3** and **TATA 4** this is most visible and these

are cations that are held closer to the micelle due to the higher hydrophobicity of the longer alkyl chains. Combining the two facts that binding leads to destabilization of the ground state and the corresponding red shifted band in the emission spectrum of **TATA 3** and **TATA 4** reveal a potential binding induced perturbation of the geometry. This perturbation can be attributed to tight binding of the alkyl groups to the hydrophobic core of the micelle with the cationic disc of the triazatriangulenium ion lying tangential to the surface of the micelle or as “Spider-on-an apple” topology as illustrated in the cartoon (figure 3.21) Such a topology definitely affect the planarity of the triangular disc of the cation and a “disc – to – bowl” type of geometric change can occur in **TATA 3** and **TATA 4**. Though this mode of binding affects the geometry of the molecule the intercalative mode do not induce such changes. In this case the emission spectrum is not perturbed and this could be the case observed for **TATA 1** and **TATA 2**. The changes in the ground state and excited state energies and the effect on the radiative transitions are illustrated in the energy level diagram presented in figure 3.22.

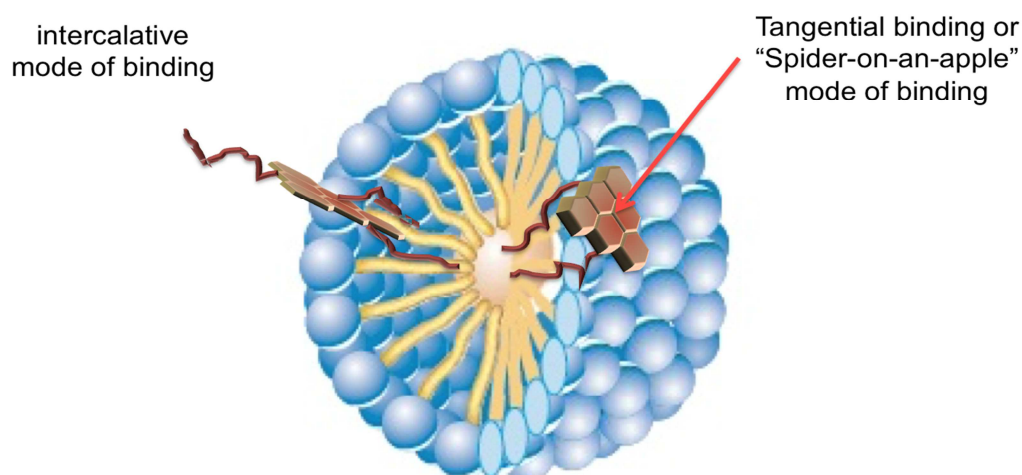


Figure3.21. Cartoon showing “*spider-on-the-apple*” and intercalative type binding topology of triazatriangulenium – anionic micelle association

In all these cases of tangential binding **TATA-SDS** assemblies could exist as a loosely bound ensemble and another fraction, which is strongly bound to the micelle. The relative proportion of these fraction depend on the length of the alkyl chain, as observed in the case **TATA 3** and **TATA 4**. The growth kinetics observed for the emitting species at 629 nm is an evidence for such loosely bound assemblies. In such loosely bound assemblies we can safely assume an additional excited state deactivation channel involving a “disc–bowl” or “pseudo bowl – bowl” transformation and pyramidalisation of the central sp^2 hybrid carbon atom (figure **3.22 A** and **B**). **TATA 1**–SDS assembly, which shows photophysical properties very similar to that in homogenous acetonitrile medium suggests that there is no such structure perturbation is affecting this cation when getting bound to SDS micelle. In this case the binding could be purely from intercalative mode. For **TATA 2**, which shows a slight destabilization in the ground state and no destabilization in the excited state, the mode of binding can be intercalative. The absorption and emission from this assembly is best described by the energy level diagram figure **3.22 B**. Such dual emission was already reported for structurally similar planarised triarylboranes by Kushida et al.¹⁵ In this report the dual emission is explained by both theory and experiment that there exists a second minima for the excited states of these molecules with a pyramidal geometry.

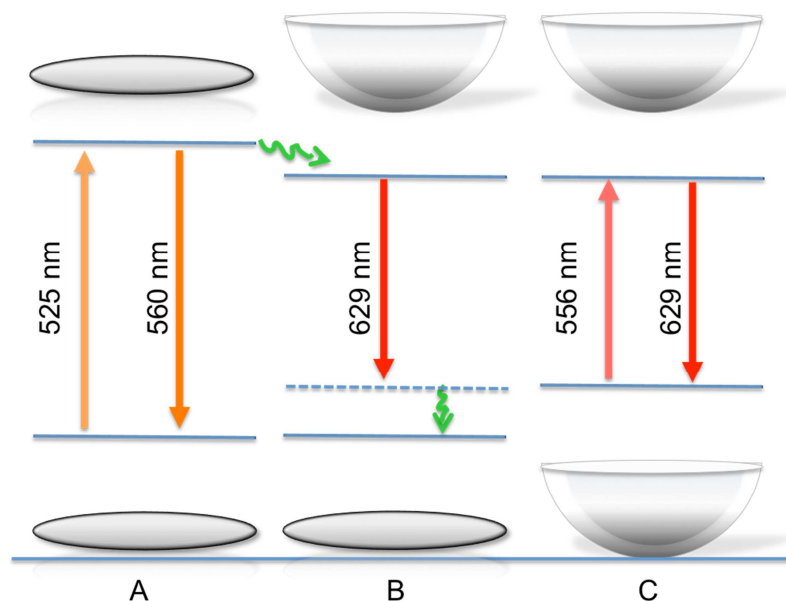


Figure 3.22 The energy level diagram showing effect of ground state “disc – bowl” geometric change and excited state “disc – bowl” change on the radiative transitions in TATA-micelle assemblies

3.3.2.8. Effect of temperature on the fluorescence emission spectra of lipophilic triazatriangulenium cations (TATA 1-4) in SDS micelles

To further support the “disc to bowl” shape transformation and the pyramidalisation of the sp^2 hybrid central carbon atom of the micelle bound cation we conducted a temperature dependent emission measurement for **TATA 3** and **TATA 4** in SDS micelle. Typically, anionic micelle tend to increase the rigidity of the assembly and compactness with increasing temperature up to $55\text{ }^{\circ}\text{C}$ and above that temperature they start to dissociate.^{16,17} Interestingly this transformation was clearly seen in the temperature dependent emission spectra of **TATA 3** and **TATA 4** in SDS solutions. Figures 3.23 and 3.24 show the temperature dependent emission spectrum of **TATA 3** and **TATA 4** in SDS micelle. At temperatures above $55\text{ }^{\circ}\text{C}$ the spectra recorded start showing an increase in the intensity of the band at 558 nm and with a concomitant decrease in the intensity of the 620

nm band. This observation supports the binding of the **TATA 3** and **TATA 4** with “spider-on-an-apple” topology. The temperature-induced disassociation can release the strain on the triazatriangulenium cation favouring a reverse “bowl to disc” transformation of the tightly bound cations resulting in the observed changes in the emission spectrum.

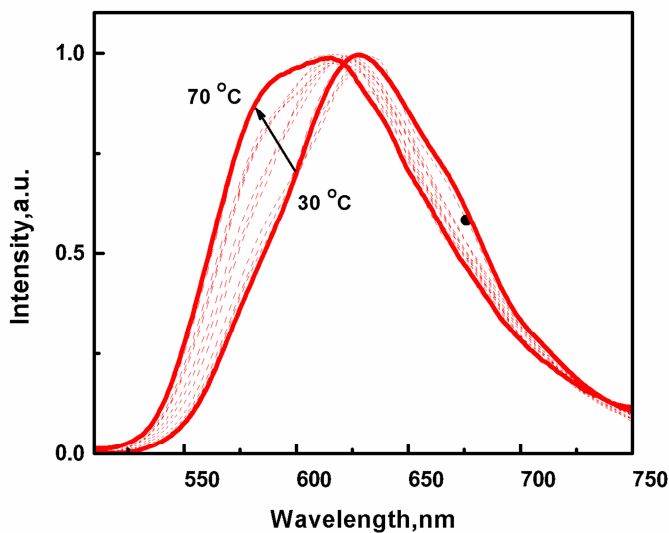


Figure 3.23 The temperature dependent emission spectrum of **TATA 3** in SDS micelle. $\lambda_{\text{ex}}=480$ nm.

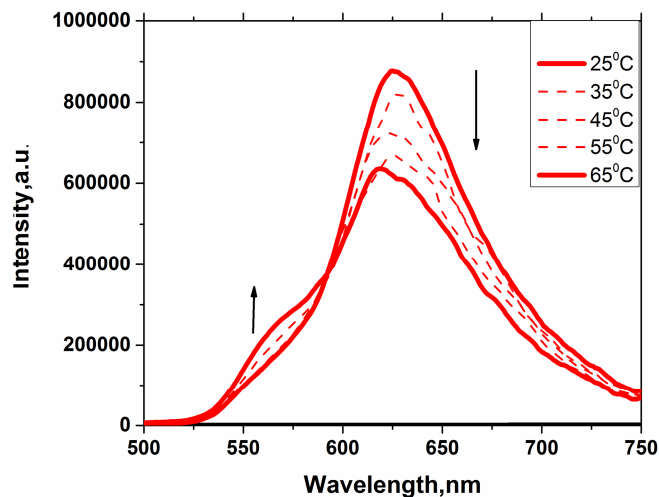


Figure 3.24 The temperature dependent emission spectrum of **TATA 4** in SDS micelle. $\lambda_{\text{ex}}=480$ nm.

3.3.3. Theoretical Calculations

From the photophysical studies it was concluded that in micellar medium the triazatriangulenium cations with long alkyl substituent on the bridging N atoms experiences a distortion in geometry upon binding with micelles. This distortion is indicated by a red shift in the absorption spectrum and appearance of a new emission band at 629 nm in the emission spectrum. The distortion in the geometry could be a pyramidalisation of the sp^2 hybrid central carbon atom bearing the positive charge and indicated in TRES and TRANES measurements in the micellar medium. Such pyramidalisation of the geometry and its role on the electronic properties was reported earlier for a structurally similar planarised triarylboranes.¹⁵ In order to further verify the nature of geometrical perturbation we have carried out DFT calculations using model structural geometries of triazatriangulenium cation. All computations were done at B3LYP/6-31+G* level. Model system chosen was an N-ethyl substituted triazatriangulenium cation with the assumption that alkyl chains do not perturb significantly the molecular orbitals of TATA series of cations under study. Test geometries are chosen with a view to study how a planar - bowl geometry change affect the electronic transitions. A series of structure with a fixed geometry was chosen where the angle between a dummy atom placed perpendicular to the plane of the ring and the C+ - C-phenyl bond is varied systematically to induce a planar to bowl shape perturbation. The optimized geometry for these structures were computed and presented in figures 3.25, 3.27 and 3.29. The first test geometry has the central carbon fixed at the plane of the molecule. Then for the second and third geometry, an angle of 2 and 4 degrees were chosen to ensure the pyramidalisation of central carbon. Using the optimized structure TD-DFT calculations were carried out to compute the radiative transitions from ground state to various excited states. The absorption calculated in this

geometry is shown in figure 3.26. The absorption spectrum computed for the planar cation consists of bands at 265 nm, 290 nm, 325 nm, 477 nm, 495 nm which were in good agreement with the experimental absorptions. The two long wavelength (low energy) transitions are between HOMO-1 to LUMO and HOMO to LUMO.

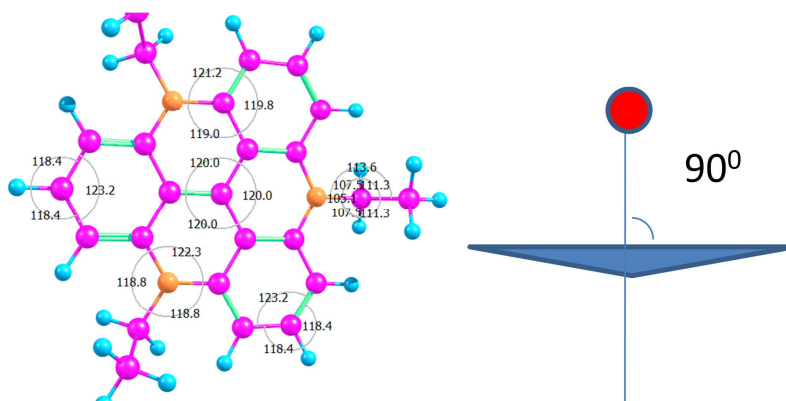


Figure 3.25 The optimized geometry of N- ethyl substituted TATA when the geometry is fixed with the central carbon at the plane of the molecule

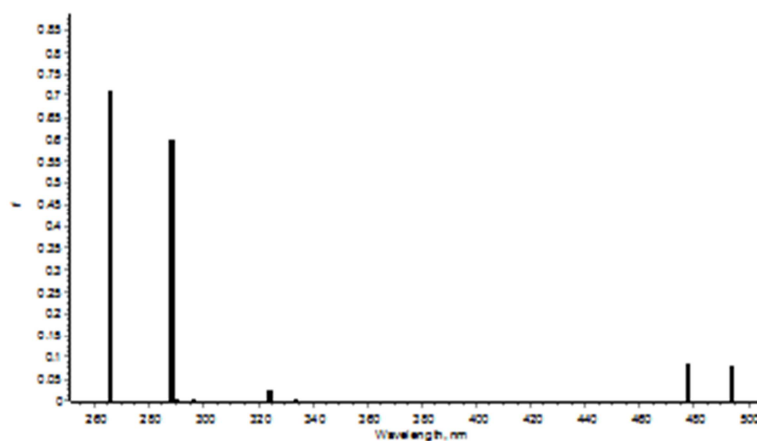


Figure 3.26 The calculated absorption spectrum of N- ethyl substituted TATA when the geometry is fixed with the central carbon at the plane of the molecule

The optimized geometry obtained when the angle between the dummy atom and the plane of the molecule changed to 92° was used for computing the radiative transitions from ground state to various excited states for this non-planar geometry. The transitions between different states computed by TD-DFT are given in figure 3.28. The computed spectrum consists of bands at 265 nm, 290 nm, 325 nm, 482 nm, where the two long wavelength transitions at 477 nm and 495 nm observed for the planar cation was now became degenerate with maximum at 482 nm. Thus pyramidalisation of the central carbon and the transformation of planar to bowl shape affected the electronic transitions in particular the low energy transition.

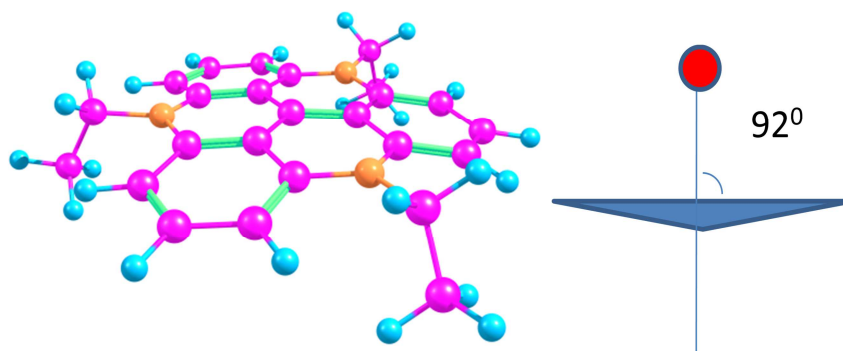


Figure 3.27 The optimized geometry of N-ethyl substituted TATA when the geometry is fixed with the angle of central carbon atom shifted to 92°

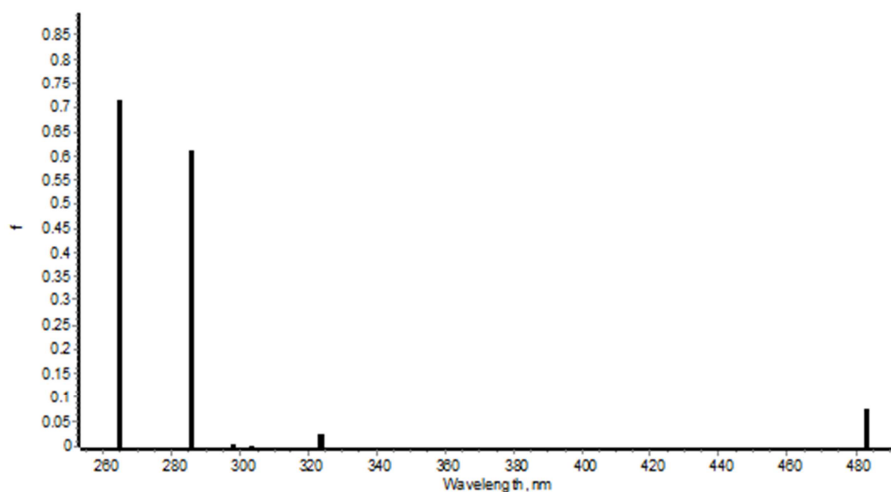


Figure 3.28 The calculated absorption spectrum of N-ethyl substituted TATA when the geometry is fixed with the angle of central carbon atom shifted to 92°

Further pyramidalisation was induced by forcing the angle between the dummy atom and the plane of the cation to 94° . The optimized geometry for this structure was used for TD-DFT computation of the absorption spectrum (figure 3.30). The absorption spectrum consists of bands at 265 nm, 290 nm, 325 nm, 504 nm. All other transitions except the one at longer wavelength (504 nm) were unaffected by the increased pyramidalisation. Only the long wavelength transition got red shifted by 22 nm. Thus a small distortion from a planar geometry to bowl shape geometry can lead to a significant change in the absorption properties of lipophilic triazatriangulenium cations. This study validates our arguments on the “disc – to – bowl” shape geometrical change upon association with micelles.

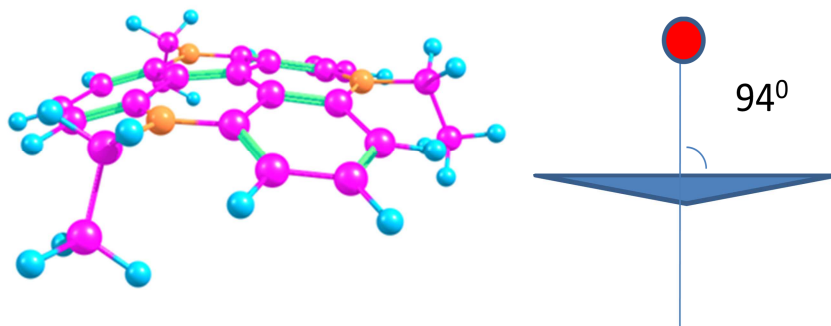


Figure 3.29 The optimized geometry of N-ethyl substituted TATA when the geometry is fixed with the angle of central carbon atom shifted to 94°

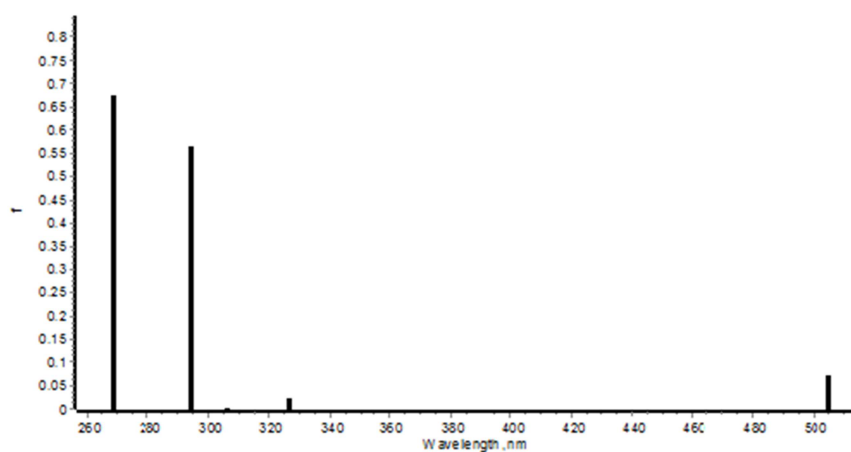


Figure 3.30 The calculated absorption spectrum of N-ethyl substituted TATA when the geometry is fixed with the angle of central carbon atom shifted to 94°

3.4. Conclusions

The lipophilic triazatriangulenium cations show chain length dependent red shift in the absorption and emission spectrum in anionic micellar medium. The increase in the chain length makes the cations more hydrophobic and strengthens the binding. The stronger binding perturbs the geometry of the molecules as a result a planar to bowl shape transformation occurs as observed in the case of dodecyl substituted triazatriangulenium

derivative. We can safely assume the topology of cation binding with the micelles as like a “spider sitting on an apple” with its legs piercing the apple.

3.5. Experimental

3.5.1 General Techniques

All reactions were carried out using oven dried glasswares. The solvents used were distilled and dried prior to use. All reagents were purchased from either Sigma - Aldrich or Spectrochem Pvt.Ltd and were used as received. Surfactant solutions (100 mM) were prepared by dissolving respective surfactants in ultrapure water from Millipore water purification system. Absorption spectra were recorded using Evolution 201 UV-visible spectrophotometer. Fluorescence, Fluorescence lifetime studies, Time resolved emission spectra, Temperature dependent emission spectra were carried out using JobinYvonFluorolog3-211UV-Vis-NIR fluorescence spectrometer.

The triazatriangulenium salts (**TATA 1-4**) were prepared based on the reported procedure.⁹ The following spectroscopic data are obtained for the compounds. **TATA 1** Yield 30 %. MS (ESI, m/z): 450. Mp: >300 °c. FT-IR (cm⁻¹) 3435, 2925, 1618, 1446, 1053. **TATA 2** Yield 32%. MS (ESI, m/z): 534. Mp: >300 °c. FT-IR (cm⁻¹) 3436, 2924, 1615, 1455, 1052. **TATA 3** Yield 28 %. MS (ESI, m/z): 618. Mp: >300 °c. FT-IR (cm⁻¹) 3447, 2931, 1616, 1335, 1048. **TATA 4** Yield 30%. MS (ESI, m/z): 786. Mp: >300 °c. FT-IR (cm⁻¹) 3437, 2924, 1617, 1390, 1088. ¹H NMR (500MHz CD₃CN) δ (ppm): 8.010-7.976 (t, 1H), 7.237-7.220(d, 2H), 4.293-4.260 (t, 2H), 2.143-1.281 (m, 23H). ¹³C NMR (125 MHz, CD₃CN) δ(ppm): 141.12, 138.15, 117.87, 105.68, 48.42, 32.25, 29.66.

3.6 References

1. Wei, Y.; Quan, L.; Zhou, C.; Zhan, Q. *Nanomedicine*. **2018**, *13*, 1495.
2. Pal, P.; Zeng, H.; Durocher, G.; Girard, D.; Giasson, R.; Blanchard, L.; Gaboury, L.; Villeneuve, L. *J. Photochem. Photobiol. A*. **1996**, *98*, 65.
3. Pal, P.; Zeng, H.; Durocher, G.; Girard, D.; Li, T.; Gupta, A.K.; Giasson, R.; Blanchard, L.; Gaboury, L.; Balassy, A.; Turmel, C. *Photochem. Photobiol.* **1996**, *63*, 161.
4. Kim, J.; Michielsen, S. *Nanomaterials*. **2016**, *6*, 243.
5. Abbott, D.C. *Analyst* **1962**, *87*, 286.
6. Havelcová, M.; Kubát, P.; Němcová, I. *Dyes Pigment*. **1999**, *44*, 149.
7. Bunton, A.; Romsted, L.S.; Sepu, I.; Lveda, L.A. *J. Phys. Chem.* **1980**, *84*, 2611.
8. Pellosi, D.S.; Estevão, B.M.; Semensato, J.; Severino, D.; Baptista, M.S.; Politi, M.J.; Hioka, N.; Caetano, W. *J. Photochem. Photobiol. A*. **2012**, *247*, 8.
9. Martin, J. C.; Smith, R. G. *J. Am. Chem. Soc.* **1964**, *86*, 2252.
10. Laursen, B. W.; Krebs, F. C. *Angew. Chem. Int. Ed. Engl.* **2000**, *39*, 3432.
11. Laursen, B. W.; Krebs, F. C. *Chem. Eur. J.* **2001**, *7*, 1773.
12. Dileesh, S.; Gopidas, K.R. *J. Photochem. Photobiol. A*. **2004**, *162*, 115.
13. Lakowicz JR, editor. Principles of fluorescence spectroscopy. Springer Science & Business Media; 2013 Apr 17
14. Koti, A.S.R.; Krishna, M.M.G.; Periasamy, N. *J. Phys. Chem. A*. **2001**, *105*, 1767.
15. Kushida, T.; Camacho, C.; Shuto, A.; Irle, S.; Muramatsu, M.; Katayama, T.; Ito, S.; Nagasawa, Y.; Miyasaka, H.; Sakuda, E.; Kitamura, N. *Chem. sci.* **2014**, *5*, 1296.

16. Makowska, J.;Wyrzykowski, D.;Pilarski, B.;Chmurzyński, L. *J. Therm. Anal. Calorim.* **2015**, *121*, 257.
17. Hammouda, B. *J. Res. Natl. Inst. Stand. Technol.* **2013**, *118*, 151.

CHAPTER 4

Synthesis, Characterization and Study of Surface-Tethered Triazatriangulenium Cations

4.1. Abstract

The synthesis of heterogeneous supported sensitizers has gained much attention in recent times and has found various applications in areas including photosensitized disinfection of waste water, taking into account their advantages over the homogeneous photosensitizers. Among the heterogeneous sensitizers, silica gel supported organic dyes have received great attention. The chapter includes the synthesis of heterogeneous supported sensitizers in which triazatriangulenium is covalently anchored on silica. The silica is functionalized with amino groups using the (3-aminopropyl)trimethoxysilane and methyltrimethoxysilanes. The precursor for the triazatriangulenium salts, tris-(2,6-dimethoxyphenyl) carbenium tetrafluoroborate when cyclised in the presence of amino functionalized silica resulting in the formation of triazatriangulenium cation on the silica surface as an organic – inorganic hybrid material. The singlet oxygen sensitization capability of the triazatriangulenium-silica composites was monitored using the singlet oxygen probe disodium-9, 10-anthracenedipropionic acid. The study of disinfection of water containing pathogenic bacteria was also carried out to determine the effectiveness of the prepared triazatriangulenium-silica composites for the waste water treatment. All the four types of synthesized triazatriangulenium-silica composites produced singlet oxygen, as it is evident from the photobleaching of singlet oxygen probe disodium-9,10-anthracenedipropionic acid (ADPA). The results of the disinfection studies

using the four types of prepared triazatriangulenium-silica microparticle conjugates shows that these materials are effective in killing of bacterial pathogens when used with light.

4.2. Introduction

The photophysical and singlet oxygen production properties of triazatriangulenium salts were discussed in the previous chapters. The issues regarding solubility and isolation are two major problems found in the study of photosensitization reactions in homogeneous medium. Immobilized photosensitizers found solution to both these problems, allowing the flexibility in the solvent selection and the easy recovery after the reaction.¹ The immobilized sensitizers found applications in waste water treatment, chemical synthesis and photodynamic processes such as PDT and photo-disinfection of pathogen contaminated water.²⁻⁴ Such recoverable and reusable heterogeneous catalytic systems are cost effective when compared to methods such as ozonization, chlorination etc. Literature shows a large number of supports available for the photosensitizer immobilization, including polymers, glass plates, zeolites, silica gel etc.⁵ Among these various supports available, silica gel has an important position. The main advantage of using this inorganic matrix for the immobilization is the more rigid and inert environment and enhanced photochemical and thermal stability compared to the organic polymer matrices.⁶ Moreover silica is a low-cost material with biocompatibility making it an attractive material for both industrial and biological applications.⁷ The heterogeneous sensitizers have many advantages over the homogeneous sensitizers, but at the same time they have some limitations too. Aggregation of the sensitizer molecules on the surface of the supports is a problem faced by many hybrid systems. Since the aggregation shortens the triplet lifetime by non-radiative processes thereby affecting the singlet oxygen generation efficiency. But, a way out is

to use covalent anchoring of the photosensitizer molecule on to a solid support.⁸ The major disadvantages of using heterosensitizers are, the decreased efficiency and occasional leaching of the photosensitizer into the solution. The accessibility of oxygen to the photosensitizers may be affected by the support used and the fast quenching of the generated singlet oxygen by the support are two major issues regarding the heterosensitizers.⁹

Kuznetsova et al., developed a series of heterogeneous singlet oxygen sensitizers by immobilizing cationic phthalocyanine on silica gel having propylamine groups and propylamine groups grafted with additional propyleneimine units (Chart 4.1).¹⁰ The photophysical properties, singlet oxygen generation capacity and the photobactericidal activity of these sensitizers in aqueous suspensions were studied. The spacer length has no effect on the photophysical properties and the singlet oxygen generation efficiency but, the photobactericidal activity was found to have increased with increase in the spacer length.

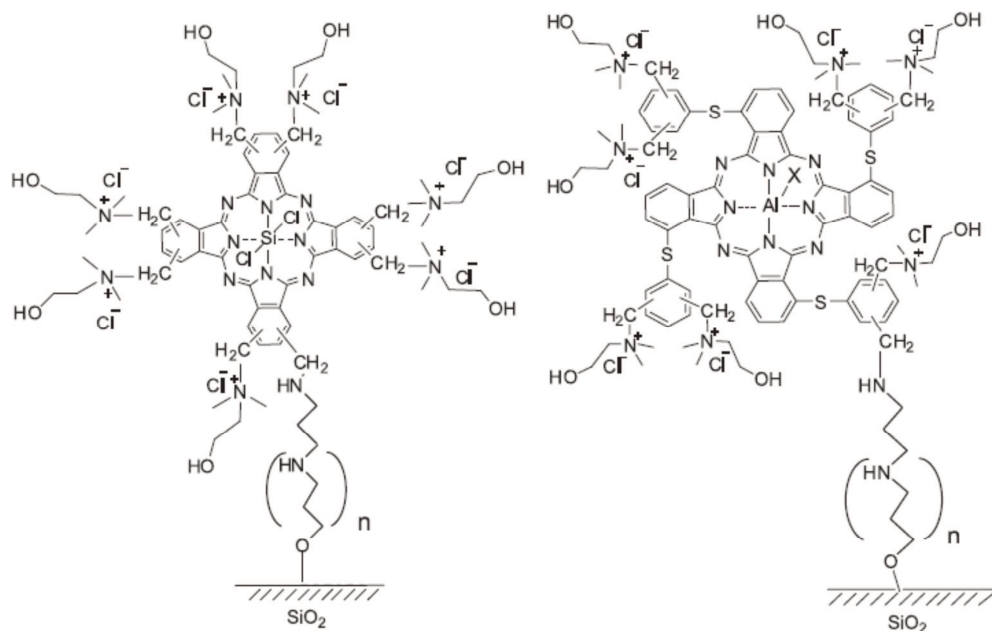


Chart 4.1(Adapted from reference 10)

Pineiro et al., synthesized a heterogeneous sensitizer in which halogenated porphyrin was covalently supported on aminoalkylated silica.⁹ The structure is shown in the following figure 4.1. The influence of support on the singlet oxygen quantum yield was studied by comparing it with another heterogeneous sensitizer in which the same halogenated porphyrin was attached to the aminoalkylated Merrifield resin. The photooxidation of α -terpinene was tested with both the heterogeneous sensitizers. Compared to the Merrifield resin, a small decrease in the singlet oxygen quantum yield was observed in the case of silica supported sensitizer because of the quenching due to the OH groups on the silica.

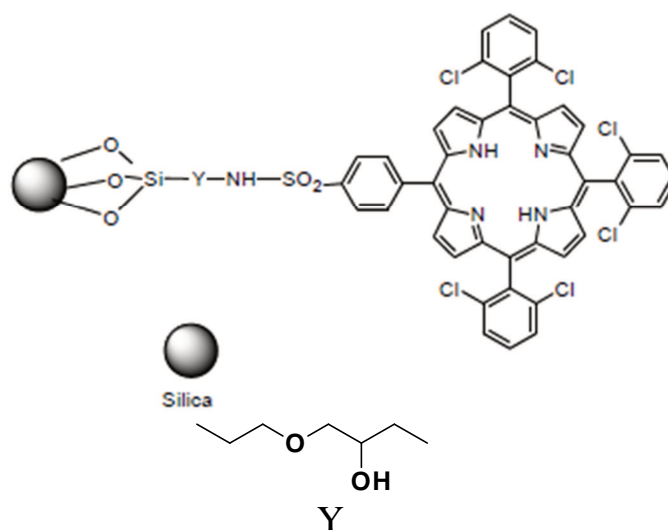


Figure 4.1 Halogenatedporphyrin was covalently supported on aminoalkylated silica. (Adapted from reference 9)

Magaraggia et al., developed a porphyrin silica microparticle conjugates in which a tetracationic meso-substituted amphiphilic porphyrin was encapsulated within the silica particle.¹¹ The porphyrin-silica microparticle conjugates show a complete stability for at least three months when suspended in neutral aqueous medium and a limited photobleaching when exposed to the full spectrum visible light. The singlet oxygen generation was observed when the particles were illuminated with visible

light. The microparticle shows a 4 log decrease in the survival of gram positive bacteria with 20 minutes irradiation and the same effect was observed in the case of gram negative bacteria with a 30 minutes irradiation in the presence of visible light. Albiter et al., incorporated a series of cationic dyes into a silica matrix by using ultrasound irradiation.⁷ Methylene blue (MB), safranin-O (SF), toluidine blue (TB), and neutral red (NR), were used in this work. The singlet oxygen generation efficiency of these dyes were monitored using photosensitized oxidation of 9, 10-dimethylanthracene (DMA). Among the four dyes doped on the silica matrix, silica-SF showed high singlet oxygen efficiency.

Cantau et al., reported the singlet oxygen quantum yield and singlet oxygen lifetime at the gas–solid interface in silica gel.¹² 9,10-dicyanoanthracene (DCA), 9,10-anthraquinone and a benzophenone derivative, 4-benzoyl benzoic acid were encapsulated in parallelepipedic xerogel monoliths. The singlet oxygen quantum yield and lifetime were determined based on time-resolved $^1\text{O}_2$ phosphorescence with 1H-phenalen-1-one included in the same xerogel as a reference sensitizer. The singlet oxygen generation efficiency of the various photosensitizers were compared based on the photooxidation of dimethylsulfide. The highest singlet oxygen efficiency was observed in the case of DCA encapsulated parallelepipedic xerogel monoliths.

The photosensitized oxidation of 9, 10-dimethylanthracene (DMA) in acetonitrile via singlet oxygen was reported by Albiter et al.¹³ They used a safranin- O/silica composite and the reaction was carried out under visible light. The only product formed was 9, 10-endoperoxianthracene. The initial concentration of DMA, the intensity of the light and the amount of the composites are the factors affecting the rate of the reaction. The schematic representation of the reaction is shown below.

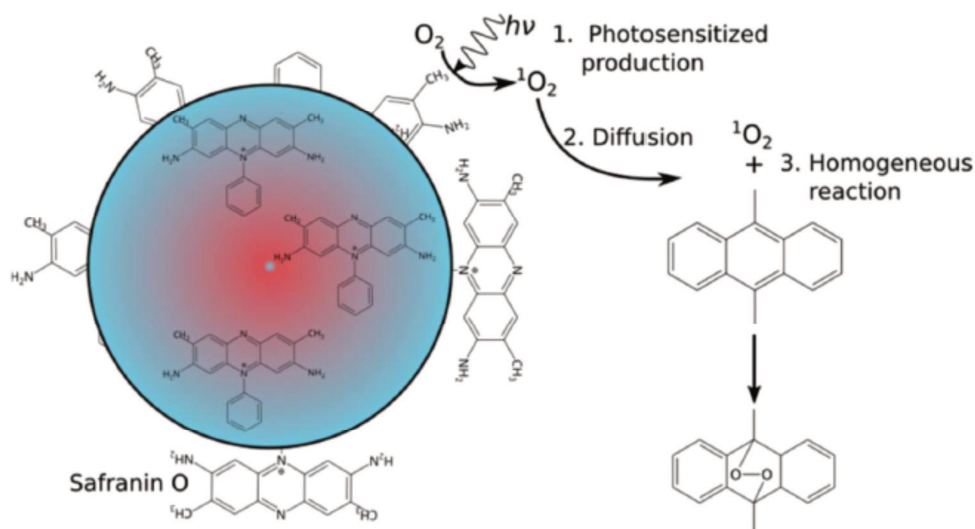


Figure 4.2 Schematic representation of the photosensitized oxidation of DMA using the SF/SiO₂ composite. (Adapted from reference 13)

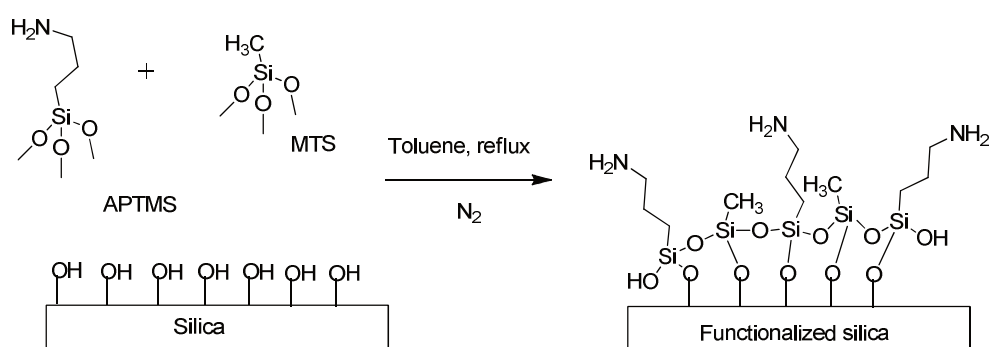
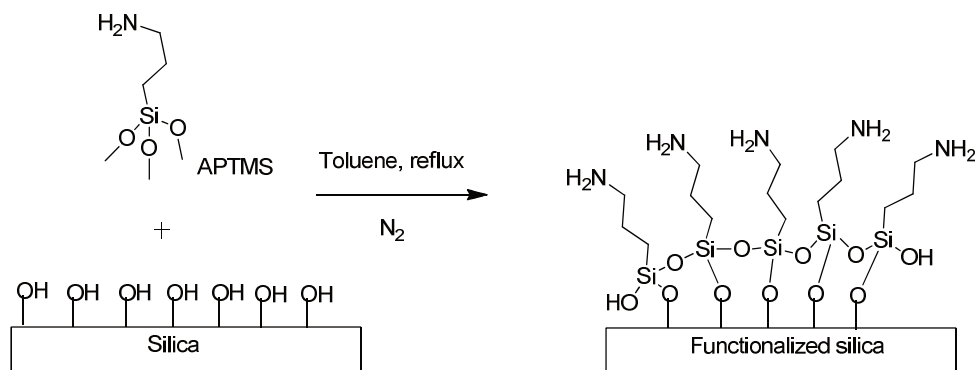
The need for the clean water is a worldwide problem. The water sources are heavily polluted by the hazardous chemicals and several kinds of pathogens such as bacteria, fungi, moulds, viruses, etc, making the problem even more severe. Therefore, there is an urgent need for the efficacious and an environmentally safe technique for the water purification and disinfection. Singlet oxygen-mediated photooxidation reactions satisfies the green chemistry demands for the development of new technologies for water treatment specially for the decontamination of organic pollutants and germs.^{1,9,14} Such processes make use of visible light (solar radiation) and oxygen (from air) as oxidant in the presence of a photosensitizer. Many known hybrid systems based on singlet oxygen mediated photo-disinfection models use dye molecules which have limited stability in aqueous environments. The mode of attachment of the sensitizer on to the heterogeneous support should also have stability under aqueous environments. Some of the known anchoring strategy uses ester or amide

linkages, which are susceptible to hydrolysis and leaching of the sensitizers. Such leaching of these toxic sensitizers is also harmful for the environment and health. In the present work, we propose the triazatriangulenium cation as a stable and visible light active sensitizer covalently anchored to the silica surface. The method adopted for anchoring is unique in which the sensitizer is strongly attached to the surface via the aza-bridging reaction used for the synthesis of the triazatriangulenium cation. The amino functionalized silica react with tris-(2,6-dimethoxyphenyl) carbenium tetrafluoroborate producing new triazatriangulenium-silica composite. This chapter describes the synthesis, characterization, singlet oxygen production and the antibacterial activity of the new triazatriangulenium-silica composites.

4.3. Results and Discussion

4.3.1. Functionalization of silica surface

Two types of amino-functionalized silica particles, S-APTMS and S-APTMS+MTS were prepared. S-APTMS was prepared by the reaction of (3-aminopropyl)trimethoxysilane (APTMS) and silica particles. In this case an appropriate ratio of APTMS to the silica particles was chosen to ensure a higher density of amino functional groups on the surface of the silica particles. In S-APTMS+MTS the ratio of APTMS with silica particles was moderated with the addition of methyltrimethoxysilane (MTS) so that the surface density of amino groups are minimum to the extent that there could be isolated amino groups present based on the reported procedure.¹⁵ General representation of the functionalization of silica is illustrated in the following schemes **4.1** and **4.2**.



4.3.2. Synthesis of Tris-(2,6-dimethoxyphenyl) carbenium tetrafluoroborate (39)

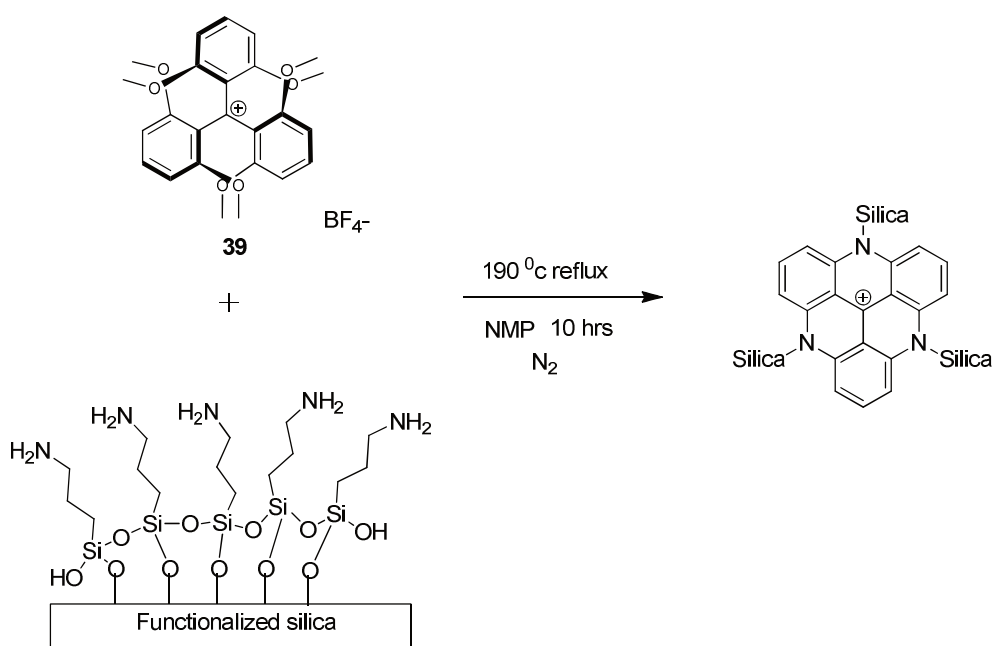
The precursor for the synthesis of triazatriangulenium salt tris-(2, 6-dimethoxyphenyl) carbenium tetrafluoroborate was prepared by a reported procedure and discuss elsewhere in the thesis (chapter 2, 2.5.2)¹⁶

4.3.3. Synthesis of triazatriangulenium- silica composites

Prior to the reaction of the amino functionalized silica particles with the tris-(2,6-dimethoxyphenyl) carbenium tetrafluoroborate, the amine capacity of the functionalized silica was measured. This was made by using acid-base titration method and was found that S-APTMS samples functionalized with (3-aminopropyl)trimethoxysilane alone contains 1.7 mmol/g

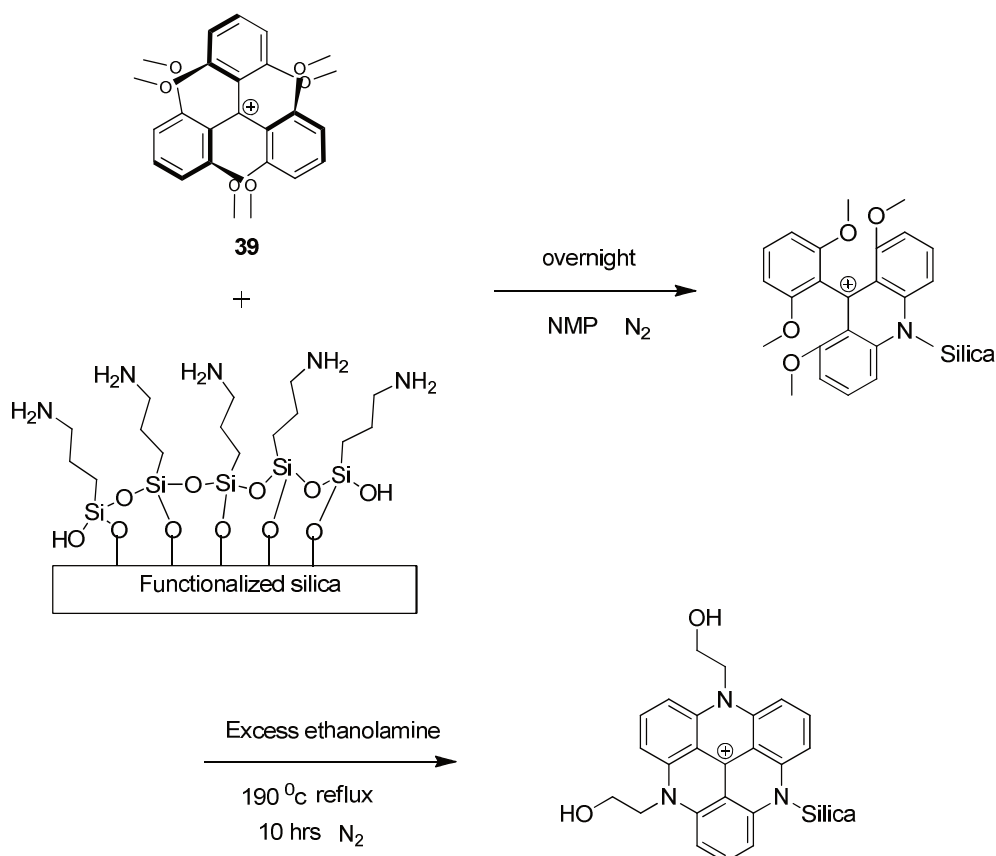
free amino groups and S-APTMS+MTS samples functionalized with mixture of (3-aminopropyl) trimethoxysilane and methyltrimethoxysilane contains 0.9 mmol/g free amino groups.

Triazatriangulenium cations are readily formed by the reaction of tris-(2, 6-dimethoxyphenyl) carbenium tetrafluoroborate with primary amines. In the synthesis of triazatriangulenium – silica composites we adopted a similar procedure and the amount of tris-(2, 6-dimethoxyphenyl) carbenium tetrafluoroborate was taken according to the amine capacity of the silica material used in the reaction. Here the primary amino groups on the amino functionalized silica were used as the N-nucleophiles in the aza-bridging reaction. Four types of triazatriangulenium - silica composites were prepared. The first one, **S1** (S1-APTMS-TATA) is the composite where all the three N-bridges on the triazatriangulenium cation formed by using surface amino groups. Scheme 4.3 illustrates its formation on the silica surface.



Scheme 4.3 Synthesis of S1-APTMS-TATA (S1)

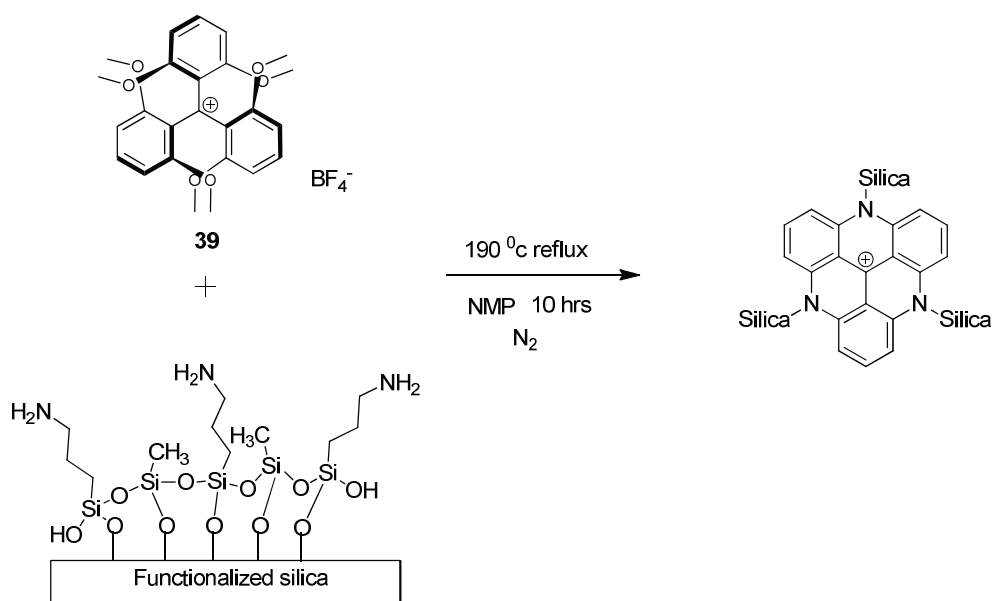
The second hybrid material, **S2** (S2-APTMS-EA-TATA), is prepared by first forming an acridinium ion by using one surface amino group on the aminofunctional silica, thereby anchoring the cation to the silica surface. The resulting material was further heated in the presence of ethanolamine to complete the second and third N-bridging reactions to form the triazatriangulenium cation. Compared to **S1** in **S2** there is only one covalent anchor to the silica surface whereas in **S1** there are three covalent anchors for a singlet cationic dye. The synthesis of **S2** is explained in scheme 4.4.



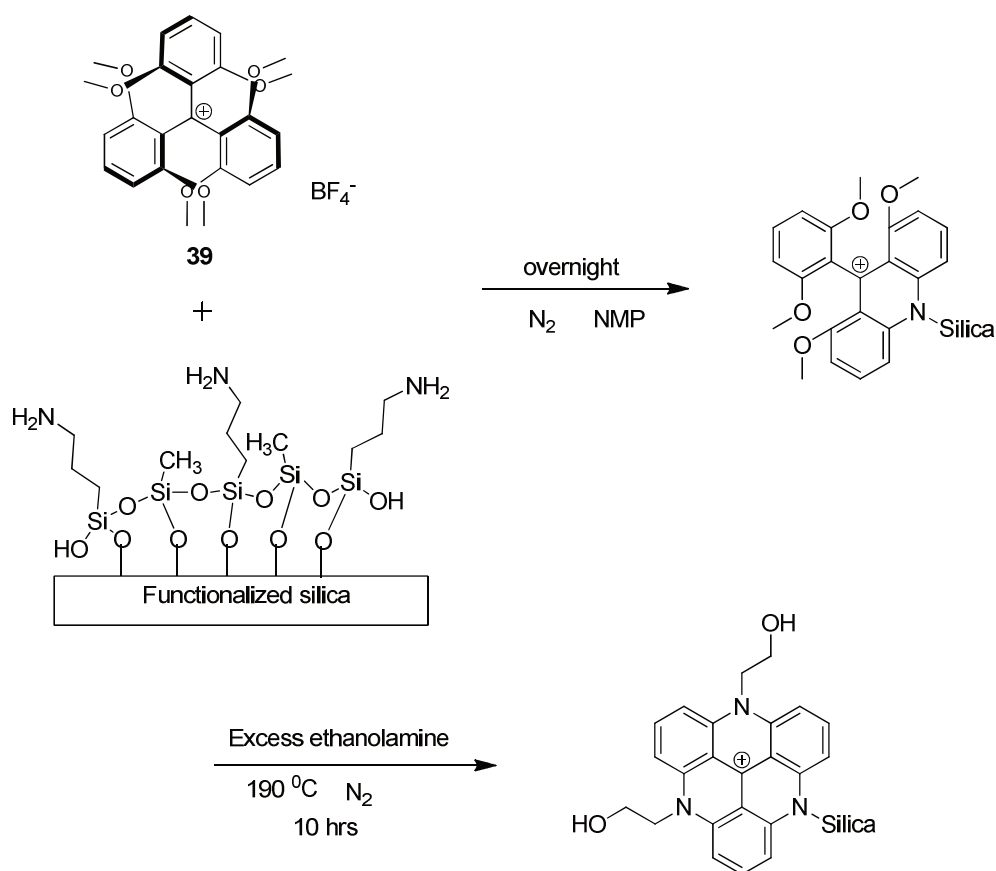
Scheme 4.4 Synthesis of S2-APTMS-EA-TATA (S2)

The remaining two materials **S3** (S3-APTMS+MTS-TATA) and **S4** (S4-APTMS+MTS-EA-TATA), were prepared by using the amino-

functionalized silica S-APTMS+MTS having lower surface density of amino groups. Here, **S3** uses all surface amino groups for the formation of all the three N bridges in the resulting cation. Whereas, in **S4** the surface amino group is used in the first bridging reaction forming the acridinium ion followed by second and third bridging reaction by using added ethanolamine. The synthesis of these two samples are illustrated in the schemes 4.5 and 4.6.



Scheme 4.5 Synthesis of S3-APTMS+MTS-TATA (S3)



Scheme 4.6 Synthesis of S4-APTMS+MTS-EA-TATA (S4)

4.3.4. Characterization of triazatriangulenium- silica composites

4.3.4.1. CHN Analysis

Introduction of organic functional groups on the silica surface was made by chemical functionalization and the extent of loading of these the aminopropyl groups and subsequent covalent attachment of triazatriangulenium cations can be estimated by CHN analysis of the prepared materials. CHN analysis was carried out and results are summarized in table 4.1. The results show that the carbon and nitrogen atoms are present on both S-APTMS and S-APTMS+MTS samples. As expected the chemical grafting of aminopropyl groups and the

corresponding percentage loading of Nitrogen was less on APTMS+MTS sample compared to that on S-APTMS. This indicates a lesser surface density of the aminopropyl groups on S-APTMS+MTS samples. Upon reaction of S-APTMS samples with tris-(2,6-dimethoxyphenyl) carbenium tetrafluoroborate, sample **S1** was obtained with triazatriangulenium cations. This led to a ~ 7% higher amount of carbon on sample **S1** without much variation in the percentage of Nitrogen. This shows that the formation of the covalently anchored cations was efficient on S-APTMS. In contrast, for sample **S3**, the similar reaction of S-APTMS+MTS with tris-(2, 6-dimethoxyphenyl) carbenium tetrafluoroborate led to only a lesser increase of 3.6% of carbon. This low loading of the cation could be due to a less efficient anchoring and bridging reaction resulting from a very low surface density of aminopropyl groups.

The preparation of **S2** and **S4** was a two step process when the initial anchoring and bridging reaction to form the acridinium ion followed by a second step involving two aza bridging reaction using amino groups of excess ethanol amine added to the reaction mixture. Among these two samples the sample **S2** show very small increase in the carbon and nitrogen content indicating a less efficient formation of the acridinium ion. Whereas, in sample **S4** there is dramatic increase of carbon loading and a very minor increase in the nitrogen loading. This shows an efficient formation of the acridinium ion but a less efficient subsequent bridging reaction with ethanolamine.

Table 4.1 Elemental composition of functionalized silica

Sample	C%	N%	H%
S-APTMS	6.62	2.25	2.42
S-APTMS+MTS	4.32	1.4	1.64
S1-APTMS-TATA	14.02	2.26	2.96
S2-APTMS-EA-TATA	7.92	2.3	2.53
S3-APTMS+MTS-TATA	7.02	1.46	2.12
S4-APTMS+MTS-EA-TATA	12.12	1.6	1.9

4.3.4.2. IR spectral studies

FT-IR spectra were recorded as KBr pellets of all the silica samples prepared to study and verify the introduction of aminopropyl groups and the formation of triazatriangulenium cations. Figure 4.3 shows the FT-IR spectra of three kinds of silica particles: silica alone, silica functionalized with APTMS and silica functionalized with a mixture of APTMS and MTS. All the FT-IR spectra present similar features. The intense and broad band appearing at 1081–1122 cm^{-1} is corresponding to the asymmetric stretching vibrations of Si–O–Si and the one at 800 cm^{-1} is due to the symmetric stretching vibration of Si–O–Si. The band at 3300–3600 cm^{-1} is responsible for the Si–OH stretching vibration and the isolated hydroxyl group stretching by hydrogen bonding. The presence of adsorbed water was reflected by $\nu(\text{O-H})$ vibration around 3446 cm^{-1} and 1640 cm^{-1} . By comparing the FTIR spectra of silica and amino functionalized silica, the decreased intensity of absorption at 3500 cm^{-1} along with the formation of new bands at 2947 cm^{-1} and 2834 cm^{-1} are observed for amine functionalized silica particles. The presence of asymmetric and symmetric stretching vibrations of $-\text{CH}_2$ on amine functionalized silica particles indicates the grafting of aminopropyl groups of APTMS on the surface of silica.^{15,17} The band at 1270 cm^{-1} is due to the C–N linkage present in the samples.

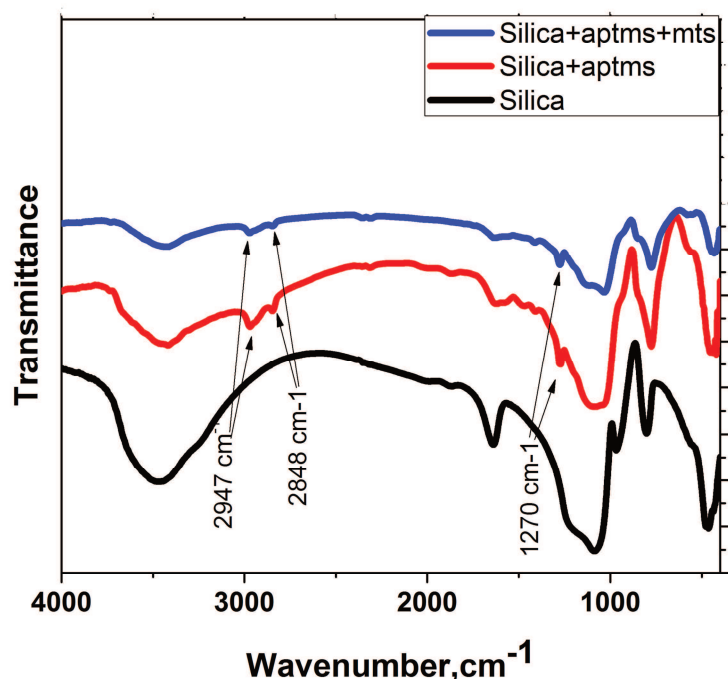


Figure 4.3 FT-IR spectra of free silica, silica functionalized with APTMS(S-APTMS) and silica functionalized with mixture of APTMS and MTS(S-APTMS+MTS)

The IR spectrum of the triazatriangulenium salt (**H-TATA 1**) is shown in the figure **4.4**. The triazatriangulenium salts show the characteristic peak in the range of 1615 cm^{-1} – 1625 cm^{-1} range corresponding to aromatic -C=C- stretching. The -OH stretching was observed in 3428 cm^{-1} . The band at 2930 cm^{-1} indicates the asymmetric stretching vibration of -CH_2 groups.

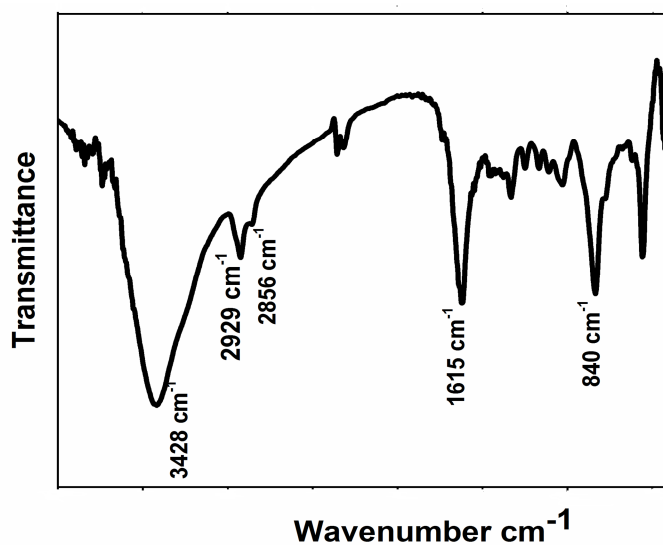


Figure 4.4 FT-IR spectra of triazatriangulenium salt (H-TATA 1)

The IR spectra of the triazatriangulenium –silica composites are shown in the figure 4.5 to 4.8. In all the composites, the appearance of a peak at 2947 cm^{-1} along with the peak at 1615 cm^{-1} - 1625 cm^{-1} range was observed. The new peak at 1615 cm^{-1} – 1625 cm^{-1} range observed in all the cases is the characteristic peak of the triazatriangulenium and is a clear evidence for the formation of triazatriangulenium –silica composites. The band at 2947 cm^{-1} indicates the asymmetric stretching vibration of $-\text{CH}_2$ groups.

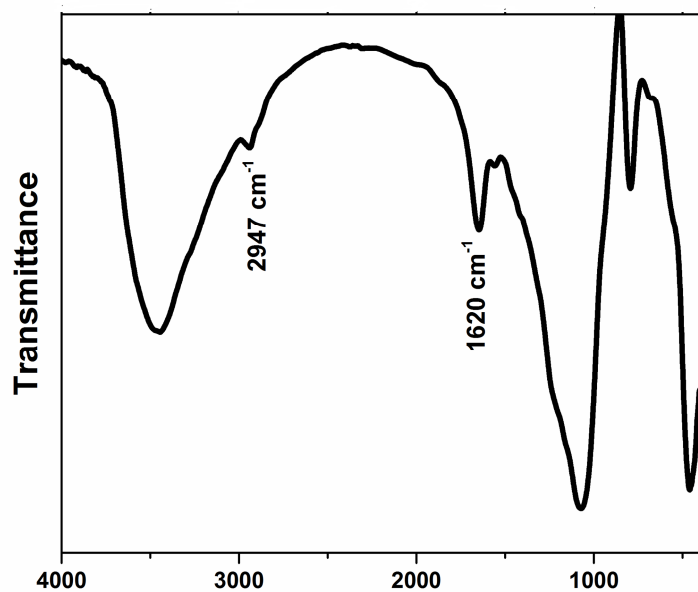


Figure 4.5. The FT-IR spectra of S1-APTMS-TATA (S1)

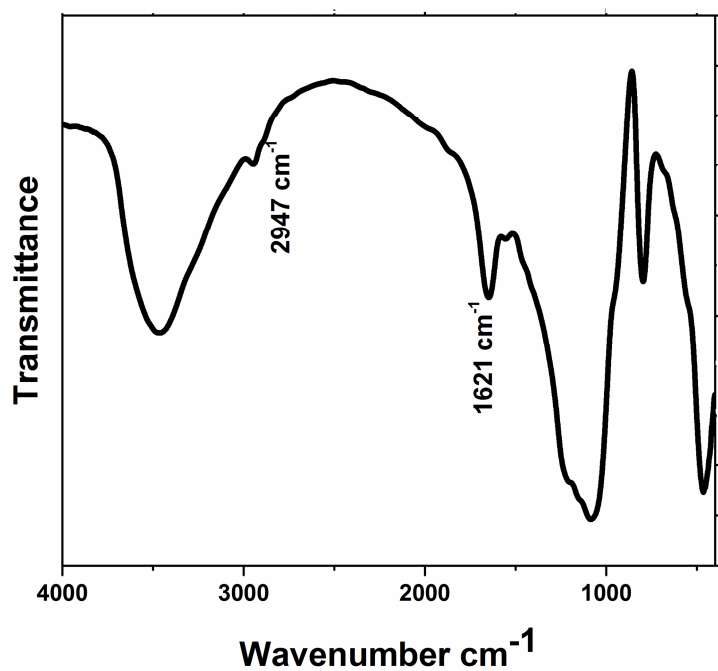


Figure 4.6. The FT-IR spectra of S2-APTMS-EA-TATA (S2)

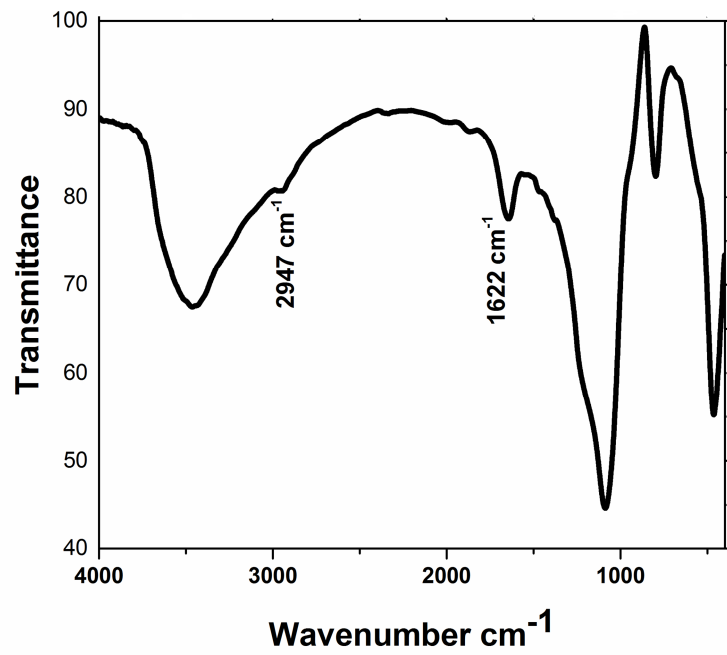


Figure 4.7 The FT-IR spectra of S3-APTMS+MTS-TATA (S3)

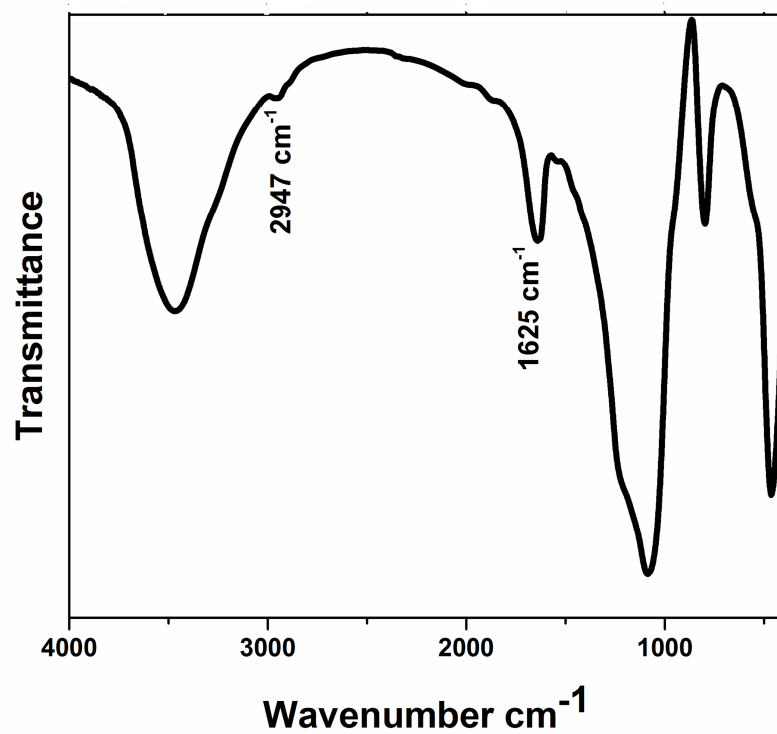


Figure 4.8. The FT-IR spectra of S4-APTMS+MTS-EA-TATA (S4)

4.3.4.3. Scanning Electron Microscopy (SEM) studies

Scanning electron micrographs (SEM) of the free silica and chemically modified silicas were observed in order to identify changes in their surface morphologies. The SEM micrographs display the rough and porous nature of the silica surface.

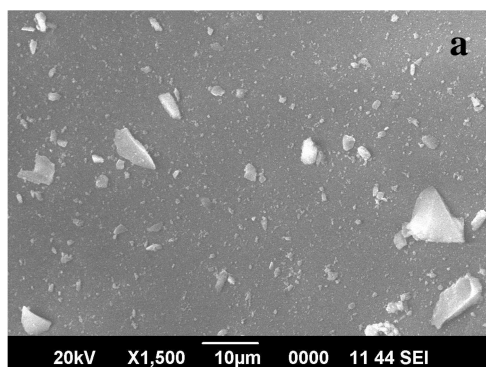


Figure 4.9 SEM image of silica gel (a)

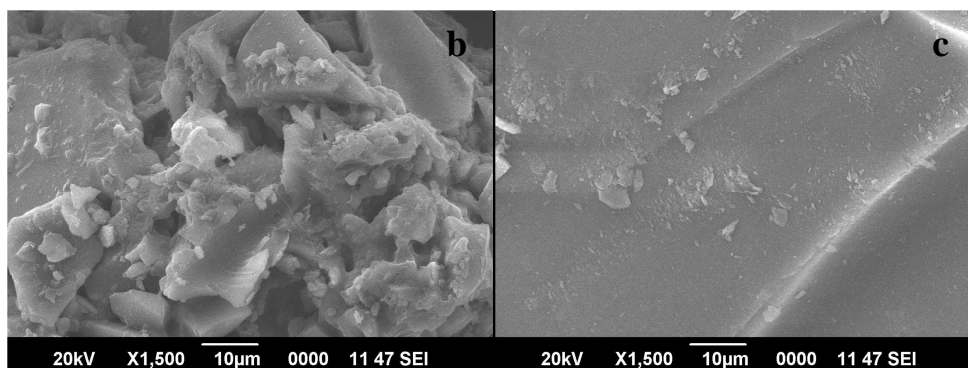


Figure 4.10 SEM images of S-APTMS (b) and S-APTMS + MTS(c)

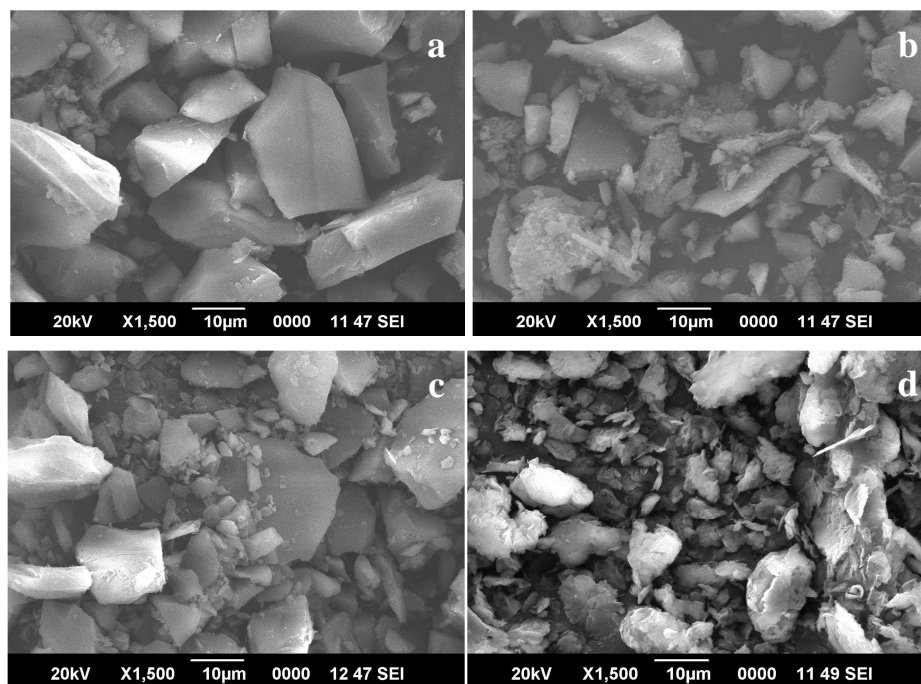


Figure 4.11 SEM micrographs of S1-APTMS-TATA (S1) (a), S2-APTMS-EA-TATA (S2) (b), S3-APTMS+MTS-TATA (S3) (c), S4-APTMS+MTS-EA-TATA (S4) (d)

The SEM images show that there is formation of smaller particles or size reduction as a result of the surface functionalization reactions. It also reveals the unagglomeration of the silica gel particle after the treatment. Other than this there is no other significant morphological changes were observed as a result of surface modification.

4.3.4.4. Transmission Electron Microscopy (TEM)

TEM images of all the samples were recorded to assess the microstructural changes if any has happened during the surface functionalization reactions. TEM images reveal that microstructures of all the samples consists agglomerates of particle of size less than 20 nm and are porous in nature. This morphological feature was not affected significantly due to the surface functionalization reactions. TEM images obtained for various samples are shown in figure 4.12 and 4.13.

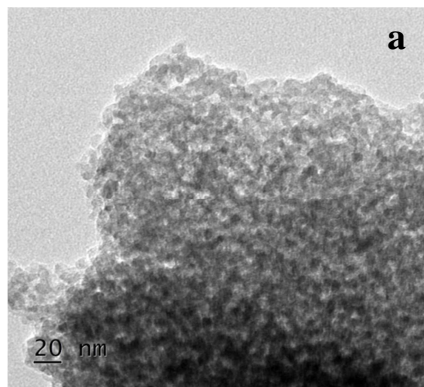


Figure 4.12 TEM image of silica gel (a)

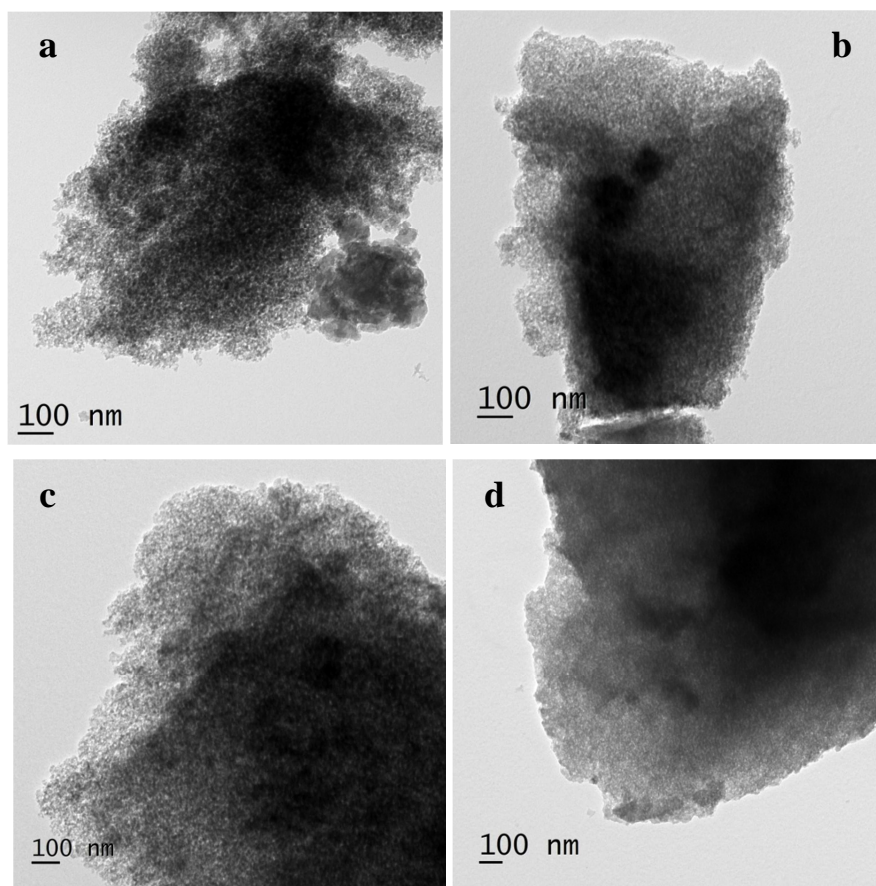


Figure 4.13 TEM images of S1-APTMS-TATA (S1) (a), S2-APTMS-EA-TATA (S2) (b), S3-APTMS+MTS-TATA (S3) (c), S4-APTMS+MTS-EA-TATA (S4) (d)

4.3.4.5. Thermo gravimetric analysis

Thermogravimetric analysis (TGA) was conducted to measure the thermal stability of the four triazatriangulenium-silica composites. The TG curves of silica are displayed in figure 4.14. As it can be seen from curve 1, silica gel shows two mass losses attributed to loss of adsorbed water molecules and also due to the condensation of silanol groups bonded to the surface respectively. The weight loss below 100 °C in all the samples was found to be decreased compared to unfunctionalized silica. This indicates that the surface has become more hydrophobic due to introduction of organic groups. Silica gel shows a weight loss of 4% in the 200 °C – 600 °C. All the triazatriangulenium-silica composites exhibited a weight loss between 200 °C – 600 °C. The composites, **S1**, **S2**, **S3**, **S4** shows weight loss of 18%, 11%, 12% and 17%, respectively. This may be due to the decomposition of the triazatriangulenium cations loaded on silica surface.

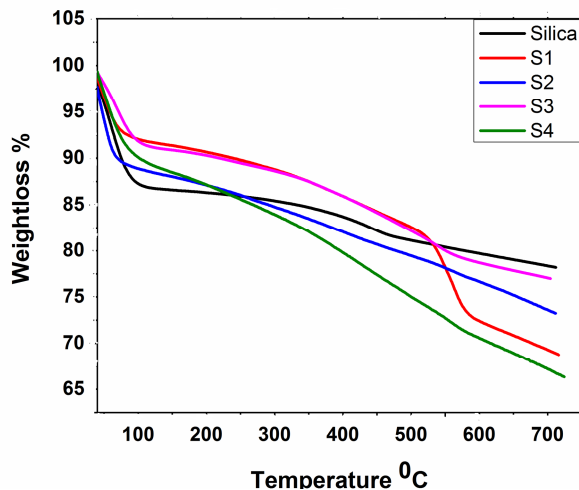


Figure 4.14 The TG plots of S1-APTMS-TATA (S1), S2-APTMS-EA-TATA (S2), S3-APTMS+MTS-TATA (S3) and S4-APTMS+MTS-EA-TATA (S4)

4.3.5. Photophysical properties

4.3.5.1. Absorption spectral properties

Since the triazatriangulenium cations loaded on the surface of the silica samples are indicated by appearance of intense red colour. This colour change itself shows that there is a significant quantity of triazatriangulenium cations on the surface of the samples. The presence of triazatriangulenium ions is indicated as absorptions in the diffuse reflectance spectrum with the characteristic absorption bands and the spectral profile appearing in the region of 400 nm – 600 nm (Figure 4.15). Only the sample **S1** showed the absorption spectral profile similar to the triazatriangulenium cation in acetonitrile solutions. The absorption maximum observed for this sample was at 485 nm with a shoulder at 510 nm. This maximum is slightly blue shifted compared to that observed for free molecules in acetonitrile and this may be due to the hydrophobic nature of the organically modified silica surface. Samples **S2** and **S4** showed additional band at 600 nm. Sample **S3** also presented with a broad absorption up to 600 nm. The presence of the new band suggests the presence of another species along with the triazatriangulenium cation (1). This is possible when the aza bridging reaction is either incomplete or due to a competing oxa bridging reaction leading to the formation of a diaza-oxatriangulenium cation (2) as shown in Chart 4.2. This cation also possess a red shifted absorption maximum as reported by Krebs and coworkers.²⁰

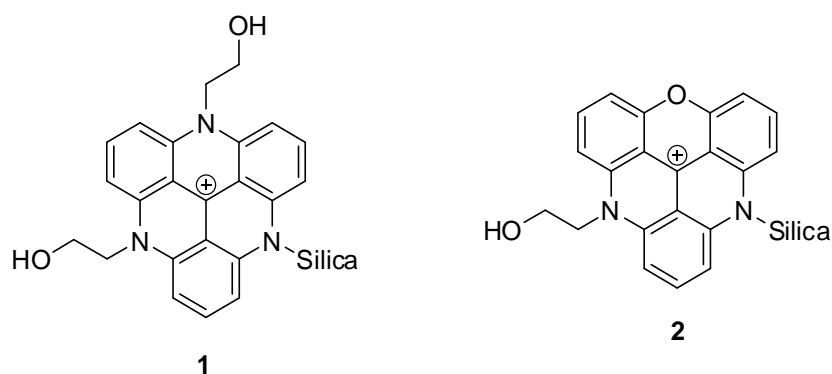


Chart 4.2

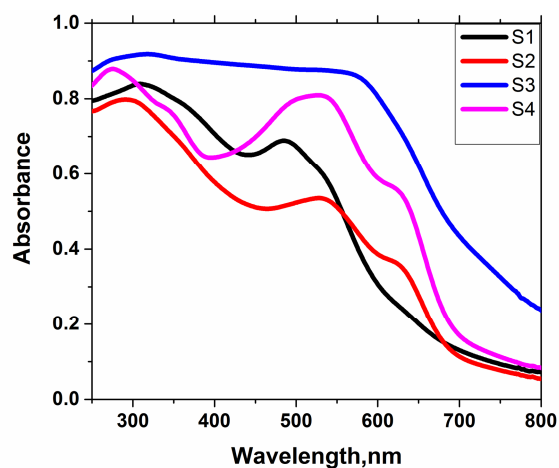


Figure 4.15 Diffuse reflectance spectra of S1-APTMS-TATA (S1), S2-APTMS-EA-TATA (S2), S3-APTMS+MTS-TATA (S3) and S4-APTMS+MTS-EA-TATA (S4)

4.3.5.2. Emission spectral properties

The fluorescence emission is another property that gives indication for the presence of triazatriangulenium cations on the surface of the modified silica samples. The emission spectra of the triazatriangulenium-silica composites obtained on excitation at 480 nm were presented in the figure 4.16.

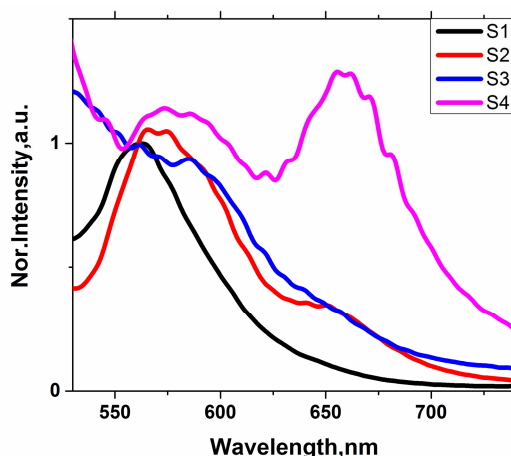


Figure 4.16 Emission spectra of S1-APTMS-TATA (S1), S2-APTMS-EA-TATA (S2), S3-APTMS+MTS-TATA (S3) and S4-APTMS+MTS-EA-TATA (S4). $\lambda_{\text{ex}} = 480 \text{ nm}$

The emission maximum in the visible region of the triazatriangulenium cations was found to be 558 nm in acetonitrile solution. A similar maximum was observed for sample **S1**, but some variations are observed for other samples. For **S2** and **S4** two emission maxima were observed at 565 nm, 651 nm and 570 nm, 655 nm respectively. This observation, once again suggest the presence of a mixture of cations on the surface of these silica samples as shown in Chart 4.2.

4.3.5.3. Lifetime Measurements

The fluorescence lifetimes of all the samples were determined by the method of Time Correlated Single Photon counting (TCSPC) in solid state by using a 510 nm pulsed laser diode as the excitation source. The fluorescence decay profiles of the compounds were shown in figure 4.17. Samples **S1** and **S3** the data fitted well with monoexponential decay function whereas **S2** and **S4** followed a bi-exponential decay function. This result also suggests presence of two emitting species present on the surface of these samples.

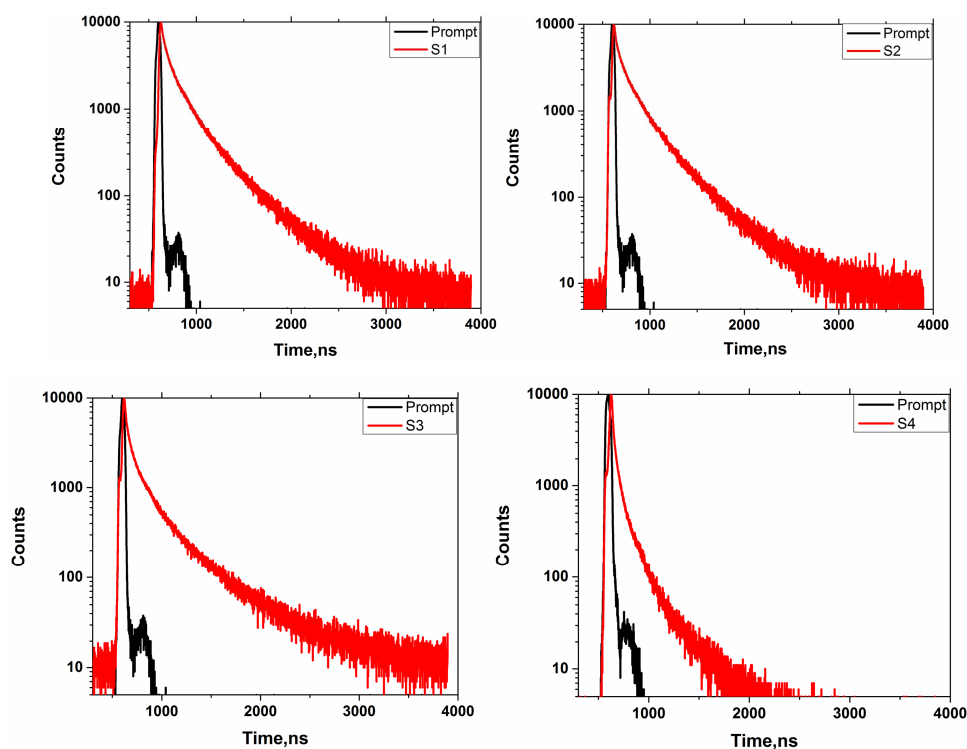


Figure 4.17 Fluorescence decay profile of S1-APTMS-TATA (S1), S2-APTMS-EA-TATA (S2), S3-APTMS+MTS-TATA (S3), S4-APTMS+MTS-EA-TATA (S4)

The photophysical properties of all the prepared triazatriangulenium-silica composites are tabulated in **table 4.2**.

Table 4.2 Absorption maxima ($\lambda_{\max}(\text{abs})$), emission max ($\lambda_{\max}(\text{em})$), singlet lifetime (τ_F) of modified silica samples

	$\lambda_{\max}(\text{abs})$, nm	$\lambda_{\max}(\text{em})$, nm ($\lambda_{\text{ex}}=480$ nm)	τ_F , ns($\lambda_{\text{ex}}=510$ nm)
S1-APTMS-TATA(S1)	485	560	2.3
S2-APTMS-EA-TATA(S2)	525,620	565,651	2.5,0.42
S3-APTMS+MTS – TATA(S3)	570	562	1.6
S4-APTMS+MTS-EA – TATA(S4)	523,620	570,655	1.30, 0.26

4.3.6. Singlet oxygen generation studies

The applicability of the prepared composites in singlet oxygen generation by photosensitization was assessed by irradiation and detection of singlet oxygen using the singlet oxygen scavenger ADPA. The triazatriangulenium- silica particle suspensions were irradiated with a monochromatic light at 530 nm using an ultrabright green LED in the presence of ADPA. Singlet oxygen generated if any would react with ADPA forming the endoperoxide leading to the decrease of absorbance due to ADPA. The progress of the reactions was monitored as a function of time of irradiation. The evolution of absorption spectrum during the photooxygenation reaction for the four silica-triazatriangulenium-composites are given in figures **4.18** to **4.21**. Bare silica samples were also irradiated in the presence of ADPA and no absorbance change was noted suggesting the role of anchored cations in the generation of singlet oxygen (figure **4.22**). The incident photon rate was kept constant in all the cases and it was ensured by chemical actinometry as described in chapter 2 and the time of irradiation is also fixed to study the initial kinetics of the photooxygenation process. All the composites produced singlet oxygen as it was evidenced by the decrease in the absorbance of ADPA over a period of 120 minutes.

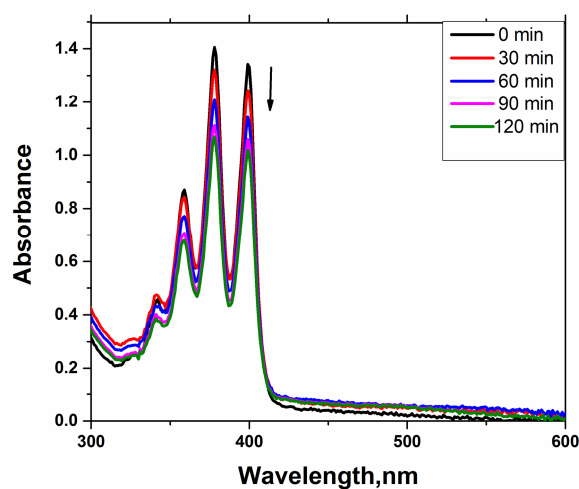


Figure 4.18 The decrease in absorbance of ADPA (1.8×10^{-4} M) during the irradiation of S1-APTMS-TATA (S1) in aqueous solution with ultrabright green LED light.

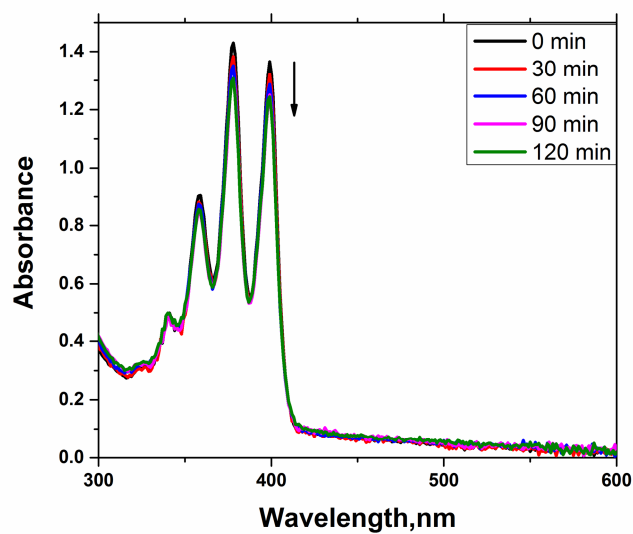


Figure 4.19 The decrease in absorbance of ADPA (1.8×10^{-4} M) during the irradiation of S2-APTMS-EA-TATA (S2) in aqueous solution with ultrabright green LED light.

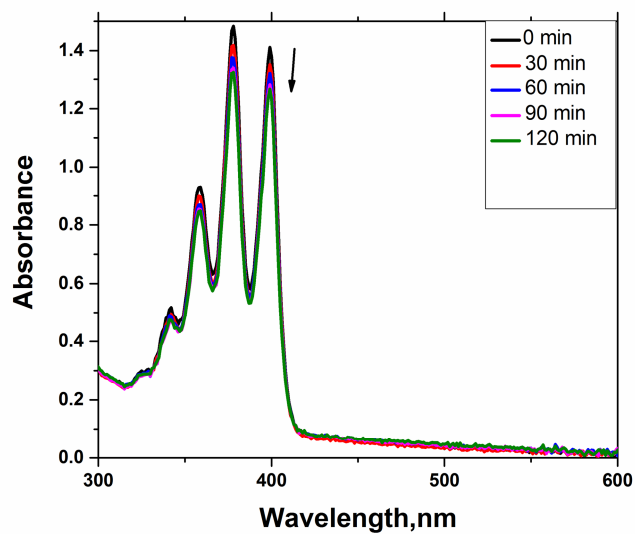


Figure 4.20 The decrease in absorbance of ADPA (1.8×10^{-4} M) during the irradiation of S3-APTMS- MTS-TATA (S3) in aqueous solution with ultrabright green LED light.

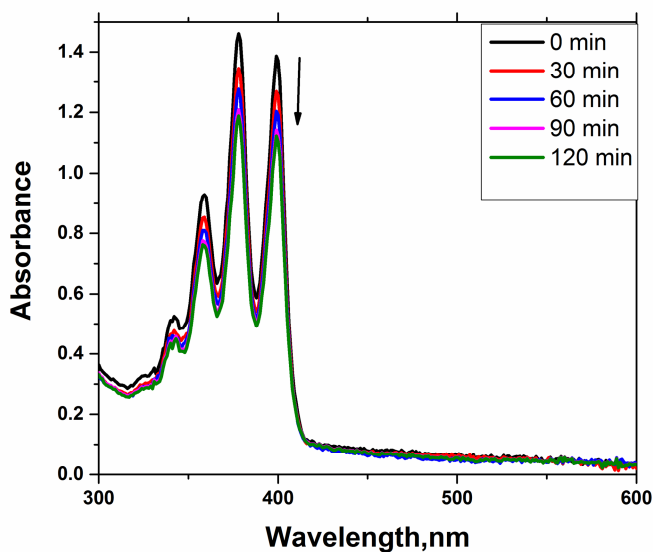


Figure 4.21. The decrease in absorbance of ADPA (1.8×10^{-4} M) during the irradiation of S4-APTMS- MTS-EA-TATA (S4) in aqueous solution with ultrabright green LED light

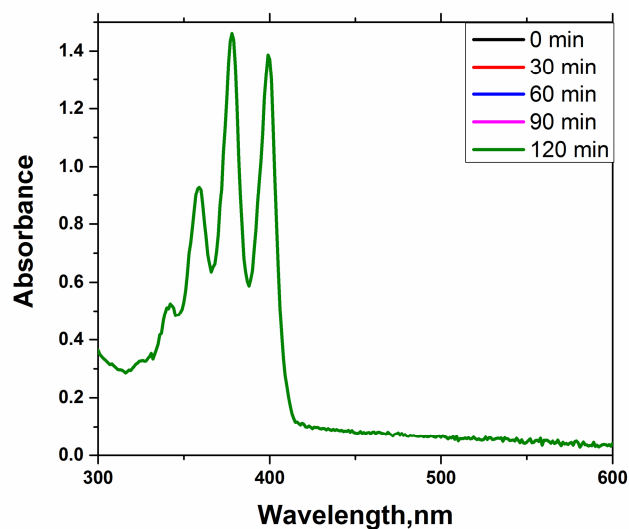


Figure 4.22 The absorbance of ADPA (1.8×10^{-4} M) during the irradiation in the presence of bare silica particles using ultrabright green LED light

4.3.6.1. Comparison of singlet oxygen production of triazatriangulenium-silica composites in the presence of ultrabright green LED light

The singlet oxygen productions of the four composites were compared under identical conditions of incident photon rate ensured by aberchrome-670 actinometry at the irradiation wavelength. The kinetic profiles obtained for the all the samples are presented in figure 4.23. Among the four samples, samples **S1** and **S4** showed the highest efficiency in the singlet oxygen generation. This is due to the higher loading of the cations on these two samples compared to that of **S2** and **S3** where the cation loading was less.

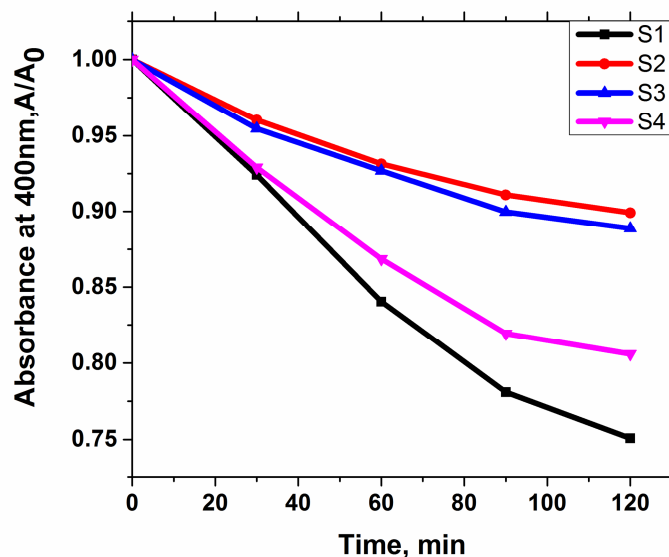
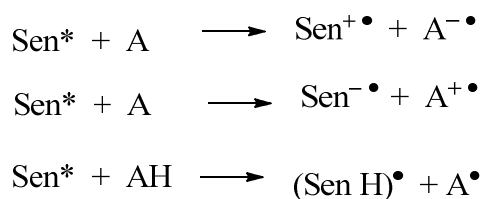


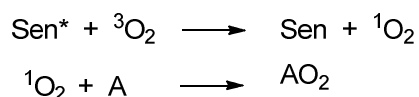
Figure 4.23 Kinetic profiles of photooxidation of ADPA (1.8×10^{-4} M) with triazatriangulenium silica composites in aqueous solution.

4.3.7. Photosensitized inactivation of bacteria

The oxidation capacity of singlet oxygen is well known. It can easily oxidize unsaturated double bonds, sulfides, phenols, amino groups and other electron-donor groups in organic compounds.²¹⁻²³ Water disinfection is an important application of heterogeneous photosensitizers and is achieved through the photodynamic action of oxygen. The photodynamic action of oxygen generally proceeds through either Type I or Type II process. Type I mechanism involves hydrogen-atom abstraction or electron-transfer between the excited sensitizer and a substrate, yielding free radicals. These radicals can react with oxygen to form an active oxygen species such as the superoxide radical anion.



In a Type II mechanism, singlet oxygen is generated via an energy transfer process during a collision of the excited sensitizer with triplet oxygen.



Sen* is the sensitizer in the triplet excited state. A is the substrate which reacts with the sensitizer in the triplet excited state.

The different steps involved in the photodynamic action are the following. The first step is the accumulation of the photosensitizer in the bacteria and upon irradiation with light of suitable wavelength reactive oxygen species are generated. In singlet oxygen mediated reaction singlet oxygen causes the lethal damage through the destruction of DNA or cytoplasmic membrane (figure 4.24). In the case of supported sensitizers the accumulation of the dye in the cells of the pathogen normally do not occur. In this case the singlet oxygen generated in the extra cellular region has a significant diffusion length during its lifetime and could meet with a pathogen cell causing photooxidative damage. On comparing the use of free and supported sensitizers, supported sensitizers have reduced efficiency. Rose bengal supported on a poly (ethylene glycol) polymer shows reduced efficiency in the heterogeneous form compared to the homogeneous form.²⁴ Pthalocyanines shows a four fold reduction in the efficiency, when attached to silicagel.⁸ Halogenated porphyrin derivatives which are covalently attached to aminoalkylated silica and aminoalkylated Merrifield polymer also show reduced efficiency compared to the free form.⁹

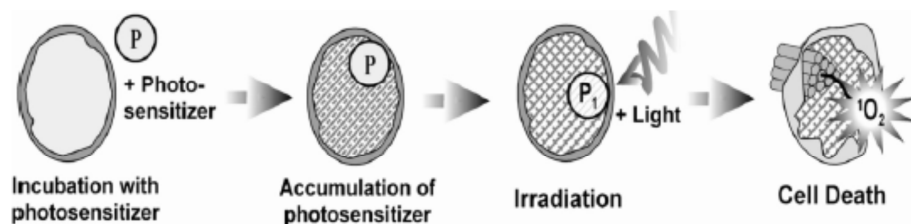


Figure 4.24 Mechanism of destructive action of photosensitization in the cell: P – photosensitizer, P_1 – excited state of photosensitizer after absorption of light, 1O_2 – singlet reactive oxygen (Adapted from reference 25)

The antibacterial activity of the four triazatriangulenium-silica composites was investigated by using the gram negative bacteria, *E.coli* contaminated water. The bacterial inactivation studies were performed by using a suspension containing the 1 mg/mL of the modified silica. The bacterial inactivation rate was determined by the colony counting method. The incubation of bacteria with the heterogeneous sensitizers under study in the absence of light did not lead to reduction in the number of *E.coli* colonies suggesting that these materials are nontoxic to *E.coli*. Incubation of the bacteria with bare silica particles was taken as control. In this case too no significant reduction in the number of *E.coli* colonies was observed. Under exposure to sunlight for 30 minutes a significant variation of the number of *E.coli* colonies was noted in the presence of prepared supported sensitizer materials. The counts obtained for various samples in the presence and absence of the light is given in table 4.3. The plate images is also presented in figure 4.25 and 4.26.

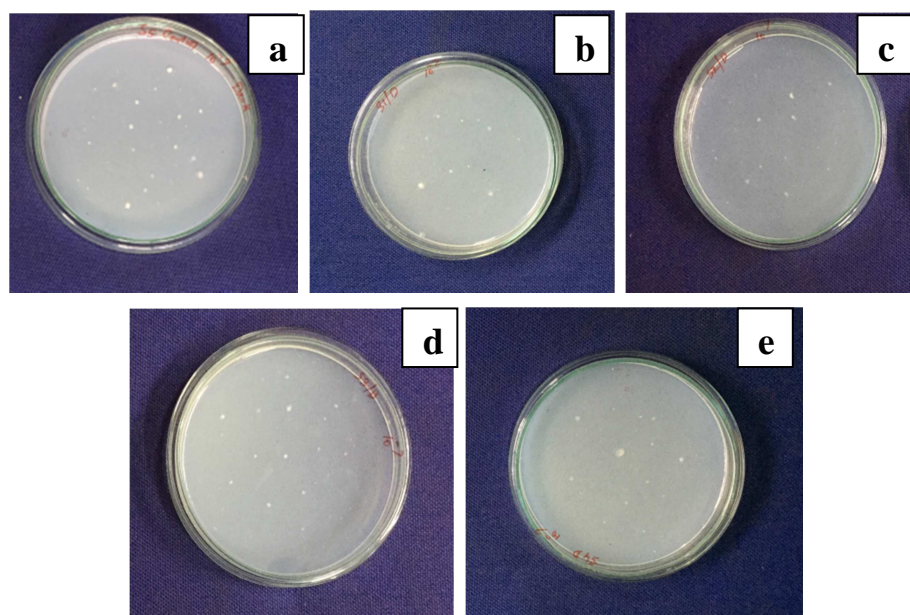


Figure 4.25. The *E.coli* treated with Control(a), S1-APTMS-TATA(S1)(b), S2-APTMS-EA-TATA(S2)(c), S3-APTMS+MTS-TATA(S3)(d), S4-APTMS+MTS-EA-TATA(S4)(e) kept in the dark

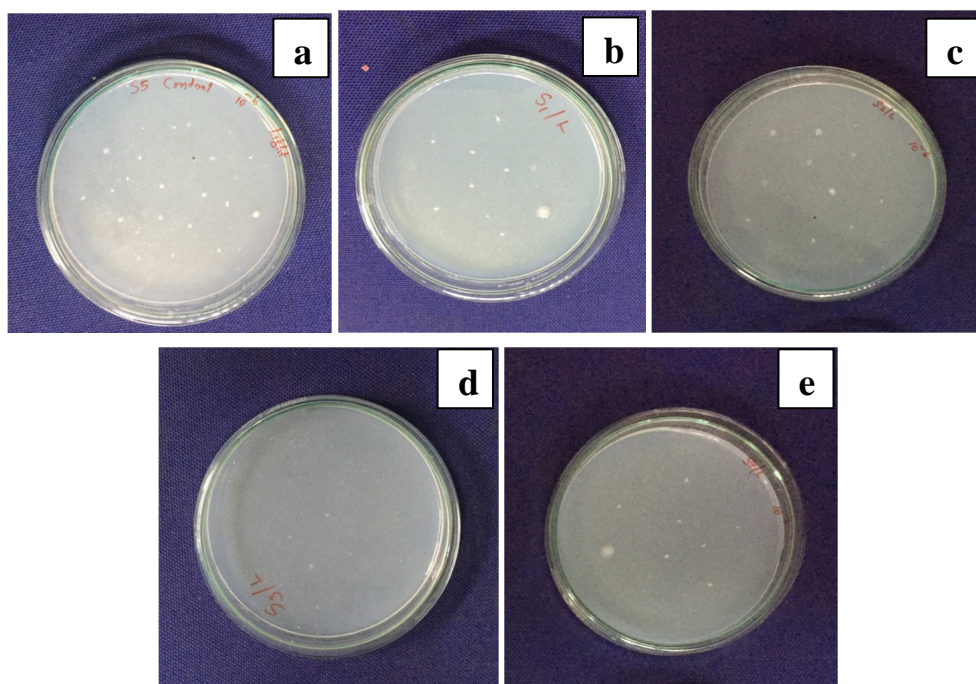


Figure 4.26. The *E.coli* treated with Control(a), S1-APTMS-TATA(S1)(b), S2-APTMS-EA-TATA(S2)(c), S3-APTMS+MTS-TATA(S3)(d), S4-APTMS+MTS-EA-TATA(S4)(e) kept in the sunlight for 30 minutes.

Table 4.3 The number of *E.coli* colonies observed by incubating the bacteria with the heterogeneous sensitizer in the dark and after keeping with 30 minutes in the presence of sunlight. The presented data is a mean of the triplicate with a standard deviation (SD) of <5%.

	Dark($\times 10^8$ CFU/ML)	Light($\times 10^8$ CFU/ML)
Control	9.9	9.7
S1	9.8	0.0002
S2	9.6	6.0
S3	9.9	4.1
S4	9.9	0.3

The results clearly demonstrate that **S1** successfully inactivated *E.coli* through the photosensitization process. The bacteria underwent 99.9% decrease in cell viability upon exposure to full spectrum visible light for 30 min.

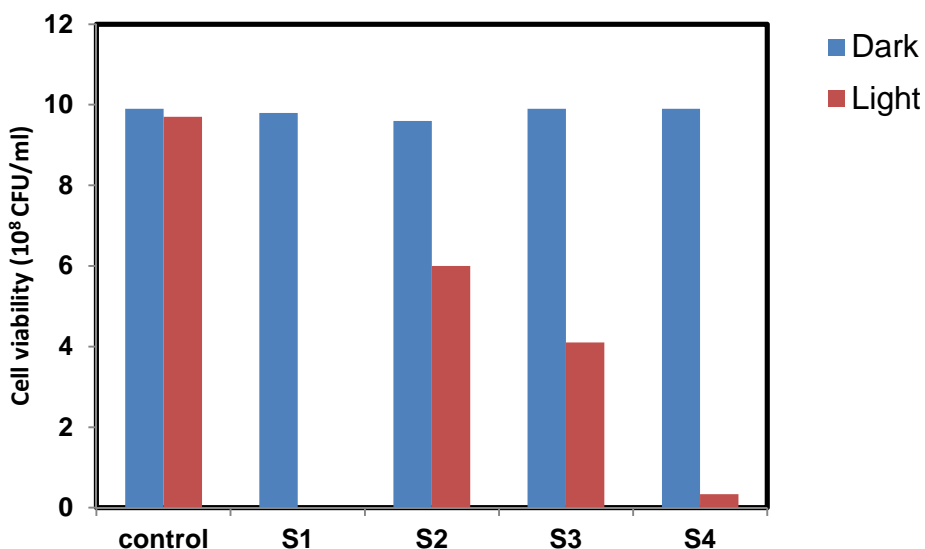


Figure 4.27. The cell survival when *E.coli* treated with Control, S1-APTMS-TATA, S2-APTMS-EA-TATA, S3-APTMS+MTS-TATA, S4-APTMS+MTS-EA-TATA

In the case of **S2** only 37% decrease in the inactivation of bacteria was observed. This is due to the fact that the amount of triazatriangulenium on the surface was low, and hence the generation of singlet oxygen is also very low. A 58% decrease in the inactivation of gram negative bacteria was observed in **S3**. In this case too the cation loading was very low compared to **S1**. In the case of **S4**, 97% reduction in the cell viability of bacteria was observed. Among the two triazatriangulenium silica surface modified with APTMS and MTS this material show higher efficiency in bacterial inactivation.

4.4. Conclusion

In the present work four types of triazatriangulenium- silica composites were synthesized and characterized. The photophysical characterization of all the four synthesized triazatriangulenium-silica composites were also carried out. The singlet oxygen production of the triazatriangulenium-silica composites during exposure to sunlight was monitored by the singlet oxygen scavenger ADPA. The disinfection studies were also conducted in order to determine the effectiveness of the synthesized triazatriangulenium-silica composites for the treatment of pathogen-contaminated water. The Gram-negative bacteria underwent 99.9% decrease in the survival of bacteria upon exposure to full spectrum sunlight for 30 min during the irradiation in the presence of **S1**.

4.5. Experimental

All solvents used were of reagent grade and used without further purification. Reagents were purchased from Sigma-Aldrich and Spectrochem Pvt. Ltd, and were used as received. Silicagel of 60-120 mesh size procured from Spectrochem Pvt.Ltd was used as the preparation of the hybrid materials. ADPA was synthesized based on a reported procedure.²⁶

Elemental analysis was performed using Elementar Vario EL III model instrument. Infrared Spectra were recorded on a JASCO FTIR Spectrometer using KBr pellets in the range 400-4000 cm^{-1} . The SEM images were obtained using JEOL ModelJSM - 6390LVScanning Electron Micrograph with an attached energy-dispersive X-raydetector. TEM images were obtained using JEOL JEM 2100 HRTEM at SAIF, CUSAT. The diffuse reflectance UV-Vis spectra of the solid samples were recorded using UV-Vis-NIR Ocean Optics fibre optics Spectrophotometer SD 2000model equipped with a diffuse reflectance probe. TG analysis was performed on Perkin Elmer Pyris Diamond 6thermogravimetric/differential thermal analyzer by heating the sample at the rate of 10 $^{\circ}\text{C}/\text{min}$ from 40 $^{\circ}\text{C}$ to 730 $^{\circ}\text{C}$ under N_2 atmosphere. Fluorescence and Fluorescence lifetime studies were carried out usingJobinYvonFluorolog3-211UV-Vis-NIR fluorescence spectrometer. Absorption spectra were recorded using Evolution 201 UV-visible spectrophotometer.

4.5.1. Synthesis of Tris-(2, 6-dimethoxyphenyl) carbenium tetrafluoroborate(39)

Synthesis of this cation is described elsewhere in the thesis (see chapter 2.Section 2.5.2.)

4.5.2. Functionalization of silica surface

Silica surface was functionalized with amino group by (3-aminopropyl) trimethoxysilane and using a mixture of (3-aminopropyl) trimethoxysilane and methyltrimethoxysilane based on the reported procedure.¹⁵ Prior to functionalization the silicagel was refluxed in water (25 mL per g of support) for 1 hr and after cooling the material was collected by filtration and washed with toluene (20 mL/g). The wet material was suspended in toluene (100 mL/g) and dried by azeotropic distillation (2.5 mL/g). After cooling to ambient temperature pure APTMS (3.6 mL/g), MTS

(2.8 mL/g) or a mixture of silanes were added to the slurry. The mixture was vigorously stirred for 14 hrs at room temperature. The residue obtained was filtered, redispersed in fresh toluene (100 mL/g) and refluxed for 1hr. The solid was collected by filtration and washed with isopropanol (20 mL/g). The functionalized material was placed in a Soxhlet apparatus and refluxed with a 2:1 diethyl ether: acetonitrile mixture for 24 hrs. The functionalized material was dried at 373 K in vacuum oven.

4.5.3. Estimation of -NH₂ group capacity

The amine content of functionalized silica was estimated via aqueous HCl consumption using the acid–base titration method. Typically, 100 mg of functionalized silica was suspended in 30 mL of 0.1 M HCl solution and stirred at ambient temperature for 24 hrs. The filtrate was titrated with NaOH solution(0.1 M) using phenolphthaleine as the indicator.

4.5.4. Synthesis of triazatriangulenium silica composites

4.5.4.1. Synthesis of S1-APTMS-TATA (S1)

Silica functionalized with APTMS (1 g) was refluxed at 190 °C with a solution of tris-(2,6-dimethoxyphenyl) carbenium tetrafluoroborate(0.3 g, 0.56 mmol) in NMP(10 mL) under N₂ atmosphere for 10 hrs. The resulting red suspension was filtered, washed with chloroform and then with water (0.1M NaCl) in order to remove any starting materials and the unbound triazatriangulenium photosensitizer. Soxhlet extraction was also performed again with chloroform and dried overnight under vacuum at 80 °C.

4.5.4.2. Synthesis of S2-APTMS-EA-TATA (S2)

Silica functionalized with APTMS (1 g) was stirred overnight at room temperature with a solution of tris-(2, 6-dimethoxyphenyl) carbenium tetrafluoroborate (0.9 g, 1.7 mmol) in NMP (10 mL) under N₂ atmosphere. The

red coloured suspension was refluxed with ethanolamine (1 mL 16 mmol) at 190 °C for 10 hrs under N₂ atmosphere. The resulting material was filtered, thoroughly washed with chloroform followed by water (0.1 M NaCl) in order to remove any starting materials and the unbound triazatriangulenium photosensitizer. Soxhlet extraction was also performed again with chloroform and dried overnight under vacuum at 80 °C.

4.5.4.3. Synthesis of S3-APTMS-TATA (S3)

Silica functionalized with a mixture of APTMS and MTS (1 g) was refluxed at 190 °C with a solution of tris-(2,6-dimethoxyphenyl) carbenium tetrafluoroborate (0.15 g, 0.3 mmol) in NMP (10 mL) under N₂ atmosphere for 10 hrs. The resulting red suspension was filtered, washed with chloroform and then with water (0.1M NaCl) in order to remove any starting materials and the unbound triazatriangulenium photosensitizer. Soxhlet extraction was also performed again with chloroform and dried overnight under vacuum at 80 °C.

4.5.4.4. Synthesis of S4-APTMS-TATA (S4)

Silica functionalized with a mixture of APTMS and MTS (1 g) was stirred overnight at room temperature with a solution of tris-(2,6-dimethoxyphenyl) carbenium tetrafluoroborate (0.9 g, 1.7 mmol) in NMP (10 mL) under N₂ atmosphere. The red coloured suspension was refluxed with ethanolamine (1 mL 16 mmol) at 190 °C for 10 hrs under N₂ atmosphere. The resulting material was filtered, thoroughly washed with chloroform followed by water (0.1 M NaCl) in order to remove any starting materials and the unbound triazatriangulenium photosensitizer. Soxhlet extraction was also performed again with chloroform and dried overnight under vacuum at 80 °C.

4.5.5. Studies on photosensitized production of singlet oxygen

The studies on photosensitized production of singlet oxygen by the prepared hybrid materials are carried by using suspensions of the silica supported dyes in a 1.8×10^{-4} M solution of the singlet oxygen scavenger disodium-9, 10-anthracenedipropionic acid (ADPA). A volume of 3 mL of 3 mg of the suspension was stirred continuously while irradiating with ultrabright green LED light ($\lambda=530$ nm). The progress of the oxygenation reaction was monitored by recording the absorption spectrum of the suspension every 30 min. The suspension was allowed to settle for 10 min prior to recording the absorption spectrum. A blank experiment was also performed in the absence of the silica-dye composites.

4.5.6. Photobactericidal studies on microbial cell cultures with the triazatriangulenium-silica particles

Using aseptic techniques, a single pure colony was transferred into a 200 mL of nutrient broth, capped and placed in incubator overnight at 37°C . After incubation, using aseptic preparation, turbidity of suspensions was calculated and adjusted using McFarland standards as a reference. The 10 mg of samples (concentration-1 mg/mL) were added to 10 mL of culture and one set was incubated at dark and other set was incubated in sunlight. A control tube was also kept as a reference. After the incubation, the tubes were serially diluted and plated on nutrient agar. The plates are incubated for 24 hrs at 37°C . The plates were observed for colonies and the total count was determined.

4.6. References

1. García-Fresnadillo, D. *Chem Photo Chem.* **2018**, *2*, 512.
2. Valkov, A.; Nakonechny, F.; Nisnevitch, M. *Int. J. Mol. Sci.* **2014**, *15*, 14984.
3. Ronzani, F.; Saint-Cricq, P.; Arzoumanian, E.; Pigot, T.; Blanc, S.; Oelgemöller, M.; Oliveros, E.; Richard, C.; Lacombe, S. *Photochem. Photobiol.* **2014**, *90*, 358.
4. Spagnul, C.; Turner, L.C.; Boyle, R.W. *Photochem. Photobiol. Sci.* **2015**, *150*, 11.
5. Van Laar, F.M.; Holsteyns, F.; Vankelecom, I.F.; Smeets, S.; Dehaen, W.; Jacobs, P.A. *J. Photochem. Photobiol. A.* **2001**, *144*, 141.
6. Schulz-Ekloff, G.; Wöhrle, D.; van Duffel, B.; Schoonheydt, R.A. *Micropor. Mesopor Mat.* **2002**, *51*, 91.
7. Albiter, E.; Alfaro, S.; Valenzuela, M.A. *Int. J. Photoenergy.* **2012**, *2012*, 1.
8. Kuznetsova, N.A.; Kaliya, O.L. *Macroheterocycles.* **2015**, *8*, 8.
9. Pineiro, M.; Ribeiro, S.M.; Serra, A.C. *ARKIVOC* **2010**, Jan 1
10. Kuznetsova, N.A.; Yuzhakova, O.A.; Strakhovskaya, M.G.; Slivka, L.K.; Kaliya, O.L.; Lukyanetsa, E.A. *Macroheterocycles.* **2013**, *6*, 363.
11. Magaraggia, M.; Jori, G.; Soncin, M.; Schofield, C.L.; Russell, D.A. *Photochem. Photobiol. Sci.* **2013**, *12*, 2170.
12. Cantau, C.; Pigot, T.; Manoj, N.; Oliveros, E.; Lacombe, S. *Chem. Phys. Chem.* **2007**, *8*, 2344.
13. Albiter, E.; Alfaro, S.; Valenzuela, M.A. *Photochem. Photobiol. Sci.* **2015**, *14*, 597.

14. Mantareva, V.N.; Angelov, I.; Wöhrle, D.; Borisova, E.; Kussovski, V. *J. Porphyr. Phthalocyanines*. **2013**, *17*, 399.
15. Luechinger, M.; Prins, R.; Pirngruber, G.D. *Microporous Mesoporous Mater.* **2005**, *85*, 111.
16. Martin, J. C.; Smith, R. G. *J. Am. Chem. Soc.* **1964**, *86*, 2252.
17. Gao, X.; He, J.; Deng, L.; Cao, H. *Opt. Mater.* **2009**, *31*, 1715.
18. Parida, K.M.; Rath, D.J. *Mol. Catal. A. Chem.* **2009**, *310*, 93.
19. Silva, A.L.; Nascimento, R.G.; Arakaki, L.N.; Arakaki, T.; Espínola, J.G.; Fonseca, M.G. *J. Non-Cryst. Solids*. **2013**, *376*, 139.
20. Laursen, B. W.; Krebs, F. C. *Angew. Chem. Int. Ed. Engl.* **2000**, *39*, 3432.
21. Wöhrle, D.; Suvorova, O.; Gerdes, R.; Bartels, O.; Lapok, L.; Baziakina, N.; Makarov, S.; Slodek, A. *J. Porphyr. Phthalocyanines*. **2004**, *08*, 1020.
22. Skurlatov, Y.I.; Ernestova, L.S.; Vichutinskaya, E.V.; Samsonov, D.P.; Semenova, I.V.; Rod'ko, I.Y.; Shvidky, V.O.; Pervunina, R.I.; Kemp, T.J. *J. Photochem. Photobiol. A*. **1997**, *107*, 207.
23. Cai, J.H.; Huang, J.W.; Zhao, P.; Zhou, Y.H.; Yu, H.C.; Ji, L.N. *J. Mol. Catal. A. Chem.* **2008**, *292*, 49.
24. Schaap, A. P.; Thayer, A. L.; Blossey, E. C.; Neckers, D. C. *J. Am. Chem. Soc.* **1975**, *97*, 3741.
25. Lukšiene, Ž. *Food Technology and Biotechnology. Food Technol. Biotech.* **2005**, *43*, 411.
26. Icli, S.; Demić, S.; Dindar, B.; Doroshenko, A.O.; Timur, C. *J. Photochem. Photobiol. A*. **2000**, *136*, 15.

CHAPTER 5

Synthesis, Characterization and Study of Intercalated Triazatriangulenium Cations in Layered Materials

5.1. Abstract

This chapter includes the study on the triazatriangulenium cations supported on the clay minerals such as sodium montmorillonite (Mt) and Cloisite 93a (Ct). Clay minerals are layered materials and composed of tetrahedral and octahedral sheets. Their interlayer space is negatively charged and contains exchangeable charge compensating cations. These can be exchanged by using organic or inorganic cations via ionexchange. We attempted this strategy to intercalate the cationic triazatriangulenium salts (H-TATA 1 and H-TATA 4) in these layered clay materials through an ion exchange process. From the XRD analysis it was concluded that the intercalation occurred in the case of cloisite clay indicated by a 6 Å⁰ increase in the interlayer distance. All the materials were characterized by spectroscopic and photophysical studies. The chapter also reports the results of the studies of their singlet oxygen generation efficiencies and photochemical disinfection of *E coli* contaminated water samples.

5.2. Introduction

Clay is omni present and is generally formed by breaking and chemical decomposition of igneous rocks with fine texture of particle size less than 2 µm. Clay minerals are members of the phyllosilicate or sheet

silicates family consisting of hydrated alumina-silicates. Tetrahedral silicates and octahedral hydroxide sheets are the basic building blocks of clay minerals. Based on the arrangement of tetrahedral and octahedral sheets, various types of clays exist, such as 1:1, 2:1, etc. The 2:1 clay consists of an octahedral sheet sandwiched between two tetrahedral sheets (e.g., smectite, chlorite and vermiculite). Based on the metal ions present in the octahedral sheets, clay minerals are divided into two groups, namely dioctahedral and trioctahedral. Divalent metal ions such as Fe^{2+} and Mg^{2+} lead to formation of a trioctahedral clay and trivalent metal ions such as Al^{3+} form dioctahedral clay. Clay minerals are either positively charged or negatively charged, which is the main reason for their ion exchange capacity. The cationic clay minerals possess a negative charge and are widespread in nature. Smectite is an example for the cationic clay. The anionic clay minerals possess a positive charge and are relatively uncommon. The cationic clay minerals are again classified into two, such as expanding and non expanding.¹ Various types of expanding and non expanding clay minerals are shown in figure 5.1.

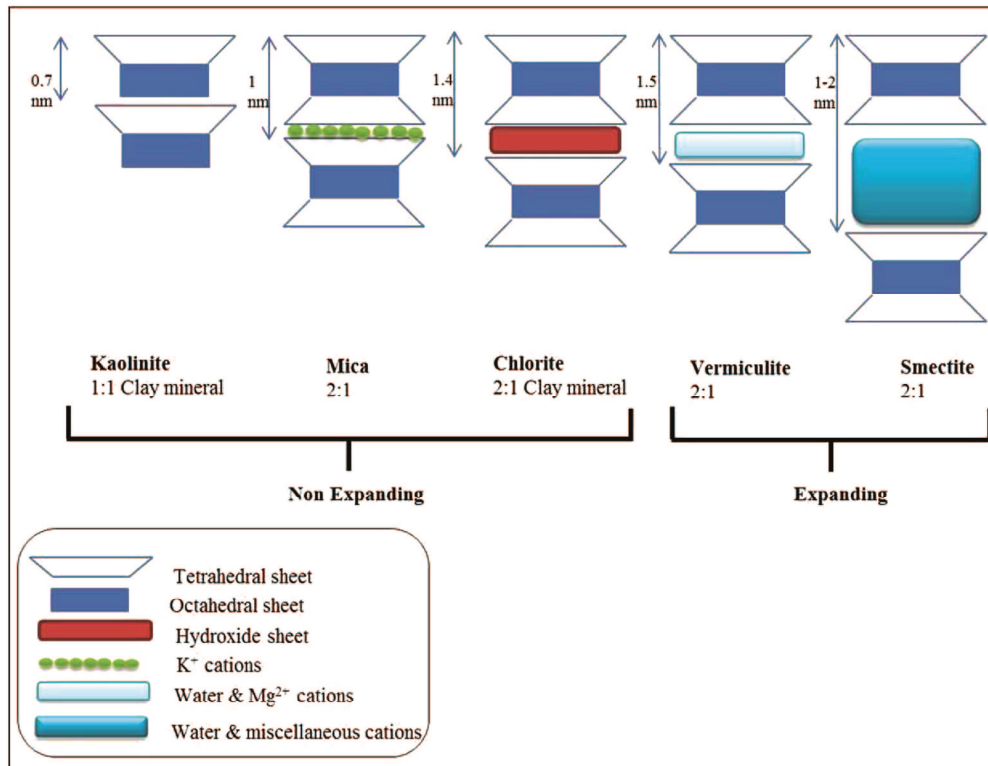


Figure 5.1 Expanding and non expanding cationic clay minerals (Adapted from reference 1)

Smectites are widely used clays by virtue of their high cation exchange capacity, excellent ability to swell, high platelet aspect ratio and ease with which their surface can be modified.² Montmorillonite belongs to the family of 2:1 smectite minerals. It is basically composed of aluminosilicate layers, where one octahedral alumina sheet is sandwiched between two tetrahedral silica sheets. The distance between the two layers is known as interlayer distance or gallery height, whereas the interlayer distance plus thickness of a single aluminosilicate layer constitutes the basal spacing as shown in figure 5.2.

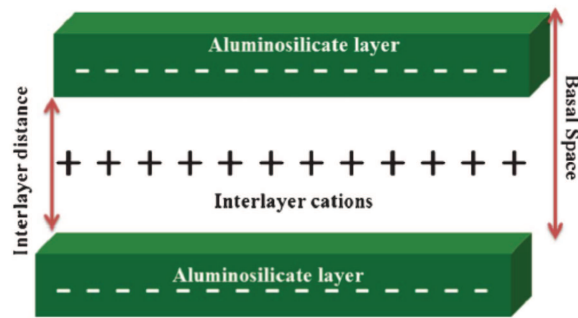


Figure 5.2 Showing interlayer distance and basal spacing in montmorillonite (MMT). (Adapted from reference 2)

In the aluminosilicate layers, partial isomorphous substitution of Si^{4+} ions by trivalent metal cations and Al^{3+} ions by divalent metal cations causes a charge deficit. To balance this charge deficit, a number of exchangeable hydrated alkali and alkaline earth metal cations occupy the interlayer space of montmorillonite (MMT). These cations in the interlayer space are highly exchangeable, thereby making montmorillonite able to accommodate various guest molecules in its interlayer space. The interlayer space of montmorillonite can be varied by introduction of many organic surfactant species and robust metal oxides as pillars (pillared clays), which push apart the clay layers, thereby increasing the surface area generating a large platform to accommodate other cationic species.²

Cation exchange capacity (CEC) is the characteristic property of soil provided by clay and organic matter. It is expressed as meq/100g.³ It is the capacity of the soil to hold cations, like Al^{3+} , Ca^{2+} , Mg^{2+} , Mn^{2+} , Zn^{2+} , Cu^{2+} , Fe^{2+} , Na^+ , K^+ and H^+ .⁴ It is understood as the quantity of positively charged ions held by the negatively charged surface of clay mineral. But in general most of the clay minerals tend to have a negative charge, due to substitution of silica cation (Si^{4+}), by aluminum cation (Al^{3+}) in the clay sheet structure. This phenomenon, referred to as isomorphous substitution, produces the capacity in clay sheets to hold positive charges.

Smectites have attracted much attention because of its potential to be intercalated by various types of cationic organic molecules between the aluminosilicate layers by ion exchange process which introduces different applications for these host-guest systems.^{5,6} Hydrophobic or organophilic surface modification of clay mineral particles by electrostatic interaction of montmorillonite with cationic surfactants, mainly quaternary alkylammonium compounds, have been widely practiced in the last decade.⁷ Cationic dyes are another group of organic compounds which are used as an intercalant and their luminescence properties have been extensively investigated.^{6,8} The interaction of cationic dyes with clay mineral surfaces changes the spectroscopic properties of the dye molecules. Metachromasy, characteristic change in the colour, caused by adsorption and aggregation of dye molecules on clay layers is one of the most studied photo-physical processes to probe the clay surface.⁹ Progress in controlling photophysical and photochemical properties of clay-dye hybrids lead to production of advanced materials.¹⁰⁻¹³ Also montmorillonite is considered as an efficient and low cost adsorbent for dye removal from coloured wastewaters due to the high absorption capacity for cationic dye molecules.^{14,15} Coloration of polymeric matrices and printing inks were prepared using cationic dye intercalated montmorillonite.¹⁶ Raha et al., reported that the colour stability of the MMT /rhodamine B nanopigment in polypropylene was improved more than ten times compared with the pure dye due to the protection offered by the silicate layers to the intercalated dye molecules.¹⁷ Validi et al., studied the intercalation of methylene blue into montmorillonite at different conditions. They reported that the intercalation process was only dependent on intercalant concentration. Other factors such as duration of the process and clay concentration had no effect on the obtained basal spacing. They found a trend of increase in basal spacing with increase in methylene blue concentration but this trend was leveled off when the concentration of

intercalant reached an amount equal to 1.3 times of cation exchange capacity.¹⁸

Madhavan et al., reported a series of photoreactions in clay media.¹⁹ Methylene blue/ rose bengal bound to the bentonite clay was used for the photooxidation of electron-rich substrates such as quinol, 1-naphthol and anthracene to the corresponding 1, 4-quinones was studied in acetonitrile medium. A [4 + 2] cycloaddition between singlet oxygen and the substrate, followed by its subsequent cleavage is the predominant reaction with clay-supported sensitizers. Even though [4 + 2] cycloaddition is the favoured pathway, in the case of anthracene, there is a possibility of electron transfer reactions also. Among the series of phenol derivatives selected only quinol and 1-naphthol are found to be oxidised efficiently with bentonite-bound methylene blue as the sensitizer. The percentage conversion of both the compounds increases with increase in the irradiation time. In the cases of quinol and anthracene the percentage conversion slows down at longer irradiation times. This may be because of the decrease in substrate concentration and also to the light absorption by the photoproducts. Madhavan et al., also reported the photooxidation of dialkyl and alkyl aryl sulfides to corresponding sulfoxides with the clay bound methylene blue in acetonitrile.²⁰

A new type of hybrid photosensitizer was obtained by efficient adsorption of a 5,10,15,20-tetrakis(4-carboxyphenyl)porphyrin by Cloisite 30B.²¹ It is a monotallowbis(hydroxyethyl) ammonium modified montmorillonite clay. The structure of the porphyrin -cloisite hybrid material is represented in figure 5.3. After the treatment of clay with the porphyrin, the basal spacing was found to be decreased from 18.7 Å⁰ to 15.4 Å⁰. This is because during the synthesis of hybrid sensitizer most probably the rearrangement or partial leaching of the surfactant from the aluminosilicate

layer occurs. The obtained material was found to be an efficient photosensitizer for the oxidation of phenol in aqueous solution under irradiation with the visible light ($\lambda > 470$ nm). The dye-sensitized photooxidation of phenol occurs with the participation of singlet oxygen.

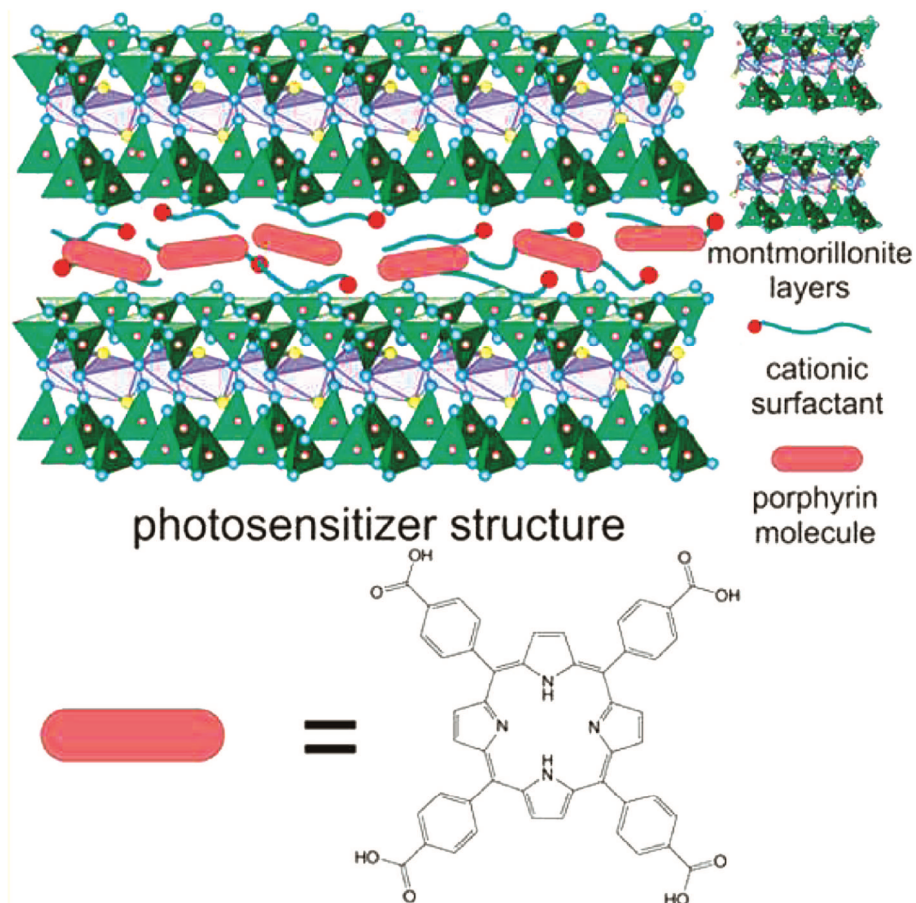


Figure 5.3 Structural Formula of 5, 10, 15, 20-Tetrakis (4-carboxyphenyl) porphyrin (Po) and Structure of Cloisite 30B. (Adapted from reference 21)

The potential of clay minerals in the field of disinfection was reported by bujudak et al., in 2009.²² The antimicrobial activity of methylene blue is found to be enhanced when attached to clay minerals. The singlet oxygen produced as a result of visible light irradiation is responsible for the antimicrobial activity but due to molecular aggregation the methylene blue attached to the clay lost the ability to produce the singlet oxygen. The

contradiction between the significant antimicrobial properties of MB in clay colloidal systems and low $^1\text{O}_2$ formation can be explained in terms of the photosensitization mechanism as well as facilitation in the contact between microorganism cells and photoactive MB. Although the dye directly bound to the clay surface exhibits significantly reduced photoactivity, the presence of clay mediates the delivery of dye molecules on the surface or inside cells.²²

Literature shows the instances of supported sensitizers for singlet oxygen production. The previous chapter discusses the singlet oxygen production by the triazatriangulenium supported on silica. Clays find wide range of applications in various areas of science due to their natural abundance and propensity with which they can be chemically and physically modified to suit practical technological needs.² In the current chapter we present a novel hybrid system in which water soluble triazatriangulenium cations **H-TATA 1** and **H-TATA 4**, with different chain length, (Chart 5.1) was applied as the photoactive component and sodium montmorillonite (Mt) and Cloisite 93a (Ct) was used as a support. Cloisite 93a was chosen for that purpose because it is one of the most commonly used organoclay mineral. It is a methyl dihydrogenated tallow ammonium montmorillonite. The hybrid photosensitizer was characterized using XRD, CHN analysis, SEM, TEM and thermogravimetric analysis. The photophysical properties of the clay supported triazatriangulenium salts were also investigated. The singlet oxygen generation capacity was monitored using the water soluble actinometer ADPA in aqueous suspensions. The disinfection properties of the new hybrid photosensitizer were also studied.

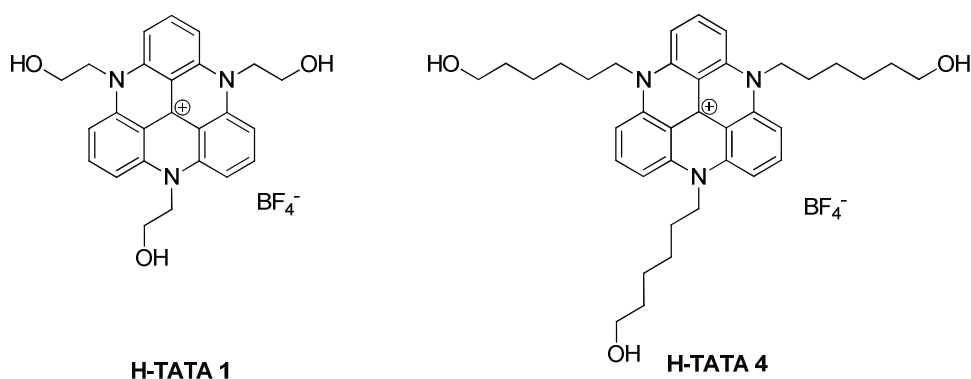


Chart 5.1

5.3. Results and discussion

5.3.1. Characterization of the H-TATA 1 and H-TATA 4 intercalated clay samples

5.3.1.1. X-ray diffraction studies

The intercalation reaction of **H-TATA 1** and **H-TATA 4** with sodium montmorillonite gave a pink solid (Mt-H-TATA 1 and Mt-H-TATA 4). The samples were analysed by powder XRD for any changes in the interlayer structure. The low angle XRD pattern of the product is shown in figure 5.4, together with that of sodium montmorillonite (Mt). XRD pattern gives the values of basal spacing. When Na⁺ ions were replaced by organic cationic ion in the clay gallery, the reflections broadened and shifted to lower angles, i.e. larger d spacing and hence larger distances between the silicate layers will be found. The basal spacing of unmodified montmorillonite clay is termed as initial basal spacing (9.93 Å⁰ at 2θ = 8.95). After modification of clay, the basal spacing changed. In the case of **H-TATA 1** and **H-TATA 4** the basal spacing is found to be slightly increased (9.98 Å⁰ at 2θ=8.85), but this is not a significant change to be considered as there is intercalation of the dyes.

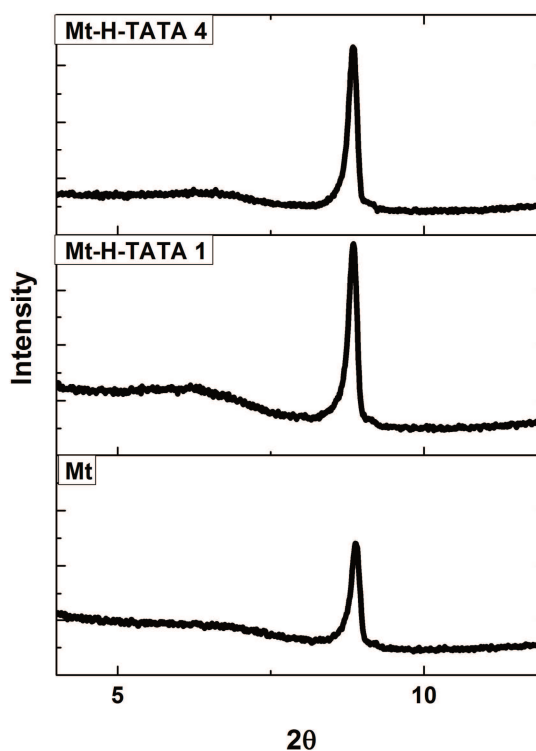


Figure 5.4 The XRD pattern of sodium montmorillonite (Mt), Sodium montmorillonite modified with **H-TATA 1** (Mt-H-TATA 1) and **H-TATA 4** (Mt-H-TATA 4)

A pink solid was also obtained by the intercalation reaction between **H-TATA 1** and **H-TATA 4** with Cloisite 93a to get the materials named as Ct-H-TATA 1 and Ct-H-TATA 4 respectively. In the case of cloisite 93a the basal spacing is found to be 25.1 \AA at $2\theta = 3.51$. After treating the cloisite clay with **H-TATA 1**, the diffraction peak shifts to lower angle *i.e.* $2\theta = 2.82$ and basal spacing increases from 25.1 \AA to 31.3 \AA . In the case of **H-TATA 4** the basal spacing is found to be decreased to 24.8 \AA at $2\theta = 3.56$ compared to free cloisite 93a. The low angle XRD pattern of the products is shown in Figure 5.5, together with that of free cloisite 93a.

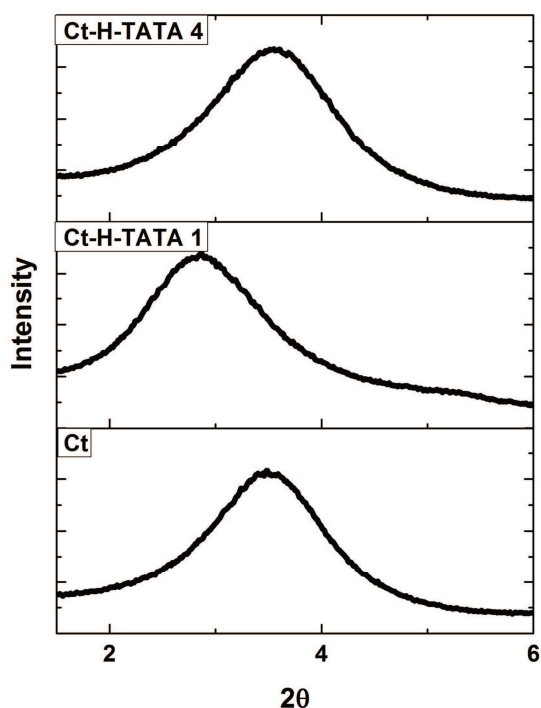


Figure 5.5 The XRD pattern of Cloisite 93a (Ct), Cloisite 93a modified with **H-TATA 1** (Ct-H-TATA 1) and **H-TATA 4** (Ct-H-TATA 4).

The scattering maximum of Sodium montmorillonite (the 001 reflection) is usually found in the range of 0.95-1.4 nm (9.5-14 Å), depending on both cation exchange capacity (CEC) and water content of the sample. When Na⁺ ions were replaced by organic cations in the clay gallery, the reflections broadened and shifted to lower angles, i.e. larger d spacing and hence larger distances between the silicate layers will be found. In the case of **H-TATA 1** and **H-TATA 4** an increase in the basal spacing of 0.05 Å⁰ is observed. Hence, both dyes did not penetrate into the interlayer space and possibly the dye must have adsorbed taken on the external surface of the clay by weaker hydrogen bonds or Van der Waals interactions between dye molecule and the O-plane of outer surface of the clay layer.

For Cloisite clay, actual d-spacing was found to be $d_{001} = 25.1 \text{ \AA}$. In the case of **Ct-H-TATA 1** a large increase in d spacing was obtained ($\Delta d =$

6.2 Å). This indicates that **H-TATA 1** molecules penetrated inside the clay layer and possibly located inside the clay layer. However from the characterization methods available, the arrangement of the molecules cannot be directly deduced. Ito et al., in his study of intercalation of cationic dyes to various clay minerals found that better dye intercalation was observed for tetraalkylammonium ion exchanged clays as the support.²³

In **H-TATA 4**, d-spacing of cloisite 93a is shifted to $d_{001} = 24.8$ Å. This decrease of d spacing shows some interaction of dye molecule with the clay. Since dye molecules have necessarily a rather flat shape a parallel mode of intercalation of these molecules within the silicate layers cannot be ruled out. This decrease of d-spacing may also be due to a reduction of surfactant modifiers in the Cloisite clay removed as a result of the intercalation process. It is observed that the peak shape changed from narrow peak to a broad peak after being treated with organic dye. Based on these results one can assume that the sample obtained after the intercalation reaction of **H-TATA 4** either contain surface adsorbed molecules or it is a mixture of both intercalated and surface adsorbed molecules, with a higher proportion having more of the cations on the outer surface of the Cloisite clay. Among Ct-H-TATA 1 and Ct-H-TATA 4, the role of alkyl chain length on the intercalation behaviour is evident from these results. A shorter alkyl chain seems to be beneficial for obtaining the H-TATA intercalated Ct-clay sample. The following figures (5.6, 5.7 and 5.8) represent the possible modes of adsorption and intercalation of the H-TATA molecules into the clays.

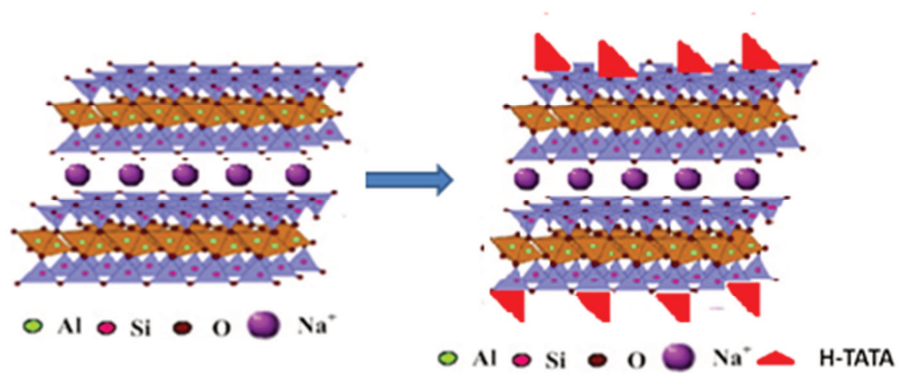


Figure 5.6 Surface adsorbed H-TATA 1 and H-TATA 4 on sodium montmorillonite.

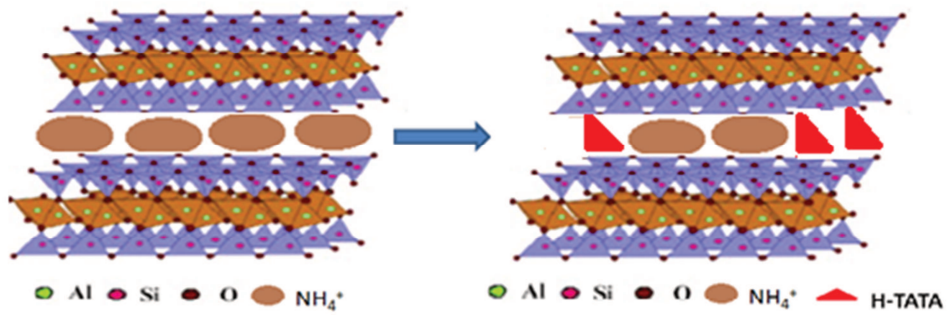


Figure 5.7 H-TATA 1 intercalated into the cloisite 93a. (montmorillonite layer structure adapted from reference 37)

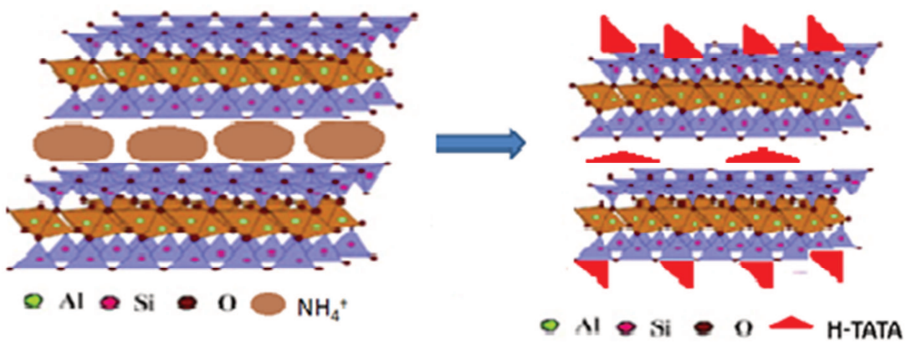


Figure 5.8 Parallel mode of intercalation of H-TATA 4 into the Cloisite 93a. (montmorillonite layer structure adapted from reference 37)

5.3.1.2. CHN Analysis

The results of CHN elemental analysis of pure clays and those modified with triazatriangulenium salts are shown in table 5.1. As expected the carbon content of Mt is negligible. There is an increase in the amount of carbon content in all cases after the intercalation reaction indicating the adsorption of the dye molecules to the clay. Since the clay dye composites were washed repeatedly to remove excess and loose bonded dye molecules, the majority of carbon content may be attributed to intercalated molecules. The discrepancy in the C/H ratio could be the difference in the level of moisture content in these samples. In the case of Cloisite 93a sample the change in C and N content do not show a significant change. This may be attributed to the loss of some of the tetraalkylammonium surfactant molecules from the interlayer spaces of the organo-clay during the process of intercalation with the **H-TATA** dyes.

Table 5.1 Elemental composition of pristine and organically modified clays

	N%	C%	H%
Sodium Montmorillonite	0.07	0.20	1.38
Mt-H-TATA 1	0.23	1.77	1.54
Mt-H-TATA 4	0.24	1.32	1.69
Cloisite 93a	1.01	25.86	4.55
Ct-H-TATA 1	1.09	26.33	4.84
Ct-H-TATA 4	1.04	26.06	4.71

5.3.1.3. Thermogravimetric analysis

Thermal stability of the materials is an essential parameter required to be assessed for determining potential technological applications and

processing conditions of organically modified clays. At a given temperature the modified montmorillonite weight loss is directly related to the rate of the modified montmorillonite decomposition process.²⁴ The thermal decomposition of montmorillonite along with the **H-TATA-1** and **H-TATA 4** intercalated samples are represented in figure 5.9.

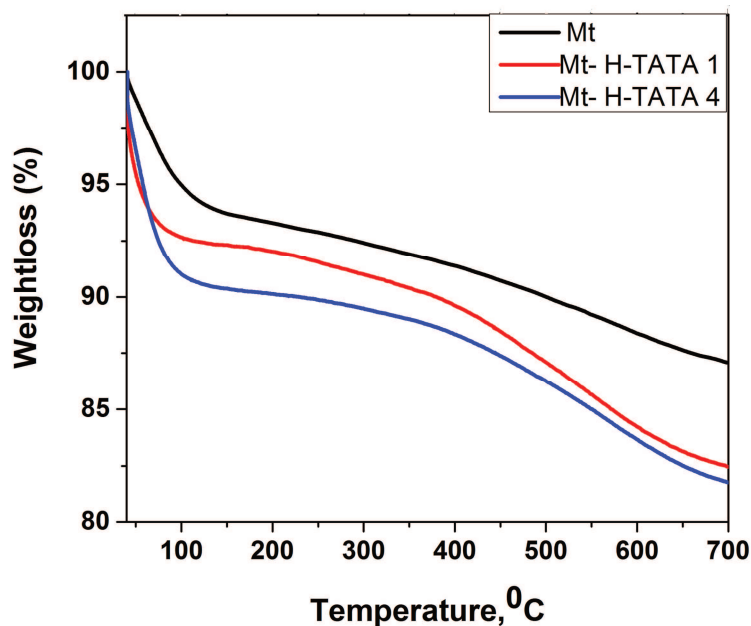


Figure 5.9 TGA plots of Mt, together with Mt-H-TATA 1 and Mt-H-TATA 4

Xie et al., divided the decomposition of the organoclay into four parts; (a) the free water region in the temperature below 200 °C (b) the region where organic substances decompose in the temperature range 200-500 °C (c) the structural water region in the temperature range 500-800 °C and (d) the region between 800-1000 °C.^{25,26} Na-MMT is usually highly hydrated due to its large hydrophilic internal surface.²⁵ Hence, free water (water between particles and sorbed on the external surfaces of crystals) are released at the temperature of below 100 °C.²⁷ The total weight loss in this region was found to be 6%. The second step of decomposition occurs at the temperature range of 400-700 °C. This is due to the structure water in the clay, bonded OH that

undergoes dehydroxylation. The total weight loss at this region is 4%. The **H-TATA 1** intercalated montmorillonite clay shows a weight loss of 8% below 100 °C and in the second step ie the decomposition of organic substance shows a weight loss of 8%. The **H-TATA 4** intercalated montmorillonite clay shows a weight loss of 10% below 100 °C and in the second step ie the decomposition of organic substance shows a weight loss of 8%. The weight loss of organic substances indicates dye molecules adsorbed on the surface of the sodium montmorillonite clay.

The thermal decomposition of cloisite 93a along with the **H-TATA-1** and **H-TATA 4** intercalated samples are represented in figure 5.10.

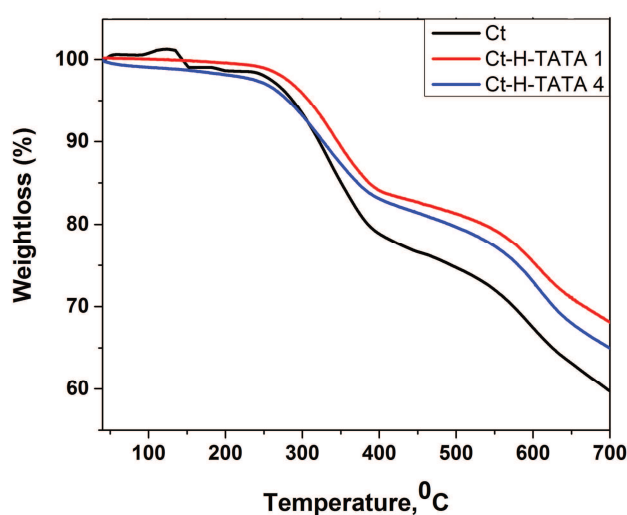


Figure 5.10 TGA plots of Ct, together with Ct-H-TATA 1 and Ct-H-TATA 4

The weight loss below 200 °C refers to the first degradation step which is related to the dehydration of physically adsorbed water and water molecules around metal cations in the interlayer. The total weight loss in the first degradation step was low in the case of cloisite 93a and two modified samples were compared to sodium montmorillonite. The onset for the decomposition of organic matter occurs around 200 °C which corresponded

to the decomposition of the surfactant within the modified montmorillonite.²⁸ The **H-TATA 1** intercalated cloisite 93a clay shows a weight loss of 19% between 200 °C to 500 °C where as **H-TATA 4** intercalated cloisite 93a clay shows a weight loss of 18%. The pristine clay shows a weight loss of 24%. The decrease in the weight percentage of organic matter may be due to the leaching out of the surfactant during the intercalation procedure. Similar observations were reported by Drozdet. al., during the intercalation of porphyrin molecule to Cloisite 30b.²¹

5.3.1.4. Scanning Electron Microscopy (SEM) studies

SEM is used to investigate the morphology of organo-modified clay. It is of importance to reveal that there are not many morphologic differences observed between organoclays despite the obvious variation observed in the XRD measurements. Figure 5.11 and 5.12 shows the morphology of sodium Montmorillonite clay before and after intercalation. Figure 5.13 and 5.14 shows the morphology of cloisite 93a clay before and after intercalation.

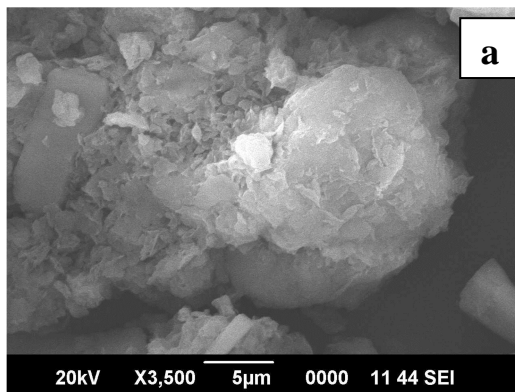


Figure 5.11 SEM image of Sodium montmorillonite(Mt).

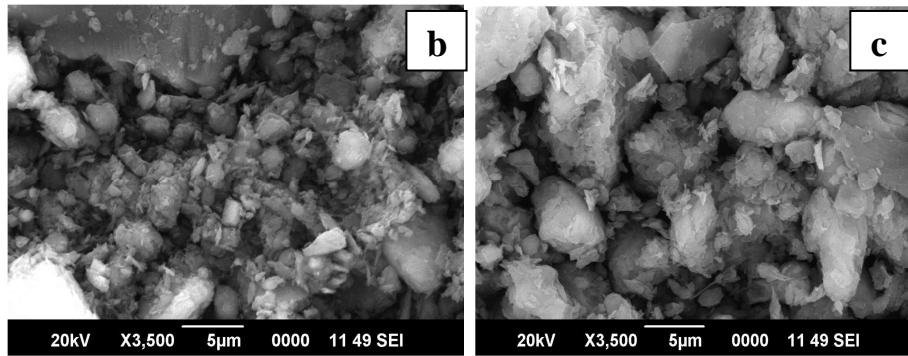


Figure 5.12 SEM images of Mt-H-TATA 1(b) and Mt-H-TATA 4(c)

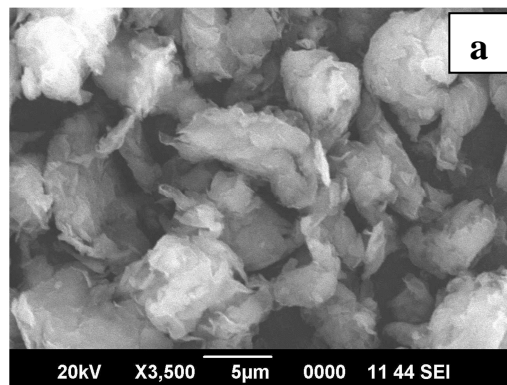


Figure 5.13 SEM image of cloisite 93a (Ct)

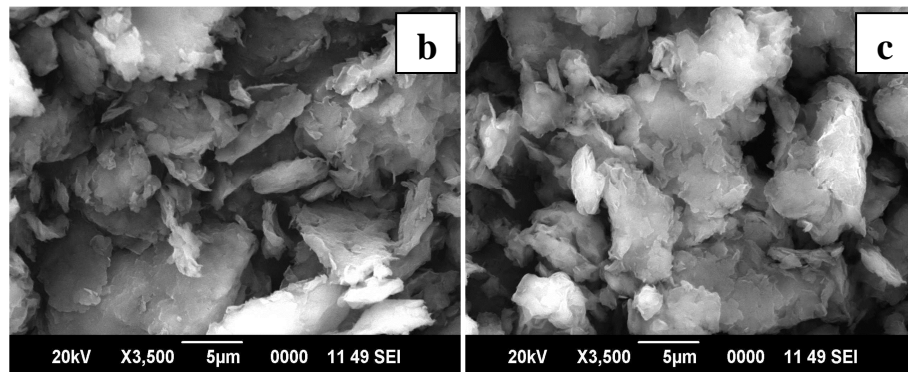


Figure 5.14 SEM images of Ct-H-TATA 1(b) and Ct-H-TATA 4 (c)

5.3.1.5. Transmission Electron Microscopy (TEM)

Transmission electron microscopy (TEM) was used to qualitatively analyze the structure of the clay-dye complex.

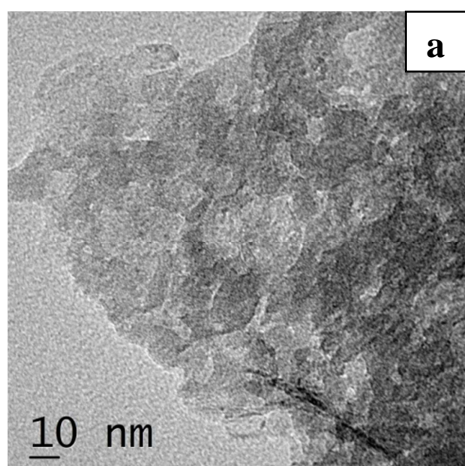


Figure 5.15 TEM image of Sodium montmorillonite

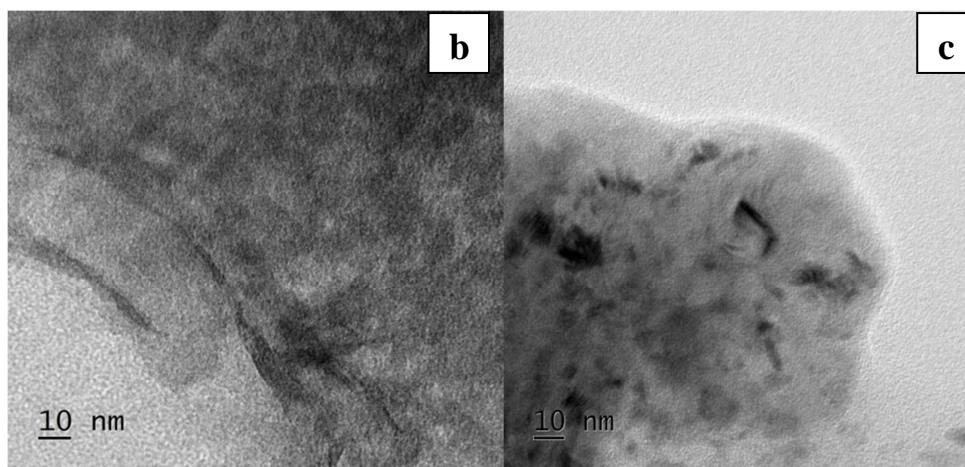


Figure 5.16 TEM images of Mt-H-TATA 1(b) and Mt-H-TATA 4 (c)

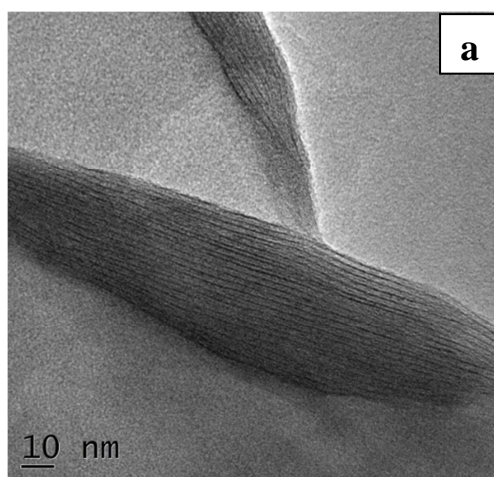


Figure 5.17 TEM image of cloisite 93a

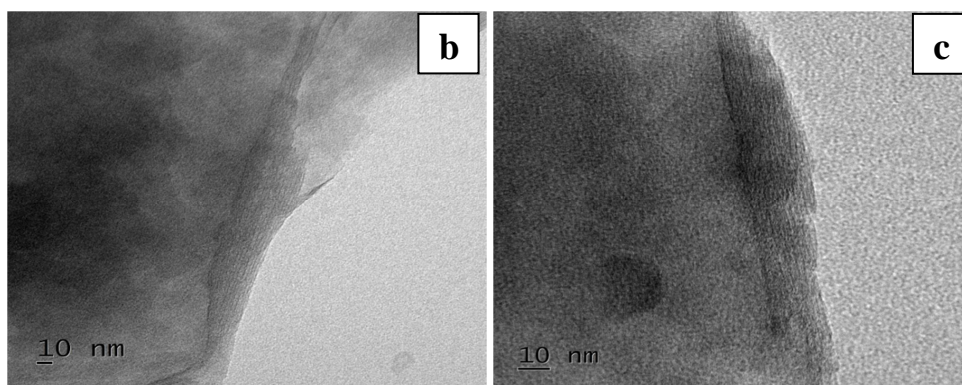


Figure 5.18 TEM images of Ct-H-TATA 1(b) and Ct-H-TATA 4(c)

TEM images obtained for Mt - H-TATA hybrids do not indicate any morphology changes upon dye adsorption. Whereas in the case of cloisite clay these images visually confirm the existence of layer structure. In cloisite clay layer structure is retained after the dye incorporation. It was reported earlier that the layer-structure images of untreated Cloisite Na⁺ cannot be observed with TEM. It was supposed that for the unmodified clay, there is water adsorbed on exchangeable cations such as Na⁺. Under high vacuum of TEM imaging conditions and due to the impact of the high-energy beams, the

adsorbed water can be expelled making the collapse of the layer structure. This forbids the structures from being readily observed in TEM images.²⁹ However, with the present materials, the unmodified Cloisite and clay modified with triazatriangulenium salts the TEM images reveal layer structures.

5.3.2. Photophysical properties

5.3.2.1. Absorption spectral properties

The diffuse reflectance spectrum showing visible light absorption by the prepared clay -triazatraingulenium cation hybrids are given in Figure 5.19 and 5.20. Both spectra are characterized by an absorption band in the region of 450-550 nm with a typical spectral profile similar to that of the free triazatriangulenium cations **H-TATA 1** or **H-TATA 4**. In the case of **H-TATA 1** and **H-TATA 4** supported on Na-MMT the absorption maximum obtained was at 526 nm and 520 nm respectively. In water (0.1 M NaCl), both **H-TATA 1** and **H-TATA 4** showed a maximum of absorption at 530 nm. A shift of 4 nm and 10 nm was observed when the dyes are adsorbed on to the Na-MMT clay.

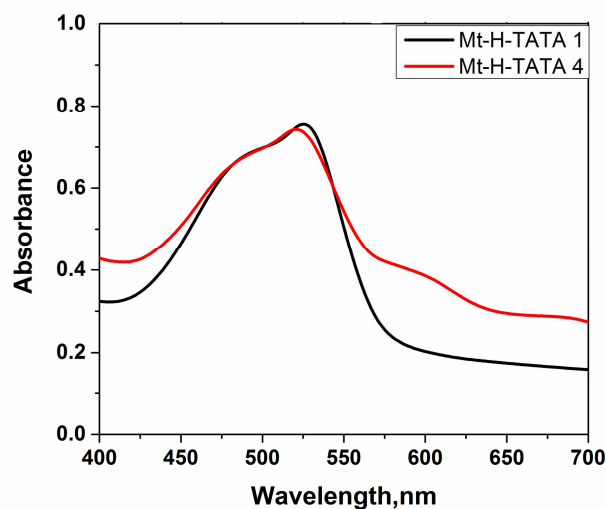


Figure 5.19 Absorption spectra of Mt-H-TATA 1 and Mt-H-TATA 4.

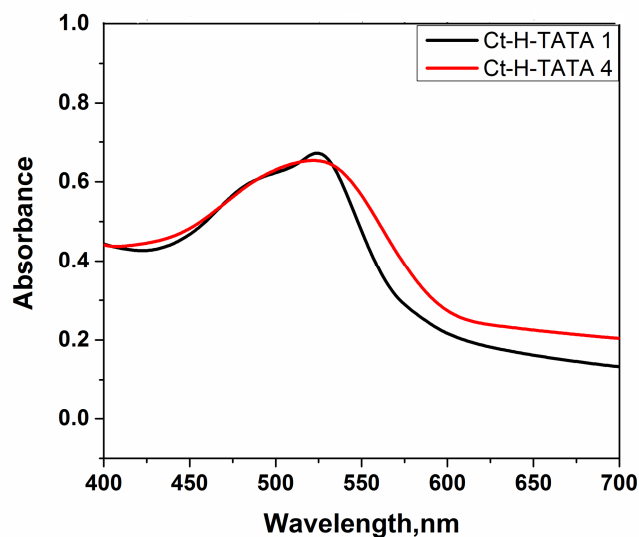


Figure 5.20 Absorption spectra of Ct-H-TATA 1 and Ct-H-TATA 4

In the case of **H-TATA 1** on Cloisite clay which shows evidence for intercalation in the XRD, the absorption maximum obtained was at 525 nm in comparison to 530 nm in aqueous solutions. However, for **H-TATA 4** on Cloisite, it showed a maximum of absorption at 521 nm without significant changes to the spectral profile.

5.3.2.2. Emission spectral properties

For **H-TATA1** and **H-TATA 4** supported on Na-MMT, the emission spectrum is characterized by a band with maximum at 567 nm and 543 nm respectively. In water (0.1 M NaCl), both **H-TATA 1** and **H-TATA 4** showed the emission maximum at 571 nm. A major difference observed in this case is the observation of a blue shifted emission maximum observed for the **H-TATA 1** and **H-TATA 4**. Since there is no corroborative evidence in x-ray diffraction on intercalation, we cannot consider this as an evidence for an intercalative binding. Moreover, the weak intensity of emission observed prevents us from making a conclusion on the possible intercalation in the interlayer spaces of Na-MMT.

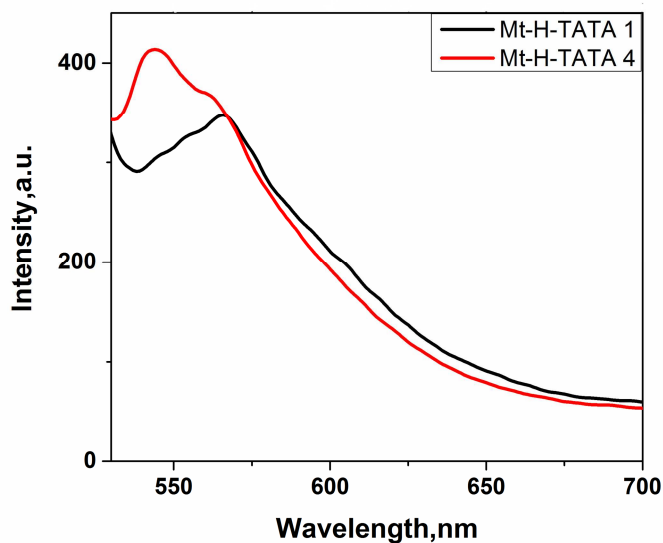


Figure 5.21 Emission spectra of Mt-H-TATA 1 and Mt-H-TATA 4.
 $\lambda_{ex} = 480$ nm

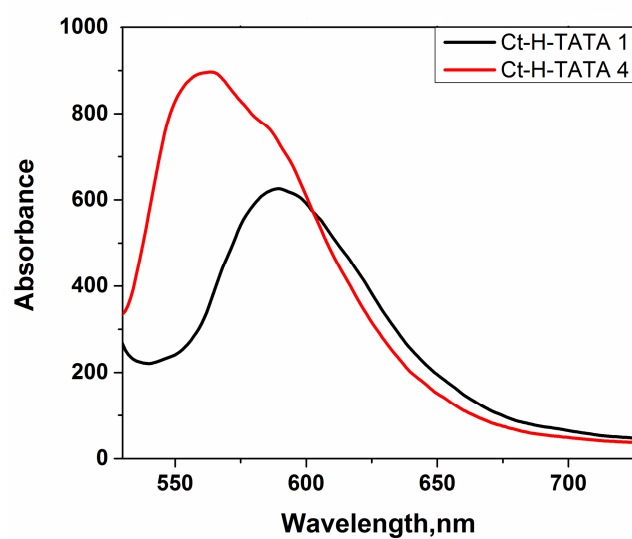


Figure 5.22 Emission spectra of Ct-H-TATA 1 and Ct-H-TATA 4
 $\lambda_{ex} = 480$ nm

Upon intercalation of **H-TATA 1** on to the interlayer space of Cloisite clay the emission spectrum showed a dramatic red shift of 19 nm compared to that for the free molecule in water (0.1 M NaCl). Whereas, **H-TATA 4**

showed a blue shift of 9 nm that observed in water. This can be considered as an evidence for the intercalative binding observed for the **H-TATA 1**. This observation is similar to that observed earlier (Chapter 3 figure 3.9) for the **TATA 4** cation, where, the emission band red shift due to a perturbation to the polarity of the molecule. Here too the intercalation led to an increase in the interlayer space which suggest a mode of intercalation that is either perpendicular or somewhat angular with respect to the plane of the layers. Such a mode of binding may introduce a strain on the plane of the ring and can lead to the observed changes in the emission band upon intercalation.

5.3.2.3. Lifetime Measurements

The fluorescence decay profiles of the samples were obtained by the method of Time Correlated Single Photon counting (TCSPC) in solid state. Fluorescence lifetime is another parameter that changed significantly upon adsorption to the clay minerals. The long lifetime of ~10 ns observed for the free cations in aqueous solutions has been shortened significantly due to binding to clay surface. This may be attributed to an enhanced interaction of vibrational modes of bonds on the clay surface with the organic cations facilitating a higher non – radiative deactivation processes.

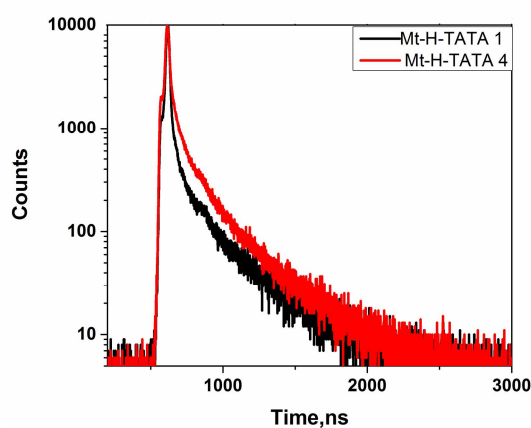


Figure 5.23 Lifetime measurement of Mt-H-TATA 1 and Mt-H-TATA 4.

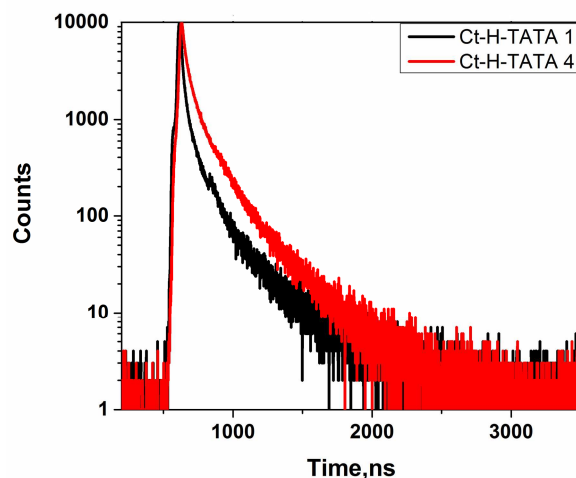


Figure 5.24 Lifetime measurement of Ct-H-TATA 1 and Ct-H-TATA 4

The photophysical properties of the modified clays are summarized in **table 5.2**.

Table 5.2 Absorption maxima ($\lambda_{\max}(\text{abs})$), emission max ($\lambda_{\max}(\text{em})$), singlet lifetime (τ_f) of modified clays.

	$\lambda_{\max}(\text{abs})(\text{nm})$	$\lambda_{\max}(\text{em})(\text{nm})$	$\tau_f(\text{ns})$
Mt-H-TATA 1	526	567	0.12
Mt-H-TATA 4	520	543	0.26
Ct-H-TATA 1	525	590	0.42
Ct-H-TATA 4	521	562	0.55

5.3.3. Singlet oxygen generation studies

The singlet oxygen generation capacity of triazatriangulenium salts were discussed earlier in chapter 2. The singlet oxygen generation capacity of clay supported triazatriangulenium salts were also studied in aqueous solutions using the water soluble actinometer ADPA. As already discussed, in the

presence of singlet oxygen ADPA undergoes photooxidation to corresponding endoperoxide. Since the endoperoxide formed does not absorb in the region where ADPA absorbs the photochemical conversion can be monitored by UV-Vis absorption spectroscopy. The singlet oxygen generation capability was demonstrated by taking the 1 mg/mL of the supported sensitizer in the presence of ADPA (1.6×10^{-4} M) in water. The irradiation was carried out with the help of ultrabright green LED for the selective excitation of the sensitizer. The incident photon rate was kept constant in all the cases and it was ensured by chemical actinometry as described in chapter 2. The duration of irradiation is limited to observe the initial kinetics of the reaction. The decrease in the absorbance of ADPA (1.6×10^{-4} M) was observed in all the cases over a period of 120 minutes of irradiation. Figure 5.25 to 5.28 shows the change in absorbance of the ADPA bands upon irradiation at 530 nm. Control experiments were performed using clay sample devoid of triazatriangulenium cations does not show change in the absorbance of ADPA.

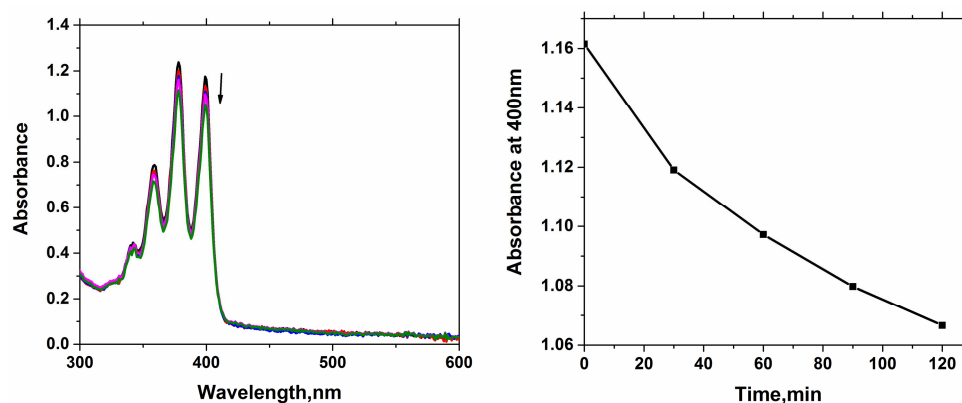


Figure 5.25 The decrease in absorbance of ADPA (1.6×10^{-4} M) during the irradiation of Mt-H-TATA 1 in aqueous solution with ultrabright green LED light.

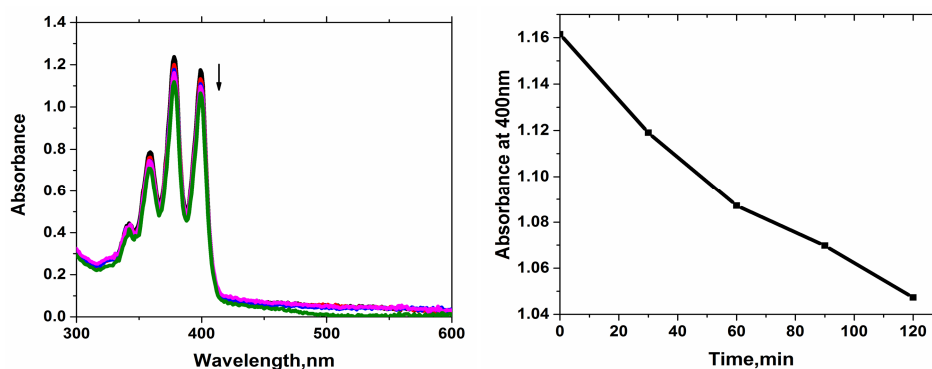


Figure 5.26 The decrease in absorbance of ADPA (1.6×10^{-4} M) during the irradiation of Mt-H-TATA 4 in aqueous solution with ultrabright green LED light.

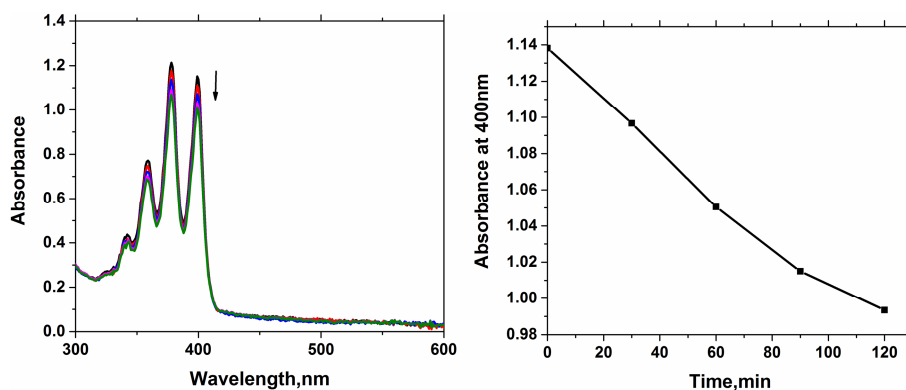


Figure 5.27 The decrease in absorbance of ADPA (1.6×10^{-4} M) during the irradiation of Ct-H-TATA 1 in aqueous solution with ultrabright green LED light.

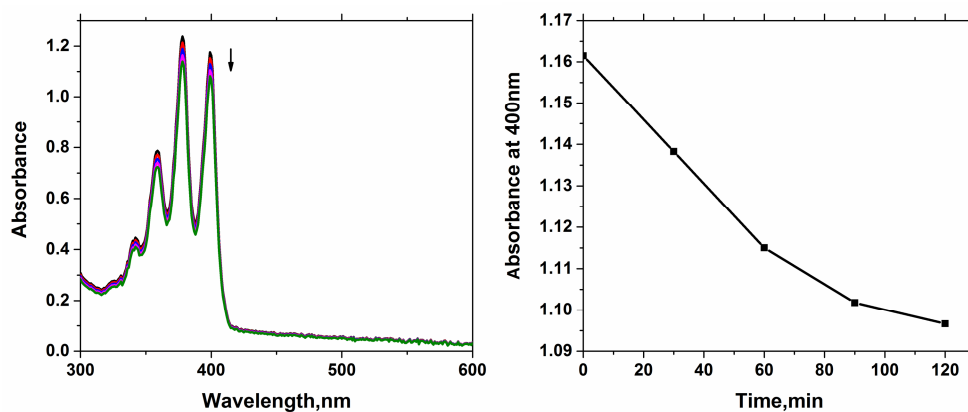


Figure 5.28 The decrease in absorbance of ADPA (1.6×10^{-4} M) during the irradiation of Ct-H-TATA 4 in aqueous solution with ultrabright green LED light.

5.3.4. Photosensitized inactivation of bacteria

Under aerobic conditions, the singlet oxygen production of clay supported triazatriangulenium salts were evident from the conversion of ADPA to its corresponding endoperoxide. This result allows the application of these supported sensitizers as a disinfection agent as a photo-antimicrobial material. The active chemical species, $^1\text{O}_2$ is formed by the energy transfer between the excited state of photosensitizer and ground state of molecular oxygen. It can easily oxidizes organic matter and is able to damages significantly, the structure of cell walls of the organism and also deactivate the antioxidant enzymes.³⁰ The high antimicrobial efficiency of $^1\text{O}_2$ was demonstrated in the literature.³¹

The penetration of photosensitizer molecules inside the cells or atleast their adsorption onto the cell walls is essential for the singlet oxygen mediated antibacterial efficiency.^{32,33} The adsorption of cationic dyes on clay mineral surface brings about the charge reversal on clay mineral particles.^{34,35} This results in the antibacterial efficiency of the clay minerals intercalated with cationic singlet oxygen sensitizers. In this case for the outer surface adsorbed triazatriangulenium cations too, they ensure an electrostatic interaction between the negatively charged gram negative bacterial cell walls with photosensitizers.

The antibacterial activity of the four clay supported triazatriangulenium salts was investigated by using the gram negative bacteria, *E. coli* contaminated water. The *E.coli* counts of irradiated and unirradiated samples were determined by colony counting method. A 1 mg/mL suspension of the prepared hybrid materials were used for the bacterial inactivation studies. The incubation of bacteria with the heterogeneous sensitizers under study in the absence of light did not lead to reduction in the number of *E.coli* colonies suggesting that these materials are nontoxic to *E. coli*. Incubation of the

bacteria with clay alone was also taken as a control. No significant reduction in the number of *E.Coli* was observed while keeping the control in the dark and in the presence of sunlight. The variation of the number of *E.coli* colonies in the presence of clay supported heterogeneous sensitizers in the presence and absence of the light is shown in table 5.3. and 5.4. The plate images are shown in figure 5.29, 5.30, 5.31 and 5.32. The reduction in the cell viability in the presence of heterogeneous sensitizer is shown in figure 5.31 and 5.34.

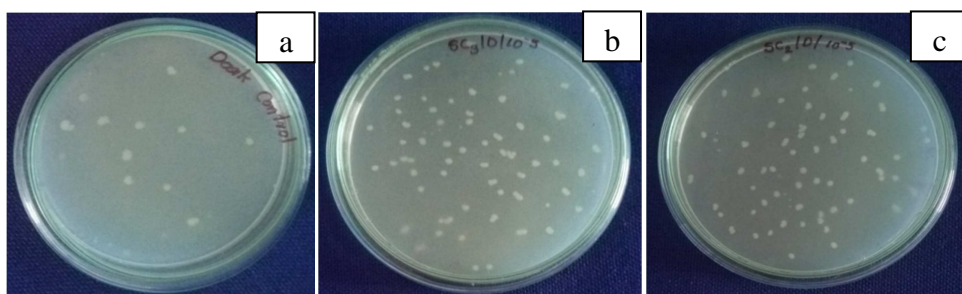


Figure 5.29 The *E.coli* treated with control(a), Mt-H-TATA 1(b),Mt-H-TATA 4(c) kept in the dark

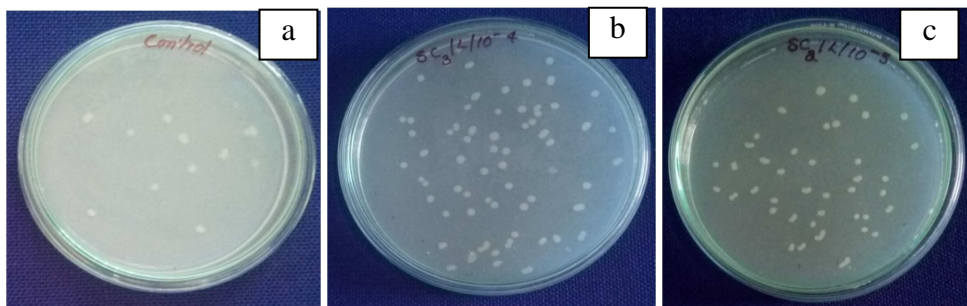


Figure 5.30 The *E.coli* treated with control (a),Mt-H-TATA 1(b), Mt-H-TATA 4(c) kept in the sunlight for 30 minutes

Table 5.3 The number of *E.Coli* colonies observed by incubating the bacteria with the heterogeneous sensitizer in the dark and after keeping with 30 minutes in the presence of sunlight. The presented data is a mean of the triplicate with a standard deviation (SD) of <5%.

	Dark($\times 10^6$ CFU/ml)	Light($\times 10^6$ CFU/ml)
Control	7.1	7.1
Mt-H-TATA 1	7.1	3.3
Mt-H-TATA 4	7.0	5.8

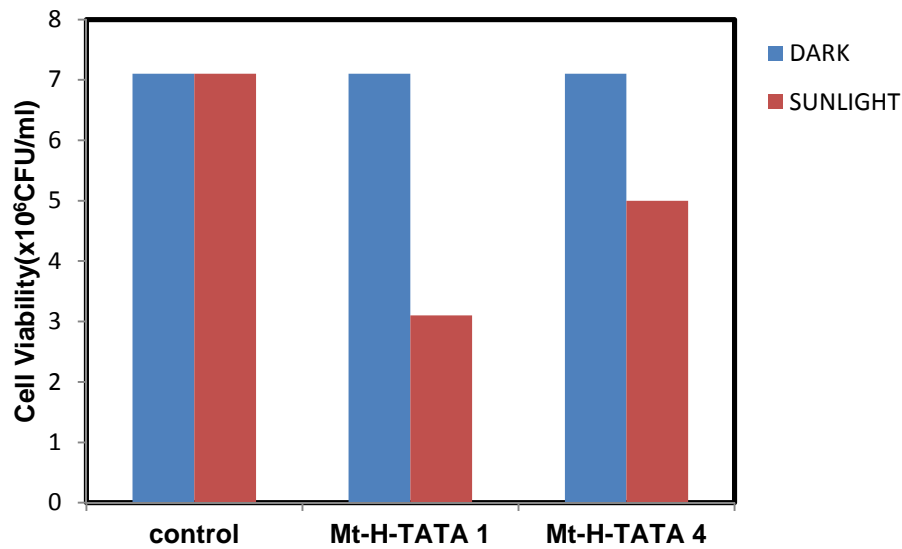


Figure 5.31 The cell survival when *E.coli* treated with Control (a), Mt-H-TATA 1(b), Mt-H-TATA 4 (c)

In the case of **H-TATA 1** intercalated to sodium montmorillonite samples show a 53% reduction where as the **H-TATA 4** intercalated samples show 17% reduction in the *E.coli* count.

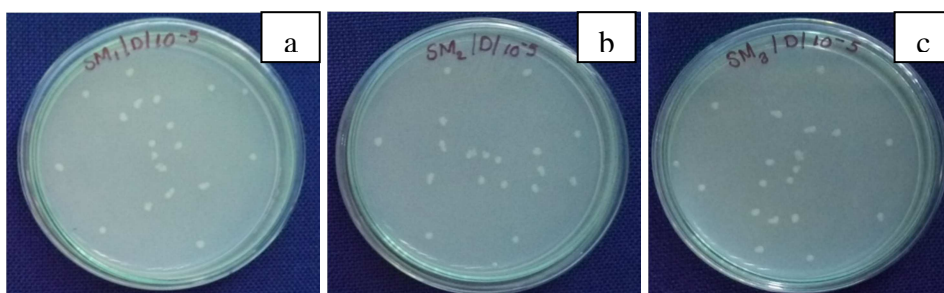


Figure 5.32 The *E.coli* treated with control (a), Ct-H-TATA 1(b), Ct-H-TATA 4 (c), kept in the dark

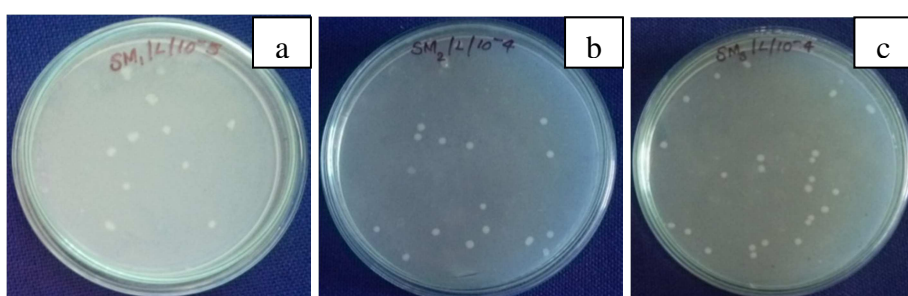


Figure 5.33 The *E.coli* treated with control (a), Mt-H-TATA 1(b), Mt-H-TATA 4 (c) kept in the sunlight for 30 minutes

Table 5.4 The number of *E.Coli* colonies observed by incubating the bacteria with the heterogeneous sensitizer in the dark and after keeping with 30 minutes in the presence of sunlight. The presented data is a mean of the triplicate with a standard deviation (SD) of <5%.

	Dark($\times 10^6$ CFU/ml)	Light($\times 10^6$ CFU/ml)
Control	2.1	2.1
Mt-H-TATA 1	2.1	0.6
Mt-H-TATA 4	2.1	0.59

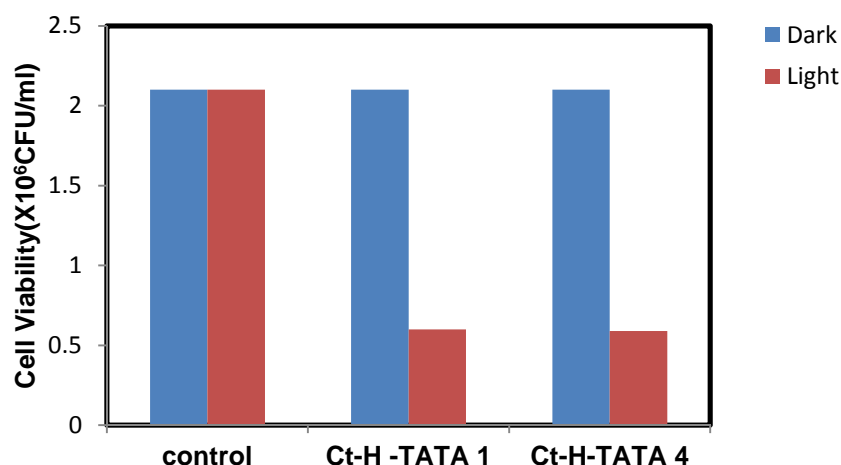


Figure 5.34. The cell survival when *E.coli* treated with (a) Control (b) Ct-H-TATA 1, (c) Ct-H-TATA 4

The better activity was observed in triazatriangulenium intercalated with cloisite 93a samples. In both the cases 75% reduction in the cell viability was observed.

5.4. Conclusions

The water soluble triazatriangulenium cations were adsorbed on to Na-montmorillonite and Cloisite clay surfaces in a solution phase intercalation method. The powder XRD data and the photophysical studies reveal that only H-TATA 1 in Cloisite clay showed intercalation behaviour whereas, all other materials may have surface adsorbed triazatriangulenium ions. The long size of the alkyl chain ($n=6$) on H-TATA 4 could be a deterrent to intercalation on Cloisite clay. All the prepared materials show singlet oxygen generation capability indicated by the photooxidation of ADPA under irradiation at 530 nm. All hybrid materials show photo-antimicrobial activity against *E. coli* bacteria with Cloisite based hybrid materials showing better activity. This higher activity may be due to a higher loading of the cations in comparison to Na-montmorillonite clay based hybrid structures.

5.5. Experimental

All solvents used were of reagent grade and used without further purification. Reagents were purchased from Sigma-Aldrich and Spectrochem Pvt.Ltd. and used as received. Montmorillonite K 10 was purchased from Sigma-Aldrich. Cloisite 93 A, a modified clay mineral, was sourced from Southern Clay Corp, USA. Elemental analysis was performed in Elementar Vario EL III model instrument in SAIF, CUSAT. Infrared Spectra were recorded using JASCO FTIR Spectrometer using KBr pellets in the range 400-4000 cm^{-1} . The SEM images were obtained using JEOL ModelJSM - 6390LVScanning Electron Micrograph with an attached energy-dispersive X-raydetector. TEM images were obtained using JEOL JEM 2100 HRTEM at SAIF, CUSAT. The diffuse reflectance UV-Vis spectra of the solid samples were recorded using UV-Vis-NIR Ocean Optics fibre optics Spectrophotometer SD 2000model equipped with a diffuse reflectance probe. TG analysis was performed on Perkin Elmer Pyris Diamond 6thermogravimetric/differential thermal analyzer by heating the sample at the rate of 10 $^{\circ}\text{C}/\text{min}$ from 40 $^{\circ}\text{C}$ to 730 $^{\circ}\text{C}$ under N_2 atmosphere. Fluorescence and Fluorescence lifetime studies were carried out using JobinYvonFluorolog3-211UV-Vis-NIR fluorescence spectrometer. Absorption spectra were recorded using Evolution 201 UV-visible spectrophotometer. XRD analysis was performed with Rigaku X-ray diffractometer.

5.5.1. Synthesis of H-TATA 1 and H-TATA 4

Synthesis of **H-TATA 1** and **H-TATA 4** were described elsewhere in the thesis (see chapter 2.Sections 2.5.3 and 2.5.6).

5.5.2 Preparation of H-TATA 1 and H-TATA 4 intercalated montmorillonite

The Na^+ exchanged montmorillonite clay was prepared by stirring 1g of the clay (Montmorillonite K10) with 50 mL 0.2 M solution of sodium

nitrate solution at 70 °C for 12hrs. It was then allowed to settle down, filtered and washed several times with water till free from nitrate. It was then kept in the vacuum at 80 °C over night. Intercalation of **H-TATA 1** and **H-TATA 4** into montmorillonite was carried out by the conventional ion-exchange method in which an aqueous suspension of sodium montmorillonite (1 g in 80 mL) was mixed with an aqueous solution (0.1 M NaCl) of the **H-TATA 1** or **H-TATA 4**(20 mg in 20 mL) and the mixture was allowed to react for one day at 70 °C. After centrifugation, the resulting pink solid was washed with water and dried. Soxhlet extraction was performed with chloroform in order to remove any trace amount of triazatriangulenium on the clay surface. It was then kept in the vacuum at 80 °C over night.

5.5.3 Preparation of **H-TATA 1** and **H-TATA 4** intercalated Cloisite 93a

Intercalation of **H-TATA 1** and **H-TATA 4** into the modified clay cloisite 93a was also done by a similar procedure described in section 5.5.2. The samples thus obtained were characterized by powder XRD, CHN analysis, thermogravimetric analysis, SEM, TEM, UV-Vis DRS and fluorescence spectroscopy.

5.5.4 Studies on photosensitized generation of singlet oxygen

The production of singlet oxygen by the triazatriangulenium-clay particles was determined using the singlet oxygen scavenger disodium-9, 10-anthracenedipropionic acid (ADPA). Typically, 1 mg/mL of the clay supported triazatriangulenium composites were added to an aqueous solution of ADPA (1.6×10^{-4} M). The particles were exposed to light at 530 nm from an ultrabright green LED for 120 minutes with periodic monitoring of UV-visible absorption spectrum of the experimental solution. Control experiment was also performed using clay sample devoid of triazatriangulenium cations.

5.5.5 Photobactericidal studies of microbial cell cultures with the triazatriangulenium-clay composites

Using aseptic techniques, a single pure colony was transferred into a 200 mL of nutrient broth, capped and placed in incubator overnight at 37 °C. After incubation, using aseptic preparation, turbidity of suspensions was measured and adjusted using McFarland standards as a reference. The 10 mg of samples (concentration-1 mg/mL) were added to 10 mL of culture and one set was incubated at dark and other set was incubated in sunlight. A control tube was kept. After the incubation, the tubes were serially diluted and plated on nutrient agar. The plates are incubated for 24 hrs at 37 °C. The plates were observed for colonies and the total count was recorded.

5.6. References

1. Ghadiri, M.; Chrzanowski, W.; Rohanizadeh, R. *RSC Adv.* **2013**, *00*, 1.
2. Xi, Y.; Frost, R.L.; He, H.; Klopogge, T.; Bostrom, T. *Langmuir.* **2005**, *21*, 8675.
3. Alexandre, M.; Dubois, P. *Mater. Sci. Eng.* **2000**, *28*, 1.
4. Greenland, D.J.; *J. Colloid Sci.* **1963**, *18*, 647.
5. Wang, X.; Liu, B.; Yu, P. *J. Nanomater.* **2015**, *1*, 4.
6. Sandri, G.; Bonferoni, M.C.; Rossi, S.; Ferrari, F.; Aguzzi, C.; Viseras, C.; Caramella, C. *In Wound Healing Biomaterials*, **2016**, *1*, 385.
7. Paiva, L.B.; Morales, A.R.; Díaz, F.R.V. *Appl. Clay Sci.* **2008**, *42*, 8.
8. Gao, S.; Zhu, J.; Zhang, Y.; Wang, Q.; Jing, X.; Meng, C. *R. Soc. open sci.* **2017**, *4*, 171258.
9. Garfinkel-Shweky, D.; Yariv, S. *Clay Miner.* **1999**, *34*, 459.
10. Valandro, S.R.; Poli, A.L.; Correia, T.F.; Lombardo, P.C.; Schmitt, C.C. *Langmuir.* **2017**, *33*, 891.
11. Ley, C.; Brendlé, J.; Miranda, M.; Allonas, X. *Langmuir.* **2017**, *33*, 6812.
12. Shinozaki, R.; Nakato, T. *Microporous Mesoporous Mater.* **2008**, *113*, 81.
13. Boháč, P.; Bujdák, J. *Clays and Clay Miner.* **2018**, *66*, 127.
14. Liu, P.; Zhang, L.; *Sep. Purif. Technol.* **2007**, *58*, 32.
15. Almeida, C.A.P.; Debacher, N.A.; Downs, A.J.; Cottet, L.; Mello, C.A.D. *J. Colloid Interface Sci.* **2009**, *332*, 46.
16. Fischer, H.; Batenburg, L.F. US patent no. 6, **2003**, 648, 959.

17. Raha, S.; Ivanov, I.; Quazi, N.H.; Bhattacharya, S.N. *Appl. Clay Sci.* **2009**, *42*, 661.
18. Validi, M.; Bazgir, S.; Saeid Rashidi, A.; Yazdanshenas, M.E. *Ceramics-Silikáty.* **2012**, *56*, 152.
19. Madhavan, D.; Pitchumani, K. *J. Photochem. Photobiol. A.* **2002**, *153*, 205.
20. Madhavan, D.; Pitchumani, K. *Tetrahedron* **2001**, *57*, 8391.
21. Drozd, D.; Szczubiałka, K.; Skiba, M.; Kepczynski, M.; Nowakowska, M. *J. Phys.Chem C.* **2014**, *118*, 9196.
22. Bujdak, J.; Jurecekova, J.; Bujadakova,H.; Lang,K.; Sersen, F. *Environ. Sci. Technol.* **2009** ,*43*, 6202.
23. Ito, K.;KoushiFukunishi,M.K.; Fujiwara, Y. *DyesPigm.* **1996**, *34*, 297.
24. Hoidy, W.H.; Ahmad, M.B.; Al Mulla, E. A.; Ibrahim, N. *Am. J. Applied Sci.* **2009**, *6* , 1567.
25. Xie, W.; Z. Gao, K.; Liu, W.P.; Pan, R.; Vaia. *ThermochimicaActa.* **2001**,*367*, 339.
26. Arroyo, M.; Lopez-Manchado, M.A.; Herrero, B. *Polymer* **2003**, *44*, 2447.
27. Magaraphan, R.; Lilayuthalert, W. *Compos Sci. Technol.* **2001**, *61*, 1253.
28. Cervantes-Uc, J.M.; Cauich-Rodriguez, J.V.; Vazquez-Torres, H.; Garfias-Mesias, L.F.; Paul, D.R.*Thermochim. Acta.* **2007**, *457*, 92.
29. Ensafi, A.A.; Heydari-Bafrooei, E.; Dinari, M.; Mallakpour, S. *J. Mater. Chem. B.* **2014**, *2*, 3022.

30. Wainwright, M.; Crossley, K. B. *Int. Biodeterioration Biodegrad.* **2004**, *53*, 119.
31. Wainwright, M.; Phoenix, D. A.; Laycock, S. L.; Wareing, D. R. A.; Wright, P. A. *FEMS Microbiol. Lett.* **1998**, *160*, 177.
32. Phoenix, D. A.; Harris, F. *Trends Mol. Med.* **2003**, *9*, 283.
33. O'Neill, J.; Wilson, M.; Wainwright, M. *J. Chemother.* **2003**, *15*, 329.
34. Eren, E.; Afsin, B. *Dyes Pigm.* **2007**, *73*, 162.
35. Eren, E.; Afsin, B. *Dyes Pigm.* **2008**, *76*, 220.
36. Icli, S.; Demic, S.; Dindar, B.; Doroshenko, A.O.; Timur, C. *J. Photochem. Photobiol. A.* **2000**, *136*, 15.
37. Jayrajsinh, S.; Shankar, G.; Agrawal, Y.K.; Bakre, L. *Journal of Drug Delivery Sci. and Tech.* **2017**, *39*, 200.

SUMMARY AND CONCLUSION

The thesis entitled “**SYNTHESIS OF WATER SOLUBLE TRIAZATRIANGULENIUM CATIONS AND STUDIES ON THEIR APPLICATION AS SINGLET OXYGEN SENSITIZERS IN HOMOGENEOUS AND HETEROGENEOUS MEDIA**” embodies the results of the investigations carried out towards assessing the use of a well known cationic and highly stable triangulenium dye as a potential singlet oxygen generator for photodynamic processes. The major objectives of the thesis were:

- ❖ To synthesize water soluble triazatriangulenium salts by incorporating polar functional groups
- ❖ Study their photophysical properties
- ❖ Study the efficiency of Triplet state formation and singlet oxygen generation
- ❖ Synthesis and study of lipophilic triazatriangulenium cations in microheterogeneous medium
- ❖ Tether covalently or intercalate triazatriangulenium salts to solid supports or layered materials
- ❖ Study the singlet oxygen production by these heterogeneous sensitizer systems

- ❖ Study the photodynamic action of singlet oxygen generated by these heterogeneous sensitizers and explores their ability in disinfection of contaminated water.

Solubility of dyes in the medium required for photodynamic applications is a major requirement. In chapter 2 we were able to demonstrate that by introduction of a hydroxyl group in the N-alkyl substituent can significantly improve the solubility in water and in non-aqueous medium such as acetonitrile. A comparison of the photophysical properties reveal that, water is ideal for obtaining a longer fluorescence lifetime, a higher triplet quantum yield, a longer triplet lifetime and a better singlet oxygen generation efficiency. In terms of singlet oxygen generation efficiency, a limiting phenomenon is the thermally activated delayed emission (TADF) due to the small energy gap between the singlet and triplet excited states. Yet another limiting reason is the possibility of photoinduced electron transfer between oxygen and excited states of triazatriangulenium cations.

Chapter 3 of the thesis explore the photophysical changes when a series of triazatriangulenium cations having lipophilic long alkyl substituents on the bridging 'N' are solubilized in microheterogenous medium such as anionic, cationic and neutral micelles. The solubility properties indicate anionic micelle is a suitable medium for these lipophilic cations. The photophysical studies show that the absorption and emission spectra changes as the length of the alkyl chain increases. Detailed studies using time resolved emission spectroscopy (TRES), studies on the temperature dependence of emission and the theoretical modelling using DFT and TD-DFT calculations identified a "disc to bowl" geometrical change to the structure of the cation when solubilized in anionic micelles. Based on these results two possible binding modes has been proposed. For triazatriangulenium cations with smaller alkyl chains intercalation between

the anionic head groups of the surfactant is the preferred mode of binding. For cation having longer alkyl chains, the preferred mode of binding is a “spider-on-an-apple” type topology with its pods penetrating the micelles.

Covalent tethering is a well established strategy to prepare organic – inorganic hybrid structures. The work presented in Chapter 4 is an attempt in this direction. We have prepared and studied four types of triazatriangulenium-silica composites. The studies on the photophysical properties show that the composite material S1 having three point tether to the silica surface has the matching characteristics with that of dye in homogenous medium. This material has the highest efficiency for singlet oxygen generation and photodynamic activity against *E. coli*.

Intercalation in layered materials is another strategy for the preparation of organic – inorganic hybrids. Clay minerals are the most studied layered materials for dye encapsulation for applications such as photocatalysis. Being cationic and planar, triazatriangulenium cations are having the perfect structural feature to be an intercalator in clay minerals. The water soluble triazatriangulenium cations were adsorbed on to Na-montmorillonite and Cloisite93a clay in a solution phase intercalation method. The powder XRD data and the photophysical studies reveal that only H-TATA 1 in Cloisite clay showed intercalation behaviour whereas, all other materials may have surface adsorbed triazatriangulenium ions. The long size of the alkyl chain (n=6) on H-TATA 4 could be a deterrent to intercalation on Cloisite clay. All the prepared materials showed singlet oxygen generation capability and showed photo-antimicrobial activity against *E. coli* bacteria with Cloisite based hybrid materials showing better activity.

List of Publications

Publications

1. **S. Seena**, N. Manoj, "Determination of the singlet oxygen quantum yield of a water soluble Triangulenium salt", *MATCON 2016 International Conference on Materials for the Millennium*. January 14 -16, 2016 (ISBN 978-93-80095-738)
2. **Seena Sebastian**, "Synthesis and characterization of a novel triazatriangulenium intercalated montmorillonite with potential antibacterial activity", *Asia Pacific Journal of Research*. LXXXVII, April 2018(ISSN: 2347-4793)

Poster Presentations

1. Determination of the singlet oxygen quantum yield of a water soluble Triangulenium salt, **S. Seena**, N. Manoj, International Conference on Materials for the Millennium (MATCON 2016) held at Cochin University of Science and Technology during 14-16th January 2016
2. Synthesis of a few water soluble triazatriangulenium salts, **S. Seena**, N. P. Pravitha, N. Manoj. Inter National Conference on Green Chemistry; Catalysis, Energy and Environment held at Goa University from 22-24th January 2015.
3. Synthesis of a few novel triazatriangulenium salts, **S. Seena** and N. Manoj. The National Conference on Current Trends in Chemistry (CTRIC 2012) held at Cochin University of Science and Technology during 20th and 21st January 2012.